"SAPIENZA" - UNIVERSITY OF ROME

DEPARTMENT OF EARTH SCIENCES

Ph.D. School "Vito Volterra", Earth-Sciences Curriculum

XXXIV DOCTORATE CYCLE

Tempo and dynamics of the peri-Tyrrhenian Quaternary explosive volcanism inferred from distal archives

Lorenzo Monaco

2018-2021

Author statement

This doctorate thesis is composed by my original work and contains published and unpublished research material produced during the three-year long Ph.D. program in Earth Sciences at “Sapienza” - University of Rome.

Supervised by:

Prof. Danilo M. Palladino
Earth Science Department, “Sapienza” - University of Rome, Rome, Italy

Dr. Biagio Giaccio
Istituto di Geologia Ambientale e Geoingegneria, CNR-IGAG, Monterotondo, Italy

Revised by:

Prof. Raffaello Cioni
Earth Science Department, University of Florence, Florence, Italy

Dr. Sabine Wulf
School of Environment, Geography & Geosciences, University of Portsmouth, Portsmouth, United Kingdom

Table of Contents

SUMMARY

The study of volcanic ashes (or "tephra") has an enormous potential for volcanic stratigraphy and explosive activity reconstruction. Indeed, tephra layers deposited and preserved in sedimentary records, located sufficiently far away from the volcanic sources, can document deposits of minor and/or older volcanic events not recorded in proximal (i.e., near-vent) sections. This allows a more rigorous and complete reconstruction of the past activity and recurrence time evaluation of a volcano, with important implications for hazard assessment in volcanically active regions.

The central Mediterranean area, and in particular central-southern Italy, represents an ideal location for tephra investigations. Indeed, the presence of numerous volcanoes, active over long periods of time, combined with that of several sedimentary (i.e., sub-aerial, lacustrine and marine) successions hosting rich tephra sequences, represents an ideal condition for the development and application of the tephrostratigraphic method.

In central Italy, the lacustrine succession of Fucino Basin recorded the deposition of tephra layers from the peri-Tyrrhenian potassic Quaternary volcanic systems over a period of at least the last ~430 kyr, representing a key site for tephrochronological investigations in the area. The study of Fucino tephra layers allowed the identification of explosive events previously undocumented (or undescribed) in proximal sections, but also provided new and more reliable chronological constraints of previously known eruptions. However, not all the Fucino tephra have been geochemically characterised and associated to their source volcano, so that the eruptive history of the Italian volcanoes during the Middle Pleistocene still remains partly unknown and unexplored.

Reconstructing this activity is fundamental, as, during the Upper-Middle Pleistocene, the Quaternary potassic peri-Tyrrhenian Italian volcanoes were intensely active and dispersed several tephra layers documented all over the central-eastern Mediterranean region and acting as marker horizons. Among these, the tephra layers known in marine records as C-22, X-5, and X-6, due to their peculiar geochemical composition, their distribution over wide regions and precise ages, are among the most valuable for tephrochronological studies. Based on their geochemical composition, the volcanic origin of these tephra was postulated to be in the Campanian area, likely from Campi Flegrei.

However, so far, they were not documented in proximal settings, leaving their specific source yet to be determined.

Furthermore, in order to confidently and undoubtedly correlate tephra layers of unknown origin to their volcanic sources and specific equivalent eruption, geochemistry of the proximal near-vent deposits must be available. Unfortunately, glass composition for the peri-Tyrrhenian potassic volcanoes is still limited, as the available literature mainly consists in whole-rock bulk analysis that can be potentially affected by the presence of crystals (phenocrysts and microlites), especially in highly porphyritic samples. Furthermore, most of the available glass analysis for the Quaternary peri-Tyrrhenian potassic volcanoes derives from studies of tephra in distal settings, resulting scattered in the literature in several papers. Also these studies are incomplete, as they cover only specific time intervals and report analysis only of selected volcanoes, whilst for others (e.g., Roccamonfina) the available glass data is completely lacking. Thus, an organized glass-based geochemistry database of proximal pyroclastic units is almost lacking and needed for future tephra investigations in the area. This Thesis represents an attempt at resolving the open issues mentioned above, which are presented as three case studies in an equivalent number of scientific articles.

The first two case studies - and related scientific articles - address two tephra sequences from the F4-F5 Fucino Basin's succession, covering the 430-365 ka and 250-170 ka time intervals, broadly corresponding to Marine Isotope Stages (MIS) 11 and 7 respectively. In both cases, the Fucino tephra layers have been lithologically, geochemically (i.e., major, minor, and trace elements, Sr and Nd isotopes) and geochronologically (i.e., $^{40}Ar/^{39}Ar$ dated) characterised. Furthermore, deposits of near-vent eruptive units emplaced during these time intervals from the Vulsini, Vico, Sabatini, and Colli Albani volcanoes have been similarly characterised with the same set of analyses to provide a glass-based geochemistry reference database. This allowed to backtrack the Fucino tephra to their specific volcanic sources, which include the Vulsini, Vico, Sabatini, Colli Albani, Roccamonfina, Ischia, and Campi Flegrei volcanic systems. For the most part, the Fucino tephra layers have been associated to their corresponding proximal equivalent eruptive units, but, in some cases, also documented previously unknown eruptive events at these volcanic systems. Thus, the Fucino

Basin's succession provided new integrative information that allowed a more rigorous and complete reconstruction of the past explosive activity at these volcanoes.

In the third case study, mid-proximal deposits from the Campanian Plain area, southern Italy, have been analysed (i.e., major, minor, trace elements, Sr and Nd isotope composition, $^{40}Ar/^{39}Ar$ dating), and allowed to trace back for the first time the proximal eruptive units of the widespread C-22, X-5, and X-6 MIS 5 Mediterranean tephra marker horizons. Furthermore, other two less-dispersed tephra markers, i.e., TM-24a and TM-24b, have been associated to eruptive units from the Campanian Plain as well. Data from this study thus allowed to confidently associate these tephra marker horizons to the Campi Flegrei volcanic system, documenting an intense and frequent explosive activity at this volcano during the 110-90 ka time interval.

In conclusion, results from this Thesis provided new integrative information that allowed refining the explosive history of the Quaternary Italian potassic volcanic systems during the Middle-Upper Pleistocene. Furthermore, the tephra layers investigated in the three case studies and presented in this Thesis have been correlated to tephra layers hosted in other Italian and central Mediterranean sedimentary archives, thus consolidating the Mediterranean tephra lattice. Finally, the approach employed in this Thesis, which combines the study of distal tephra sequences hosted in sedimentary successions with investigations in near-vent volcanic areas, showed to be an effective approach for confidently correlating tephra layers of unknown origin to their volcanic source.

Chapter I - Introduction

1. *The tephrostratigraphic method: a brief history*

The term "tephra" generically refers to all the unconsolidated (i.e., not welded or cemented) primary pyroclastic products of a volcanic eruption, independently from the grain size of the particles. It was first proposed by Sigurdur Thórarinsson, who coined the term from the Greek word τεφρα (literally "ash") referring to volcanic ash layers (Thórarinsson, 1944). Sigurdur Thórarinsson (Sigurður Þórarinsson in his native language) was a Stockholm University doctoral student of Icelandic origins, who was attempting to apply the pollen analytical method in Iceland. During his surveys, he realized that he could trace and correlate over great distances volcanic ash layers based on their lithostratigraphic characteristics, such as the colour of the deposits, the grain size and shape of the grains, the crystal contents etc. As such, he realized that tephra layers represented isochronous horizons (since eruption and deposition of volcanic materials are instantaneous events in the geological timescale) that allowed to date and synchronize natural events over great distances:

"… but I also realized that identification and correlation of the numerous tephra layers in Icelandic soils would greatly facilitate the planned pollenanalytical studies." (Thórarinsson, 1981a).

In his doctoral thesis, "Tefrokronologiska studier på Island: Þjórsárdalur och dess förödelse*"* (Thórarinsson, 1944), he also proposed the term "tephrochronology":

"…as an international term to designate a geological chronology based on the measuring, interconnecting and dating of volcanic ash layers in soil profiles" (Thórarinsson, 1944).

Thus, the term tephrochronology can be defined as a dating method which uses tephra as time-stratigraphic horizons to determine the relative age of the deposits immediately underlying/overlying a tephra layer. Later in the early '80s, in the paper entitled "Greetings from Iceland: ash falls and volcanic aerosols in Scandinavia" (Thórarinsson, 1981b), Thórarinsson provided a review, based on

historic reports from 17th-19th century newspapers and transcribed eyewitness descriptions, of Icelandic ash-fall deposits in the Scandinavian peninsula, highlighting the potential of Icelandic volcanoes to disperse volcanic ash in the European continent. This was already pointed out by Christer Persson (Davies, 2015), who had been carrying out tephra investigations in Scandinavia in the '60s (Persson, 1966, 1967, 1968, 1971).

Indeed, as predicted by Thórarinsson and Persson, at the end of the decade Dugmore (1989) first reported the discovery of an Icelandic "cryptotephra" (i.e., not visible to the naked eye) in Scotland, officially opening the "tephra hunting season" in the British Isles. In the years immediately after, several studies reported the occurrence of Icelandic cryptotephra in Scotland (Dugmore and Newton, 1992; Dugmore et al., 1995, 1996), Northern Ireland (Pilcher and Hall, 1992; Hall et al., 1993; Pilcher et al., 1995, 1996) and England (Pilcher and Hall, 1996). The discovery of Icelandic cryptotephra deposited in the European continent highlighted the possibility of finding volcanic ashes of known eruptions thousands of km away from the volcanic source, at distances and in sedimentary environments never thought before. For instance, Pyne-O'Donnel et al. (2012) reported the presence of the Alaskan tephra known as "White River Ash" (~1250 BP; Lerbekmo, 2008; Jensen et al., 2014) in a pond in Newfoundland Island (Canada), at the margins of the Atlantic Ocean, at more than 7000 km away from the source volcano!

Since the discovery of Icelandic tephra in the British Isles, tephra studies have exponentially increased (Fig. 1), and tephra-based studies are published every year from all over the globe: from northern Europe (e.g., Pouclet et al., 2008; Karatson et al., 2016; Förster et al., 2020) to the Mediterranean (e.g., Keller et al., 1978; Paterne, 1986, 1988; Narcisi and Vezzoli, 1999; Bazin et al., 2019; Insinga et al., 2020), from Japan (e.g., Smith et al., 2013; Albert et al., 2018; Ishimura and Hiramine, 2020; Maruyama et al., 2020; Miyabuchi and Sugiyama, 2020; Nishizawa and Suzuki, 2020; Suzuki et al., 2020) to New Zealand (e.g., Shane, 2000; Shane and Hoverd, 2002; Smith et al., 2005, 2018; Gherels et al., 2006; Shane et al., 2013; Peti et al., 2020), Indonesia (e.g., De Maisonneuve & Bergal-Kuvikas, 2020; Pearce et al., 2020), Alaska (e.g., de Fontaine et al., 2007; Aoki, 2020; Bolton et al., 2020), South America (e.g., Wastegård et al., 2013) and the Kamchatka peninsula (e.g., Derkachev et al., 2020; Zelenin et al., 2020).

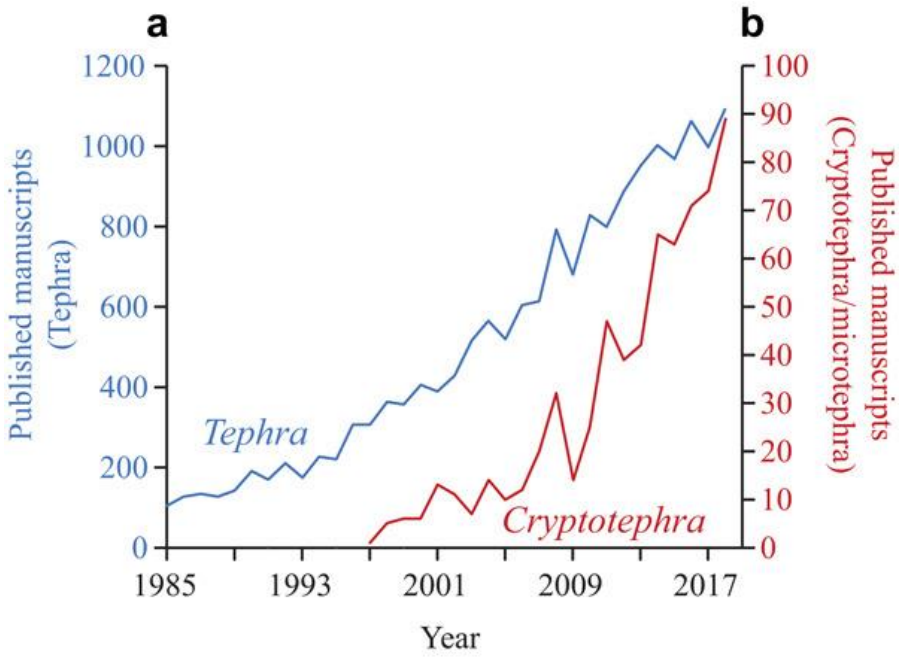

Figure 1. Number of papers published between the year 1985 and 2018 that include the terms tephra (a-blue line) and cryptotephra/microtephra (b-red line). The numbers relate to searches on Scopus using "tephra", "cryptotephra", or "microtephra" in "all fields" (i.e., including title, keywors and abstract). Image after Abbott et al. (2020).

As isochronous horizons, tephra (and cryptotephra) layers represent chronological, stratigraphic and correlation tools for addressing numerous issues in Quaternary sciences (e.g., Lowe and Hunt, 2001; Lowe, 2011; Davies, 2015; Lane et al., 2017). As defined by Lowe and Hunt (2001), "tephrostratigraphy" is:

"*… the study of sequences of tephra layers and related deposits and their relative ages.*" (Lowe and Hunt, 2001).

Indeed, tephra layers have been employed as a dating tool for the construction of age models applied to paleoclimate reconstructions (e.g., Lane et al., 2013; Giaccio et al., 2015, 2019; Regattieri et al., 2015; Kutterolf et al., 2019; Wagner et al., 2019; Abrook et al., 2020), archaeology investigations (e.g., Lane et al., 2014; Villa et al., 2020; Giaccio et al., 2008, 2017; Zanchetta et al., 2018),

palaeontological studies (e.g., Marcolini et al., 2003; Gatta et al., 2016; Marra et al., 2018) and tectonic evolution (e.g., Giaccio et al., 2012a; Galli et al., 2015). All these studies highlighted the huge potential of tephra layers as an independent dating tool and its broad applicability in different disciplines.

Most commonly, tephra layers are extremely useful when applied in volcanological investigations, especially when a succession of sequentially stratified tephras is considered. Indeed, near-vent volcanic successions can be characterised by a fragmentary record of the past activity of a volcano since deposits of older and/or minor explosive events can be: (i) eroded-pedogenized during the periods of volcanic quiescence (e.g., Schiffman et al., 2000); (ii) not preserved (e.g., due to the preferential dispersion axis of the eruptive column; this applies also, and more fully, to distal settings; e.g., Santacroce et al., 2008); (iii) covered by products of younger/major eruptions (i.e., ignimbrites; e.g., Barberi et al., 1978); (iv) altered by weathering processes and zeolitization, thus hindering the possibility to retrieve data from the glasses (e.g., Freda et al., 2011); (v) not described in detail or unreported in the literature. Thus, if only the proximal outcrops are considered, the resulting reconstructed eruptive history could be incomplete, potentially leading to an erroneous assessment of the volcanic hazard linked to a volcano. Instead, moving away from the volcanic edifice, the chances of older or minor explosive episodes to be preserved increases. Similarly, relying only on distal deposits is not sufficient and can potentially lead to erroneous reconstructions of the past explsoive activity. Thus, it is the combined study of both proximal (near-vent) and distal volcanic successions that allows a more rigorous and complete reconstruction of the explosive history at a regional scale (tephra lattice).

For instance, in Figure 2, three outcrops at a progressively increasing distance from the stratovolcano of Vico, central Italy, are shown. In the first section (Viterbo section), which is the closest to the volcano (assuming the centre of the present intra-caldera lake as the source point), only the first two units are preserved or accesible, i.e., the Pre-Vico α and Vico α units. In the Vignanello section, slightly farther away from the volcanic edifice, four more units are preserved and recorded (i.e., Vico β, Vico β_{top}, Vico γ and Vico δ). Finally, at Civita Castellana section, the farthest from the volcano, the same four units of Vignanello section are preserved, along with an extra unit (i.e., CC-2),

stratigraphically located between Vico α and Vico β, which is not recorded at Vignanello. As a downside, moving away from the volcano, the source of a given tephra starts to become uncertain, as, at more distal sites, can deposit the products with similar lithofacies characters (especially grain-size and thickness) of different volcanoes that are more or less equally distant from the site. Indeed, the tephra CC-2 recognised in the section of Civita Castella was attributed to the adjacent Sabatini volcano rather than Vico (Pereira et al., 2020).

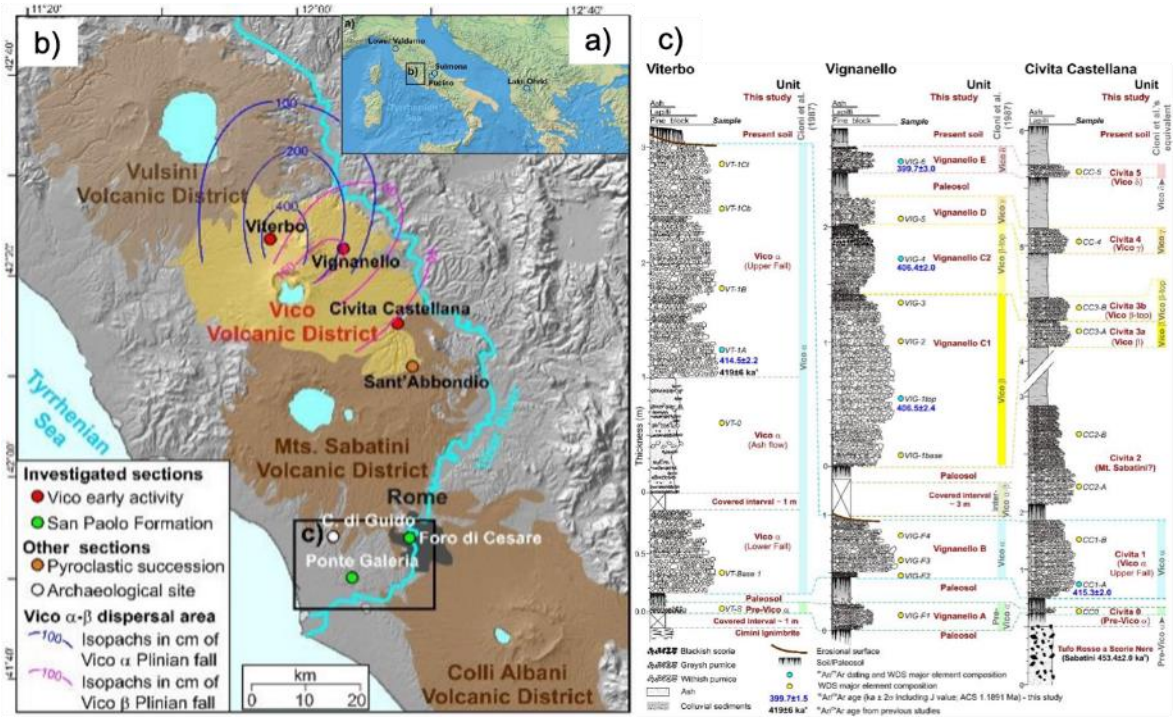

Figure 2. Proximal outcrops of the products from the Vico Period I (as defined by Perini et al., 2004) showing progressively more complete tephra sequences at increasing distance from the source volcano. a) Geographic setting of the Latium volcanic districts and b) location of the Viterbo, Vignanello and Civita Castellana sections (solid red circles). c) Tephrostratigraphic successions of the Vico Period I units at Viterbo, Vignanello and Civita Castellana sections. Image modified after Pereira et al. (2020). Isopachs (Fig. 2b) and name of the eruptions are from Cioni et al. (1987).

This (over-)simplified example shows the relevance of mid-distal outcrops for volcanic stratigraphy investigations. In reality, volcanological investigations in proximal areas usually consider several (tens of) outcrops, so that the general framework can be successfully obtained. Furthermore, in proximal settings there is a larger potential to record small scale activity, although minor explosive events, or even episodes with a Volcanic Explosivity Index (VEI; Newhall and Self, 1982) of 4 and 5,

can still be easily missed (e.g., Kiyosugi et al., 2015). In addition, the volcanic stratigraphy in proximal exposures may often lack clear evidence of intervening time breaks (i.e., soils/paleosols, erosional surfaces) between closely spaced pyroclastic deposits, so that distinct events can be erroneously reported as an individual eruption. The correct reconstruction of the eruptive history provides fundamental information needed for eruption timing and frequency estimation, as well as for quantifying the duration of quiescence intervals. In this regard, relatively long and continuous sedimentary successions, located sufficiently far away from the volcanic sources, not only can host and preserve tephra sequences with deposits of minor and/or previously unknown explosive events (Fig. 3), but also the time interval elapsed between eruptions, to be confidentially assessed. The study of such sequences thus allows a more rigorous and complete reconstruction of the explosive history, which is fundamental to properly reconstruct the temporal evolution of volcanic systems and hazard assessment at volcanically active regions.

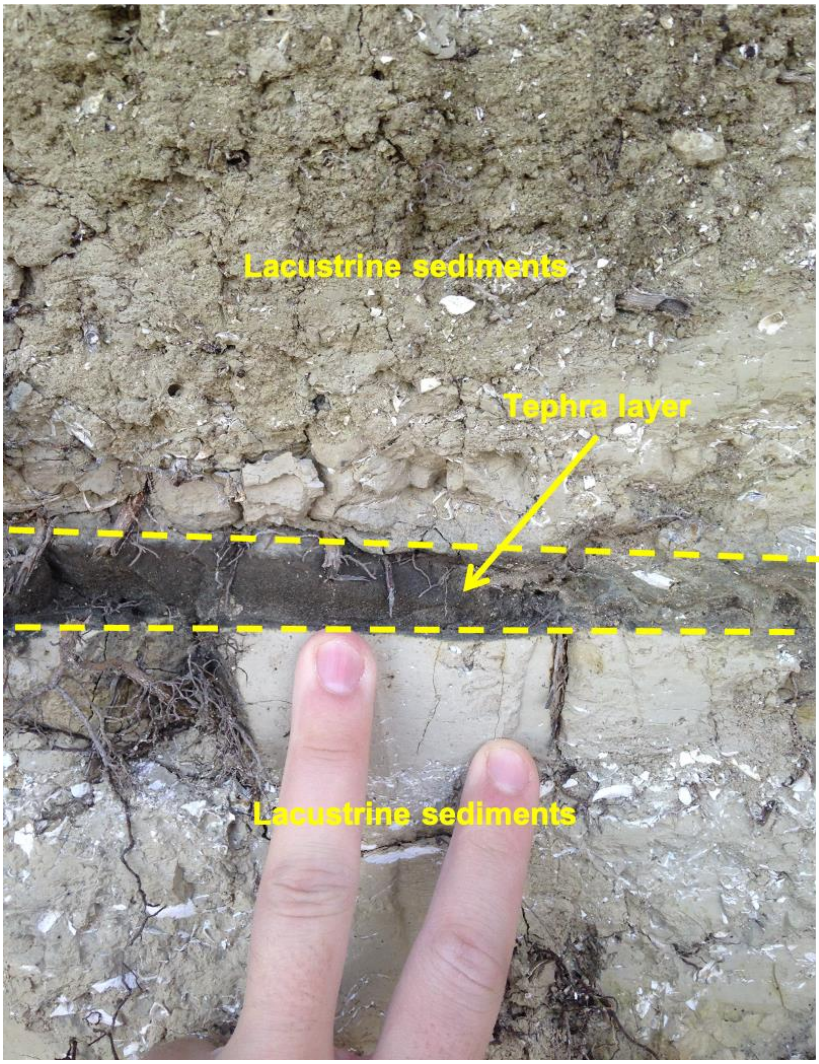

Figure 3. Cm-thick tephra layer sandwiched between lacustrine (silty) sediments of Sulmona Basin, in central Italy. A faint fining upward (FU) lamination is observable in the tephra deposit.

2. *The Central Mediterranean tephra lattice*

The tephrostratigraphic method is most successfully applied when long and continuous sedimentary successions containing well-preserved tephra layers are located in a suitable range of distance from sources of recurrent explosive activity. These requirements are fulfilled in the European-Mediterranean area, which is characterised by several volcanic regions - including Iceland, the Massif Central (France), the Eifel Volcanic Field (western Germany), the Italian peninsula and Sicily, the Hellenic Arc in Greece, Central Anatolia - and an outstanding number of tephra-hosting sequences. Since the first discovery of Icelandic tephra in Scotland (Dugmore, 1989), tephrostratigraphy has been exported and widely employed in the region, given birth to a series of international projects aiming at building a European "tephra lattice" and relative databases.

The first of such initiatives was entitled INTIMATE ("INTegrating Ice core, MArine and TErrestrial records"), a core programme of the International Quaternary Union (INQUA) Palaeoclimate Commission, which aimed at:

"…*synthesise data from the marine, terrestrial and ice-core realms for the North Atlantic region during the Last (Glacial) Termination*" (Björck et al., 1998).

In order to build a network of palaeoclimate records based on independent timescales, one of the INTIMATE project main objectives was to individuate tephra layers that could have been used as time-horizons and develop tools and techniques for tephra characterisation (Blockley et al., 2014).

Another ambitious international research programme, the RESET project ("RESponse of humans to abrupt Environmental Transitions"; Lowe et al., 2015; Bronk Ramsey et al., 2015a, 2015b), funded by the Natural Environment Research Council in the 2008-2013 period, aimed at establishing the links between abrupt environmental transitions and human dispersal and development. The RESET project, in particular, employed tephra layers to

"…*reduce the chronological uncertainty that compromises archaeological and palaeo-environmental records*" (Lowe et al., 2015).

In order to do so, RESET aimed at selecting tephra layers (and the associated eruptive events) that satisfied a certain number of requisites, those being: (a) distinct chemical and/or physical features; (b) widespread dispersion; (c) high state of preservation; (d) quantifiable age. Simultaneously, several sites hosting two or more of these tephra layers has been individuated, building a European tephra lattice (Fig. 4). This is schematically pictured as an underground railway network, where metro stations are represented by key sites where tephra of two or more volcanoes are hosted, whilst the metro lines represent the tephrostratigraphical links between the stations. As depicted in the sketch map (Fig. 4), the interconnection between the North Atlantic-Europe and the Mediterranean sections is mainly provided by tephra repositories in the Italian peninsula and tephra layers originating at Italian volcanoes. Indeed, 6 out of the 16 tephrostratigraphical links are represented by eruptions at Italian volcanoes, those being the Agnano Pomici Principali (APP, 12,380-12,140 BP; Blockley et al., 2008), the Neapolitan Yellow Tuff (NYT, 14,190 ± 680 BP; Siani et al., 2004), the Y-3 tephra (or Masseria del Monte Tuff, MdMT, 28,680-29,420; Albert et al., 2015, 2019) and the Campanian Ignimbrite (CI, 39.85 ± 0.14 ka; Giaccio et al., 2017) of Campi Flegrei, the Green Tuff/Y-6 of Pantelleria volcanic Island (45.7 ± 1.0 ka; Scaillet et al., 2013), and the Biancavilla Montalto Ignimbrite/Y-1 (14,240 ± 90 ^{14}C; Siani et al., 2001) of Etna volcano.

Most of these eruptions originated at the Campi Flegrei Caldera, in southern Italy (Fig. 5), which originated several widespread tephras in both the Mediterranean and the European continent. For instance, ashes of the greatest CI super-eruption, with an estimated volume (expressed as the Dense Rock Equivalent, DRE; Walker, 1973) of > 200 km^3 of erupted magma, have been found as far as Kostenki, and even beyond the Don River, in Russia (Pyle et al., 2006; Giaccio et al., 2008; Fig. 6).

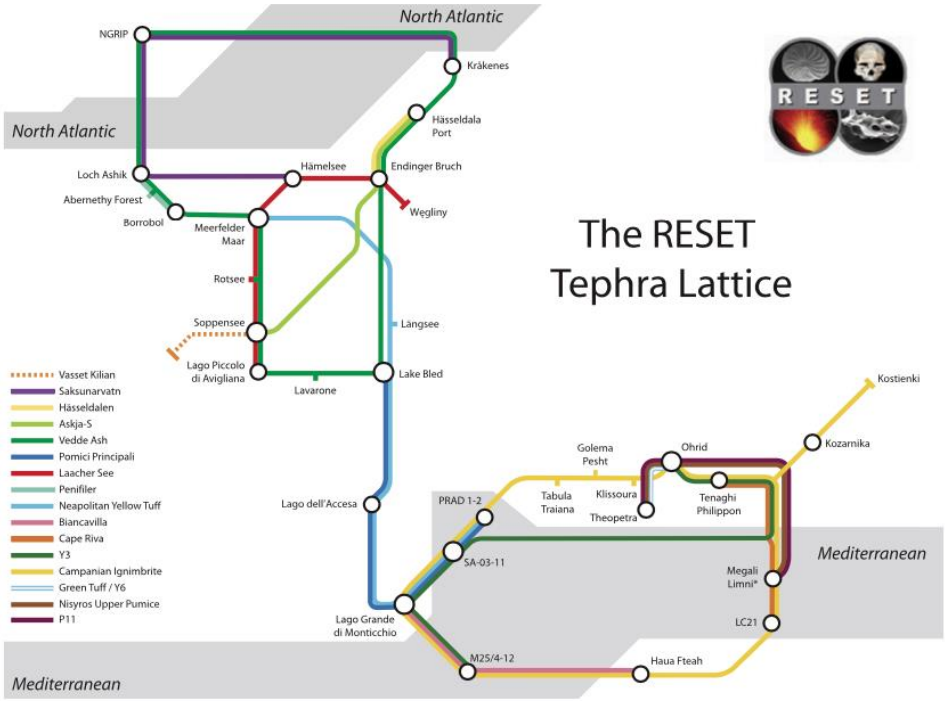

Figure 4. The RESET tephra lattice schematically showing the key sites selected by the project (pictured as metro stations) and the main tephrostratigraphical links (metro lines) through Europe and the Mediterranean. Note that this tephra lattice is not up-to-date, as recent studies (e.g., Ott et al., 2016; Wulf et al., 2016; Kearney et al., 2018) identified major early Holocene Icelandic tephras. Image after Lowe et al. (2015).

Given the wide dispersal of Italian tephras, especially those of Campi Flegrei eruptions, previous studies focused particularly on this volcano and its products. Following the pivotal study of Narcisi (1996), during the first decade of the 21st century Wulf et al. (2004, 2008, 2012) carried on a detailed tephra investigation of cores retrieved from the lacustrine succession of Lago Grande di Monticchio (LGdM). This is one of the two intra-caldera maar lakes (the other one is named "Lago Piccolo", Italian for "small lake", whilst "Lago Grande" stands for "big lake") hosted in Mt. Vulture, one of the Quaternary volcanic edifices in southern Italy (Fig. 7). The LGdM succession is characterised by a continuous annual lamination (varved sequence) of the lacustrine sediments, which allowed dating of the tephra layers to be assessed by layer-counting of the varved intervals. The succession hosted almost 400 tephra layers (primary and reworked) spanning the last 133 kyr (Wulf et al., 2004, 2012). Due to the relative position of the lake with respect to the Neaopolitan Volcanic District (Fig. 7), most LGdM tephra were backtracked to its volcanoes (i.e., Somma-Vesuvius, Ischia, Campi Flegrei). The

succession also hosted some tephra of other Italian volcanoes, including products of the Sabatini, Alban Hills (Colli Albani), Stromboli, Etna, and Aeolian Islands.

Figure 5. Satellite image of the Gulf of Naples, in southern Italy, with location of the city of Naples and the Ischia, Procida, Somma-Vesuvius and Campi Flegrei volcanic edifices. The caldera rim of Campi Flegrei volcano is shown by the dashed red line. Image taken with Google Earth Pro in August 2021.

The unique features of the LGdM succession - varved succession with sequentially ordered tephra, position relative to the prevalent dispersion of the ashes - allowed it to become one of the key tephra archives in southern Italy and the Mediterranean and is still used as a reference site for tephrostratigraphical studies in the region. On a broader point of view, the Italian peninsula is home to several rich tephra repositories, which, combined to the numerous and frequently active Quaternary volcanic districts (Fig. 7), makes the region one of the most fertile for tephra investigations. An increasing number of studies on marine (Keller et al., 1978; Paterne et al., 1986, 1988, 2008; Bourne et al., 2010, 2015; Tamburrino et al., 2012; Insinga et al., 2014; Morabito et al., 2014; Matthews et al., 2015; Petrosino et al., 2015, 2016; D'Antonio et al., 2016), lacustrine (Wulf et al., 2008; Petrosino et al., 2014; Giaccio et al., 2015; Di Roberto et al., 2018; Leicher et al., 2019;

Regattieri et al., 2019) and sub-aerial (Giaccio et al., 2012b; Gatta et al., 2016; Donato et al., 2016; Zanchetta et al., 2018; Bini et al., 2020) sedimentary environments of the Mediterranean region have documented this potential.

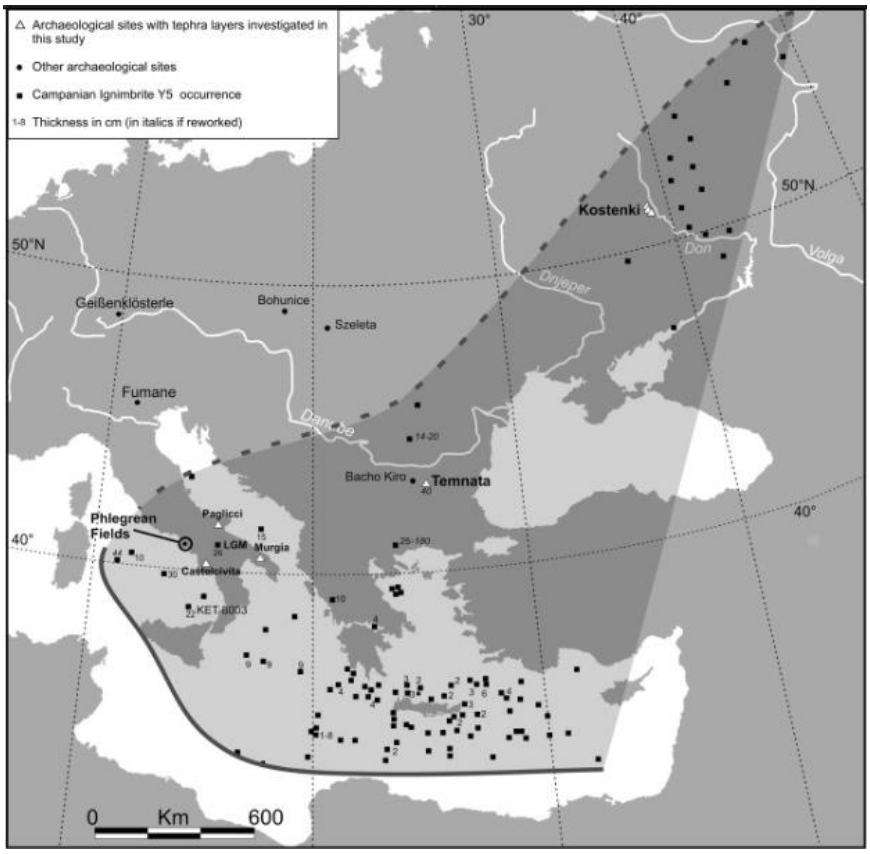

Figure 6. Distribution of the Campanian Ignimbrite (CI) distal tephra layer in eastern Mediterranean and Europe. After Giaccio et al., 2008.

Despite the great step forwards made in recent years, the tephrostratigraphic framework of the central Mediterranean area is still fragmentary and largely unexplored, especially for the Middle Pleistocene (~780-130 ka), and further investigations are needed to complete this gap of knowledge.

Figure 7. Digital Elevation Model (DEM) map of central and southern Italy showing the Quaternary volcanic districts and centres (yellow) and the main basinal sedimentary successions (aqua green) reported hosting tephra sequences.

References

Abbott, P.M., Jensen, B.J.L., Lowe, D.J., Suzuki, T., Veres, D., 2020. Crossing new frontiers: extending tephrochronology as a global geoscientific research tool. Journal of Quaternary Science, 35, 1-2, 1-8. https://doi.org/10.1002/jqs.3184.

Abrook, A.M., Matthews, I.P., Candy, I., Palmer, A.P., Francis, C.P., Turner, L., Brooks, S.J., Self, A.E., Milner, A.M., 2020. Complexity and synchrony of climatic drivers and environmental responses during the Last Glacial-Interglacial Transition (LGIT) in north-west Europe. Quaternary Science Reviews, 250, 106634. https://doi.org/10.1016/j.quascirev.2020.106634.

Albert, P.G., Giaccio, B., Isaia, R., Costa, A., Niespolo, E.M., Nomade, S., Pereira, A., Renne, P.R., Hinchliffe, A., Mark, D.F., Brown, R.J., Smith, V.C., 2019. Evidence for a large-magnitude eruption from Campi Flegrei Caldera (Italy) at 29 ka. Geology, 47:7, 595-599. https://doi.org/10.1130/G45805.1.

Albert, P.G., Hardiman, M., Keller, J., Tomlinson, E.L., Smith, V.C., Bourne, A.J., Wulf, S., Zanchetta, G., Sulpizio, R., Müller, U.C., Pross, J., Ottolini, L., Matthews, I.P., Blockley, S.P.E., Menzies, M.A., 2015. Revisiting the Y-3 tephrostratigraphic marker: a new diagnostic glass geochemistry, age estimate, and details on its climatostratigraphic context. Quaternary Science Reviews, 118, 105-121. https://doi.org/10.1016/j.quascirev.2014.04.002.

Albert, P.G., Smith, V.C., Suzuki, T., Tomlinson, E.L., Nakagawa, T., McLean, D., Yamada, M., Staff, R.A., Schlolaut, G., Takemura, T., Nagahashi, Y., Kimura, J., Suigetsu 2006 Project Members, 2018. Constraints on the frequency and dispersal of explosive eruptions at Sambe and Daisen volcanoes (South-West Japan Arc) from the distal Lake Suigetsu record (SG06 core). Earth Science Reviews, 185, 1004-1028. https://doi.org/10.1016/j.earscirev.2018.07.003.

Aoki, K., 2020. Dawson tephra, a widespread 29-ka marker bed, in a marine core from Patton Seamount off the Alaska Peninsula and its potential marine-terrestrial correlation. Journal of Quaternary Science, 35, 1-2, 93-101. https://doi.org/10.1002/jqs.3176.

Barberi, F., Innocenti, F., Lirer, L., Munno, R., Pescatore, T., Santacroce, R., 1978. The Campanian ignimbrite: a major prehistoric eruption in the Neapolitan area (Italy). Bulletin Volcanologique 41, 10-31. https://doi.org/10.1007/BF02597680.

Bazin, L., Lemieux-Dudon, B., Siani, G., Govin, A., Landais, A., Genty, D., Michel, E., Nomade, S., 2019. Construction of a tephra-based multi-archive coherent chronological framework for the last deglaciation in the Mediterranean region. Quaternary Science Reviews, 216, 45-57. https://doi.org/10.1016/j.quascirev.2019.05.018.

Bini M., Zanchetta G., Drysdale R.N., Giaccio B., Stocchi P., Vacchi M., Hellstrom J.C., Couchoud I., Monaco L., Ratti A., Martini, F., Sarti L., 2020. An end to the Last Interglacial highstand before 120 ka: Relative sea-level evidence from Infreschi Cave (Southern Italy). Quaternary Science Reviews 250, 106658. https://doi.org/10.1016/j.quascirev.2020.106658.

Björk, S., Walker, M.J.C., Cwynar, L.C., Johnsen, S., Knudsen, K.-L., Lowe, J.J., Wohlfarth, B., INTIMATE Members, 1998. An event stratigraphy for the Last Termination in the North Atlantic region based on the Greenland ice-core record: a proposal by the INTIMATE group. Journal of Quaternary Science, 13, 4, 283-292. https://doi.org/10.1002/(SICI)1099-1417(199807/08)13:4%3C283::AID-JQS386%3E3.0.CO;2-A.

Blockley, S.P.E., Bourne, A.J., Brauer, A., Davies, S.M., Hardiman, M., Harding, P.R., Lane, C.S., MacLeod, A., Matthews, I.P., Pyne-O'Donnel, S.D.F., Rasmussen, S.O., Wulf, S., Zanchetta, G., 2014. Tephrochronology and the extended intimate (integration of ice-core, marine and terrestrial records) event stratigraphy 8-128 ka 2bk. Quaternary Science Reviews, 106, 88-100. https://doi.org/10.1016/j.quascirev.2014.11.002.

Blockley, S.P.E., Bronk Ramsey, C., Pyle, D.M., 2008. Improved age and high-precision age estimates of late Quaternary tephras, for accurate palaeoclimate reconstruction. Journal of Volcanology and Geothermal Research, 177, 251-262. https://doi.org/10.1016/j.jvolgeores.2007.10.015.

Bolton, M.S.M., Jensen, B.J.L., Wallace, K., Praet, N., Fortin, D., Kaufman, D., De Batist, M., 2020. Machine learning classifiers for attributing tephra to source volcanoes: an evaluation of methods for Alaska tephras. Journal of Quaternary Science, 35, 1-2, 81-92. https://doi.org/10.1002/jqs.3170.

Bourne, A.J., Albert, P.G., Matthews, I.P., Trincardi, F., Wulf, S., Asioli, A., Blockley, S.P.E., Keller, J., Lowe, J.J., 2015. Tephrochrunology of core PRAD 1-2 from the Adriatic Sea: insights into Italian explosive volcanism for the period 200-80 ka. Quaternary Science Reviews, 116, 28-43. https://doi.org/10.1016/j.quascirev.2015.03.006.

Bourne, A.J., Lowe, J.J., Trincardi, F., Asioli, A., Blockley, S.P.E., Wulf, S., Matthews, I.P., Piva, A., Vigliotti, L., 2010. Distal tephra record for the last ca 105,000 years from core PRAD 1-2 in the central Adriatic Sea: implications for the marine tephrostratigraphy. Quaternary Science Reviews, 29, 23-24, 3079-3094. https://doi.org/10.1016/j.quascirev.2010.07.021.

Bronk Ramsey, C., Albert, P.G., Blockley, S.P.E., Hardiman, M., Housley, R.A., Lane, C.S., Lee, S., Matthews, I.P., Smith, V.C., Lowe, J.J., 2015a. Improved age estimates for key Late Quaternary European tephra horizons in the RESET lattice. Quaternary Science Reviews, 118, 18-32. https://doi.org/10.1016/j.quascirev.2014.11.007.

Bronk Ramsey, C., Housley, R.A., Lane, C.S., Smith, V.C., Pollard, A.M., 2015b. The Reset tephra database and associated analytical tools. Quaternary Science Reviews, 118, 33-47. https://doi.org/10.1016/j.quascirev.2014.11.008.

Cioni, R., Sbrana, A., Bertagnini, A., Buonasorte, G., Landi, P., Rossi, U., Salvati, L., 1987. Tephrostratigraphic correlations in the Vulsini, Vico and Sabatini volcanic succession. Periodico di Mineralogia, 56, 137-155.

D'Antonio, M., Mariconte, R., Arienzo, I., Mazzeo, F.C., Carandente, A., Perugini, D., Petrelli, M., Corselli, C., Orsi, G., Principato, M.S., Civetta, L., 2016. Combined Sr-Nd isotopic and geochemical fingerprinting as a tool for identifying tephra layers: Application to deep-sea cores from Eastern Mediterranean Sea. Chemical Geology, 443, 121-136. https://doi.org/10.1016/j.chemgeo.2016.09.022.

Davies, S.M., 2015. Cryptotephras: the revolution in correlation and precision dating. Journal of Quaternary Science, 30, 2, 114-130. https://doi.org/10.1002/jqs.2766.

de Fontaine, C.S., Kaufman, D.S., Anderson, R.S., Werner, A., Waythomass, C.F., Brown, T.A., 2007. Late Quaternary distal-fall deposits in lacustrine sediments, Kenai Peninsula, Alaska. Quaternary Research, 68, 1, 64-78. https://doi.org/10.1016/j.yqres.2007.03.006.

De Maisonneuve, C.B. & Bergal-Kuvikas, O., 2020. Timing, magnitude and geochemistry of major Southeast Asian volcanic eruptions: identifying tephrochronologic markers. Journal of Quaternary Science, 35, 1-2, 272-287. https://doi.org/10.1002/jqs.3181.

Derkachev, A.N., Gorbarenko, S.A., Ponomareva, V.V., Portnyagin, M.V., Malakhova, G.I., Liu, Y., Middle to late Pleistocene record of explosive volcanic eruptions in marine sediments offshore Kamchatka (Meiji Rise, NW Pacific). Journal of Qauternary Science, 35, 1-2, 362-379. https://doi.org/10.1002/jqs.3175.

Di Roberto, A., Smedile, A., Del Carlo, P., De Martini, P.M., Iorio, M., Petrelli, M., Pantosti, P., Pinzi, S., Todrani, A., 2018. Tephra and cryptotephra in a ~60,000-year old lacustrine sequence from the Fucino Basin: new insights into the major explosive events in Italy. Bulletin of Volcanology, 80:20. https://doi.org/10.1007/s00445-018-1200-x.

Donato, P., Albert, P.G., Crocitti, M., De Rosa, C., Menzies, M.A., 2016. Tephra layers along the southern Tyrrhenian coast of Italy: Links to the X-5 & X-6 using volcanic glass geochemistry. Journal of Volcanology and Geothermal Research, 317, 30-41. https://doi.org/10.1016/j.jvolgeores.2016.02.023.

Dugmore, A.J. & Newton, A.J., 1992. Thin tephra layers in peat revealed by X-radiography. Journal of Archaeological Science, 19, 2, 163-170. https://doi.org/10.1016/0305-4403(92)90047-7.

Dugmore, A.J., Larsen, G., Newton, A.J., 1995. Seven tephra isochrones in Scotland. The Holocene, 5, 3, 257-266. https://doi.org/10.1177%2F095968369500500301.

Dugmore, A.J., Newton, A.J., Edwards, K.J., Larsen, G., Blackford, J.J., Cook, G.T., 1996. Long-distance marker horizons from small-scale eruptions: British tephra deposits from the AD 1510 eruption of Hekla, Iceland. Journal of Quaternary Science, 11, 6, 511-516. https://doi.org/10.1002/(SICI)1099-1417(199611/12)11:6%3C511::AID-JQS284%3E3.0.CO;2-C.

Dugmore, A.J., 1989. Icelandic volcanic ash in Scotland. Scottish Geographical Megazine, 105:3, 168-172. https://doi.org/10.1080/14702548908554430.

Freda, C., Gaeta, M., Giaccio, B., Marra, F., Palladino, D.M., Scarlato, P., Sottili, G., 2011. CO2-driven large mafic explosive eruptions: the Pozzolane Rosse case study from the Colli Albani Volcanic District (Italy). Bulletin of Volcanology, 73, 241-256. https://doi.org/10.1007/s00445-010-0406-3.

Forster, M.W., Zemlitskaya, A., Otter, L.M., Buhre, S., Sirocko, F., 2020. Late Pleistocene Eifel eruptions: insights from clinopyroxene and glass geochemistry of tephra layers from Eifel Laminated Sediment Archive sediment cores. Journal of Quaternary Science, 35, 1-2, 186-198. https://doi.org/10.1002/jqs.3134.

Galli, P., Giaccio, B., Peronace, E., Messina, P., 2015. Holocene Palaeoearthquakes and Early-Pleistocene Slip Rate on the Sulmona Fault (Central Apennines, Italy). Bulletin of the Seismological Society of America, 105, 1, 1-13. https://doi.org/10.1785/0120140029.

Gatta, M., Sinopoli, G., Giardini, M., Giaccio, B., Hajdas, I., Pandolfi, L., Bailey, G., Spikins, P., Rolfo, M.F., Sadori, L., 2016. Pollen from Late Pleistocene hyena (Crocuta Crocuta spelaea) coprolites: An interdisciplinary approach from two Italian sites. Review of Palaeobotany and Palynology, 233, 56-66. https://doi.org/10.1016/j.revpalbo.2016.07.005.

Gehrels, M.J., Lowe, D.J., Hazell, Z.J., Newnham, R.M., 2006. A continuous 5300-yr Holocene cryptotephrostratigraphic record from northern New Zealand and impllications for tephrochronlogy and volcanic hazard assessment. The Holocene, 16, 2, 173-187. https://doi.org/10.1191%2F0959683606hl918rp.

Giaccio, B., Isaia, R., Fedele, F.G., Di Canzio, E., Hoffecker, J., Ronchitelli, A., Sintsyn, A.A., Anikovich, M., Lisitsyn, S.N., Popov, V.V., 2008. The Campanian Ignimbrite and Codola tephra layers: Two temporal/stratigraphic markers for the Early Upper Palaeolithic in southern Italy and eastern Europe. Journal of Volcanology and Geothermal Research, 177, 1, 208-226. https://doi.org/10.1016/j.jvolgeores.2007.10.007.

Giaccio, B., Galli, P., Messina, P., Peronace, E., Scardia, G., Sottili, G., Sposato, A., Chiarini, E., Jicha, B., Silvestri, S., 2012b. Fault and basin depocentre migration over the last 2Ma in the L'Aquila 2009 earthquake region, central Italian Apennines. Quaternary Science Reviews, 56, 69–88. https://doi.org/10.1016/j.quascirev.2012.08.016.

Giaccio, B., Leicher, N., Mannella, G., Monaco, L., Regattieri, E., Wagner, B., Zanchetta, G., Gaeta, M., Marra, F., Nomade, S., Palladino, D.M., Pereira, A., Scheidt, S., Sottili, G., Wonik, T., Wulf, S., Zeeden, C., Ariztegui, D., Cavinato, G.P., Dean, R.J., Florindo, F., Leng, M.J., Macrì, P., Niespolo, E., Renne, P.R., Rolf, C., Sadori, L., Thomas, C., Tzedakis, P.C., 2019. Extending the tephra and paleoenvironmental record of the Central Mediterranean back to 430 ka: A new core from Fucino Basin, central Italy. Quaternary Science Reviews, 225, 106003. https://doi.org/10.1016/j.quascirev.2019.106003.

Giaccio, B., Niespolo, E.M., Pereira, A., Nomade, S., Renne, P.R., Albert, P.G., Arienzo, I., Regattieri, E., Wagner, B., Zanchetta, G., Gaeta, M., Galli, P., Mannella, G., Peronace, E., Sottili, G., Florindo, F., Leicher, N., Marra, F., Tomlinson, E.L., 2017. First integrated tephrochronological record for the last ~190 kyr from the Fucino Quaternary lacustrine succession, central Italy. Quaternary Science Reviews, 158, 211-234. https://doi.org/10.1016/j.quascirev.2017.01.004.

Giaccio, B., Nomade, S., Wulf, S., Isaia, R., Sottili, G., Cavuoto, G., Galli, P., Messina, P., Sposato, A., Sulpizio, R., Zanchetta, G., 2012a. The late MIS 5 Mediterranean tephra markers: a reappraisal from peninsular Italy terrestrial records. Quaternary Science Reviews, 56, 31-45. https://doi.org/10.1016/j.quascirev.2012.09.009.

Giaccio, B., Regattieri, E., Zanchetta, G., Wagner, B., Galli, P., Mannella, G., Niespolo, E., Peronace, E., Renne, P.R., Nomade, S., Cavinato, G.P., Messina, P., Sposato, A., Boschi, C., Florindo, F., Marra, F., Sadori, L., 2015. A key continental archive for the last 2 Ma of climatic history of the central Mediterranean region: A pilot drilling in the Fucino Basin, central Italy.

Scientific Drilling, 20, 13-19. https://doi.org/10.5194/sd-20-13-2015.
Hall, V.A., Pilcher, J.R., McCormac, F.G., 1993. Tephra-dated lowland landscape history of the north of Ireland, A.D. 750-1150. New Phytologist, 125, 1, 193-202. https://doi.org/10.1111/j.1469-8137.1993.tb03876.x.
Insigna, D.D., Petrosino, P., Alberico, I., De Lange, G.J., Lubritto, C., Molisso, F., Sacchi, M., Sulpizio, R., Wu, J., Lirer, F., 2020. The Late Holocene tephra record of the central Mediterranean Sea: Mapping occurrences and new potential isochrones for the 4.4-2.0 ka time interval. Journal of Quaternary Science, 35, 1-2, 213-231. https://doi.org/10.1002/jqs.3154.
Insinga, D.D., Tamburrino, S., Lirer, F., Vezzoli, L., Barra, M., De Lange, G.J., Tiepolo, M., Vallefuoco, M., Mazzola, S., Sprovieri, M., 2014. Tephrochronology of the astronomically-tuned KC01B deep-sea core, Ionian Sea: insights into the explosive activity of the Central Mediterranean area during the last 200 ka. Quaternary Science Reviews, 85, 63-84. https://doi.org/10.1016/j.quascirev.2013.11.019.
Ishimura, D., & Hiramine, R., 2020. Proximal-distal fall deposit correlation of VEI-5 tephra (Towada-Chuseri) from Towada volcano, northeast Japan. Journal of Quaternary Science, 35, 1-2, 334-348. https://doi.org/10.1002/jqs.3161.
Jensen, B.J.L., Pyne-O'Donnel, S., Plunkett, G., Froese, G., Huges, P.D.M., Sigl, M., McConnel, J.R., Amesbury, M.J., Blackwell, P.G., van den Bogaard, C., Buck, C.E., Charman, D.J., Clague, J.J., Hall, V.A., Koch, J., Mackay, H., Mallon, G., McColl, L., Pilcher, J.R., 2014. Transatlantic distribution of the Alaskan White River Ash. Geology, 42 (10): 875-878. https://doi.org/10.1130/G35945.1.
Karátson, D., Wulf, S., Veres, D., Magyari, E. K., Gertisser, R., Timar-Gabor, A., Novothny, Á., Telbisz, T., Szalai, Z., Anechitei-Decau, V., Appelt, O., Bormann, M., Jánosi, Cs., Hubay, K., Schäbitz, F., 2016. The latest explosive eruptions of Ciomadul (Csomád) volcano, East Carpathians - A tephrostratigraphic approach for the 51-29 ka BP time interval. Journal of Volcanology and Geothermal Research, 319, 29-51. https://doi.org/10.1016/j.jvolgeores.2016.03.005.
Kearney, R., Albert, P.G., Staff, R.A., Pál, I., Veres, D., Magyari, E., Bronk Ramsey, C., 2018. Ultra-distal fine ash occurrences of the Icelandic Askja-S Plinian eruption deposits in Southern Carpathian lakes: New age constraints on a continental scale tephrostratigraphic marker. Quaternary Science Reviews, 188, 174-182. https://doi.org/10.1016/j.quascirev.2018.03.035.
Keller, J., Ryan, W.B.F., Ninkovich, D., Altherr, R., 1978. Explosive volcanic activity in the Mediterranean over the last 200,000 yr as recorded in deep-sea sediments. Geological Society of America Bulletin, 89:4, 591-604. https://doi.org/10.1130/0016-7606(1978)89%3C591:EVAITM%3E2.0.CO;2.
Kyosugi, K., Connor, C., Sparks, R.S.J., Crosweller, H.S., Brown, S.K., Siebert, L., Wang, T., Takarada, S., 2015. How many explosive eruptions are missing from the geologic record? Analysis of the quaternary record of large magnitude explosive eruptions in Japan. Journal of Applied Volcanology, 4:17. https://doi.org/10.1186/s13617-015-0035-9.
Kutterolf, S., Schindlbeck, J.C., Jegen, M., Freundt, A., Straub, S.M., 2019. Milankovitch frequencies in tephra records at volcanic arcs: The relation of kyr-scale cyclic variations in volcanism to global climate changes. Quaternary Science Reviews, 204, 1-16. https://doi.org/10.1016/j.quascirev.2018.11.004.
Lane, C.S., Brauer, A., Blockley, S.P.E., Dulski, P., 2013. Volcanic ash reveals time-transgressive abrupt climate change during the Younger Dryas. Geology, 41:12, 1251-1254. https://doi.org/10.1130/G34867.1.
Lane, C.S., Cullen, V.L., White, D., Bramham-Law, C.W.F., Smith, V.C., 2014. Cryptotephra as a dating and correlation tool in archaeology. Journal of Archaeological Science, 42, 42-50. https://doi.org/10.1016/j.jas.2013.10.033.
Lane, C.S., Lowe, D.J., Blockley, S.P.E., Suzuki, T., Smith, V.C., 2017. Advancing tephrochronology as a global dating tool: Applications in volcanology, archaeology, and palaeoclimatic research. Quaternary Geochronology, 40, 1-7. https://doi.org/10.1016/j.quageo.2017.04.003.
Leicher, N., Giaccio, B., Zanchetta, G., Wagner, B., Francke, A., Palladino, D.M., Sulpizio, R., Albert, P.G., Tomlinson, E.L., 2019. Central Mediterranean explosive volcanism and tephrochronology during the last 630 ka based on the sediment record from Lake Ohrid. Quaternary Science Reviews, 226, 106021. https://doi.org/10.1016/j.quascirev.2019.106021.
Lerbekmo, J.F., 2008. The White River Ash: largest Holocene Plinian tephra. Canadian Journal of Earth Sciences, 45, 6, 693-700. https://doi.org/10.1139/E08-023.
Lowe, D.J., & Hunt, J.B., 2001. A summary of terminology used in tephra-related studies. In Juvigne, E.T. & Raynal, J.P. (eds.), Tephras: Chronology, Archaeology. Les Dossiers de L'Archeo-Logis, 1, 17-22.
Lowe, D.J., Bronk Ramsey, C., Housley, R.A., Lane, C.S., Tomlinson, E.L., RESET Team, Reset Associates, 2015. The RESET project: constructing a European tephra lattice for refined synchronisation of environmental and archaeological events during the last c. 100 ka. Quaternary Science Reviews, 118, 1-17. https://doi.org/10.1016/j.quascirev.2015.04.006.
Lowe, D.J., 2011. Tephrochronology and its application: A review. Quaternary Geochonology, 6, 2, 107-153. https://doi.org/10.1016/j.quageo.2010.08.003.
Marcolini, F., Bigazzi, G., Bonadonna, F.P., Centamore, E., Cioni, R., Zanchetta, G., 2003. Tephrochronology and tephrostratigraphy of two Pleistocene continental fossiliferous successions from central Italy. Journal of Quaternary Science, 18, 6, 545-556. https://doi.org/10.1002/jqs.768.
Marra, F., Nomade, S., Pereira, A., Petronio, C., Salari, L., Sottili, G., Bahain, J.J., Boschian, G., Di Stefano, G., Falguères, C., Florindo, F., Gaeta, M., Giaccio, B., Masotta, M., 2018. A review of the geological sections and the faunal assemblages of Aurelian Mammal Age of Latium (Italy) in the light of a new chronostratigraphic framework. Quaternary Science Reviews, 181, 173-199. https://doi.org/10.1016/j.quascirev.2017.12.007.
Maruyama, S., Takemura, K., Hirata, T., Yamashita, T., Danhara, T., 2020. Major and trace element abundances in volcanic glass shards in visible tephras in SG93 and SG06 drillcore samples from Lake Suigetsu, central Japan, obtained using femtosecond LA-ICP-MS. Journal of Quaternary Science, 35, 1-2, 66-80. https://doi.org/10.1002/jqs.3124.
Matthews, I.P., Trincardi, F., Lowe, J.J., Bourne, A.J., MacLeod, A., Abbott, P.M., Andersen, N., Asioli, A.,

Blockley, S.P.E., Lane, C.S., Oh, Y.A., Satow, C.S., Staff, R.A., Wulf, S., 2015. Developing a robust tephrochronological framework for Late Quaternary marine records in the Southern Adriatic Sea: new data from core station SA03-11. Quaternary Science Reviews, 118, 84-104. https://doi.org/10.1016/j.quascirev.2014.10.009.

Miyabuchi, Y., & Sugiyama, S., 2020. Vegetation history after the late period of the Last Glacial Age based on phytolith records in Nangodani Valley basin, southern part of the Aso caldera, Japan. Journal of Quaternary Science, 35, 1-2, 304-315. https://doi.org/10.1002/jqs.3153.

Morabito, S., Petrosino, P., Milia, A., Sprovieri, M., Tamburrino, S., 2014. A multidisciplinary approach for reconstructing the stratigraphic framework of the last 40 ka in a bathyal area of eastern Tyrrhenian Sea. Global and Planetary Change, 123, Part A, 121-138. https://doi.org/10.1016/j.gloplacha.2014.10.005.

Narcisi, B., 1996. Tephrochronology of a late quaternary lacustrine record from the Monticchio Maar (Vulture volcano, Southern Italy). Quaternary Science Reviews, 15 (2-3), 155-165. https://doi.org/10.1016/0277-3791(95)00045-3.

Narcisi, B. & Vezzoli, L., 1999. Quaternary stratigraphy of distal tephra layers in the Mediterranean - an overview. Global and Planetary Change, 21, 31-50. https://doi.org/10.1016/S0921-8181(99)00006-5.

Newhall, C.G., & Self, S., 1982. The volcanic explosivety index (VEI) an estimate of explosive magnitude for historical volcanism. Journal of Geophysical Research, 87, C2, 1231-1238. https://doi.org/10.1029/JC087iC02p01231.

Nishizawa, F., & Suzuki, T., 2020. Characterization and correlation of the Hegawa-kasamori 5 tephra, a widespread tephra aged c. 450 ka associated with large-scale pyroclastic flows from southern Kyushu, SW Japan. Journal of Quaternary Science, 35, 1-2, 288-303. https://doi.org/10.1002/jqs.3172.

Ott, F., Wulf, S., Serb, J., Słowiński, M., Obremska, M., Tjallingii, R., Błaszkiewicz, M., Brauer, A., 2016. Constraining the time span between the Early Holocene Hässeldalen and Askja-S tephras through varve counting in the Lake Czechowskie sewdiment record, Poland. Journal of Quaternary Science, 31 (2), 103-113. https://doi.org/10.1002/jqs.2844.

Paterne, M., Guichard, F., Duplessy, J.C., Siani, G., Sulpizio, R., Labeyrie, J., 2008. A 90,000-200,000 yrs marine tephra record of Italian volcanic activity in the Central Mediterranean Sea. Journal of Volcanology and Geothermal Research, 177, 187-196. https://doi.org/10.1016/j.jvolgeores.2007.11.028.

Paterne, M., Guichard, F., Labeyrie, J., 1988. Explosive activity of the south Italian volcanoes during the past 80,000 years as determined by marine tephrochronology. Journal of Volcanology and Geothermal Research, 34, 3-4, 153-172. https://doi.org/10.1016/0377-0273(88)90030-3.

Paterne, M., Guichard, F., Labeyrie, J., Gillot, P.Y., Duplessy, J.C., 1986. Tyrrhenian Sea tephrochronology of the oxygen isotope record for the past 60,000 years. Marine Geology, 72, 3-4, 259-285. https://doi.org/10.1016/0025-3227(86)90123-4.

Pearce, N.J.G., Westgate, J.A., Gualda, G.A.R., Gatti, E., Muhammad, R.F., 2020. Tephra glass chemistry provides storage and discharge details of five magma reservoirs which fed the 75 ka Youngest Toba Tuff eruption, northern Sumatra. Journal of Quaternary Science, 35, 1-2, 256-271. https://doi.org/10.1002/jqs.3149.

Pereira, A., Monaco, L., Marra, F., Sébastien, N., Gaeta, M., Leicher, N., Palladino, D.M., Sottili, G., Guillou, H., Scao, V., Giaccio, B., 2020. Tephrochronology of the central Mediterranean MIS 11c interglacial (~425-395 ka): New constraints from the Vico volcano and the Tiber delta, central Italy. Quaternary Science Reviews, 243, 106-470. https://doi.org/10.1016/j.quascirev.2020.106470.

Perini, G., Francalanci, L., Davidson, J.P., Conticelli, S., 2004. Evolution and Genesis of Magmas from Vico Volcano, Central Italy: Multiple Differentiation Pathways and Variable Parental Magmas. Journal of Petrology, 45, 1, 139-182. https://doi.org/10.1093/petrology/egg084.

Persson, C., 1966. Försök till tefrokronologisk datering av några svenska torvmossar. Geologiska Foereningan i Stockholm Foerhandlingar, 88, 361-395. https://doi.org/10.1080/11035896609448933.

Persson, C., 1967. Försök till tefrokronologisk datering I tre norska myrar. Geologiska Foereningan i Stockholm Foerhandlingar, 89, 181-197. https://doi.org/10.1080/11035896709448363.

Persson, C., 1968. Försök till tefrokronologisk datering I tre norska färöiska. Geologiska Foereningan i Stockholm Foerhandlingar, 90, 241-266. https://doi.org/10.1080/11035896809451887.

Persson, C., 1971. Tephrochronological investigation of peat deposits in Scandinavia and on the Faroe Islands. Geological Survey of Sweden, C, 656.

Peti, l., Gadd, P.S., Hopkins, J.L., Augustinus, P.C., Itrax m-XRF core scanning for rapid tephrostratigraphic analysis: a case study from the Auckland Volcanic Field maar lakes. Journal of Quaternary Science, 35, 1-2, 54-65. https://doi.org/10.1002/jqs.3133.

Petrosino, P., Jicha, B.R., Mazzeo, F.C., Ciaranfi, N., Girone, A., Maiorano, P., 2015. The Montalbano Jonico marine succession: An archive for distal tephra layers at the Early-Middle Pleistocene boundary in southern Italy. Quaternary International, 383, 89-103. https://doi.org/10.1016/j.quaint.2014.10.049.

Petrosino, P., Jicha, B.R., Mazzeo, F.C., Russo Ermolli, E., 2014. A high-resolution tephrochronological record of MIS 14-12 in the Southern Apennines (Acerno Basin, Italy). Journal of Volcanology and Geothermal Research, 274, 34-50. https://doi.org/10.1016/j.jvolgeores.2014.01.014.

Petrosino, P., Morabito, S., Jicha, B.R., Milia, A., Sprovieri, M., Tamburrino, S., 2016. Multidisciplinary tephrochronological correlation of marker events in the eastern Tyrrhenian Sea between 48 and 105 ka. Journal of Volcanology and Geothermal Research, 315, 79-99. https://doi.org/10.1016/j.jvolgeores.2016.02.001.

Pilcher, J.R., & Hall, V.A., 1992. Towards a tephrochronology for the Holocene of the north of Ireland. The Holocene, 2, 3, 255-259. https://doi.org/10.1177%2F095968369200200307.

Pilcher, J.R., & Hall, V.A., 1996. Tephrochronological studies in northern England. The Holocene, 6, 1, 100-105. https://doi.org/10.1177%2F095968369600600112.

Pilcher, J.R., Hall, V.A., McCormac, F.G., 1995. Dates of Holocene Icelandic volcanic eruptions from tephra layers in Irish peats. The Holocene, 5, 1, 103-110. https://doi.org/10.1177%2F095968369500500111.

Pilcher, J.R., Hall, V.A., McCormac, F.G., 1996. An outline tephrochronology for the Holocene of the north

of Ireland. Journal of Quaternary Science, 11, 6, 485-494. https://doi.org/10.1002/(SICI)1099-1417(199611/12)11:6%3C485::AID-JQS266%3E3.0.CO;2-T.

Pouclet, A., Juvigné, E., Pirson, S., 2008. The Rocourt Tephra, a widespread 90-74 ka stratigraphic marker in Belgium. Quaternary Research, 70, 1, 105-120. https://doi.org/10.1016/j.yqres.2008.03.010.

Pyle, D.M., Ricketts, G.D., Margari, V., van Andel, T.H., Sinitsyn, A.A., Praslov, N.D., Lisitsyn, S., 2006. Wide dispersal and deposition of distal tephra during the Pleistocene "Campanian Ignimbrite/Y-5" eruption, Italy. Quaternary Science Reviews, 25, 21-22, 2713-2728. https://doi.org/10.1016/j.quascirev.2006.06.008.

Pyne-O'Donnel, S.D.F., Hughes, P.D.M., Froese, D.G., Jensen, B.J.L., Kuehn, S.C., Mallon, G., Amesbury, M.J., Charman, D.J., Daley, T.M., Loader, N.J., Mauquoy, D., Street-Perrot, F.A., Woodman-Ralph, J., 2012. High-precision ultra-distal Holocene tephrochronology in North America. Quaternary Science Reviews, 52, 6-11. https://doi.org/10.1016/j.quascirev.2012.07.024.

Regattieri, E., Giaccio, B., Mannella, G., Zanchetta, G., Nomade, S., Tognarelli, A., Perchiazzi, N., Vogel, H., Boschi, C., Drysdale, R.N., Wagner, B., Gemelli, M., Tzedakis, P., 2019. Frequency and dynamics of millennial-scale variability during marine isotope stage 19: insights from the Sulmona Basin (central Italy). Quaternary Science Reviews, 214, 28-43. https://doi.org/10.1016/j.quascirev.2019.04.024.

Regattieri, E., Giaccio, B., Zanchetta, G., Drysdale, R.N., Galli, P., Nomade, S., Peronace, E., Wulf, S., 2015. Hydrological variability over the Apennines during the Early Last Glacial precession minimum, as revelated by a stable isotope record from Sulmona basin, Central Italy. Journal of Quaternary Science, 30, 19-31. https://doi.org/10.1002/jqs.2755.

Santacroce, R., Cioni, R., Marianelli, P., Sbrana, A., Sulpizio, R., Zanchetta, G., Donahue, D. J., Joron, J. L., 2008. Age and whole rock-glass compositions of proximal pyroclastics from the major explosive eruptions of Somma-Vesuvius: A review as a tool for distal tephrostratigraphy. Joournal of Volcanology and Geothermal Research, 177, 1-18. https://doi.org/10.1016/j.jvolgeores.2008.06.009.

Scaillet, S., Vita-Scaillet, G., Rotolo, S.G., 2013. Millennial-scale phase relationships between ice-core and Mediterranean marine records: insights from high-precision $^{40}Ar/^{39}Ar$ dating of the Green Tuff of Pantelleria, Sicily Strait. Quaternary Science Reviews, 78, 141-154. https://doi.org/10.1016/j.quascirev.2013.08.008.

Shane, P., & Hoverd, J., 2002. Distal record of multi-sourced tephra in Onepoto Basin, Auckland, New Zealand: implications for volcanic chronology, frequency and hazards. Bulletin of Volcanology, 64, 441-454. https://doi.org/10.1007/s00445-002-0217-2.

Shane, P., Gehrels, M., Zawalna-Geer, A., Augustinus, P., Lindsay, J., Chaillou, I., 2013. Longevity of a small shield volcano revealed by crypto-tephra studies (Rangitoto volcano, New Zealand): Change in eruptive behavior of a basaltic field. Journal of Volcanology and Geothermal Research, 257, 174-183.https://doi.org/10.1016/j.jvolgeores.2013.03.026.

Shane, P., 2000. Tephrochronology, a New Zealand case study. Earth-Science Reviews, 49, 1-4, 223-259. https://doi.org/10.1016/S0012-8252(99)00058-6.

Shiffman, P., Spero, H.J., Southard, R.J., Swanson, D.A., 2000. Controls on palagonization versus pedogenic weathering of basaltic tephra: Evidence from consolidation and geochemistry of the Keanakako'I Ash Member, Kilauea Volcano. Geochemistry, Geophysics, Geosystems, 1 (8), 2000GC000068. https://doi.org/10.1029/2000GC000068.

Siani, G., Paterne, M., Michel, E., Sulpizio, R., Sbrana, A., Arnold, M., Haddad, G., 2001. Mediterranean Sea Surface Radiocarbon Reservoir Age Changes Since the Last Glacial Maximum. Science, 294, 5548, 1917-1920. https://doi.org/10.1126/science.1063649.

Siani, G., Sulpizio, R., Paterne, M., Sbrana, A., 2004. Tephrostratigraphy study for the last 18,000 14C years in a deep-sea sediment sequence for the South Adriatic. Quaternary Science Reviews, 23, 2485-2500. https://doi.org/10.1016/j.quascirev.2004.06.004.

Smith, E.I., Jacobs, Z., Johnsen, R., Ren, M., Fisher, E.C., Oestmo, S., Wilkins, J., Harris, J.A., Karkanas, P., Fitch, S., Ciravolo, A., Keenan, D., Cleghorn, N., Lane, C.S., Matthews, T., Marean, C.W., 2018. Humans thrived in South Africa through the Toba eruption about 74,000 years ago. Nature, 555, 511-515. https://doi.org/10.1038/nature25967.

Smith, V.C., Shane, P., Nairn, I.A., 2005. Trends in rhyolite geochemistry, mineralogy, and magma storage during the last 50 kyr at Okataina and Taupo volcanic centres, Taupo Volcanic Zone, New Zealand. Journal of Volcanology and Geothermal Research, 148, 3-4, 372-406. https://doi.org/10.1016/j.jvolgeores.2005.05.005.

Smith, V.C., Staff, R.A., Blockley, S.P.E., Bronk Ramsey, C., Nakagawa, T., Mark, D.F., Takemura, K., Danhara, T., Suigetsu 2006 Project Members, 2013. Identification and correlation of visible tephras in the Lake Suigetsu SG06 sedimentary archive, Japan: chronostratigraphic markers for synchronising of east Asian/west Pacific palaeoclimatic records across the last 150 ka. Quaternary Science Reviews, 67, 121-137.

Suzuki, T., Maruyama, S., Danhara, T., Hirata, T., Machida, H., Arai, F., 2020. Identification of Lower Pleistocene widespread tephras associated with large caldera-forming eruptions in the Tohoku area, north-east Japan. Journal of Quaternary Science, 35, 1-2, 316-333. https://doi.org/10.1002/jqs.3162.

Tamburrino, S., Insinga, D.D., Sprovieri, M., Petrosino, P., Tiepolo, M., 2012. Major and trace element characterization of tephra layers offshore Pantelleria Island: insights into the last 200 ka of volcanic activity and contribution to the Med- iterranean tephrochronology. Journal of Quaternary Science, 27, 129-140. https://doi.org/10.1002/jqs.1504.

Thorarinsson, S., 1944. Tefrokronologiska studier på Island. Geografiska Annaler, 26, 1-217. https://doi.org/10.1080/20014422.1944.11880727.

Thorarinsson, S., 1981a. Greetings from Iceland. Ash-falls and volcanic aerosols in Scandinavia. Geografiska Annaler: Series A, Physical Geography, 63:3-4, 109-118. https://doi.org/10.1080/04353676.1981.11880024.

Thorarinsson, S., 1981b. Tephra studies and tephrochronology: a historical review with special reference to Iceland. In: S. Self, R.S.J., Sparks (Eds.), Tephra Studies, Reidel, Dordrecht (1981), pp. 1-12. https://doi.org/10.1007/978-94-009-8537-7_1.

Villa, P., Soriano, S., Pollarolo, L., Smriglio, C., Gaeta, M., D'Orazio, M., Conforti, J., Tozzi, C., 2020.

Neanderthals on the beach: Use of marine resources at Grotta dei Moscerini (Latium, Italy). PLoS ONE 15(1):e0226690. https://doi.org/10.1371/journal.pone.0226690.

Wagner, B., Vogel, H., Francke, A., Friederich, T., Donders, T., Lacey, J.H., Leng, M.J., Regattieri, E., Sadori, L., Wilke, T., Zanchetta, G., Albrecht, C., Bertini, A., Combourieu-Nebout, N., Cvetkoska, A., Giaccio, B., Grazhdani, A., Hauffe, T., Holtvoeth, J., Joannin, S., Lagoos, M., Leicher, N., Levkov, Z., Lindhorst, K., Masi, A., Melles, M., Mercuri, A.M., Nomade, S., Nowaczyk, N., Panagiotopoulos, K., Peyron, O., Reed, J.M., Sagnotti, L., Sinopoli, G., Stellbrink, B., Sulpizio, R., Timmermann, A., Tofilovska, S., Torri, P., Wagner-Cremer, F., Wonik, T., Zhang, X., 2019. Mediterranean winter rainfall in phase with African monsoons during the past 1.36 million years. Nature, 573, 256-260. https://doi.org/10.1038/s41586-019-1529-0.

Walker, G.P.L., 1973. Explosive volcanic eruptions - a new classification scheme. Geologische Rundschau, 62, 431-446. https://doi.org/10.1007/BF01840108.

Wastergård, S., Veres, D., Kliem, P., Hahn, A., Ohlendorf, C., Zolitschka, B., The PASADO Science Team, 2013. Towards a late Quaternary tephrochronological framework for the southernmost part of South America - the Laguna potrok Aike tephra record. Quaternary Science Reviews, 71, 81-90. https://doi.org/10.1016/j.quascirev.2012.10.019.

Wulf, S., Dräger, N., Ott, F., Serb, J., Appelt, O., Guðmundsdóttir, E., van den Bogaard, C., Słowiński, M., Błaszkiewicz, M., Brauer, A., 2016. Holocene tephrostratigraphy of varved sediment records from Lakes Tiefer See (NE Germany) and Czechowskie (N Poland). Quaternary Science Reviews, 132, 1-14. https://doi.org/10.1016/j.quascirev.2015.11.007.

Wulf, S., Keller, J., Paterne, M., Mingram, J., Lauterbach, S., Opitz, S., Sottili, G., Giaccio, B., Albert, P.G., Satow, C., Tomlinson, E.L., Viccaro, M., Brauer, A., 2012. The 100-133 ka record of Italian explosive volcanism and revised tephrochronology of Lago Grande di Monticchio. Quaternary Sciences Reviws, 58, 104-123. https://doi.org/10.1016/j.quascirev.2012.10.020.

Wulf, S., Kraml, M., Keller, J., 2008. Towards a detailed tephrostratigraphy in the Central Mediterranean: The last 20,000 yrs record of Lago Grande di Monticchio. Journal of Volcanology and Geothermal Research, 177, 1, 118-132. https://doi.org/10.1016/j.jvolgeores.2007.10.009.

Wulf, S., Kraml., M., Brauer, A., Keller, J., Negendank, J.F.W., 2004. Tephrochronology of the 100 ka lacustrine sediment record of Lago Grande di Monticchio (Southern Italy). Quaternary International, 122, 1, 7-30. https://doi.org/10.1016/j.quaint.2004.01.028.

Zanchetta, G., Giaccio, B., Bini, M., Sarti, L., 2018. Tephrostratigraphy of Grotta del Cavallo, Southern Italy: insights of the chronology of Middle to Upper Paleolithic transition in the Mediterranean. Quaternary Science Reviews, 182, 65-77. https://doi.org/10.1016/j.quascirev.2017.12.014.

Zelenin, E., Kozhurin, A., Ponomareva, V., Portnyagin, M., 2020. Tephrochronological dating of palaeoearthquakes in active volcanic arcs: A case of the Eastern Volcanic Front on the Kamchatka Peninsula (northwest Pacific). Journal of Quaternary Science, 35, 1-2, 349-361. https://doi.org/10.1002/jqs.3145.

Chapter II - Aims, structure and methods of the Thesis

1. Aims and structure of the Thesis

As outlined in paragraph 2, Chapter I, the central Mediterranean tephrostratigraphic framework is still incomplete since previous studies have largely focused on the Upper Pleistocene (126-11.7 ka) and Holocene (~11.7 ka-present). On the contrary, the Middle Pleistocene (781-126 ka) remains still largely unexplored, and only few of the sedimentary successions covering this time interval have been investigated in detail. In this period, the potassic and ultrapotassic Italian Quaternary volcanism started and reached its acme (~400 ka) of activity. Products emplaced during this interval of time have been widely investigated and chemically characterised but, however, glass-geochemistry of proximal pyroclastic products are scant and/or missing. This is a fundamental requirement as glass-geochemistry of proximal products is needed as a reference to compare with the composition of tephra of unknown origin to backtrack their source volcano and equivalent eruptive event.

The main objective of this Ph.D. Thesis is to improve the general knowledge on timing, dynamics, and evolution of the Quaternary Italian volcanoes, aiming at filling the gap of knowledge relative to the Middle Pleistocene peri-Tyrrhenian explosive history.

To achieve this objective, an integrated approach has been carried out. On one side, tephra investigation in a series of repositories from central Italy sedimentary deposits and successions has been performed, in particular from the 430 kyr-long Fucino Basin succession. On the other side, investigations of near-vent volcanic areas, including lithostratigraphic, geochemical and geochronological analyses of main pyroclastic units from the Italian volcanoes, has been carried out as well. This allowed acquiring glass-geochemistry composition of proximal Italian volcanoes products to build a reference dataset for direct comparison with the distal tephra sequences and for future investigations in the region. Indeed, despite the huge geochemical dataset available in the literature for the peri-Tyrrhenian volcanoes, a comprehensive glass-based database is still pending. This has been achieved with the employment of the Electron Probe Micro Analyser (EPMA), or Electron Microprobe, and the Laser Ablation - Inductively Coupled Plasma - Mass Spectrometry (LA-

ICP-MS). Major and minor element composition allowed a first tentative correlation of tephra of unknown origin to their source volcano, by direct comparison with proximal units' glass-geochemistry and the aid of classification diagrams. For selected tephra layers - i.e., those for which major/minor element composition failed to undoubtedly backtrack their source volcano - trace element composition has been also determined, allowing a more rigorous source volcano attribution and eruptive event correlation.

A selected number of tephra layers and proximal pyroclastic units were chosen for further analysis to perform isotopic composition (i.e., Sr and Nd) and $^{40}Ar/^{39}Ar$ age determinations. This type of analysis, combined with the major and trace element ones, provided the full geochemical fingerprint of the tephra layers and fundamental time constraints to build age-depth models in the Fucino Basin, which in turn provided modelled ages for all the other tephra. In this Thesis, whilst I personally aquired major, minor and trace elements with the EPMA and LA-ICP-MS (except for the work in Chapter V, where trace element data were aquired by Dr. P. G. Albert), Sr and Nd isotope composition and $^{40}Ar/^{39}Ar$ age determinations have been carried out in collaboration with researchers from other national and international institutes.

Indeed, results from this Thesis represent a contribution to the international project entitled "FUTURE (FUcino Tephrochronology Unites Quaternary REcords)", supported by the Italian Ministry of Education, University and Research (MIUR, grant PRIN No. 20177TKBXZ_003; G. Zanchetta: coordinator; M. D'Antonio, B. Giaccio and D. Palladino, UR responsibles) and co-funded by DFG (German Research Foundation) grant WA 2109/16. This project, which involves researchers from both national (Universities of Pisa, Rome-Sapienza, and Naples-Federico II, IGAG-CNR, IGG-CNR, INGV-OV) and international (University of Cologne, LSCE-Paris Saclay) research institutes and universities, aims at building a high-precision $^{40}Ar/^{39}Ar$ dated tephrochronological record for the last ~430 kyr anchored to a detailed paleoclimate multiproxy record, from Fucino lacustrine succession, that may be regionally to globally spread via tephrostratigraphic, paleomagnetic and cosmogenic nuclide peak synchronization and paleoclimatic alignments. To achieve this objective, the project employs the 430-kyr long tephra sequence from Fucino Basin, through their geochemical fingerprinting and $^{40}Ar/^{39}Ar$ dating. Each one of the research institutes and universities, which are

referred as “operational units”, is responsible of one (or more) aspect(s) of the project, and are listed below:

-University of Pisa, IGG-CNR: Fucino sediments’ lithology, stable isotopes (i.e., O, C), XRF, CNS, XRD, Raman, pollen, and biogenic silica analysis.

-University of Rome-Sapienza, IGAG-CNR: field sampling in proximal (near-vent) volcanic areas, major, minor (EPMA), and trace element (LA-ICP-MS) analysis of proximal pyroclastic units and distal (Fucino’s) tephra layers.

-University of Naples-Federico II, INGV-OS: Sr and Nd isotope analysis of proximal pyroclastic units and Fucino’s tephra layers.

Furthermore, a series of international research institutes and universities are actively involved in the project by providing their expertites:

-University of Cologne: XRF-core scanning, tephra sampling and analysis (EPMA).

-Laboratoire des Sciences du Climat et de l’Environnement (LSCE), University of Paris Saclay: $^{40}Ar/^{39}Ar$ dating of K-bearing minerals (i.e., K-feldspar and/or leucite/dark mica) from tephra (proximal and distal) deposits.

As a collaborator of the Rome-Sapienza and CNR-IGAG operational units, the author of this Thesis was responsible of Fucino tephra analysis as well as field sampling in the peri-Tyrrhenian volcanic areas (i.e., Vulsini, Vico, Sabatini, Colli Albani, Campi Flegrei). This aimed at describing and collecting samples from the proximal pyroclastic units, as well as their subsequent geochemical characterisation (i.e., major and minor elements; EPMA) along with the Fucino and other sedimentary successions’ tephra layers. Selected samples have been also characterised in terms of trace element composition by means of LA-ICP-MS in collaboration with and under the supervision of Dr. P. Albert (Swansea University) and Dr. M. Petrelli (University of Perugia).

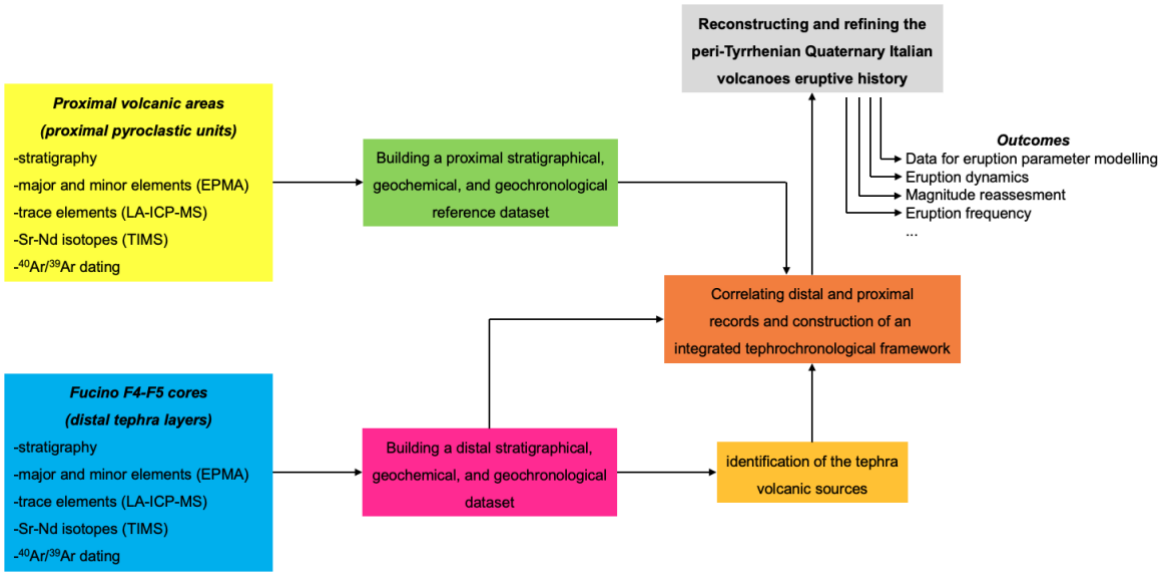

Figure 1. Flow chart of the Thesis highlighting the main steps of the workflow.

To resume, the multidisciplinary approach adopted included the following steps, which are also summarized in Figure 1:

i) Characterisation of tephra layers from Fucino Basin and other sedimentary successions in central-southern Italy in terms of stratigraphy, litology and, major and minor elements by means of the Electron Microprobe (EPMA).

ii) Characterisation of a selected number of these tephra layers also in terms of trace elements by means of Laser Ablation - Inductively Coupled Plasma - Mass Spectrometry (LA-ICP-MS).

iii) Field investigations in proximal (i.e., near-vent) settings, including lithostratigraphic analysis, sampling of key pyroclastic units (i.e., fall deposits) emplaced by the peri-Tyrrhenian Quaternary Italian volcanoes during specific time-intervals.

iv) Chemical characterisation by means of EPMA and LA-ICP-MS of the peri-Tyrrhenian volcanoes proximal pyroclastic units to build a reference dataset for direct comparison with distal tephra layers and for future investigations in the region.

v) Isotopic composition (i.e., Sr and Nd) and $^{40}Ar/^{39}Ar$ age determinations to obtain the full geochemical fingerprint of the tephra and fundamental chronological constraints.

vi) Distal-proximal correlation between Fucino tephra layers and the peri-Tyrrhenian Quaternary Italian volcanoes pyroclastic products to determine tephra layer source volcano and individual eruption.

vii) Construction of sequentially ordered tephra sequences and age-depth models to obtain modelled ages for all the other tephra.

viii) Comparison with other tephra repositories in the central Mediterranean area.

ix) Identification of potential tephra marker horizons and undocumented eruptive episodes recorded by tephra layers.

The Thesis is structured in a series of chapters, each one referring to a peer-review published, unpublished or submitted original manuscript.

Chapter III and IV - The third and fourth chapters consist in scientific papers addressing two tephra sequences from the F4-F5 record of Fucino Basin. In the first one, entitled "*Mediterranean tephrostratigraphy and peri-Tyrrhenian explosive activity revaluated in light of the 430-365 ka record from Fucino Basin (central Italy)*" and published in the prestigious Earth-Science Reviews journal (Monaco et al., 2021), the explosive activity of the Quaternary peri-Tyrrhenian Italian volcanoes in the period 365-430 ka is revised based on the newly presented record of 28 Fucino tephra layers. In the second original (unpublished) research article, temporaneously entitled "*Central Mediterranean volcanism during marine isotope stages 7 and 6 (250-170 ka): a new tephra record from Fucino Basin, central Italy*", similarly the peri-Tyrrhenian explosive activity during the time interval of 250-170 ka is revaluated based on the tephra record of Fucino Basin.

These two papers represent a contribution to the international project "FUTURE".

Chapter V - The fifth chapter addresses the pre-Campanian Ignimbrite activity (i.e., older than 40 ka) at Campi Flegrei volcanic system, where a medial-proximal sequence relative to the 90-110 ka activity of the volcano is presented. In this manuscript, entitled "*Tracing the proximal occurrences of the largest Campi Flegrei explosive eruptions preceding the Campanian Ignimbrite (~40 ka), southern Italy"*, the medial-proximal record allowed to backtrack for the first time ever the famous C-22, X-5, and X-6 widespread marine tephra layers to the Campi Flegrei volcanic district. Occurrences

of these fundamental Middle Pleistocene tephra horizons at other central Mediterranean sedimentary sequences is critically revaluated and reviewed and the new high-precision $^{40}Ar/^{39}Ar$ dating of the investigated units provide new fundamental temporal constraints for refining and consolidating the chronology of MIS 5d-c period.

Chapter VI - The sixth chapter collects a series of co-authored publications showing examples of possible applications of the tephrostratigraphic method for tephra, volcanological and paleoclimatic reconstructions in central-southern Italy. The papers collect data relative to tephra repositories in sedimentary - sub-aerial and basinal - successions from central-southern Italy. The papers' abstracts are presented in order of year of publication, from the oldest to the most recent.

Chapter VII - Finally, in the seventh and last chapter, a general overview on the main results and objectives achieved with this Thesis is critically exposed, evaluating also future perspectives in the region and possible advancements.

2. Analytical procedures

In order to use tephra layers as stratigraphic horizons, their lithological features, (geo-)chemical (major, minor, and trace elements, Sr-Nd isotopes) composition must be first determined. In this chapter, a brief review of the main analytical techniques employed in tephra studies, as well as in this thesis, is provided. Note that, concerning the analytical data presented in the figures of this Thesis, each data point in the plots corresponds to a single analysis. In some cases, for those samples where the paucity of the analysable material limited the number of analyses (i.e., alteration of the glasses, cryptotephra nature), multiple analysis were performed on the same pumice fragment/glass shard.

2.1. Tephra extraction and concentration

The first step in tephra analysis consists in the extraction from the hosting sediment of a sufficient amount of glass shards to be analysed. After the discovery of Icelandic cryptotephras in the British Isles (Dugmore, 1989), it become fundamental to develop techniques that allowed the removal of

undesired material and extraction of the shards in concentrations that allowed tephra characterisation.

A preliminary, useful, and widely employed technique, which at the same time is incredibly effective and non-destructive, is X-ray fluorescence (XRF) scanning of the cores extracted from the sedimentary succession hosting tephra, which allows to obtain the chemical composition of an entire core section. In this way, the “invisible” cryptotephra can be spotted where a chemical contrast between the scanned host material and the volcanic ashes is revealed (e.g., Kylander et al., 2012), thus allowing sediment sampling at specific core depths. Then, glass shards extraction and concentration can be carried out on the sampled sediments.

One of the main (destructive) techniques for organic material removal is “ashing”, introduced in tephra investigations by Dugmore (1989). It consists in drying water-rich (like peat deposits) sediments in a high-temperature oven and subsequently suspend the resulting ash in 10% HCl to remove the soluble inorganic fraction. For the removal of organic material, acid treatment of the sediments can also be performed, the main techniques being acid digestion (e.g., Dugmore et al., 1992, 1995) and alkali treatment (for removal of biogenic silica; Rose et al., 1996).

In mineral-rich sediments, magnetic separation showed to be an effective technique for the retrieval of magnetic (like basalts) volcanic material, exploiting minerals with high Fe contents (e.g., Mackie et al., 2002; Griggs et al., 2014).

If an ice core is retrieved, volcanic ashes can be extracted simply by melting the ice (e.g., Davies et al., 2010) and recovering the sediment from the molten solution.

One of the main techniques used for cryptotephra extraction from a marine and/or lacustrine succession is density separation (e.g., Turney, 1998). It is a stepped floating technique that employs floatation media (i.e., heavy liquids) at different densities and centrifuging to isolate fractions at desired densities. This technique allows concentration of sediments at specific densities that can be successively ashed to remove the organic material, allowing retrieval of volcanic ashes of proper size and density ranges.

Note that all the above-mentioned techniques are mainly adopted for cryptotephra extraction, but in the case of thicker, visible tephra layers, glass shards/pumices can be directly sampled from the sediment core, as for the Fucino tephra.

Once a sufficient amount of glass shards is recovered, samples can be embedded in epoxy resin and mounted either on thin sections or embedded in 1-inch epoxy pucks (Fig. 2), to be subsequently polished in order to expose fresh sections of the micro-pumices for analytical purposes.

Figure 2. Multi-sample 1-inch epoxy puck holder for EMPA and LA-ICP-MS analysis. Description of the preparation, in Lowe (2011).

2.2. Electron Microprobe

Volcanic glasses, consisting in micro-pumices, pumice fragments and/or glass shards, are the major component of a tephra layer, along with free (loose) crystals, the nature of which depending on the distance between the volcanic source and the tephra archive (i.e., low-density minerals can travel for further distances). The characterisation of the glasses allows to distinguish tephra from one

another, as well as to backtrack the source volcano of the tephra. Glass geochemistry of tephra has also been widely shown to allow distinguishing between eruptive products of the same volcano, and major element glass-composition can be sufficient to discriminate tephra from one another and correlate them over different repositories.

The most common technique employed for major element characterisation is the electron microprobe analysis (EMPA). This analytical technique was developed in the first half of the 20th century and introduced in the market in the 50s. Nowadays, the two major (and only) producing companies are CAMECA (France) and JEOL (Japan).

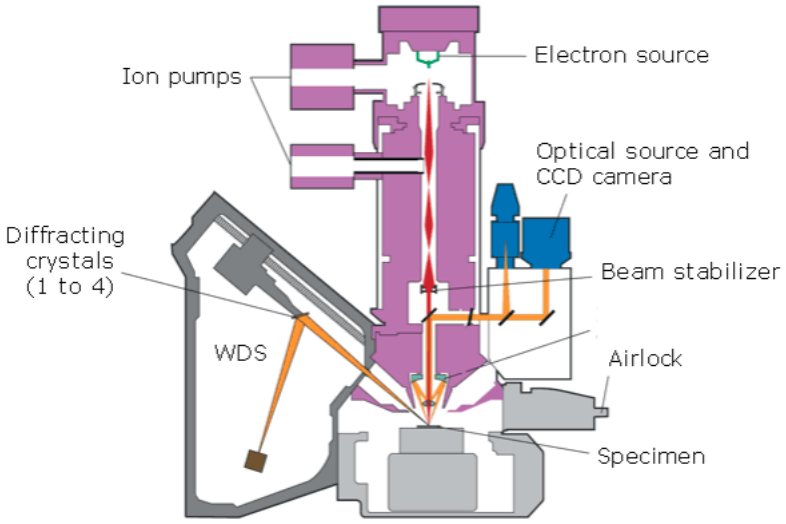

Figure 3. Sketch representation of the internal structure of an electron microprobe. Image taken from the CAMECA official website at https://www.cameca.com/products/epma/technique.

In the electron microprobe, an electron beam is produced by heating of a metal filament (generally tungsten, W) and accelerated through the column (Fig. 3) via an anode. Then, the beam is collimated and focalized via a series of magnetic lenses, producing a beam with a diameter that, in modern machines, can be varied at the operator's choice. Once the beam reaches the sample, incident electrons interact with the electrons of the specimen and, if an electron of the specimen is scattered and ejected by the incident ones, this will cause a vacancy in the atom. Then, an electron from the outer shield of the same atom can fill this vacancy and substitute the ejected electron and in doing

so, moving from an outer more energetic shell to a less energetic one, it will release part of its energy in form of a photon (X-ray). These X-rays (photons) will have a characteristic wavelength depending on the element from which the X-rays are emitted. The Electron Microprobe is equipped with detectors which measure the wavelength of the emitted X-rays, called Wavelength Dispersive Systems (WDS). These WDS spectrometers operate based on the Bragg's Law (Fig. 4) and with the employment of specific monocrystals which operates as monochromators (a device that filters selected wavelengths of light or other radiations). The Bragg's Law is defined as:

$$n\lambda = 2d \sin(\theta) \quad [1]$$

where *n* is a positive integer, λ is the wavelength of the incident wave (unknown), *d* is the intraplane distance (known), and θ is the incident angle. The monocrystals have known intraplane distance and can be rotated, thus capable of measuring X-rays emitted at different angles, allowing measurement of wavelengths of different elements. Each of these monochromators (e.g., PET, LIF, TAP, etc.) can "analyse" wavelengths of X-rays emitted from a certain range of elements. In an EMP device, up to five of these WDS spectrometers are installed (usually 3 to 5 different WDS can be installed) allowing to detect a broad range of major and minor elements (elements in concentration > than 1 wt.% and between 0.1-1 wt.% respectively), as oxides. The main 10 major element oxides generally measured in geological samples are SiO_2, TiO_2, Al_2O_3, FeO, MnO, MgO, CaO, Na_2O, K_2O and P_2O_5.

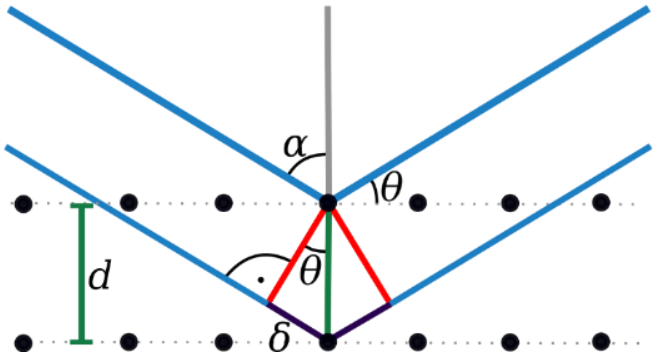

Figure 4. Bragg's Law sketch representation. WDS spectrometers are movable (rotating) crystals with known intraplane distance d. Image source: https://it.wikipedia.org/wiki/Legge_di_Bragg

EMP devices are widely used in geosciences for the characterisation of rock-forming minerals and natural, as well as synthetized, materials, the main advantage being the ability to perform single-point analysis. The EMPA was first employed for the characterisation of glass-shards to correlate tephra by Smith and Westgate (1969). Since then, major element characterisation of tephra by means of glass-WDS analysis has become a routine technique in tephra studies. This technique has, however, some issues and limitations that must be considered when performing major element glass-analysis.

A first issue is linked to alkali mobilization and loss during the analytical session. To avoid such alkali loss (especially for Na), a beam diameter of 10 μm or more is preferred (Hayward, 2012). This, however, can lead to a second issue, linked to shards and septa size. Indeed, the septa of a micro-pumice can be as small as 10 μm or even smaller, limiting the number of measurable septa and making the acquisition of a satisfying number of analysis (generally more than 10-15 analytical points are required for the characterisation of a tephra layer) more challenging. This is even more complicated for cryptotephra studies, where glass materials can be extremely small and in very low concentration. Another major issue is linked to the state of preservation of the pumices. In marine and lacustrine sedimentary environments, pumices might be altered during post-depositional processes, making the glass not analysable. It is thus mandatory to retrieve the most pristine and "fresh" glasses to obtain unaffected analysis.

One of the main limitations in tephra studies can be linked to the lack of a satisfying literature glass-composition chemical dataset of proximal volcanic deposits, making comparison of a tephra layer of unknown provenance to its proximal counterpart quite challenging. This is especially true in the Italian peninsula, where proximal volcanic materials have been mainly characterised by means of X-ray fluorescence (XRF), which provides whole rock bulk-composition that can sensibly differ from the glass composition, especially in highly porphyritic samples (e.g., Lowe et al., 2017). Furthermore, the available glass analysis for the Quaternary peri-Tyrrhenian potassic volcanoes is scattered in the literature in several papers and thus not organised in a database. Efforts for the organisation of the available glass analyses in such a database have been made by the RESET project (Bronk Ramsey

et al., 2015b). Another issue is represented by the fact that proximal deposits of large eruptions are frequently characterised by compositionally zoned eruption sequences (e.g., Pompeii eruption; Santacroce et al., 2008), that might not be fully represented in distal settings, due to variations of the dispersal axes of the eruptive products.

Finally, a major limitation is linked to tephra (often) having very similar major element composition, potentially leading to erroneous tephra attribution and correlation. To overcome this limitation, tephra correlation must rely also on other data and indications, such as the stratigraphic order with respect to other tephra, and chronological indications, both direct and indirect (e.g., position relative to climatic or geomagnetic events), in order to not income into erroneous correlations (e.g., Giaccio et al., 2009). Staying on the geochemical tools, minor elements composition or other techniques, capable to quantify trace elements (concentration < 0.1 wt.%), which are more sensible to magma differentiation processes, can be more effective in distinguishing tephra with very similar major element composition. One of such techniques is the Laser Ablation Inductively Coupled Plasma Mass Spectrometry, which is discussed in the next paragraph.

2.3. Laser Ablation Inductively Coupled Plasma Mass Spectrometry

The study of trace element composition is usually employed as a supplementary (and complementary) analytical procedure for obtaining the geochemical fingerprint of a tephra. Indeed, tephra layers of different volcanoes, as well as those erupted from the same one, can display similar major (and even minor) element chemical composition, leading to possible miscorrelations. Instead, small variations in trace elements allow discrimination of tephra exhibiting similar chemical composition in terms of major and minor elements.

The main analytical technique employed for the characterisation of trace elements in tephra studies is the laser ablation-inductively coupled plasma-mass spectrometry (LA-ICP-MS). As the name suggests, this technique couples a pulsing laser to an ICP-MS device which ablates the material directly from the solid sample. Then, the material is ionised by the plasma torch (Fig. 5) and elements (and/or isotopes) counting is performed by the mass spectrometer detector, as in a standard ICP-MS device, at ppb (parts per billion) concentrations. Thus, in a LA-ICP-MS device the material is

directly removed from the sample with the laser without the preparation of a solution and is particularly suitable for solid materials.

First studies employed the LA-ICP-MS for the analysis of bulk samples (e.g., Pearce et al., 2004) and subsequently evolved allowing single-shard analysis. As in an EMP device, single shards as small as 10 μm in diameter can be now successfully analysed with the LA-ICP-MS (e.g., Tomlinson et al., 2010).

A recent advancement in LA-ICP-MS devices is represented by the femtosecond LA-ICP-MS (fs LA-ICP-MS), which allows characterisation of up to 58 major, minor and trace elements simultaneously (e.g., Maruyama et al., 2020). The possibility to analyse both major/minor and trace elements at the same time makes this device particularly advantageous for single shards analysis of tephra. Indeed, in a standard LA-ICP-MS device the acquired data must first be processed using the composition of the sample itself (generally the mean value of Si or Ca is used), which is not required in a fs LA-ICP-MS. Theoretically, since the major element composition of a tephra can slightly change from shard to shard, the specific Si or Ca content of a shard should be used when acquiring trace element data from the same shard, which will make the acquisition process extremally time consuming.

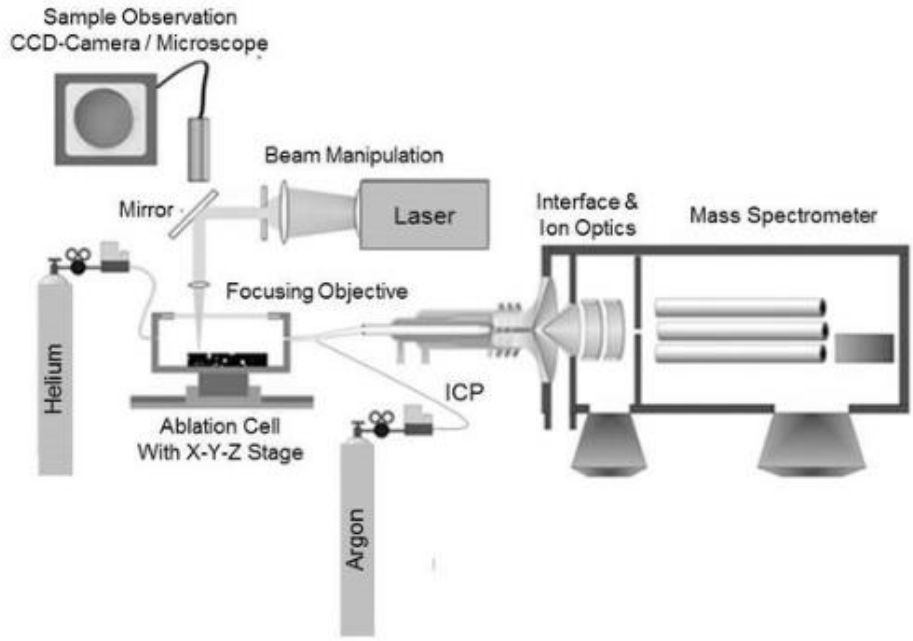

Figure 5. Schematic view of the experimental set-up used for LA-ICP-MS. Image source: https://www.researchgate.net/publication/281442167_Surface_micro-structuring_of_intercalation_cathode_materials_for_lithium-ion_batteries_-_A_study_of_laser-Assisted_cone_formation/figures?lo=1.

Another limitation of the LA-ICP-MS technique is represented by the micro-phenocrysts "hidden" underneath the glass shard's surface, that can be accidently ablated with the glass in the process (Fig. 6), contaminating the analysis. As outlined by Pearce (2014), the larger the ablation crater diameter, the greater the number of micro-phenocrysts potentially ablated with the sample that could contaminate the analysis. Nevertheless, contaminated analyses can be easily identified, and micro-phenocrysts ablation can be avoided with the employment of smaller crater volumes (i.e., ablation diameter). A smaller crater is also recommended by Pearce (2014) to avoid ablation of the epoxy resin englobing the shards, which can contaminate the acquired analysis as well.

Furthermore, the employment of a bigger crater can limit the number of analysable shards, as glass shards in cryptotephra deposits can be as small as < 100 μm. Thus, a proper ablation crater must be employed based on dimensions of the micro-pumices/shards. Besides these possible complications in the acquisition process, the LA-ICP-MS is the most reliable technique in trace element characterisation of glass shards, and it is widely used in tephra studies as a volcanic source and eruption discriminating tool, as well as tephra correlation between different sites (e.g., Albert et al., 2012).

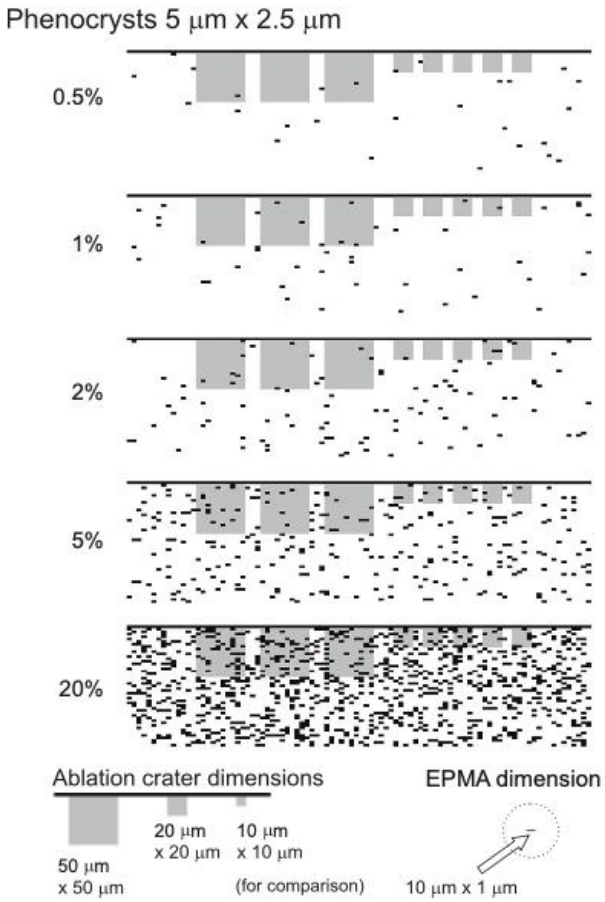

Figure 6. Comparison of the cross-sectional area of ablated material for different crater sizes in specimens with varying amounts of randomly distributed 2.5 x 5-mm phenocrysts. Image after Pearce (2014).

2.4. Sr-Nd isotopes

In chemistry (as well as other scientific disciplines such as nuclear physics) isotopes of an element are characterised by the same atomic number (Z) but a different nucleon number (A), thus having the same number of protons in the nucleon but differing in the number of neutrons and atomic weight. As such, some isotopes can be physically stable, while others are instable and naturally decay radioactively, thus being defined as radioactive (or radioisotopes). There are several types of radioactive decay, the main three being the alpha, beta, and gamma decays, during which an instable radioactive isotope will “transform” in a more stable isotope of the same element or of a different one. The time required for half of the original population of a radioisotope to decay is called the “half-life”, and each radioisotope has its own half-life and decay constant (being that defined as the rate at

which the radioisotope population decreases). Since the decay constants of radioisotopes are known, the absolute age of natural materials can be quantified (radiometric dating) by comparing the abundance of a radioisotope with its decay products employing the formula:

$$D^* = D_0 + N(t)\,(e^{\lambda t} - 1) \qquad [2]$$

Where D^* is the number of atoms of the radiogenic ("daughter") isotope, D_0 is the original (initial) number of atoms of the daughter isotope, $N(t)$ is the number of atoms of the radioisotope ("parent") in the sample at time t, λ is the decay constant of the parent isotope and t is the age of the sample (unknown). There are different types of radiometric dating, the main ones being the uranium-lead (U-Pb), the uranium-thorium (U-Th), the samarium-neodymium (Sm-Nd), the potassium-argon (K-Ar), the argon-argon (Ar-Ar) and the rubidium-strontium (Rb-Sr).

Besides being employed for radiometric dating, some isotopes can have an application also in tephra studies. Indeed, products of different volcanoes can display distinct concentrations of specific isotopes (isotopic composition), and isotope ratios can be employed to backtrack the volcanic source of an unknown tephra. For instance, D'Antonio et al. (2016) determined the isotopic composition (Sr and Nd isotope ratios) of tephra layers from six marine cores from the Mediterranean (Ionian and Aegean Seas) area, which allowed them to backtrack tephra layers to Italian and Hellenic volcanoes, as well as to specific eruptive events (i.e., Campanian Ignimbrite super-eruption). Furthermore, volcanoes from the same region can display different and time-variable isotopic ratios, allowing unknown tephra to be backtracked to their volcanic source. For instance, in the Italian peninsula, volcanic provinces display variable Sr, Nd and Pb isotopic ratios that allow their products to be distinguished from one another (Fig. 7).

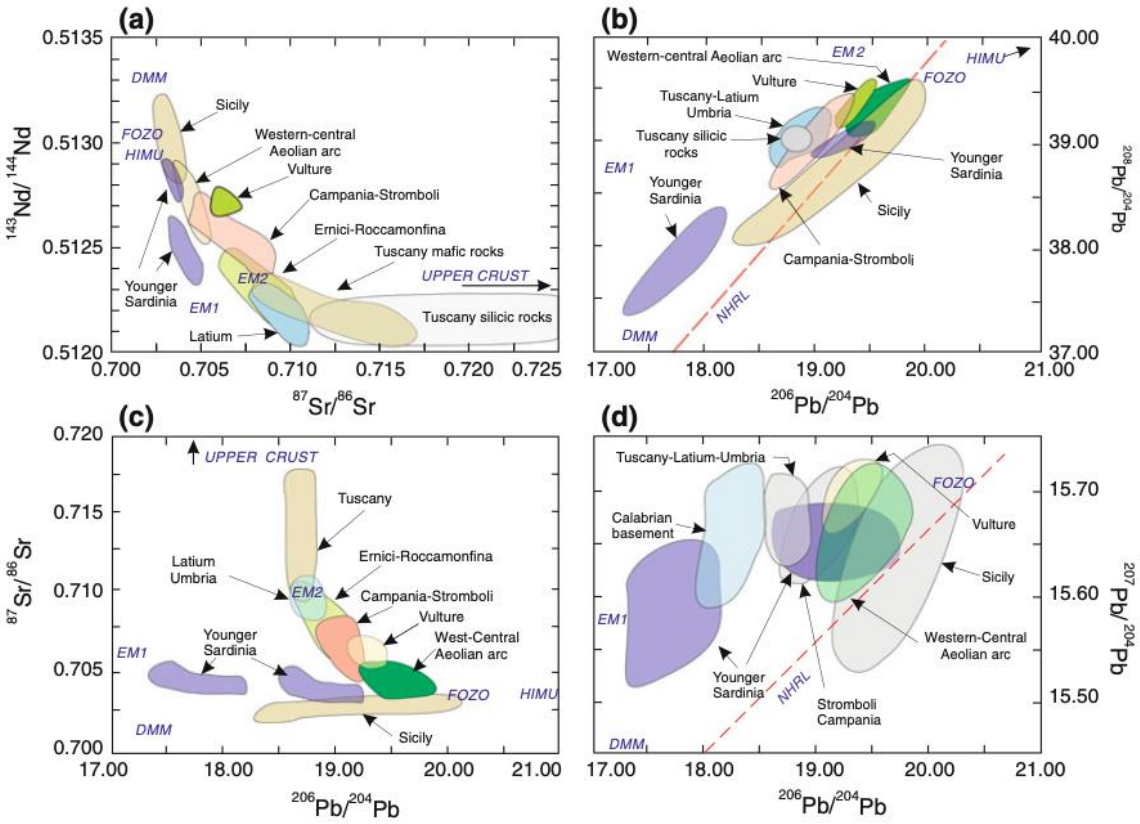

Figure 7. Sr, Nd and Pb isotope variations for Cenozoic mafic volcanic rocks from the Tyrrhenian Sea region. Image after Peccerillo, 2017.

To avoid contamination by loose crystals and lithic fragments, as in the case of whole-rock sample analysis, Sr-Nd isotope compositions in this Thesis were determined on glass fragments and sialic crystals (i.e., plagioclase, k-feldspar). Even though being a reliable discriminating tool, isotope composition of products from the same region/district or volcano can display very similar ranges of isotope ratios, making the correlation to a specific eruptive period or event quite challenging. For this reason, isotopic composition should be considered as a complementary tool to be coupled with major, minor and trace element geochemical composition of a tephra.

2.5. Dating techniques

The major prerequisite of a tephra layer is that of providing a precise age and building a robust chronology, which possibly is independent from orbital tuning procedures. Ages of tephra

layers can be determined with the employment of a radiometric technique (see previous section), the main two being the ^{14}C and $^{40}Ar/^{39}Ar$ dating.

The first technique is based on quantification of the radiogenic isotope of carbon, ^{14}C. This is produced in the atmosphere by the interaction of cosmic rays with atmospheric nitrogen (N), which successively combines with the atmospheric oxygen (O) to form CO_2. This enters the biosphere through plants photosynthesis, and, at animals/plants death, it undergoes radioactive decay with a half-life of ~5730 years. Although widely employed, ^{14}C dating has an empirical limit of applicability of ~50,000 years, meaning that organic materials older than 50 ka cannot be dated because around 50 ka the content of ^{14}C is ca. 1/500 of the originary content, i.e., near to zero and in any case too low to be detected with the present technology. In tephra studies, soils and/or paleosols, as well as charcoal, interlayered within tephra layers, can be ^{14}C dated, giving an "indirect" age of the tephra.

In the second method, the potassium (K) contained in minerals is artificially (through nuclear irradiation) converted in radiogenic argon (Ar). Successively, the crystals are laser-fused, and the so-produced extracted gas is purified, so that Ar isotopes can be measured in a mass spectrometer. The ratio of $^{40}Ar/^{39}Ar$ must be estimated with the employment of a standard of known age (e.g., Alder Creek Sanidine, ACs, 1.1891 Ma; Niespolo et al., 2017), that was co-irradiated with the sample, to measure the so-called J-factor, which is needed for the age determination. In this case, the technique allows "direct" age measurements of million years-old minerals (Fig. 8). As a matter of fact, this technique requires K-rich minerals, which in volcanic deposits are generally represented by K-feldspar (e.g., sanidine), feldspathoids (e.g., leucite) and dark mica (e.g., biotite and phlogopite) crystals, thus limiting its applicability to tephra layers with such mineral components.

The $^{40}Ar/^{39}Ar$ dating has been widely employed in tephra studies in the Mediterranean region, particularly in central-southern Italy. Indeed, the recurrent and continuous - starting from the Middle Pleistocene or "Chibanian" (770-126 ka; IUGS, 01/2020) - explosive activity of the peri-Tyrrhenian volcanism was fed by potassic to ultrapotassic magmas (e.g., Peccerillo, 2017), with K-bearing minerals suitable for this radiometric dating technique. The presence of such potassic magma-fed volcanism, as well as that of numerous Quaternary tectonic basins hosting thick sedimentary

successions, constitute a unique combination which has allowed the retrieval of extremely rich tephra repositories and, consequently, eruption event stratigraphies in the Italian peninsula.

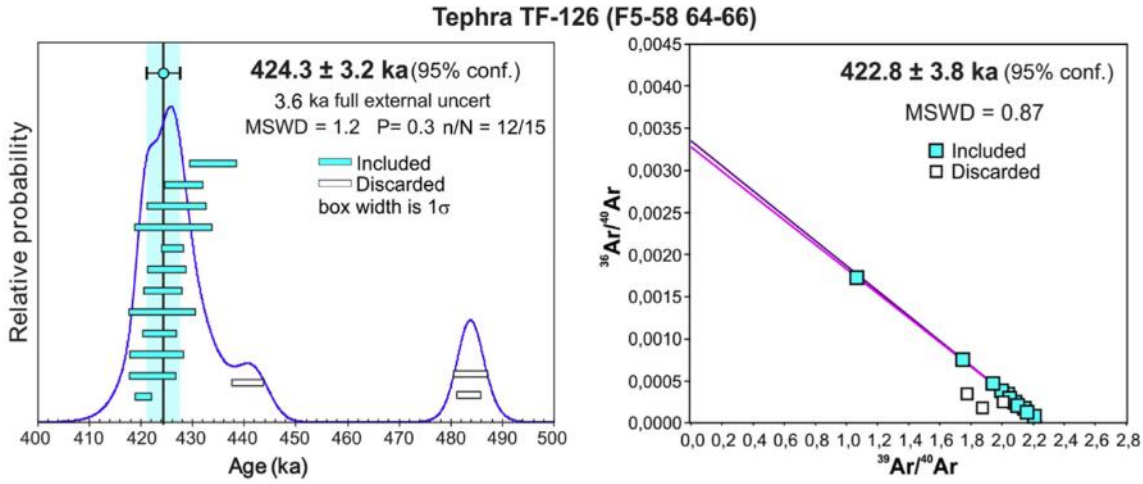

Figure 8. Example of an age probability density spectra diagram (left) and inverse isochrone (right) of a tephra (TF-126 from Fucino Basin, central Italy) acquired by means of $^{40}Ar/^{39}Ar$ dating. Image after Giaccio et al. (2019).

References

Albert, P.G., Tomlinson, E., Smith, V.C., Di Roberto, A., Todman, A., Rosi, M., Marani, M., Muller, W., Menzies, M.A., 2012. Marine-continental tephra correlations: Volcanic glasses from the Marsili Basin and the Aeolian Islands, Southern Tyrrhenian Sea, Italy. Journal of Volcanology and Geothermal Research, 229-230, 74-94. https://doi.org/10.1016/j.jvolgeores.2012.03.009.

Bronk Ramsey, C., Housley, R.A., Lane, C.S., Smith, V.C., Pollard, A.M., 2015b. The Reset tephra database and associated analytical tools. Quaternary Science Reviews, 118, 33-47. https://doi.org/10.1016/j.quascirev.2014.11.008.

D'Antonio, M., Mariconte, R., Arienzo, I., Mazzeo, F.C., Carandente, A., Perugini, D., Petrelli, M., Corselli, C., Orsi, G., Principato, M.S., Civetta, L., 2016. Combined Sr-Nd isotopic and geochemical fingerprinting as a tool for identifying tephra layers: Application to deep-sea cores from Eastern Mediterranean Sea. Chemical Geology, 443, 121-136. https://doi.org/10.1016/j.chemgeo.2016.09.022.

Davies, S.M., Wastegård, S., Abbott, P.M., Barbante, C., Bigler, M., Johnsen, S.J., Rasmussen, T.L., Steffensen, J.P., Svensson, A., 2010. Tracing volcanic events in the NGRIP ice-core and synchronising North Atlantic marine records during the last glacial period. Earth and Planetary Science Letters, 294, 69-79. https://doi.org/10.1016/j.epsl.2010.03.004.

Dugmore, A.J. & Newton, A.J., 1992. Thin tephra layers in peat revealed by X-radiography. Journal of Archaeological Science, 19, 2, 163-170. https://doi.org/10.1016/0305-4403(92)90047-7.

Dugmore, A.J., Larsen, G., Newton, A.J., 1995. Seven tephra isochrones in Scotland. The Holocene, 5, 3, 257-266. https://doi.org/10.1177%2F095968369500500301.

Dugmore, A.J., 1989. Icelandic volcanic ash in Scotland. Scottish Geographical Megazine, 105:3, 168-172. https://doi.org/10.1080/14702548908554430.

Giaccio, B., Leicher, N., Mannella, G., Monaco, L., Regattieri, E., Wagner, B., Zanchetta, G., Gaeta, M., Marra, F., Nomade, S., Palladino, D.M., Pereira, A., Scheidt, S., Sottili, G., Wonik, T., Wulf, S., Zeeden, C., Ariztegui, D., Cavinato, G.P., Dean, R.J., Florindo, F., Leng, M.J., Macrì, P., Niespolo, E., Renne, P.R., Rolf, C., Sadori, L., Thomas, C., Tzedakis, P.C., 2019. Extending the tephra and paleoenvironmental record of the Central Mediterranean back to 430 ka: A new core from Fucino Basin, central Italy. Quaternary Science Reviews, 225, 106003. https://doi.org/10.1016/j.quascirev.2019.106003.

Giaccio, B., Messina, P., Sposato, A., Voltaggio, M., Zanchetta, G., Galadini, F., Gori, S., Santacroce, R., 2009. Tephra layers from Holocene lake sediments of the Sulmona Basin, central Italy: implications for volcanic activity in Peninsular Italy and tephrostratigraphy in the Central Mediterranean area. Quaternary Sceince Reviews, 28, 2710-2733. https://doi.org/10.1016/j.quascirev.2009.06.009.

Griggs, A.J., Davies, S.M., Abbott, P.M., Rasmussen, T.L., Palmer, A.P., 2014. Optimising the use of marine tephrochronology in the North Atlantic: a detailed investigation of the Faroe Marine Ash Zones II, III and IV. Quaternary Science Reviews, 106, 122-139. https://doi.org/10.1016/j.quascirev.2014.04.031.

Hayward, C., 2012. High spatial resolution electron probe microanalysis of tephras and melt inclusions without beam-induced chemical modification. The Holocene, 22, 1, 119-125. https://doi.org/10.1177%2F0959683611409777.

Kylander, M.E., Lind, E.M., Wastergård, S., Löwemark, L., 2011. Recommendations for using XRF core scanning as a tool in tephrochronology. The Holocene, 22, 3, 371-375. https://doi.org/10.1177%2F0959683611423688.

Lowe, D.J., 2011. Tephrochronology and its application: A review. Quaternary Geochonology, 6, 2, 107-153. https://doi.org/10.1016/j.quageo.2010.08.003.

Lowe, D.J., Pearce, N. J. G., Jorgensen, M. A., Kuehn, S. C., Tryon, C. A., Hayward, C. L., 2017. Correlating tephras and cryptotephras using glass compositional analyses and numerical and statistical methods: Review and evaluation. Quaternary Sceince Reviews, 175, 1-44. https://doi.org/10.1016/j.quascirev.2017.08.003.

Mackie, E.A.V., Davies, S.M., Turney, C.S.M., Dobbyn, K., Lowe, J.J., Hill, P.G., 2002. The use of magnetic separation techniques to detect basaltic microtephra in last glacial-interglacial transition (LGIT; 15-10 ka cal. BP) sediment sequence in Scotland. Scottish Journal of Geology, 38, 21-30. https://doi.org/10.1144/sjg38010021.

Maruyama, S., Takemura, K., Hirata, T., Yamashita, T., Danhara, T., 2020. Major and trace element abundances in volcanic glass shards in visible tephras in SG93 and SG06 drillcore samples from Lake Suigetsu, central Japan, obtained using femtosecond LA-ICP-MS. Journal of Quaternary Science, 35, 1-2, 66-80. https://doi.org/10.1002/jqs.3124.

Monaco, L., Palladino, D.M., Gaeta, M., Marra, F., Sottili, G., Leicher, N., Mannella, G., Nomade, S., Pereira, A., Regattieri, E., Wagner, B., Zanchetta, G., Albert, P.G., Arienzo, I., D'Antonio, M., Petrosino, P., Manning, C., Giaccio, B. 2021. Mediterranean tephrostratigraphy and peri-Tyrrhenian explosive activity revaluated in light of the 430-365 ka record from Fucino Basin (central Italy). Earth-Science Reviews, 220, 103706. https://doi.org/10.1016/j.earscirev.2021.103706.

Niespolo, E.M., Rutte, D., Deino, A.L., Renne, P.R., 2017. Intercalibration and age of the Alder Creek Sanidine $^{40}Ar/^{39}Ar$ standard. Quaternary Geochronology, 39, 205-213. https://doi.org/10.1016/j.quageo.2016.09.004.

Pearce, N.J.G., Westgate, J.A., Perkins, W.T., Preece, S.J., 2004. The application of ICP-MS methods to tephrochronological problems. Applied Geochemistry, 19, 3, 289-322. https://doi.org/10.1016/S0883-2927(03)00153-7.

Pearce, N.J.G., 2014. Towards a protocol for the trace element analysis of glass from rhyolitic shards in tephra deposits by laser ablation ICP-MS. Journal of Quaternary Science, 29, 7, 627-640. https://doi.org/10.1002/jqs.2727.

Peccerillo, A., 2017. Cenozoic Volcanism in the Tyrrhenian Sea Region. In: IAVCEI, Advances in Volcanology, 2 ed. Springer, p. 400.

Rose, N.L., Golding, P.N.E., Battarbee, R.W., 1996. Selective concentration and enumeration of tephra shards from lake sediment cores. The Holocene, 6, 2, 243-246. https://doi.org/10.1177%2F095968369600600210.

Santacroce, R., Cioni, R., Marianelli, P., Sbrana, A., Sulpizio, R., Zanchetta, G., Donahue, D. J., Joron, J. L., 2008. Age and whole rock-glass compositions of proximal pyroclastics from the major explosive eruptions of Somma-Vesuvius: A review as a tool for distal tephrostratigraphy. Joournal of Volcanology and Geothermal Research, 177, 1-18. https://doi.org/10.1016/j.jvolgeores.2008.06.009.

Smith, D.G.W., & Westgate, J.A., 1969. Electron probe technique for characterising pyroclastic deposits. Earth and Planetary Science Letters, 5, 313-319. https://doi.org/10.1016/S0012-821X(68)80058-5.

Tomlinson, E.L., Thordarson, T., Muller, W., Thirlwall, M.T., Menzies, M.A., 2010. Microanalysis of tephra by LA-ICP-MS - strategies, advantages and limitations assessed using the Thorsmork ignimbrite (Southern Iceland). Chemical Geology, 279, 3-4, 73-89. https://doi.org/10.1016/j.chemgeo.2010.09.013.

Turney, C.S.M., 1998. Extraction of rhyolitic component of Vedde microtephra from minerogenic lake sediments. Journal of Paleolimnology, 19, 199-206. https://doi.org/10.1023/A:1007926322026.

Chapter III - Mediterranean tephrostratigraphy and peri-Tyrrhenian explosive activity revaluated in light of the 430-365 ka record from Fucino Basin (central Italy)

In this manuscript (Monaco et al., 2021), the activity of the peri-Tyrrhenian potassic Quaternary Italian volcanoes in the period 430-365 ka - i.e., broadly corresponding to Marine Isotope Stage 11 - is revised and updated based on the tephra sequence from Fucino Basin. It collects data of 28 newly presented tephra layers, characterised in terms of major, minor (EPMA-WDS), and trace (LA-ICP-MS) elements, Sr isotopic composition and $^{40}Ar/^{39}Ar$ dating. Results from this study revealed that the Fucino tephra all originated from the peri-Tyrrhenian potassic volcanoes, including the Vulsini, Vico, Sabatini, Colli Albani, and Roccamonfina volcanic districts. Data allowed backtracking of the tephra layers to known eruptive events, but also identifying eruptions undocumented in proximal settings, thus revising length of the quiescence periods and time of recurrency, with important implications for hazard assessment in the area. Finally, data from this study also allowed to identify new potential tephra marker horizons for the Middle Pleistocene period and the tephra sequence presented in this study is compared with other repositories across the Mediterranean covering this time interval.

This paper was published in the *Earth Science Reviews* journal (Monaco et al., 2021) with the contribution of: L. Monaco (manuscript writing and revision, EPMA and LA-ICP-MS data acquisition, data elaboration and interpretation, images preparation, First Author); B. Giaccio (manuscript writing, tephra correlation, images preparation, Corresponding author); D.M. Palladino, M. Gaeta, F. Marra, G. Sottili, N. Leicher, G. Mannella, E. Regattieri, B. Wagner, G. Zanchetta (manuscript writing, data and manuscript revision); S. Nomade, A. Pereira ($^{40}Ar/^{39}Ar$ data aquisition); P.G. Albert, C. Manning (LA-ICP-MS data acquisition and elaboration); I. Arienzo, M. D'Antonio, P. Petrosino (Sr isotope data acquisition and elaboration). Supplementary Materials (major and minor elements, trace elements, Sr-Nd isotope composition, $^{40}Ar/^{39}Ar$ ages) can be found at:

https://www.sciencedirect.com/science/article/pii/S0012825221002075#s0200.

ABSTRACT

Accurately reconstructing the scale and timing of dynamic processes, such as Middle-Late Pleistocene explosive volcanism and rapid climatic change, requires rigorous and independent chronological constraints. In this framework, the study of distal volcanic ash layers, or tephra, transported and deposited over wide regions during explosive volcanic eruptions, is increasingly being recognised as a fundamental chronostratigraphic tool for addressing these challenging issues. Here we present a high-resolution distal tephra record preserved in the lacustrine sedimentary succession of the Fucino Basin, central Italy. The investigated record spans the 430-365 ka time interval, covering the entirety of Marine Isotope Stage 11 (MIS 11), and provides important insights into peri-Tyrrhenian potassic explosive volcanism from sources located in central Italy against a backdrop of Mediterranean paleoclimate records. The succession of ash fall events of this time interval is reconstructed through a detailed lithostratigraphic, geochemical and $^{40}Ar/^{39}Ar$ geochronological characterisation of the deposits preserved as discrete layers in the Fucino F4-F5 sediment core. This work is complemented by similarly detailed characterisation of selected proximal pyroclastic units from the peri-Tyrrhenian potassic volcanoes. Geochemical fingerprinting of the tephra deposits by means of their major, minor and trace elements and Sr isotope compositions indicates that all the thirty-two investigated ash layers derived from the peri-Tyrrhenian potassic volcanoes. The stratigraphically continuous succession of the Fucino tephra layers allowed the development of a fully independent, $^{40}Ar/^{39}Ar$ age-constrained, Bayesian age-depth model for the investigated time interval. The age-model allows us to establish modelled ages for the tephra layers within the succession that are not directly dated. The resulting dated tephra record clearly reveals a highly time resolved and previously unparalleled chronicle of explosive activity from the Vulsini, Vico, Sabatini, Colli Albani and Roccamonfina volcanic complexes. Our study provides a benchmark and valuable geochemical and geochronological dataset to be used as a reference for any future development and application of the tephrostratigraphic methods across the central Mediterranean area both during the investigated 430-365 kyr time interval, and deeper in time. This contribution

underlines the importance of integrating proximal and distal sedimentary records to more accurately establish long-term and comprehensive volcanic eruption records.

1. Introduction

Reconstructing the history of explosive volcanism, including the dynamics, timing, and recurrence intervals of eruptions, is a fundamental requirement for understanding the temporal evolution of the volcanic systems and for assessing the related hazards (e.g., Gehrels et al., 2006). The required stratigraphic, chronological and volcanological data are commonly acquired in near-vent (proximal) volcanic areas, where the geological record provides key data for evaluating eruptive and emplacement dynamics, as well as the evolution of the volcanic edifices. Furthermore, the presence of coarse-grained K-rich crystals in proximal deposits from volcanoes fed by highly potassic evolved magmas enables direct and precise radiometric dating using the $^{40}Ar/^{39}Ar$ technique. However, due to the intense volcano-tectonic and sedimentary processes occurring in near-source volcanic regions, many proximal deposits are often buried, inaccessible, or partially eroded. In contrast, intermediate and distal archives, usually located downwind with respect to volcanic sources, can offer a more continuous record of volcanic ash layers (or “tephra”) derived from sustained columns and co-ignimbrite ash clouds, thus enabling the reconstruction of the eruptive history and dynamics of individual volcanic systems and regions (e.g., Paterne et al., 1986, 1988; Newnham et al., 1999; de Fontaine et al., 2007; Dugmore et al., 2013; Giaccio et al., 2014; Leicher et al., 2016, 2019; Albert et al., 2018, 2019; Larsen et al., 2020; Wulf et al., 2020).

The relevance of tephrostratigraphy extends beyond volcanological applications, as these instantaneously deposited layers are also outstanding chronological, stratigraphic and correlation tools for addressing numerous issues in Quaternary sciences (e.g., Lowe et al., 2011). Through diagnostic geochemical, stratigraphic, and chronological features, the volcanic ash, widely dispersed during explosive eruptions and deposited on regional to global scale (Ponomareva et al., 2015), can be recognized and correlated to eruptive events or distal tephra of known ages. This provides an effective and reliable way through which sedimentary archives with co-located tephra can be accurately and precisely dated and correlated over wide regions. Indeed, when combined with high-

precision and accurate radiometric $^{40}Ar/^{39}Ar$ dating and detailed multiproxy series, long and continuous distal tephra successions become the cornerstones for reconstructing both the paleoclimatic change and the history of explosive volcanism (e.g., Thorarinson, 1981a, 1981b; Paterne, 1986, 1988; Dugmore, 1989; Narcisi and Vezzoli, 1999; Wastergard, 2002; Wulf et al., 2004, 2008, 2012; Lane et al., 2013; Giaccio et al., 2015a; Kousis et al., 2018; Leicher et al., 2019; Mannella et al., 2019; Regattieri et al., 2019).

Tephrostratigraphy is most successfully applied when long and continuous sedimentary successions containing well-preserved tephra layers are in a suitable range of distances from sources of recurrent explosive activity. These requirements are fulfilled in the Mediterranean area, particularly in central-southern Italy. Indeed, the recurrent and continuous explosive activity of the peri-Tyrrhenian volcanism, fed by potassic to ultrapotassic magmas (e.g., Peccerillo, 2017), as well as the presence of numerous Quaternary tectonic basins hosting thick sedimentary successions, constitute a unique combination which has allowed the retrieval of extremely rich tephra repositories and, consequently, eruption event stratigraphies. An increasing number of studies on marine (Keller et al., 1978; Paterne et al., 2008; Bourne et al., 2010, 2015; Tamburrino et al., 2012; Insigna et al., 2014; Morabito et al., 2014; Matthews et al., 2015; Petrosino et al., 2015, 2016; D'Antonio et al., 2016), lacustrine (Wulf et al., 2004, 2008; Petrosino et al., 2014a; Giaccio et al., 2015a; Di Roberto et al., 2018; Leicher et al., 2019; Regattieri et al., 2019) and sub-aerial (Giaccio et al., 2012a; Gatta et al., 2016; Donato et al., 2016; Zanchetta et al., 2018; Bini et al., 2020) sedimentary environments of the Mediterranean region have documented this potential. However, despite these recent advances, the tephrostratigraphic framework of the central Mediterranean area is still fragmentary and unexplored, especially for the Middle Pleistocene (~780-130 ka).

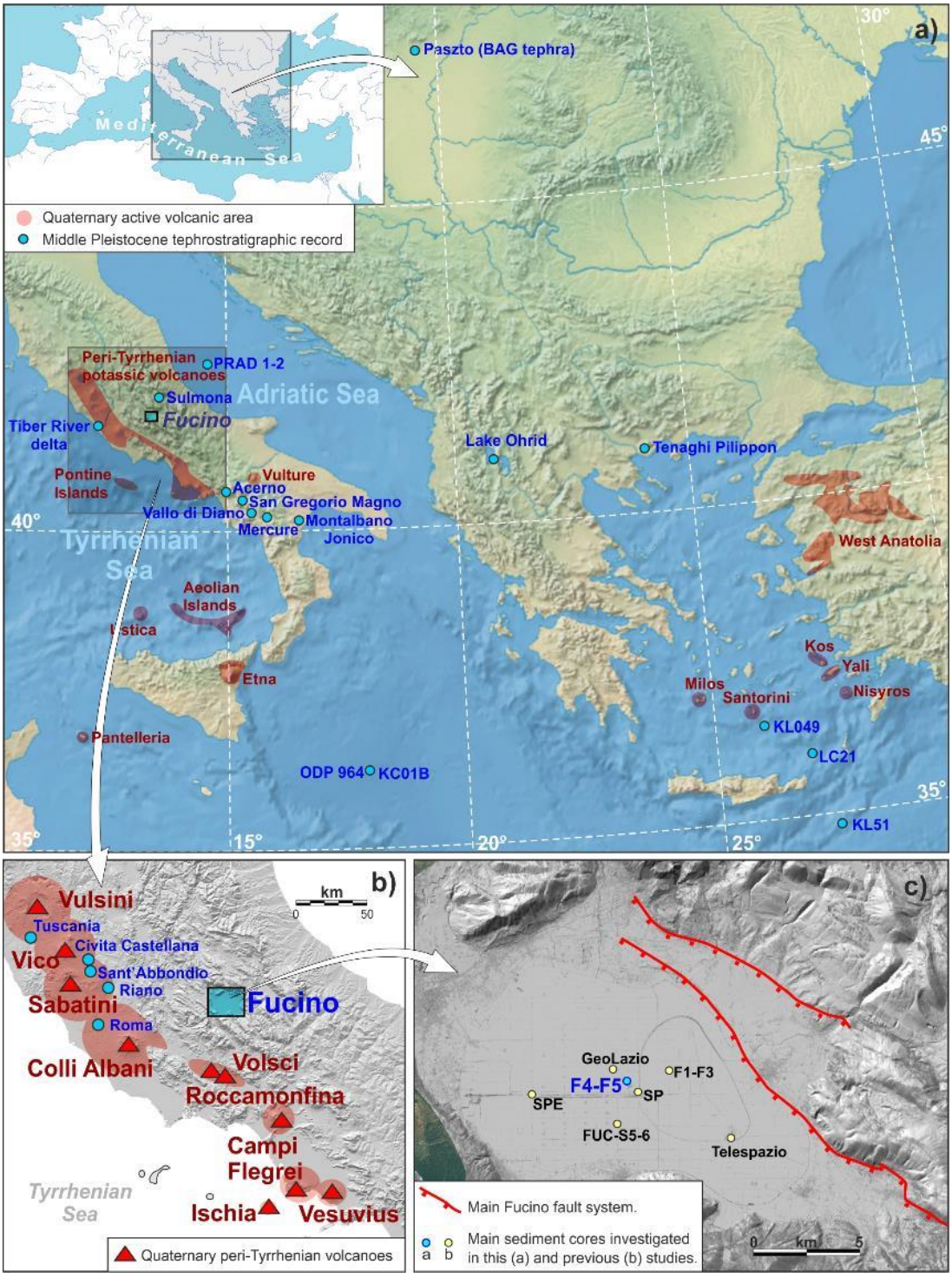

Figure 1. Reference maps. **a**) The Fucino Basin and the peri-Tyrrhenian potassic volcanoes in the context of the Mediterranean Quaternary volcanism and the Middle Pleistocene tephrostratigraphic records (blue dots) cited in the text. **b)** Magnification of the area highlighted in a) showing in detail the location of Fucino Basin relative to the peri-Tyrrhenian potassic volcanic systems of central-southern Italy. **c)** DEM map of Fucino Basin highlighting the location of the F4-F5 core, along with other cores from this lacustrine basin.

Among the lacustrine successions hosted in the Pliocene-Quaternary inter-mountain tectonic basins of the central-southern Apennines (Italy), Fucino's is the most continuous and temporally resolved, with ~900 m of seemingly uninterrupted sedimentary infill, documenting the sediment accumulation since the Lower Pleistocene up to historical times (Cavinato et al., 2002; Giaccio et al., 2015b) and a rich tephra record (Giaccio et al., 2017, 2019; Di Roberto et al., 2018; Mannella et al., 2019; Del Carlo et al., 2020). Three factors make the Fucino Basin unique for reconstructing the eruptive history of the Italian peri-Tyrrhenian potassic to ultra-potassic volcanic activity and improving the central Mediterranean Middle Pleistocene tephrostratigraphic framework: (i) its relatively short distance from the peri-Tyrrhenian volcanoes of central Italy (~70 to ~150 km, Fig. 1a); (ii) its downwind location with respect to these volcanoes, i.e., along the preferential dispersal direction (Fig. 1b); (iii) the occurrence of tephra with K-rich minerals, which facilitates the laser fusion single crystals $^{40}Ar/^{39}Ar$ dating approach.

Recently, Giaccio et al. (2019) reported the presence of ~130 volcanic ash layers in a composite ~98 m-long sediment core (F4-F5) from Fucino Basin spanning the last 430 kyr (Fig. 2) confirming the great potential of this succession to become one of the cornerstones in the tephrostratigraphic network of the entire Mediterranean region. However, so far less than a quarter of these ~130 tephra layers have been stratigraphically, geochemically, and chronologically characterised (Giaccio et al., 2017, 2019). In this paper, we present detailed lithostratigraphic, geochemical and chronological data for the lowermost 28 tephra layers from the F4-F5 core, along with proximal deposits from 5 selected volcanic units of the peri-Tyrrhenian volcanoes, all constrained within the Marine Isotope Stage (MIS) 11 period (i.e., ~430-365 ka). The MIS 11 period is particularly important both in terms of volcanological and tephrochronological investigations. Indeed, it marks the onset of activity at Vico volcano (e.g., Perini et al., 2004; Pereira et al., 2020), thus adding a further volcanic source to the already rich central Mediterranean Middle Pleistocene tephrostratigraphic framework (Fig. 3). Furthermore, currently only very few tephrostratigraphic records spanning the MIS 11 period in the Mediterranean region have been investigated (Leicher et al., 2019; Vakhrameeva et al., 2018, 2021; Fig. 1a). The results of this study are discussed in the general context of the Middle Pleistocene

Mediterranean tephrostratigraphy and that of the central Italy peri-Tyrrhenian explosive volcanism, providing a major contribution towards improved framework of the regional to extra-regional tephrochronology and of the explosive volcanism history. They also provide the basis for developing a robust and independent age-model for the multi-proxy paleoclimate information of the Fucino succession during MIS 11, a key period in the Late Quaternary climatic history, whose analogies with the Holocene have long been debated (e.g., McManus et al., 2003; Tzedakis, 2010).

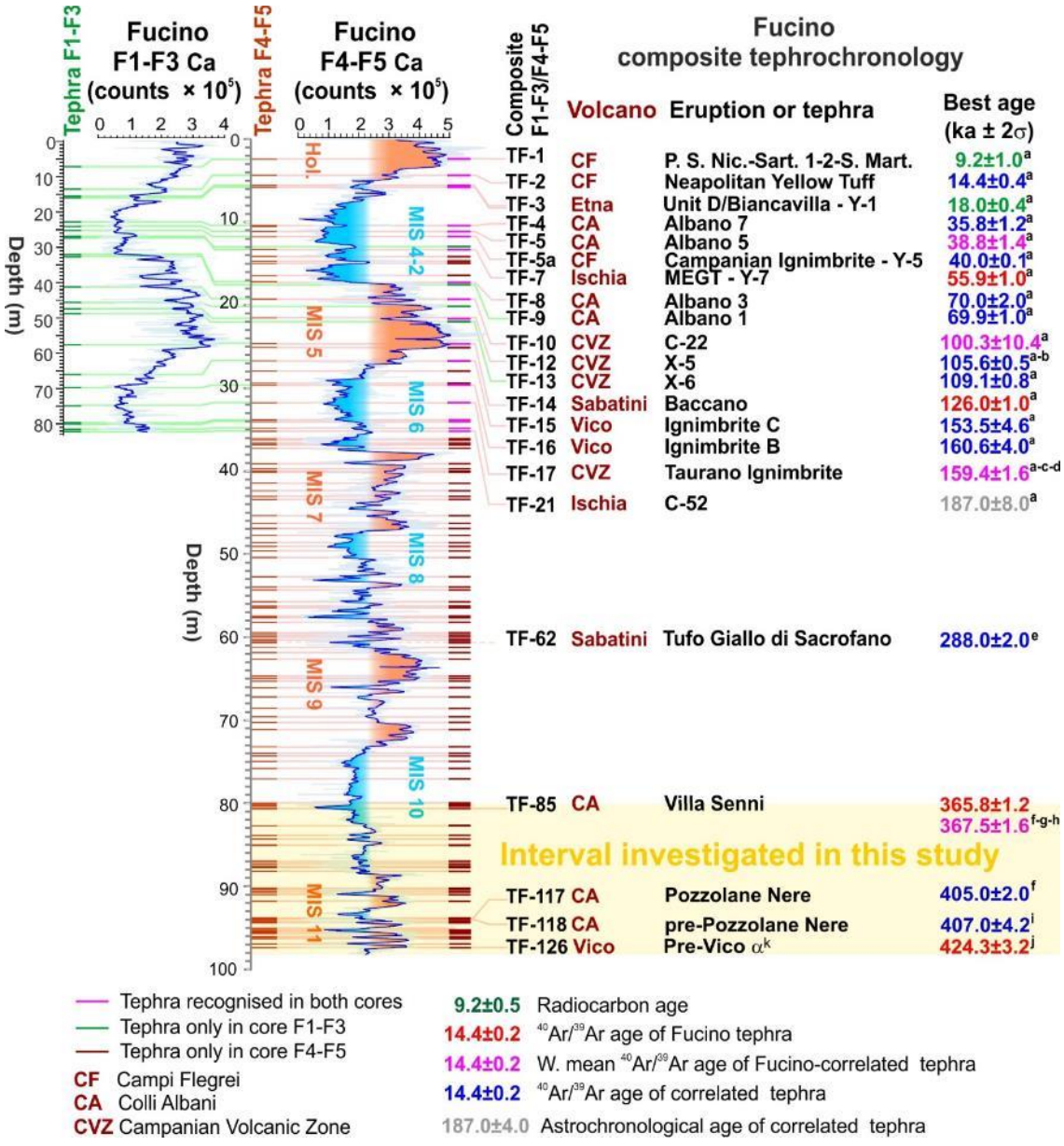

Figure 2. Stratigraphic interval of the F4-F5 Fucino Basin sediment core investigated in this study (modified from Giaccio et al., 2019). $^{40}Ar/^{39}Ar$ ages are recalculated relatively to an age of 1.1891 Ma for the Alder Creek sanidine monitor standard (Niespolo et al., 2017), with the uncertainty expressed at 2σ. $^{40}Ar/^{39}Ar$ ages data source: [a] Mannella et al. (2019 and references therein); [b] Petrosino et al. (2016); [c] Amato et al. (2018); [d] De Vivo et al. (2001); [e] Sottili et al. (2010); [f] Marra et al. (2009); [g] Marra et al. (2019); [h] Giaccio et al. (2012a, 2012b); [i] Pereira et al. (2018); [j] Giaccio et al. (2019).

2. Geological and volcanological setting

2.1. The Fucino Basin

The Fucino Basin (42° 00' 00'' N; 013° 30' 00'' E) is one of the larger inter-Apennine tectonic basins that developed during the extensional phase related to the geodynamic evolution of the Tyrrhenian Basin and central-southern Apennine chain (e.g., Doglioni et al., 1996). Extensional tectonics, mainly acting along E-W, NE-SW and NW-SE oriented high-angle faults, caused the stretching of the mountain chain (e.g., D'Agostino et al., 2001). The opening and evolution of these intermountain basins started from the Late Pliocene-Lower Pleistocene period (Galadini and Galli, 2000; Boncio et al., 2004; Giaccio et al., 2012a; Amato et al., 2014). The Plio-Quaternary tectonic and sedimentary evolution of the Fucino Basin was driven by the *Fucino Fault System* (FFS, Galadini and Galli, 2000; Fig. 1c), which depicts a semi-graben architecture with a thickness of the Plio-Quaternary sedimentary infilling increasing up to ~900 m from west to east toward the depocenter (Cavinato et al., 2002; Patacca et al., 2008).

The Fucino Basin, unlike other intra-Apennine basins, has likely undergone continuous sedimentation (~0,45 mm/yr in average in the central-eastern sector of the basin; Giaccio et al., 2017, 2019; Mannella et al., 2019) since the Plio-Pleistocene and to recent historical times, i.e., potentially covering the last ~2.0 Ma (Giaccio et al., 2015). Indeed, the basin hosted a lake, *Lacus Fucinus*, which was first partially reclaimed during Emperors Claudius and Adrian reigns (1st-2nd century CE), and then completely drained by the Torlonia family at the end of the 19th century.

2.2. The peri-Tyrrhenian potassic volcanic systems

The Quaternary peri-Tyrrhenian volcanic systems of central-southern Italy (hereafter peri-Tyrrhenian potassic volcanoes) belong to the *Roman Comagmatic Region* of Washington (1906),

which comprises the volcanic centers and areas fed by potassic and ultrapotassic magmas extending from southern Tuscany, through Latium and Campania, i.e., from north-west to south-east (Fig. 1a and 1b): Vulsini, Vico, Sabatini and Colli Albani (grouped in the *Roman Province s.s.* by Peccerillo, 2017), Volsci and Roccamonfina (*Ernici-Roccamonfina Province*; Peccerillo, 2017) and the active volcanoes of the so-called *Campanian Volcanic Zone* (Rolandi et al., 2003) or *Campanian Province* (Peccerillo, 2017), including Campi Flegrei, Ischia, Procida and Somma-Vesuvius, also known as the *Neapolitan* volcanoes. Volcanism in the region started at the beginning of the Middle Pleistocene, but the volcanic centers have been active during different time intervals (Fig. 3). Direct evidence, i.e., near-vent deposits, of the oldest activity is documented within the Volsci Volcanic Field (Cardello et al., 2020; Marra et al., 2021), which covers the 760-230 ka interval (Boari et al., 2009; Centamore et al., 2010; Marra et al., 2021). Possible evidence of similarily old activity at Sabatini is provided by distal tephra layers found in Tiber River delta, dated between 750 and 810 ka (Marra et al., 2014). During the ~600-415 ka interval, the Vulsini, Sabatini, Colli Albani, Volsci and Roccamonfina volcanic complexes were all simultaneously active (e.g., Sottili et al., 2004; Rouchon et al., 2008; Boari et al., 2009; Palladino et al., 2010; Soligo and Tuccimei, 2010). Around ~415 ka, volcanic activity also started at Vico volcano (Pereira et al., 2020). Finally, the onset of volcanic activity at Neapolitan volcanoes occurred around ~300 ka (Rolandi et al. 2003), although there is growing evidence from distal settings which reveal significantly older activity in this region, extending as far back as at least 560 ka or perhaps more (e.g., Giaccio et al., 2014; Petrosino et al., 2015; Wagner et al., 2019).

In summary, all the Latium (i.e., Vulsini, Vico, Sabatini, Colli Albani and Volsci) and Roccamonfina volcanoes were active during the interval investigated in this study (i.e., 430-365 ka), consequently there is quite a degree of complexity when trying to establish the volcanic source of distal ash layers deposited during this interval (Fig. 3).

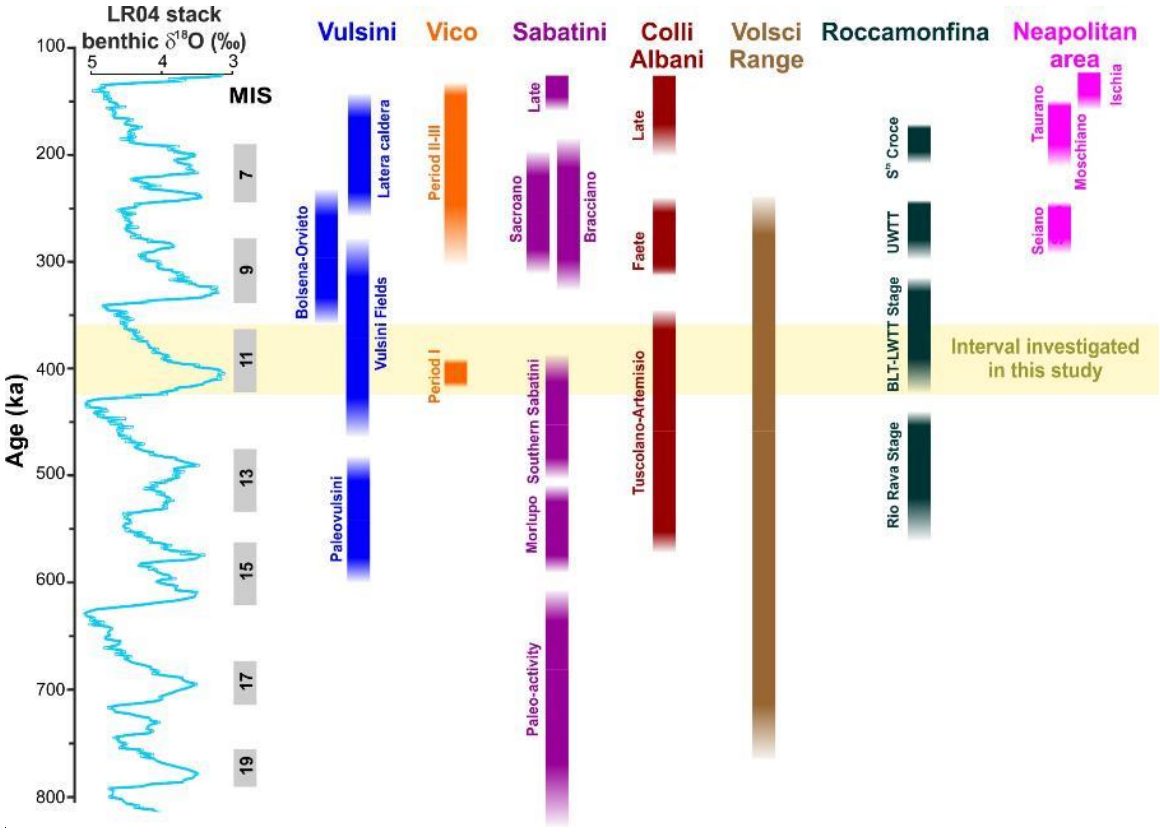

Figure 3. Temporal distribution of the Middle Pleistocene volcanic activity from the peri-Tyrrhenian potassic volcanic systems, plotted against the LR04 benthic stack record (Lisiecki and Raymo, 2005) Data source: Vulsini volcanic district: Palladino et al. (2010), Marra et al. (2020a); Vico: Perini et al. (2004), Pereira et al. (2020); Monti Sabatini volcanic district: Sottili et al. (2010), Marra et al. (2014, 2020b); Colli Albani: Marra et al. (2009); Volsci Volcanic Field: Boari et al. (2009), Centamore et al. (2010), Marra et al. (2021); Roccamonfina: Giannetti (1996a, 1996b), Giannetti and De Casa (2000), Rouchon et al. (2008), Scaillet et al. (2008); Neapolitan area: De Vivo et al. (2001), Rolandi et al. (2003), Belkin et al. (2016), Sbrana et al. (2018).

3. Materials and methods

3.1. Investigated tephra from F4-F5 cores and Roman volcanic province

A summary of the here investigated tephra from Fucino and the Roman volcanic area in this study, and those available in the literature, is reported in Table 1.

Two cores were recovered at the F4-F5 drill site in the central area of the basin (Fig. 1c) and combined to a composite profile 98 meters long. Drilling site selection strategy and recovery procedures are reported in Giaccio et al. (2019). The F4-F5 composite record contains at least 130 tephra (Giaccio et al., 2019; Fig. 2). Based on correlations with tephra layers from the nearby F1-F3 record covering the last 190 kyr (Fig. 2; Giaccio et al., 2017), the geochemical fingerprinting of 11

relevant tephra markers, one direct $^{40}Ar/^{39}Ar$ age determination, and the recognition of a climatic proxy variability linked to glacial-interglacial cyclicity, the sediment succession from F4-F5 was ascribed to the last 430 kyr (Fig. 2; Giaccio et al., 2019). In this paper, we focus on the lowermost ~17-meter-thick interval (between ~80 and ~98 m composite depth) of the F4-F5 core, spanning a ~60 kyr time interval. The interval includes the lowermost tephra layer labelled TF-126, which is directly dated by $^{40}Ar/^{39}Ar$ method at 424.3 ± 3.2 ka (Giaccio et al., 2019), and up to TF-85, correlated to the Villa Senni eruption (i.e., Tufo Lionato) from the Colli Albani volcano (Giaccio et al., 2019), which is dated at 367.6 ± 1.6 ka (Marra et al., 2009; Giaccio et al., 2012b; Fig. 2). This interval contains 32 ash layers, out of which 28 are investigated and presented in this study, while 4 (i.e., TF-85, TF-117, TF-118 and TF-126) were already studied and reported in Giaccio et al. (2019; Table 1).

Table 1. Data acquired in this study and available from literature for each investigated Fucino tephra or proximal volcanic unit.

Tephra	Site/Section	Type of analysis			
		Glass-WDS (EMPA)	Trace elements (LA-ICP-MS)	Sr isotopes (TIMS)	$^{40}Ar/^{39}Ar$
TF-85	F4-F5	Yes[a]	No	Yes[b]	Yes[b]
TF-88	F4-F5	Yes[b]	No	No	No
TF-89	F4-F5	Yes[b]	No	No	No
TF-90	F4-F5	Yes[b]	No	No	No
TF-93	F4-F5	Yes[b]	No	No	No
TF-94	F4-F5	Yes[b]	No	No	No
TF-96	F4-F5	Yes[b]	No	No	No
TF-97	F4-F5	Yes[b]	No	No	No
TF-98	F4-F5	Yes[b]	No	No	No
TF-99	F4-F5	Yes[b]	No	No	No
TF-100	F4-F5	Yes[b]	No	No	No
TF-102	F4-F5	Yes[b]	No	No	No
TF-103	F4-F5	Yes[b]	No	No	No
TF-104	F4-F5	Yes[b]	No	No	No
TF-106	F4-F5	Yes[b]	No	No	No
TF-107	F4-F5	Yes[b]	Yes[b]	Yes[b]	No
TF-108	F4-F5	Yes[b]	No	No	No
TF-109	F4-F5	Yes[b]	No	No	No
TF-110	F4-F5	Yes[b]	No	No	No
TF-111	F4-F5	Yes[b]	Yes[b]	Yes[b]	No
TF-114	F4-F5	Yes[b]	No	No	No
TF-115	F4-F5	Yes[b]	No	No	No
TF-116	F4-F5	Yes[b]	Yes[b]	No	No
TF-117	F4-F5	Yes[a]	No	No	Yes[b]
TF-118	F4-F5	Yes[a]	No	No	No
TF-120	F4-F5	Yes[b]	No	No	No
TF-121	F4-F5	Yes[b]	No	No	No
TF-122	F4-F5	Yes[b]	No	No	No
TF-123	F4-F5	Yes[b]	No	No	No
TF-124	F4-F5	Yes[b]	No	No	No
TF-125	F4-F5	Yes[b]	Yes[b]	No	No
TF-126	F4-F5	Yes[a]	Yes[b]	Yes[b]	Yes[a]
Casale delle Piane	Tuscania	Yes[b]	No	No	No
Castel Broco	Tuscania	Yes[a]	Yes[b]	Yes[b]	No
Vico α (TSP-1)	Tuscania	Yes[b]	No	No	No
TSP-2	Tuscania	Yes[b]	No	No	No
TSP-3	Tuscania	Yes[b]	No	Yes[b]	No
TSP-4	Tuscania	Yes[b]	No	No	No
Riano R-1	Riano	Yes[b]	Yes[b]	Yes[b]	Yes[c]
Pozzolane Nere	Rome	Yes[d]	No	Yes[f]	Yes[b]

Vico β	Vignanello	Yes[e]	Yes[b]	No	Yes[e]
Vico α type locality	Viterbo	Yes[e]	Yes[b]	No	Yes[e]

[a] Giaccio et al. (2019); [b] This study; [c] Marra et al. (2018); [d] Marra et al. (2009); [e] Pereira et al. (2020); [f] Gaeta et al. (2006).

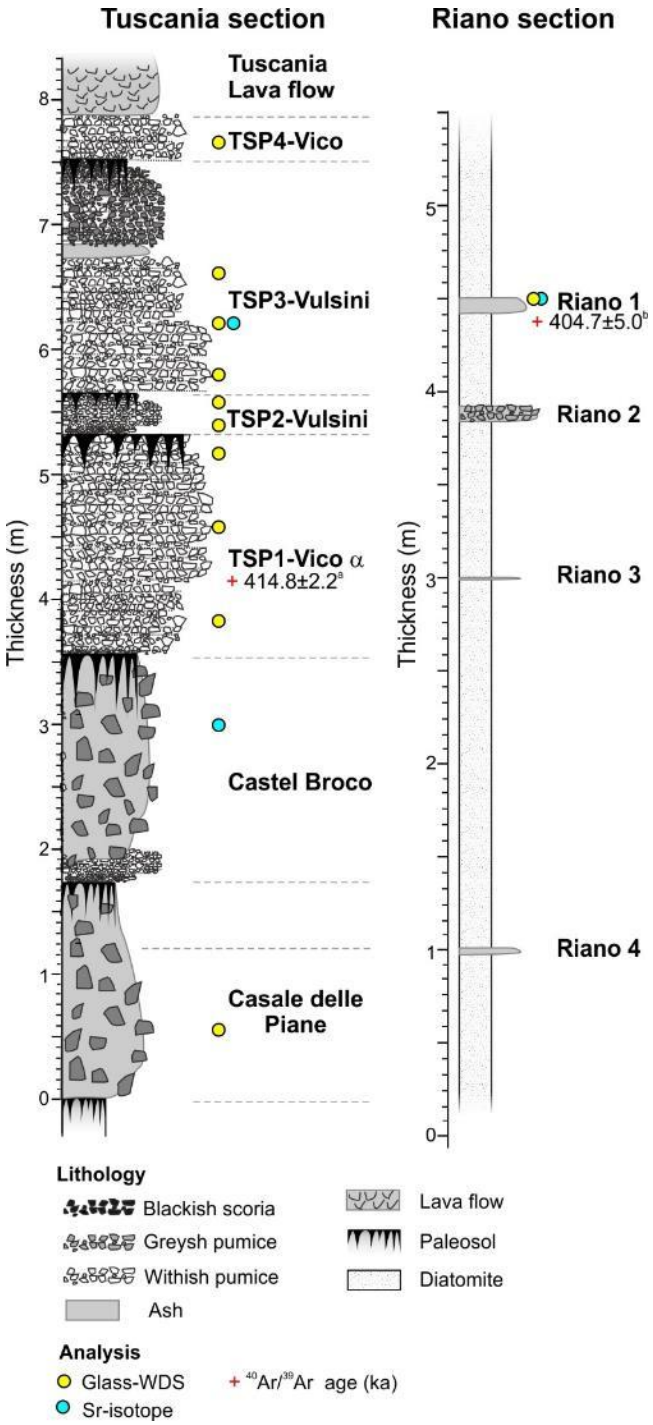

Figure 4. Reference stratigraphic successions outcropping at Tuscania-San Pietro (southern Vulsini) and Riano (eastern Sabatini) (see Fig. 1b for locations). The stratigraphic position of the samples used for geochemical analyses in this study are also shown. $^{40}Ar/^{39}Ar$ dating: [a] Pereira et al. (2020); [b] Marra et al. (2018).

In order to improve the reference geochemical dataset required for establishing reliable tephra correlations of the Fucino tephra, we re-examined the key pyroclastic succession at Tuscania-San Pietro (southern Vulsini; Cioni et al., 1987; Palladino et al., 1994, 2010; 42° 24' 43.32'' N, 011° 52' 45.13'' E; Figs. 1b, 4) and performed new analyses on four pumice fall units (TSP#). Of these, TSP-1 is correlated to the Vico α Plinian fall marker (Cioni et al., 1987), while TSP-2 and TSP-3 are referred to the Plinian activity of the Vulsini Fields (although with undefined source locations). TSP-3 in particular is tentatively correlated to the Pumice Fall 0 (PF-0) of Turbeville (1992, 1993) dated at 399.8 ± 18.0 ka (Turbeville, 1992; age recalculated according to the Alder Creek sanidine at 1.1891 Ma). We stress that this attribution is just putative until it can be corroborated by stratigraphic and geochemical characterisation of proximal PF-0 products collected in the type locality. Finally, the Plinian fall horizon TSP-4 is attributed to Vico Plinian activity, although with an uncertain correlation. The TSP succession also includes the Casale delle Piane and Castel Broco major pyroclastic flow deposits (investigated also in the present study, see below) and is topped by the Tuscania lavas (Palladino et al., 1994, 2010), which are broadly coeval with the Quarticciolo lavas (356 ± 15 ka; Funicello et al., 2012) outcropping in other nearby localities.

To supplement the major element datasets for Vico volcano presented in Pereira et al., (2020), we provide trace element glass analysis of selected proximal Vico α and β samples collected from Viterbo (Vico α; Lower fall [VT-Base Vico α] and Upper fall [VT-1A, VT-1B and VT-1C]) and Vignanello (Vico β; [VIG-3]) sections.

With the same aim, we also analysed the Riano R-1 tephra (Fig. 4), found within a lacustrine (diatomite) succession outcropping along the Flaminia road (42° 05' 24.06" N, 012° 31' 57.43'' E), north of Rome (Fig. 1b), and dated at 404.7 ± 5.0 ka by Marra et al. (2018). The Riano R-1 tephra is a 10-cm-thick, coarse to fine blackish ash layer, likely representing a relatively distal occurrence of a major fall deposit, of uncertain, Sabatini or external (i.e., from another Latium volcano), source area. The Riano diatomite succession contains three additional tephra layers (R-2, R-3, and R-4;

Fig. 4). However, while R-2 is a 10-cm-thick layer of dense scoria lapilli, likely deriving from a minor local (i.e., Sabatini) Strombolian eruption, the ash layers R-3 and R-4 did not yield fresh glass suitable for geochemical analyses.

Finally, in order to acquire a new $^{40}Ar/^{39}Ar$ age for the Colli Albani Pozzolane Nere caldera-forming eruption, we sampled an exposure in Rome City (41° 50' 44.74'' N, 012° 28' 40.56'' E). Indeed, since we could not establish which of the two different monitor standards was used for determining the previous set of $^{40}Ar/^{39}Ar$ ages for this deposit (Karner and Renne, 1998), the existing age of 407 ± 2 ka can not be recalculated with respect to the current monitor standard improved ages, and thus does not allow direct comparisons.

3.2. EPMA-WDS

Major and minor element compositions were determined on micro-pumice fragments and/or glass shards of the 28 tephra layers from the F4-F5 record (Table 1), which were labelled following the same criterions adopted in previous studies of the F1-F3 and F4-F5 cores (Giaccio et al., 2017, 2019), and for the above described five proximal samples (Table 1). To have a good statistical expression of the tephra composition and their geochemical variability, we aimed at analysing at least 10-15 shards/micro-pumices from each tephra. However, in some cases (i.e., TF-96, TF-100, TF-103, TF-104, TF-123 and TF-124), the dense microlitic texture of the juvenile clasts or the incipient alteration of the glass prevented us to acquire such a satisfactory number of analyses. Neverthless, also in those cases, the relative homogeneity and/or geochemical consistency of the analysed glasses indicate a satisfactory reliability and representativity of the compositional data for tephrochronological purposes. A synthesis of all acquired data for each of the 28 tephra and 4 proximal pyroclastic units can be found in Table 1, along with information relative to previously investigated tephra from F4-F5 core and proximal volcanics.

Polishing and carbon coating of the epoxy slides were performed for electronprobe microanalyser wavelength dispersive spectroscopy (EPMA-WDS) analysis at the *Istituto di Geologia Ambientale e Geoingegneria* of the Italian National Research Council (IGAG-CNR, Rome). Major and minor elements quantitative analyses were performed with a CAMECA SX-50 EPMA equipped with five-

wavelength dispersive spectrometers (WDS), operating at 15 kV accelerating voltage, 15 nA beam current, 10 μm defocused beam diameter - to limit Na mobilization and loss - and 20 s element counting time for all elements. Wollastonite (Si and Ca), corundum (Al), periclase (Mg), magnetite (Fe), rutile (Ti), orthoclase (K), jadeite (Na), phlogopite (F), potassium chloride (Cl), barite (S), F-apatite (P) and metals (Mn) were used as calibration standards. The Kakanui augite and Rhyolite RLS132 glasses from the United States Geological Survey were measured prior to each analytical run to evaluate the accuracy of the electron-microprobe analysis. Obtained mean values are shown in Supplementary Dataset-4 (SD-4), along with the % difference between each oxide with respect to the recommended values. The mean values show ~0.5% difference for SiO_2, ranging in concentrations from 50 wt% to 77 wt%, <0.2% for oxides in the 15-16 wt% concentration range, 3.3-1.8% for oxide concentrations between 5 and 12 wt%, 4.2-0.1% for oxides in the 2-5 wt% range, up to 5.7% for the oxides ranging from 0.2 wt% to 2 wt% and up to 39% for minor elements (i.e., oxides with concentrations <0.2 wt%).

In order to test the quality and reproducibility of our data, we also performed a series of analyses on the MPI-DING glass standards of Jochum et al. (2006) and a rhyolitic Lipari obsidian (i.e., ID3506; Kuehn et al., 2011). The results show <1.1% difference for SiO_2, ranging between 46 wt% and 77 wt% range, 2.8-0.2% for oxides ranging from 15 wt% to 27 wt%, 4.0-1.0% for oxides in the 5-13 wt% range, 5.2-0.6% for oxides ranging from 2 wt% to 5 wt%, 8.1-1.5 for oxides in the 0.2-2 wt% range and up to 62% for minor elements (SD-4).

Data reduction was carried out using the PAP correction, while data processing was performed in Microsoft Excel. We adopted 93 wt% as a threshold for the measured total: analyses with total values lower than 93 wt% were discarded. All compositional data are shown as oxide weight percentages (wt%) in the Total Alkali vs Silica (TAS; Le Maitre et al., 2002) classification diagram - as well as bi-plots diagrams - with total iron (FeOt) expressed as FeO and normalized to 100% on a volatile-free basis (i.e., excluding Cl, SO_3 and F volatiles) for correlation purposes. Collected data are all reported in Supplementary Dataset-1 (SD-1), along with secondary standards and MPI-DING measured values.

3.3. LA-ICP-MS

Trace element analyses were conducted on volcanic glasses from five Fucino tephra units, i.e., TF-107, TF-111, TF-116, TF-125, and TF-126, and four proximal-medial pyroclastic deposits, i.e., the Castel Broco unit, from the above described Tuscania-San Pietro section at Vulsini (Fig. 4), Vico α and β, and the Riano R-1 Tephra (unknown source) (Table 1). These samples have been selected (i) to test if compositions of the trace elements and/or the ratios of incompatible trace elements allow distinguishing of tephra layers with similar major element composition (e.g., TF-107, TF-111, TF-126, Castel Broco, Riano R-1), and (ii) to obtain the complete geochemical composition of the products form the two major eruptions of Vico Period I (i.e., Vico α and Vico β), likely dispersed over wide areas of the central Mediterranean and thus representing potential tephra markers for this region. The analysis was performed using an Agilent 8900 triple quadrupole ICP-MS (ICP-QQQ) coupled to a Resonetics 193nm ArF excimer laser-ablation at the Department of Earth Sciences, Royal Holloway, University of London. Full analytical procedures used for volcanic glass analysis are reported in Tomlinson et al. (2010). Spot sizes of 25 and 34 µm were used depending on the sample vesicularity and/or size of glass surfaces available for analysis. The repetition rate was 5 Hz, with a count time of 40 s on the sample, and 40 seconds on the gas blank to allow the subtraction of the background signal. Typically, blocks of eight or nine glass shards and one MPI-DING reference glass were bracketed by the NIST612 glass adopted as the calibration standard. The internal standard applied was ^{29}Si (determined by EPMA-WDS analysis). In addition, MPI-DING reference glasses were used to monitor analytical accuracy (Jochum et al., 2006). LA-ICP-MS data reduction was performed in Microsoft Excel, as outlined in Tomlinson et al. (2010). Accuracies of LA-ICP-MS analyses of the MPI-DING reference glasses, ATHO-G and StHs6/80-G, were typically ≤ 5% for most elements measured. These measurements are provided in Supplementary Dataset-2 (SD-2), along with those of selected proximal eruption units and the full Fucino dataset.

3.4. Isotopic composition of strontium

Strontium (Sr) isotope compositions were determined on glass shards/pumices and mineral phases (i.e., feldspar, leucite, and pyroxene) from six selected samples, as summarised in Table 1.

The rationale underlying the selection of these samples is similar to that for LA-ICP-MS analysis, i.e., obtaining a further geochemical characterisation of the tephra from some major eruptions of the peri-Tyrrhenian volcanoes during MIS 11 period, in order to have, if any, an additional fingerprinting tool for strengthening their recognition/discrimination in distal settings. The variable fractions were handpicked under a binocular microscope. When possible, the cleanest crystals were selected, avoiding the presence of glass rinds attached. Before chemical dissolution, glass shards and pumices were acid leached three to five times to reduce alteration effects. Leaching was carried out each time by placing the beakers containing samples and high-purity 6 N HCl on a hot plate for 10 min. Feldspar and pyroxene separates coated by a thin film of glass were leached with high-purity 7% HF for 10 min in an ultrasonic bath. After leaching, samples were rinsed with Milli Q® H_2O and dissolved with high-purity HF–HNO_3–HCl mixtures. Sr was separated from the matrix through conventional ion-exchange procedures at the clean chemistry laboratory of the *Istituto Nazionale di Geofisica e Vulcanologia, Osservatorio Vesuviano*. Sr blank was on the order of 0.3 ng during chemistry processing.

Sr isotopic compositions were determined by thermal ionization mass spectrometry (TIMS) at DiSTAR (Naples, Italy), using a Thermo Scientific Triton Plus mass spectrometer equipped with one fixed and eight adjustable Faraday cups. $2\sigma_{mean}$, i.e., the standard error with N = 150, was better than ± 0.000008 for all Sr measurements. Measured $^{87}Sr/^{86}Sr$ ratios were normalized for within-run isotopic fractionation to $^{88}Sr/^{86}Sr = 8.37521$. During the period of isotopic data collection, replicate analyses of NIST–SRM 987 ($SrCO_3$) international reference standard were carried out to check for external reproducibility at 2σ level (where σ is the standard deviation of the standard results, according to Goldstein et al., 2003). No correction has been applied to the measured $^{87}Sr/^{86}Sr$ values, since the mean measured value of $^{87}Sr/^{86}Sr$ for NIST–SRM 987 standard was 0.710248 ± 0.000006 (2σ, N = 17), which is indistinguishable from the recommended value of $^{87}Sr/^{86}Sr = 0.710248$ (Thirlwall, 1991).

3.5. $^{40}Ar/^{39}Ar$ geochronology

In order to improve the chronology of the investigated interval of the F4-F5 record, three new $^{40}Ar/^{39}Ar$ dating were performed on TF-85 and TF-117 samples, correlated to to the Villa Senni and Pozzolane Nere eruptions, respectively (Giaccio et al., 2019), and on a sample of the proximal Pozzolane Nere (PN) unit collected from the above-mentioned outcrop in Rome City (Table 1). Samples were sieved and cleaned in distilled water, while undesirable magnetic crystals were removed by magnetic separation. Approximately thirty crystals were selected from each sample and loaded into an aluminium disk in three individual pits. All crystals from the individual samples were irradiated for 120 min in the Cd-lined, in-core CLICIT facility of the Oregon State University TRIGA reactor (IRR CO002). Interference corrections were based on the nucleogenic production ratios given in Renne et al. (2015). After irradiation, samples were transferred into a copper sample holder and loaded individually into a differential vacuum Cleartan© window. All measurements were done in the LSCE $^{40}Ar/^{39}Ar$ facility (France). Detailed analytical procedures can be found in Nomade et al. (2010). Single crystals were fused individually using a 25 Watts Synrad CO_2 laser at about 10 to 15 % of the nominal power. Extracted gas was then purified for 10 min by two hot GP 10 and two GP 50 getters (ZrAl). Argon isotopes (^{40}Ar, ^{39}Ar, ^{38}Ar, ^{37}Ar and ^{36}Ar) were successively measured using a VG 5400 mass spectrometer equipped with an electron multiplier (Balzer SEV 217 SEN) coupled with an ion counter. Each argon isotope measurement consisted of 20 cycles of peak-hopping. Neutron fluence J for each sample was calculated-using co-irradiated Alder Creek sanidine standard (ACs at 1.1891 Ma; Niespolo et al., 2017) and the K total decay constant of Renne et al. (2011). This calibration produces ages independent of the astronomical tuning. J-values are the followings: TF-85 (Villa Senni) = 0.00053020 ± 0.00000053, TF-117 (Pozzolane Nere) = 0.00052950 ± 0.00000053 and PN = 0.00053260 ± 0.00000059. Mass discriminations were monitored by analysis of air pipette throughout the analytical period, and relative to a $^{40}Ar/^{36}Ar$ ratio of 298.56 (Lee et al., 2006). Procedural blank measurements were achieved after every two or three unknown samples. For 10 min times of isolation typical backgrounds are about 2.5-4.0 x 10^{-17} and 5.0 to 7.0 x 10^{-19} moles for ^{40}Ar and ^{36}Ar, respectively.

3.6. Age-depth modelling

The age model and corresponding 95%-confidence interval were both obtained using the Bacon software (Blaauw and Christen, 2011) written in the open-source statistical environment R (R Core Team, 2016).

To accommodate large differences in the sedimentation rate occurring during the investigated interval, we split the record into three sedimentary zones A to C. Zone boundaries are defined through a preliminary evaluation of changes in sedimentary facies and on the availability of the dated points. The definition of sedimentary facies is based on the analysis of the composite profile derived by stacking consecutive core images acquired by the ITRAX core scanner (Giaccio et al., 2019). For each interval, the mean sedimentation rate is estimated by dividing the thickness of the interval for the time span elapsed between the deposition of the youngest and oldest dated tephra layers bracketing the interval, or at least, a large part of it. In the case of multiple dated layers in close stratigraphic position, we choose those featuring the most accurate dating. Sedimentary intervals and estimated mean sedimentation rates are as follows:

- Zone A: 80.520 – 91.810 m, 33.33 cm/kyr
- Zone B: 91.810 – 95.950 m, 30.30 cm/kyr
- Zone C: 95.950 – 98.100 m, 4.76 cm/kyr

These zones do not represent homogeneous sedimentary facies; however, they represent the most accurate approximation of long term (>4 kyr) changes in mean sedimentation rate that can be made based on currently available tephrochronological information.

4. Results

4.1. Depositional and sedimentological features of the Fucino tephra succession

Tephra horizons in the Fucino lacustrine succession occur as discrete layers of ash with variable thickness (Table 2) and grain-size, well separated from each other by fine lake sediments (marl) (Fig. 5). Despite a slight bioturbation and/or mechanic disturbance related to the drilling operation (Fig. 5),

each tephra layer shows distinctive lithological (i.e., grain-size, shape, colour, vesicularity pattern and textural features of the juvenile clasts, type, and assemblage of the crystal and lithic components) and geochemical (glass-WDS major element composition) features. These circumstances are verified also in the case of closely clustered tephra layers, i.e., each layer forming the cluster presents its own distinctive lithological and geochemical characteristics with respect to the adjacent ones. In some cases, tephra layers are also characterised by a sharp lower boundary and by an upsection lithological zonation (e.g., TF-126; Fig. 5). These features undoubtedly indicate that tephra layers are undoubtedly primary fallout deposits and that post-depositional processes are negligible and did not affect the integrity of the tephra succession.

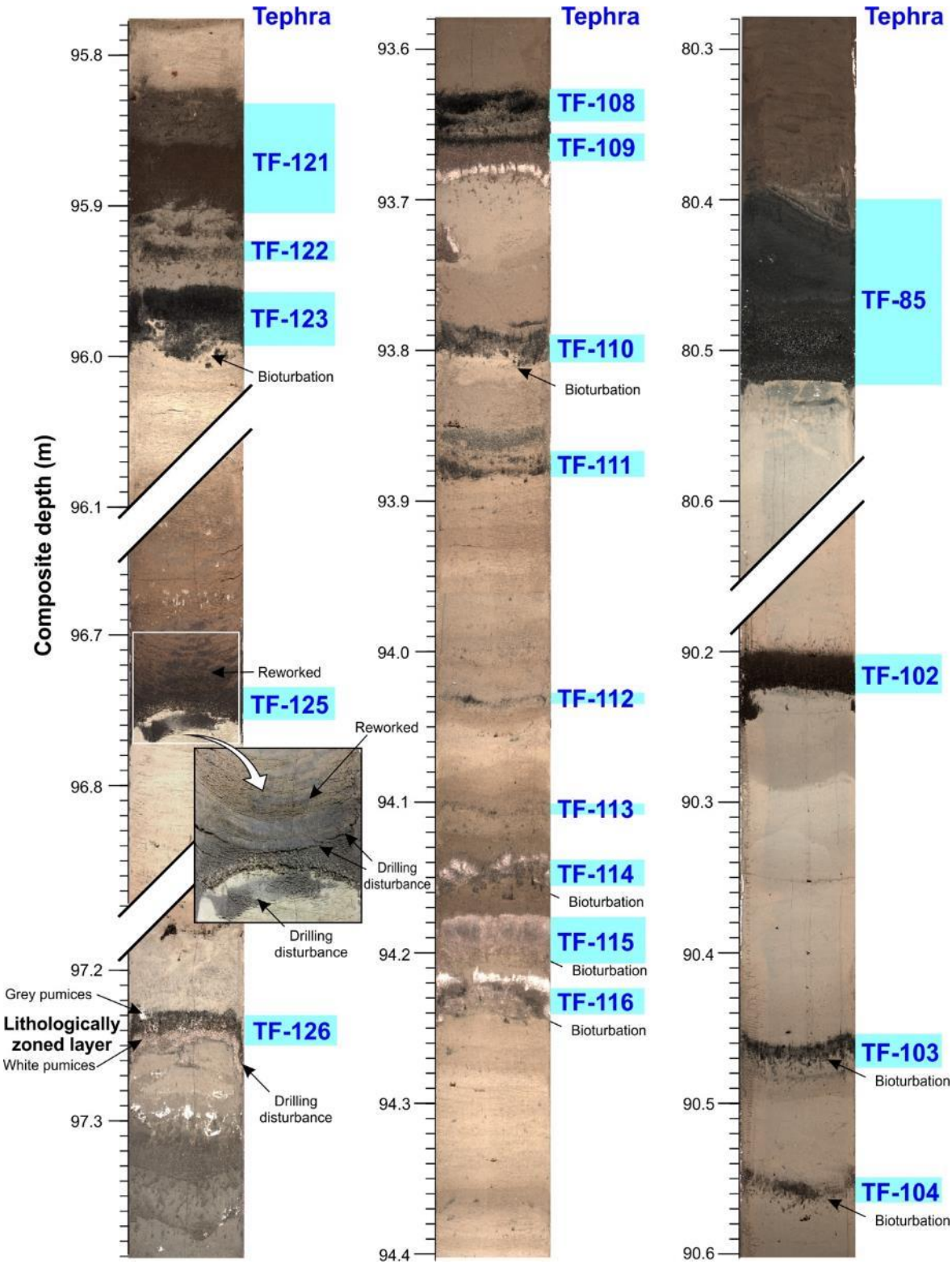

Figure 5. Representative, selected intervals of Fucino core sections, showing the general sedimenological and lithological features of the investigated tephra.

4.2. Tephra lithology and glass composition

4.2.1. Data summary

The thickness and main lithological features of the 32 Fucino tephra and proximal volcanic units are summarized in Tables 2 and 3, respectively. Full glass compositions are provided in Supplementary Dataset-1 (SD-1), while their classification according to the total alkali vs silica (TAS) diagram (Le Maitre et al., 2002) is shown in Figure 6. Description of the geochemistry (i.e., major, minor and trace elements and Sr-isotopes) of the volcanic glasses is given in the following sections.

Table 2. Main lithological, mineralogical, and geochemical features of the 365-430 ka F4-F5 Fucino tephra.

Tephra	Thickness (cm)	Composite depth (m)	Core section and depth (cm)	CG	Lithology			Rock type
					Juvenile clasts	Loose crystals	Lithic content	
TF-85*	14.00	80.520	F5-49 74-88	*ND*	Black-brown scoria	Lc>bmca>cpx	Poor	K-f
TF-88	1.25/2.00	83.770	F4-51 131-133/ F5-51 65-66	CG-2	White pumice and grey-brown scoria	Kfs>cpx>bmca	Poor	ph-tr
TF-89	2.00	84.168	F5-51 107-109	CG-2	Grey scoria	Kfs>cpx>bmca	Poor	Ph
TF-90	2.00	84.388	F5-51 130-131	CG-2	Black-grey scoria	Kfs>cpx>bmca	Rich	Tr
TF-93	0.90	86.140	F4-53 51.3-52.2/ F5-52 149-150	CG-2	White pumice	Kfs>cpx	No	tph-ph
TF-94	0.75	86.853	F4-53 53.6-54.6	CG-2	White pumice	Kfs	No	ph-tr
TF-96	1.20	87.166	F4-53 85-86.2	CG-2	White pumice and grey scoria	Kfs>cpx	Poor	Ph
TF-97	2.50	87.470	F4-53 110-112	CG-2	Grey scoria	Kfs>bmca	Poor	Lat
TF-98	1.00	87.575	F4-53 119-120	CG-2	Grey scoria and whitish pumice	Kfs>bmca	Poor	lat-tph-ph-tr
TF-99	1.00	87.677	F4-53 128-129	CG-3	Highly vesicular white pumice and brown scoria	Kfs>bmca	Poor	K-tr-rhy
TF-100	6.75	88.045	F5-54 0-4.5	CG-1	Dense black scoria	Lc	Poor	K-f
TF-102	2.00	90.230	F4-55 58-60/ F5-54 125-126	CG-2	Poorly vesicular black scoria	Kfs>Lc>bmca	Poor	t-pht
TF-103	3.00	90.485	F4-55 83-86/ F5-54 133-134.2	CG-2	Poorly vesicular black scoria	Kfs>Lc>bmca	Poor	pht-tph
TF-104	2.00	90.560	F4-55 92-93/ F5-54 142-144	CG-2	Poorly vesicular grey scoria	Kfs>Lc>bmca	Poor	pht-tph
TF-106	1.40	90.860	F4-55 123-124.4	CG-2	Poorly vesicular grey scoria	Kfs>Lc>bmca	Rich	trb-pht-tph-sho
TF-107	2.00	91.620	F4-56 29-31/ F5-55 57.2-59	CG-2	Moderately vesicular whitish pumice and poorly vesicular greyish scoria	Kfs>bmca>cpx	Rich	ph-tr
TF-108	3.00	93.650	F5-56 110-113	CG-1	Dense, leucite-bearing black scoria	Lc	No	K-f
TF-109	3.00	93.690	F5-56 114-117	CG-3	Highly vesicular white pumice and greyish scoria	Kfs>bmca	Poor	K-ph-tr-rhy
TF-110	2.00	93.810	F5-56 126-128	CG-2	Highly vesicular white pumice and greyish scoria	Kfs>bmca	Poor	ph-tr
TF-111	3.00	93.885	F4-57 47-50	CG-2	Highly vesicular white pumice	Kfs>bmca	Very poor	ph-tr
TF-114	2.00	94.166	F4-57 77-79	CG-3	Highly vesicular white pumice and greyish scoria	Kfs>bmca>cpx	Poor	K-tr-rhy
TF-115	2.00	94.211	F4-57 81-83	CG-3	Highly vesicular white pumice	Kfs>bmca>cpx	Poor	K-tr-rhy
TF-116	2.00	94.251	F4-57 85-87	CG-3	Highly vesicular white pumice	Kfs>bmca>cpx	Poor	K-ph-tr-rhy
TF-117*	9.00	95.130	F4-57 151-152/ F5-57 0-7	*ND*	Poorly vesicular leucite-bearing black scoria	Lc>cpx	Poor	K-f
TF-118*	5.50	95.290	F5-57 16-23	*ND*	Poorly vesicular leucite-bearing black scoria	Lc	Poor	K-f
TF-120	2.00	95.540	F5-57 45-47	CG-2	Highly vesicular white pumice	Kfs>bmca	Very poor	ph-tr
TF-121	8.00	95.910	F5-57 77-85	CG-2	Poorly vesicular greyish-brownish scoria	bmca>Kfs>Lc	Poor	tph-ph-tr
TF-122	1.00	95.930	F5-57 85-86	CG-2	Dense, leucite-bearing brown scoria	Kfs>bmca>Lc	Poor	tph-ph-lat-tr
TF-123	5.50	96.005	F5-57 87-94	CG-2	Poorly vesicular black scoria	Lc>cpx>Kfs> bmca	Very rich	pht-tph
TF-124	0.75	96.155	F5-57 107-110	CG-2	Poorly vesicular black scoria and whitish pumice	Lc>cpx>bmca	Rich	Sho
TF-125	3.50	96.775	F5-58 16-19.5	CG-3	Highly vesicular white pumice	Kfs>bmca>cpx>op	Poor	K-ph-tr-rhy
TF-126*	2.00	97.250	F5-58 64-66	*ND*	Highly vesicular white (base) and honey (top) pumice	Kfs>bmca>cpx>op	Poor	ph-tr

*=EPMA data in Giaccio et al. (2019); *ND*=Not determined in this study. Rock type abbreviations: K- = potassium- (suffix); f = foidite; ph = phonolite; tr = trachyte; tph = tephriphonolite; lat = latite; rhy = rhyolite. Mineral abbreviations: Kfs = K-feldspar; bmca = black mica; cpx = clinopyroxene; Lc = leucite; op = opaques. CG = compositional group (see Fig. 6).

Table 3. Geochemical and mineralogical data summary of the investigated proximal units.

Outcrop/ Location	Coordinates	Unit	Volcanic source	Lithology		Rock type
				Juvenile clasts	Minerals	
Tuscania-San Pietro	42° 24' 43.32'' N – 11° 52' 45.13'' E	Casale delle Piane	Vulsini	Highly vesicular dark grey, Kfs+bmca-bearing scoria	Kfs>bmca	Ph
		Vico α	Vico	Highly vesicular white, Kfs+bmca-bearing pumice and grey scoria	Kfs>>bmca>cpx	K-tr-rhy
		TSP-2	Vulsini	Moderately vesicular grey Kfs-bearing pumice	Kfs>cpx	Ph
		TSP-3 (PF-0?)	Vulsini	Highly vesicular white, Kfs+bmca-bearing pumice	Kfs>bmca>cpx	Ph
		TSP-4	Vico	Reddish (thermally altered) Kfs-bearing pumice	Kfs>cpx	K-tr-rhy
Riano	42° 05' 24.06" N – 12° 31' 57.43'' E	Riano R-1	*ND (Sabatini?)*	Blackish ash	Kfs>cpx>lc	Ph-tph-lat
Rome	41° 50' 44.74'' N – 12° 28' 40.56'' E	Pozzolane Nere	Colli Albani	Lc-bearing black scoria	Lc>cpx>bmca	K-f

ND=undetermined. Rock type abbreviations: K- = potassium- (suffix); f = foidite; ph = phonolite; tr = trachyte; tph = tephriphonolite; lat = latite; rhy = rhyolite. Mineral abbreviations: Kfs = K-feldspar; bmca = black mica; cpx = clinopyroxene; lc = leucite.

4.2.2. Major and minor elements

In the TAS diagram, the analysed tephra layers can be conveniently divided into three compositional groups (CGs; see also Table 2 for a classification summary). CG-1 (green area in Fig. 6) comprises of two tephra layers (i.e., TF-100 and TF-108), plus the previously investigated TF- 85, TF-117 and TF-118 layers (Giaccio et al., 2019), all displaying a K-foiditic composition. CG-2 (light-orange area) includes twenty-one F4-F5 tephra, plus two proximal units (TSP-2 and TSP-3), and the Riano R-1 tephra, and are classified as potassic phonotephrites, tephriphonolites, phonolites, latites and trachytes, each being often variable in composition and covering two or more fields of the TAS diagram (Fig. 6). Finally, CG-3 (blue area) includes six F4-F5 tephra (i.e., TF-99, TF-109, TF-114, TF-115, TF-116 and TF-125), and two proximal units (TSP-1/Vico α and TSP-4), which are phonolites-trachytes-rhyolites, trachytes-rhyolites, and rhyolites. Although partially overlapping with CG-2 (Fig. 6), CG-3 tephra layers are clearly distinguishable owing to their distinctive rhyolitic components.

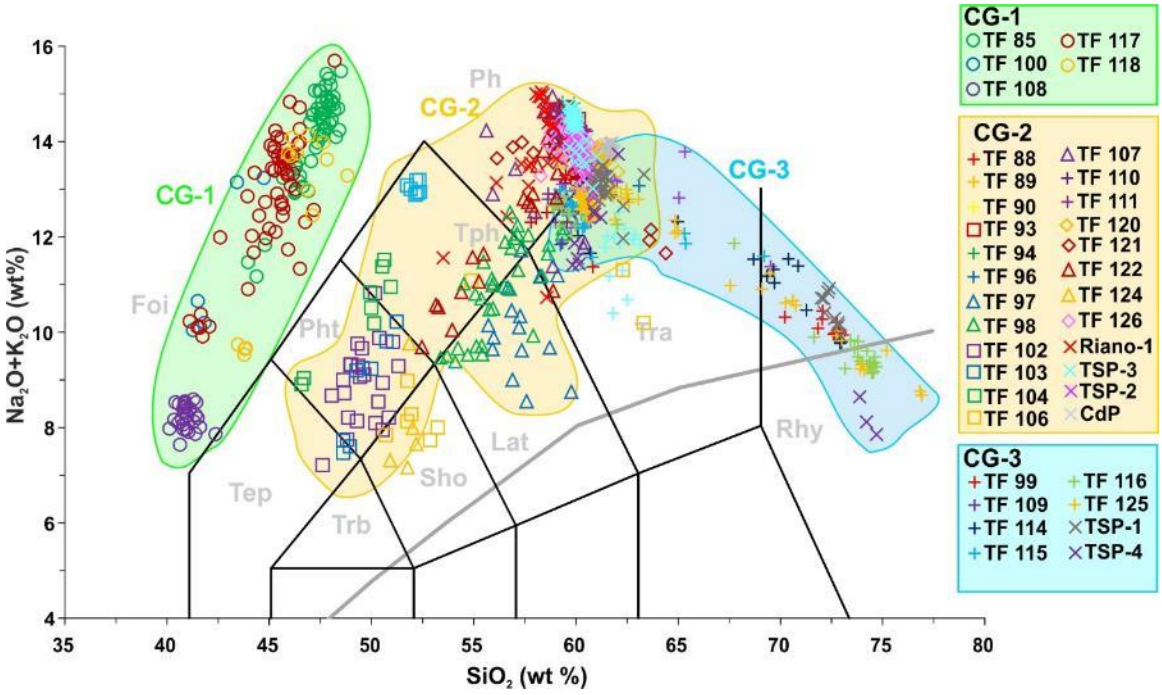

Figure 6. *Total alkali vs silica* (TAS) classification diagram (Le Maitre et al., 2002). The thirty-two F4-F5 MIS11 tephra and the proximal pyroclastic units plot in three compositional groups (CG-1, CG-2 and CG-3). Data source: glass-WDS of TF-85, TF-117, TF-118 and TF-126: Giaccio et al. (2019); glass-WDS compositions of all others Fucino tephra and proximal pyroclastic units: this study. Foi=foidite; Pht=phonotephrite; Tph=Tephriphonolite; Ph=phonolite; Rhy=rhyolite; Tra=Trachyte; Lat=latite; Sho=Shoshonite; Trb=trachybasalt; Tep=tephrite; CdP=Casale delle Piane unit (Tuscania-San Pietro section).

4.2.3. Trace elements

The full trace element glass dataset of the tephra samples can be found in Supplementary Dataset-2 (SD-2).

Phonolite tephra layers TF-107 and TF-111 (CG2) display relatively heterogeneous, yet largely overlapping trace element concentrations. For instance, Th contents range from 67-91 ppm and 66-95 ppm, respectively (Fig. 7a). Despite the variability in absolute incompatible trace element concentrations, ratios of High Field Strength Element (HFSE) to Th in both TF-107 (Nb/Th = 0.39 ± 0.02; Ta/Th = 0.021 ± 0.001; Zr/Th = 5.5 ± 0.5 [2 s.d.]) and TF-111 (Nb/Th = 0.39 ± 0.03; Ta/Th = 0.021 ± 0.001; Zr/Th = 5.6 ± 0.3 [2 s.d.]) remain constant, and indistinguishable from one another, possibly implying a common volcanic source.

TF-116 belongs to CG3 and comprises phonolitic-trachytic to rhyolitic glasses. However, our trace element analyses derive from glass shards relating to the phonolite-trachyte end-member only. These TF-116 glasses are heterogeneous in terms of their trace element contents (e.g., 82-139 ppm Th; 31-55 ppm Nb; 469-718 ppm Zr) and are more enriched in incompatible trace element than the overlying phonolitic tephra layers (TF-107 and TF-111) (Fig. 7a). Ratios of HFSE to Th in these glasses remain constant, including Nb/Th ratio (0.41 ± 0.04 [2 s.d.]), Ta/Th (0.020 ± 0.001 [2 s.d.]) and Zr/Th (5.3 ± 0.4 [2 s.d.]) which all remain largely consistent with the overlying tephra (TF-107 and TF-111) (Fig. 7b).

TF-125 also belongs to CG3, ranging from phonolitic-trachytic (mainly trachytic) to rhyolitic glasses, and this major element variability is captured by a large degree of trace element heterogeneity (e.g., 57-184 ppm Th; 1462-151 ppm Sr; 522-879 ppm Rb). Incompatible trace element concentrations observed in the phonolite-trachyte end-member glasses are consistent with TF-107 and TF-111 glasses. The TF-125 phonolite-trachyte glasses are more enriched in Sr, Ba and Eu relative to the rhyoltic end-member glasses, illustrating their compatibility during K-feldspar fractionation. Ratios of HFSE to Th in TF-125 glasses also differ between the phonolitic-trachytic (Nb/Th = 0.39 ± 0.2; Zr/Th = 5.5 ± 0.3; Hf/Th = 0.13 ± 0.005 [2 s.d.]) and rhyolitic (Nb/Th = 0.30 ± 0.3; Zr/Th = 2.7 ± 0.7; Hf/Th = 0.07 ± 0.01 [2 s.d.]) end-members. Moreover, HFSE to Th ratios in the rhyolitic glasses show more variability than those of the phonolite-trachyte glasses, particularly in terms of Zr/Th, where Zr becomes depleted, probably driven by zircon fractionation (Fig. 11a).

TF-126, previously reported in Giaccio et al. (2019), has a phonolite-trachyte composition and plots in CG-2. Incompatible trace element concentrations reveal a relatively homogeneous composition (e.g., 79 ± 7 ppm Th; 29 ± 1 ppm Nb; 393 ± 29 ppm Zr [2 s.d.]), and as such the ratios of HFSE to Th, show very limited variability, consistent with the homogeneous major element composition of the tephra (e.g., Nb/Th (0.37 ± 0.01; Ta/Th = 0.020 ± 0.001; Zr/Th = 4.9 ± 0.5 [2 s.d.]).

Concerning the proximal pyroclastic deposits, the Castel Broco phonolitic glasses show a slight heterogeneity and are anriched in certain incompatible trace elements (e.g., 138-188 ppm Th [Fig. 7a]; 627-750 ppm ppm Zr; 30-42 ppm Y). Ratios of HFSE to Th remain constant within these glasses (Nb/Th = 0.32 ± 0.02; Zr/Th = 4.1 ± 0.5 [2.d.]).

Vico α trace element glass compositions are extremely heterogeneous (75-194 ppm Th; 1303-87 ppm Sr; 248-955 ppm Rb), consistent with their major element variability ranging from phonolite-trachytes to rhyolites (Pereira et al., 2020). The less evolved phonolite-trachyte glasses are more enriched in Sr, Ba and Eu relative to the rhyoltic end-member glasses, where these elements clearly behave compatibly during K-feldspar fractionation. Ratios of HFSE to Th in these glasses also differ between the phonolitic-trachytic (Nb/Th ~ 0.38; Zr/Th ~ 5.6) and rhyolitic (Nb/Th ~ 0.29; Zr/Th = 1.9-5.6) end-members.

Vico β analyses focused on the predominantly rhyolitic sub-unit (VIG-3; Pereira et al., 2020); these rhyolitic glasses are relatively heterogeneous in the case of some incompatible elements (e.g., 137-169 ppm Th; 948-995 ppm Rb). Sr, Ba and Eu contents are more depleted in the rhyolitic glasses of Vico β than in Vico α.

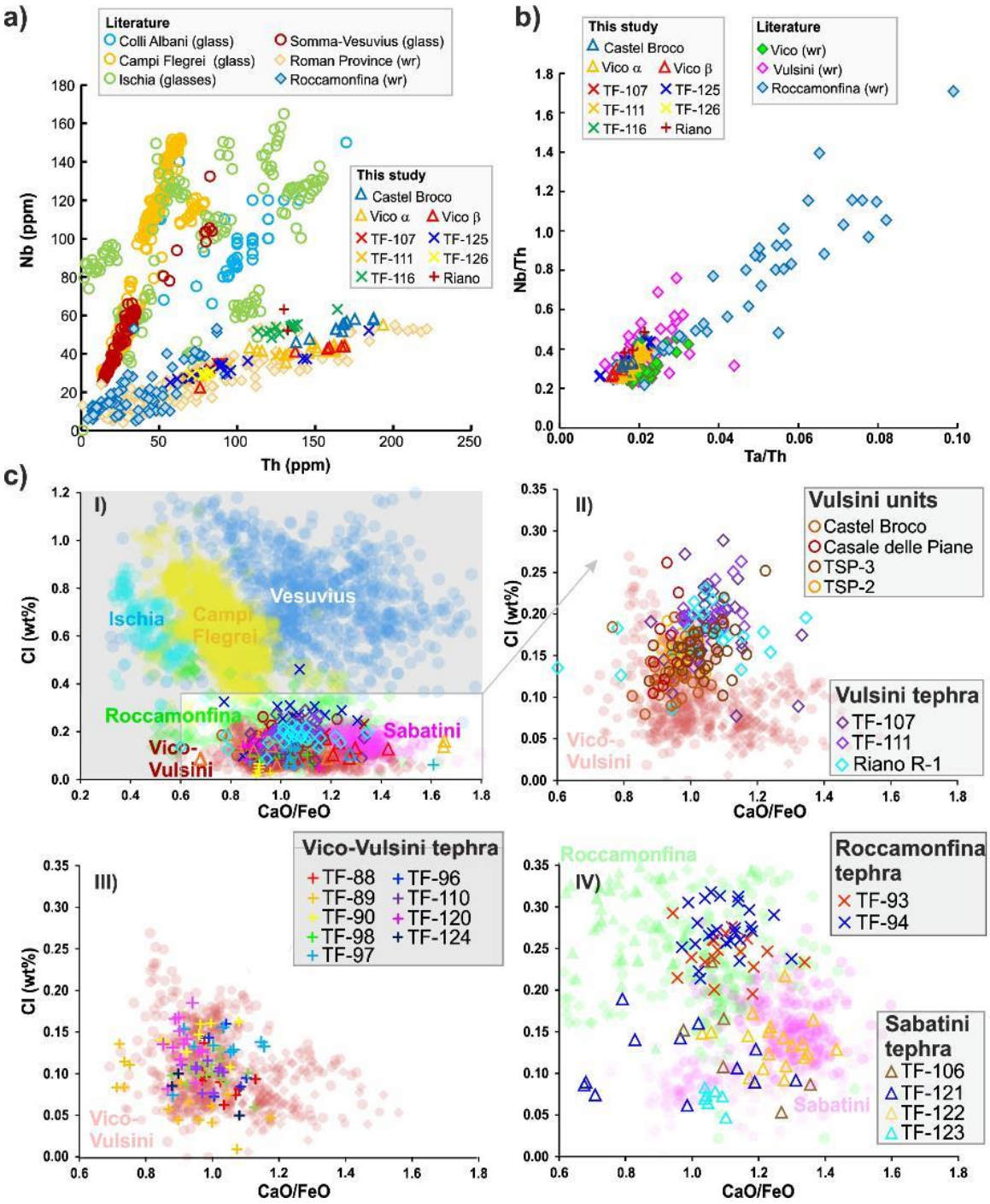

Figure 7. Discrimination diagrams for F4-F5 tephra. **a)** Th vs Nb bi-plot of the investigated tephra compared with literature data for the glasses of Neapolitan (i.e., Campi Flegrei, Somma-Vesuvius and Ischia) and Colli Albani volcanoes, which are characterised by a higher Nb/Th ratio than Roman/Latium (Vulsini, Sabatini, Vico) and Roccamonfina volcanoes; the compositions of the four tephra are compatible with either a Latium or Roccamonfina origin. **b)** Ta/Th vs Nb/Th discrimination diagram for Roccamonfina and Latium Volcanoes; the four tephra here investigated are characterised by a ratio compatible with either a Vulsini or Vico origin. Data source: TF-107, TF-111, TF-116 and TF-126: this study; literature data of whole rock

(wr) compositions of products from Latium volcanoes and Roccamonfina: Lustrino et al. (2011) and references therein; glass composition of products from Colli Albani: Cross et al., 2014; Ischia: Tomlinson et al., 2014; Campi Flegrei: Smith et al., 2011, Tomlinson et al., 2012; Somma-Vesuvius: Tomlinson et al., 2015. **c)** CaO/FeO vs Cl discriminating diagram of the volcanic sources of the Italian potassic trachyte-phonolite and tephriphonolite tephra (modified after Giaccio et al., 2017) for the F4-F5 and Riano R-1 tephra here shown in the Vulsini group for comparison. The compositions of the Vico and Vulsini pyroclastic units collected at Tuscania-San Pietro section, are also shown.

Only two successful analyses were obtained from the phonolitic Riano R-1 tephra, but the compositions are internally consistent for most incompatible elements, with the noticeable exception being the variable Nb content leading to a Nb/Th ratio of 0.39-0.48. Levels of incompatible trace element enrichement in the R-1 glasses (of unknown source area) appear more akin to those of Vulsini (e.g., Castel Broco), rather than Vico (Fig. 7b). Unfortunately, available trace element data for Sabatini are scant and cannot be considered here for comparison.

Ratios of HFSE to Th are seemingly useful when evaluating the origin of the five tephra layers characterised here in the context of peri-Tyrrhenian potassic volcanism, particularly given the limited trace element glass data available for some regional volcanic sources, and thus a reliance on whole-rock datasets, which are not always directly comparable to volcanic glass data (e.g., Tomlinson et al., 2012). The Nb/Th ratios of the five Fucino layers analysed (TF-107, TF-111, TF-116, TF-125 and TF-126) clearly preclude an origin from the Neapolitan volcanic zone (e.g., Campi Flegrei, Ischia, Vesuvius), where Nb values are far higher at overlapping Th content, and Nb/Th ratios are typically > 1.5 (glass datasets; Fig. 7a).

TF-107, TF-111, TF-116, TF-125 and TF-126 all have incompatible trace element concentrations and ratios of HFSE to Th compatible with the published analyses of the Latium and Roccamonfina volcanics (Fig. 7a). However, Roccamonfina appears an unlikely source of the five Fucino tephra layers owing to its typically higher Ta/Th ratios (Fig. 7b). In the investigated timespan, Colli Albani exclusively erupted K-foidites (CG-1) and can easily be discounted as the possible volcanic source of these Fucino layers, thus leaving the remaining Latium (Vulsini, Sabatini and Vico) volcanoes as the most obvious candidates. Indeed, ratios of HFSE to Th observed in TF-107, TF-111, TF-116, TF-125 and TF-126 are broadly consistent with those from published whole-rock (e.g., Lustrino et al.,

2011) and our preliminary glass (reported above) data from Vulsini and Vico (although similarities to Sabatini products cannot be excluded owing to a paucity of data).

4.2.4. Strontium (Sr) Isotopes

Results for each analysed sample, along with associated uncertainty (2σ), are presented in Table 4, while a comparison with values from the literature of proximal Vulsini, Vico, Sabatini and Colli Albani rock samples, erupted in the time interval 430-350 kyr, is shown in Figure 8. In literature there are very few Sr-isotopic data (i.e., just one from Perini et al., 2004) for the Vico activity in the investigated 430-365 ka time interval, thus making it challenging to identify eruptive units from this volcano based on Sr-isotope signature. This knowledge gap should be filled in the future to better constrain the attribution of several TF tephra layers.

$^{87}Sr/^{86}Sr$ values were measured on either pyroxene or feldspar minerals on each sample, except for TSP-3, for which a matrix (pumice) measurement was obtained as well. For sample TF-85 a mineral fraction enriched in leucite crystals was analysed. The lowest value (0.7095) was measured on pumice fragments from the TF-111. Pyroxenes and feldspar from TF-111 are featured by $^{87}Sr/^{86}Sr$ ratio of 0.710149 and 0.710671, respectively. The highest value (0.71120) was mesured on feldspars of TSP-3. Therefore, all the measured ratios suggest a Roman province origin for the investigated tephra (Fig. 8). Minerals from TF-85=Villa Senni have an $^{87}Sr/^{86}Sr$ ratio of 0.71043, which agrees with literature data (Gaeta et al., 2016). Measured values of proximal units from Vulsini (i.e., TSP-3 and Castel Broco) range up to 0.71125 (TSP-3 fsp), thus slightly extending the literature range for Vulsini (Fig. 8). The Riano R-1 tephra value of 0.71081 is broadly compatible with either a Sabatini or Vulsini source (rather than Vico). Finally, TF-126 has $^{87}Sr/^{86}Sr$ ratio of 0.71111 that would support the attribution of this tephra to a Vulsini eruption, as already suggested by Giaccio et al. (2019).

Overall, the measured $^{87}Sr/^{86}Sr$ values do not provide sufficient evidence to be used as correlation tool for the Latium volcanoes, except for perhaps Vico: indeed, the amount of literature data on proximal samples is still too limited to allow solid attributions to a specific volcano. Nevertheless, the Latium volcanics, as previously known and confirmed by our data, show similar $^{87}Sr/^{86}Sr$ ranges, which are different from the products of other Italian volcanoes (e.g., Peccerillo, 2017). Thus,

$^{87}Sr/^{86}Sr$ ratio can support an ascription of a tephra of unknown origin to the Latium volcanism, narrowing down the list of possible sources.

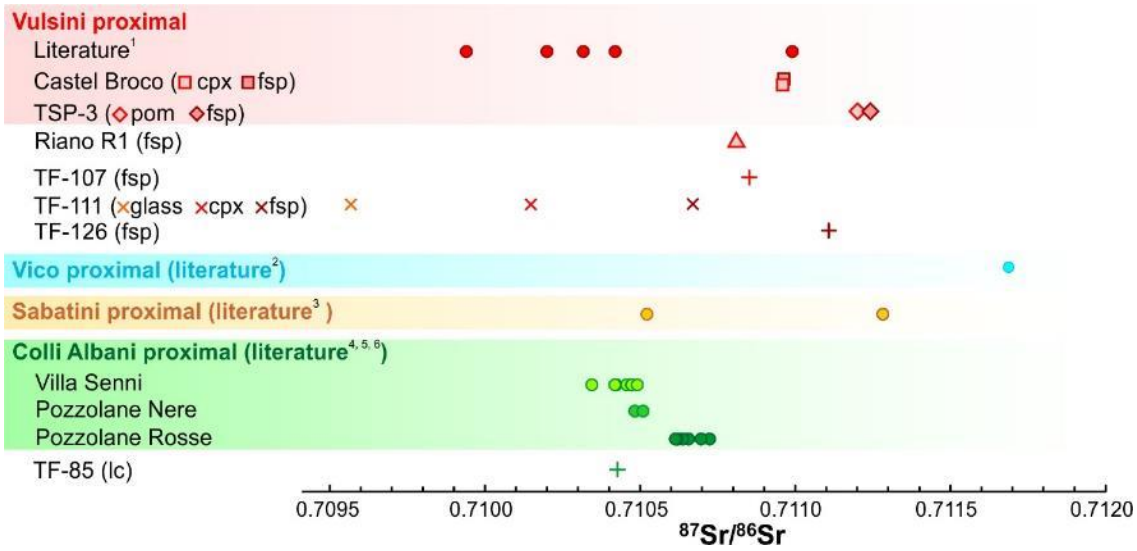

Figure 8. $^{87}Sr/^{86}Sr$ ratio values of selected tephra layers and literature proximal references for the 430-350 ka time interval. Abbreviations: cpx=clinopyroxene; fs=feldspar; pom=pumice. Data source: TF-85, TF-107, TF-111, TF-126, Castel Broco, TSP-3, Riano R-1: this study; literature data: [1] Peccerillo (2017); [2] Perini et al. (2004); [3] Sottili et al. (2019); [4] Gaeta et al. (2006; 2016); [5] Giaccio et al. (2013a).

Table 4. $^{87}Sr/^{86}Sr$ ratio values of the selected four Fucino tephra and three proximal units.

Tephra/ sample	Setting	Volcano	Glass composition	Analysed material	$^{87}Sr/^{86}Sr$	2σ
TF-85	distal	Colli Albani	K-foidite	lc	0.710430	±0.000007
TF-107	distal	unknown	phonolite	fsp	0.710851	±0.000006
TF-111	distal	Vulsini-Vico	phonolite	pum	0.709507	±0.00006
				fsp	0.710671	±0.000006
				cpx	0.710149	±0.000007
TF-126	distal	Vulsini	phonolite	fsp	0.711105	±0.000007
Castel Broco	proximal	Vulsini	phonolite	cpx	0.710960	±0.000006
				fsp	0.710965	±0.000006
TSP-3	proximal	Vulsini	phonolite	pum	0.711199	±0.000007
				fsp	0.711245	±0.000006
Riano R-1	mid-proximal	Vulsini	phonolite	K-fsp	0.710810	±0.000007

Abbreviations: K-fsp=K-feldspar; fsp=feldspar; cpx=clinopyroxene; pum=pumice.

4.3. $^{40}Ar/^{39}Ar$ age of TF-85, TF-117 and Pozzolane Nere

The results for each dated deposit are presented as probability diagrams in Figure 9. Reported uncertainties are analytical at a 95.5% of confidence limit (J-value included), as well as

fully propagated ones. Detailed analytical data are available in Supplementary Dataset-3 (SD-3).

TF-85 (Villa Senni): A total of eleven leucite single crystals were dated. All crystals yielded an undistinguishable age, allowing us to calculate a meaningful weighted mean age of 365.8 ± 1.4/1.8 ka (MSWD =0.7, P=0.7).

TF-117 (Pozzolane Nere): Nine leucite crystals were individually dated. All crystals yielded an undistinguishable age, allowing the straightforward calculation of a weighted mean age of 407.7 ± 4.0/4.4 ka (MSWD =0.04, P=1.0).

Pozzolane Nere (Rome proximal setting): Twelve leucite crystals were dated. They all share a similar age within uncertainties, allowing us to calculate a statistically meaningful weighted mean age of 408.5 ± 1.2/2.0 ka (MSWD =0.8, P=0.6). In Figure 9 we also combined the 21 single leucite ages obtained on the Pozzolane Nere from both the proximal deposits (PN) and distal equivalent (TF-117), allowing us to propose a new, more precise weighted mean age of 408.5 ± 1.4/2.0 ka (MSWD =0.4, P=1.0) for the Pozzolane Nere regional marker.

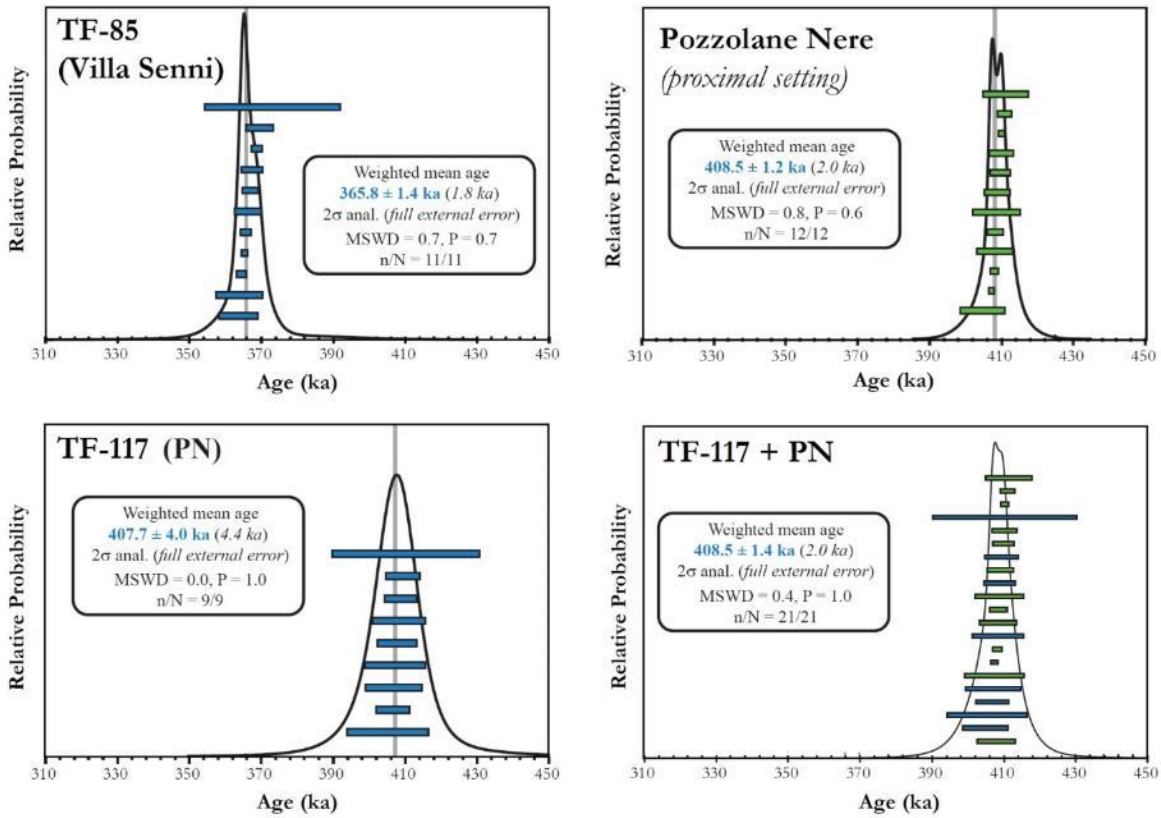

Figure 9. $^{40}Ar/^{39}Ar$ on single grain results (leucite crystals), presented as probability diagrams, for TF-85 (Villa Senni), TF-117 (Pozzolane Nere) and Pozzolane Nere (Rome proximal setting). A combined weighted mean age of TF-117/Pozzolane Nere is then proposed. Ages are calibrated according to Renne et al. (2011) total ^{40}K decay constant and from the optimization calibrated age of 1.1891 Ma for the flux standard ACs-2 (Niespolo et al., 2017). Individual crystal error bars are at 1σ of uncertainties.

5. Discussion

5.1. Volcanic sources of tephra layers from core F4-F5

5.1.1. K-foidites (CG-1)

The K-foidite compositions of the two tephra layers from CG-1 (Fig. 6) are distinctive within the context of Quaternary Italian volcanism, being limited to a few eruptive sources (e.g., Peccerillo, 2017). Among these, the Colli Albani volcanic district has produced and dispersed several K-foiditic tephra (e.g., Marra et al., 2009) from moderate to major eruptions that have been traced in both medial and distal settings (e.g., Giaccio et al., 2013a, 2014; Petrosino et al., 2014b; Leicher et al.,

2016). Consequently, Colli Albani should be regarded as the most likely source of TF-100 and TF-108.

5.1.2. Potassic phonotephrites, tephriphonolites, phonolites, trachytes, trachyte-phonolites and latites (CG2)

The glass geochemical compositions of tephra from CG-2 (i.e., potassic phonotephrites, tephriphonolites, phonolites, trachytes, trachyte-phonolites and latites) are quite common and shared by almost all peri-Tyrrhenian potassic volcanoes of central-southern Italy (e.g., Peccerillo, 2017). However, considering the time interval investigated here (430-365 ka), we can confidently exclude the Neapolitan volcanoes (i.e., Ischia, Procida, Campi Flegrei and Somma-Vesuvius) as possible sources of any of the twenty-one CG-2 tephra layers, since the so-far oldest known eruption from these volcanoes is significantly younger (i.e., the ~289.6 ± 1.9 ka Seiano Ignimbrite; De Vivo et al., 2001; Rolandi et al., 2003; Belkin et al., 2016; Fig. 3). Nevertheless, a geochemical fingerprinting approach remains essential, as there is always the possibility that Neapolitan volcanism may be extended deeper in time with future investigations, particularly since some distal archives seem to suggest older activity in the region (e.g., Giaccio et al., 2014; Petrosino et al., 2015).

To discriminate the source of this large group of tephra, we employed the CaO/FeO vs Cl classification diagram (Giaccio et al., 2017), which defines quite distinct fields for the individual sources of the Latium and Neapolitan pyroclastic rocks with a SiO_2 content ranging from 52 wt% to 67 wt% (Fig. 7c-I). This confirms the lack of products from the Neapolitan volcanoes and points to the Latium or Roccamonfina volcanoes as the only plausible sources of 17 out of 21 - i.e., those with 52 < SiO_2 wt% < 67 - CG-2 Fucino tephra (Fig. 7c-I). Furthermore, the trace element compositions of all the phonolite and trachyte glass shards from the CG-2 (and CG-3) tephra layers also clearly precludes the Neapolitan volcanoes as possible eruptive sources (Fig. 7a-b).

Vulsini – In the CaO/FeO vs Cl diagram TF-107 and TF-111 plot at the boundary between Vulsini-Vico (northern Latium) and Roccamonfina fields (Figs. 7c-II, IV), making the attribuition to one of these sources not straightforward. However, a slight difference in Cl content between Vulsini-Vico

and and Roccamonfina tephra, clustering between 0.05 wt% up to 0.20 wt% and 0.25-0.33 wt%, respectively (cfr. Fig. 7c-II with 7c-IV), makes the distinction between the two volcanic sources still tenable. More importantly, in this diagram, TF-107 and TF-111 overlap the composition of the Vulsini proximal pyroclastic units analysed in the present study (especially TSP-3 Pumice fall from Tuscania-San Pietro section; Fig. 7c-II), suggesting that Vulsini is the most probable source of these tephra layers. More detailed, individual tephra correlations are discussed below (see section *5.2.3.3.*) and fully support this volcanic source attribution. Finally, despite the paucity of the proximal reference dataset, $^{87}Sr/^{86}Sr$ ratios also support a Vulsini origin for these two tephra layers (Fig. 8), while the trace elements confirm an origin from northern Latium (Vulsini or Vico) volcanoes (Fig. 7b).

The Riano R-1 tephra (404.7 ± 5.0 ka; Marra et al., 2018), for which a clear stratigraphic/compositional correlation is still lacking, also matches the compositions of the Vulsini units analysed in this study. It is therefore compatible with a possible distal origin from Vulsini, rather than from the nearest Sabatini source.

Vulsini-Vico – Cl contents and CaO/FeO ratios of TF-88, TF-89, TF-90, TF-96, TF-97, TF-98, TF-110, TF-120 and TF-124 are consistent with either Vico or Vulsini compositions, and thus do not allow a further discrimination between these two potential sources (Fig. 7c-III). However, a discrimination is possible based on further oxides composition as discussed in section 5.2.3.4.

Sabatini – According to the CaO/FeO vs Cl diagram, TF-106 and TF-122 can be related to the Sabatini Volcanic District based on the high (i.e., >1.15) CaO/FeO ratio (Fig. 7c-IV). TF-106 forms along with TF-102, TF-103 and TF-104 a well-defined cluster of tephra that share a similar phonotephritic composition (Fig. 6; SD-1) and lithology (Table 2). Therefore, though the CaO/FeO vs Cl discrimination diagram cannot be applied to TF-102, TF-103 and TF-104 because of their SiO_2 content being lower than 52 wt%, (Giaccio et al., 2017), they can be reliaby regarded as part of a cluster of eruptions from Sabatini. Although showing a more scattered composition in the CaO/FeO vs Cl diagram (Fig. 7c-IV), TF-121 can be attributed to the Sabatini as well, because of its close geochemical similarity with the directly underlying TF-122 layer (Fig. 5). Finally, TF-123 can be also

likely attributed to the Sabatini, because of its homogenous composition in the CaO/FeO vs Cl diagram that matches a second well-defined compositional cluster of the Sabatini rock types (Fig. 7c-IV).

Roccamonfina – TF-93 and TF-94 can be confidently attributed to the Roccamonfina volcano, based on the relatively high Cl content (i.e., >0.25 wt%), and thus their clear position in the Rocamonfina field of the CaO/FeO vs Cl diagram (Fig. 7c-IV), which is quite distinctive with respect to the Latium volcanoes (Fig. 7c-IV).

5.1.3. K-rhyolites (CG-3)

The six tephra layers forming CG-3 (TF-99, 109, 114, 115, 116, 125; Fig. 6) show K-rich rhyolitic and trachy-rhyolitic compositions, which is quite unusual within the context of the peri-Tyrrhenian Quaternary Italian volcanism, and peculiar to Vico Volcano (e.g., Perini et al., 1997, 2000, 2003, 2004; Perini and Conticelli, 2002; Pereira et al., 2020), hence the most probable source of the Fucino CG-3 tephra layers.

In summary, based on distinctive chemical compositions, stratigraphic clues and lithological features and affinities, we propose an attribution of the Fucino tephra layers to the peri-Tyrrhenian potassic volcanoes, as summarized in Table 5.

Table 5. Volcanic sources of the investigated Fucino tephra, inferred from glass chemical composition and lithological features.

Volcano	**Fucino tephra**
Vulsini	TF-107, TF-111
Vico	TF-99, TF-109, TF-114, TF-115, TF-116, TF-125
Vulsini or Vico	TF-88, TF-89, TF-90, TF-96, TF-97, TF-98, TF-110, TF-120, TF-124
Sabatini	TF-102, TF-103, TF-104, TF-106, TF-121, TF-122, TF-123
Colli Albani	TF-100, TF-108
Roccamonfina	TF-93, TF-94

5.2. Individual tephra correlation

5.2.1. Tephra from Colli Albani (CG-1)

TF-100 and TF-108 - These two K-foiditic tephra layers (CG-1), ascribed to the Colli Albani activity, occur between TF-85 and TF-117 (Fig. 2), which were attributed to the Villa Senni (365.8 ± 1.4 ka) and Pozzolane Nere (408.5 ± 1.4 ka) eruptions, respectively (Giaccio et al., 2019). The $^{87}Sr/^{86}Sr$ composition determined in this study for TF-85 further supports its attribution to the Villa Senni eruption. Indeed, $^{87}Sr/^{86}Sr$ ratios of the Colli Albani products show a strong time-dependent variability (Gaeta et al., 2006, 2016; Giaccio et al., 2013a) and the $^{87}Sr/^{86}Sr$ value obtained for TF-85 precisely matches that of Villa Senni (Fig. 8).

Considering the available chronological constraints and its relative proximity to the TF-117/Pozzolane Nere, TF-108 can be attributed to the post-caldera phase of the Pozzolane Nere eruptive cycle (*sensu* Gaeta et al., 2016), which is equivalent to the Centogocce fall succession of Giordano et al. (2006). In proximal settings, the Centogocce deposits consist in a series of scoria-lapilli fall beds and lava flows overlying the Pozzolane Nere deposits, emplaced in the 403.4 ± 5 ka - 396.4 ± 5 ka time interval (recalculated ages from Marra et al. (2009) and Gaeta et al. (2016)). Unfortunately, no glass composition is available for this scoria fall succession, and therefore, we used the composition of TF-117/Pozzolane Nere for comparison (Fig. 10a). Furthermore, Pereira et al. (2020) have recently reported the occurrence, within the San Paolo Formation aggradational succession, of a tephra layer (SPF4), with a polymodal rhyolite, K-foidite and phonotephrite composition, interpreted as a reworked volcaniclastic layer containing both Vico and Colli Albani eruption products. Pereira et al. (2020) reported an age of 403.5 ± 4.2 ka for SPF4, which is consistent with the time interval (403.4 ± 5 ka - 396.4 ± 5 ka) covered by the Centogocce fall succession, despite a geochemical mismatch of TF-108 with SPF4 (Fig. 10a), which can be expected for multiple explosive and effusive eruptions occurred during a relatively long interval. Based on glass composition and stratigraphic position relatively to the TF-117/Pozzolane Nere, we attribute TF-108 to the Centogocce activity. The stratigraphic position of TF-100, between the TF-117/Pozzolane Nere and the TF-85/Villa Senni (Fig. 2), suggests an age substantially younger than the Centogocce equivalent TF-108. In spite of this, for its composition which partially overlaps the wide composition

field of the Pozzolane Nere (Fig. 10a), TF-100 could still be considered as part of the final stage of the Pozzolane Nere eruptive cycle.

5.2.2. Tephra from Vico (CG-3).

TF-125 – This tephra occurs in the lowermost portion of the F4-F5 record, ~50 cm upsection from TF-126 that was directly dated at 424.3 ± 3.2 ka (Giaccio et al., 2019). TF-125 is characterised by a heterogeneous phonolite-trachyte to rhyolite composition, with a silica content ranging from 59 to 77 wt% and an alkali content from 14 to 8 wt%. Recently, Pereira et al. (2020) published new glass geochemical compositions for the early-emplaced volcanics of Vico activity (Vico Period I; Perini et al., 2004), including Vico α and Vico β Plinian fall markers (Cioni et al., 1987), both with a dominant rhyolitic composition, along with the characterisation of three minor events (i.e., Vico β_{top}, Vico γ and Vico δ; Cioni et al., 1987). In addition, Pereira et al. (2020) acquired very precise $^{40}Ar/^{39}Ar$ ages for Vico α (414.8 ± 2.2 ka), Vico β (406.5 ± 2.4 ka), Vico β_{top} (406.4 ± 2.0 ka) and Vico δ (399.7 ± 3.0 ka).

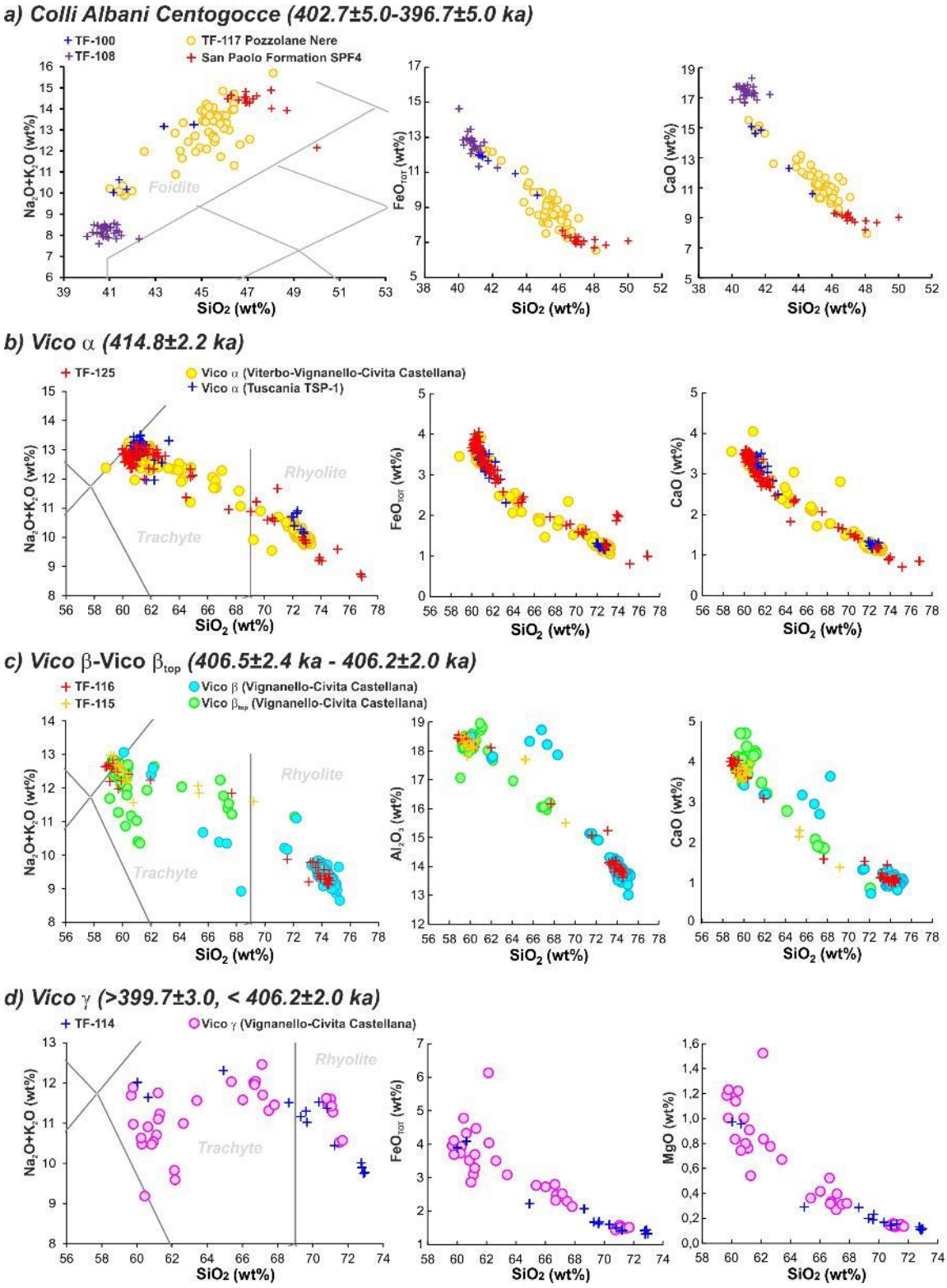

Figure 10. Total alkali versus silica (TAS) classification diagram after Le Maitre et al. (2002) and representative bi-plots for TF-100, TF-108, TF-114, TF-115, TF-116 and TF-125 from the F4-F5 tephra record, compared with SPF4 tephra layer from the San Paolo aggradational succession, Pozzolane Nere (TF-117), proximal Vico α, Vico β, Vico β_{top} and Vico γ units from

Vico volcano. Data source: WDS glass composition of TF-100, TF-108, TF-114, TF-115, TF-116, TF-125 and Vico α (TSP-1): this study; WDS glass composition of TF-117/Pozzolane Nere: Giaccio et al. (2017); WDS glass composition and $^{40}Ar/^{39}Ar$ age of tephra SPF4, Vico α, Vico β, Vico β_{top} and Vico γ, sampled at Viterbo (VT), Civita Castellana (CC) and Vignanello (VIG): Pereira et al. (2020). $^{40}Ar/^{39}Ar$ ages are recalculated relative to an age of 1.1891 Ma for the Alder Creek sanidine monitor standard (Niespolo et al., 2017), with the uncertainty expressed at 2σ.

Using this updated geochemical dataset for the Vico Period I products, we found that TF-125 major element composition matches that of Vico α of Pereira et al. (2020) and of Tuscania-San Pietro TSP-1 (this study; Fig. 10b), and this correlation is further strengthened by the similarities in the trace element glass compositions obtained here for Vico α and TF-125 (Fig. 11a). Considering this geochemical affinity and its stratigraphic position between TF-126 (424.3 ± 3.2 ka) and TF-117/Pozzolane Nere (408.5 ± 1.4 ka), consistent with an age of 414.8 ± 2.2 ka, we can confidently correlate TF-125 to the Vico α Plinian eruption.

TF-116 and TF-115 – TF-116 is located less than 1 m upsection from TF-117, the latter dated at 407.7 ± 4.0 ka and correlated to the Pozzolane Nere eruption (Giaccio et al., 2019), which has been dated here more precisely at 408.5 ± 1.4 ka (Fig. 9). Like TF-125, this tephra is characterised by a heterogeneous trachytic-rhyolitic composition, with a dominant SiO_2-rich (>75 wt%) rhyolitic component, and a minor scattered phonolitic-trachytic one (58-68 wt% SiO_2), which is a distinctive, common features of the Vico Period I units (Pereira et al., 2020). Trace element analyses (Fig. 7a-b) also support a Latium origin for this tephra. Specifically, the glass rhyolitic composition of TF-116 matches that of Vico β (Fig. 10c) that, along with its position on top of TF-117/Pozzolane Nere, allows us to correlate TF-116 to Vico β eruption (406.5 ± 2.4 ka; Pereira et al., 2020). Noteworthy, TF-116 contains a significant trachyte-phonolite component that is poorly represented or documented in proximal settings (Fig. 10c).

TF-115 tephra is found 2 cm above TF-116 and is characterised by a heterogeneous composition, consisting of a main phonolitic-trachytic component (SiO_2 59-66 wt%) and a minor SiO_2-rich (~69 wt%) rhyolitic one. These geochemical features allow unambiguous correlation to Vico β_{top} (Fig. 10c),

consistent with the superposition of the tephra just on top of TF-116/Vico β. Furthermore, consistent with its strict stratigraphic proximity to TF-116/Vico β, the proximal Vico β_{top} has a $^{40}Ar/^{39}Ar$ age of 406.5 ± 2.4 ka that is indistinguishable from that of Vico β (Pereira et al., 2020). Noteworthy, Pereira et al. (2020) also pointed out that the combined glass composition of Vico β and Vico β_{top} is to some extent similar to that of Vico α, so that, in the absence of strong chronological and/or tephrostratigraphic constraints, the geochemical composition of the two units could be potentially confused. However, in the F4-F5 record, the TF-115 and TF-116 couplet occurs on top of the 408.5 ± 1.2 ka Pozzolane Nere tephra, well upsection from the Vico α correlative (TF-125). Furthemore, when dealing with sedimentary archives not so well constrained chronostratigraphically as Fucino, trace element analysis of the Vico eruption products may offer useful means to discriminate the distal equivalents of Vico α and Vico β. In fact, the phonolite-trachyte end-member glasses of TF-116/Vico β extend to greater levels of incompatible trace element enrichement with respect to TF-125/Vico α (Fig. 11a-left), whilst the analysis of proximal and distal Vico rhyolitic products reveals greater depletions in Sr associated with the Vico β tephra (Fig. 11a-right), likely induced by major K-feldspar fractionation. In conclusion, the general stratigraphic, chronological, and geochemical features of TF-116 and TF-115 consistently support their unambiguous attribution to Vico β and Vico β_{top}, respectively.

TF-114 - This tephra is separated from the underlying TF-115 by 2-cm-thick lacustrine sediments. It is characterised by a heterogeneous trachyte-rhyolite composition, with a silica content ranging from 60 to 73 wt% and an alkali content from 9 to 13 wt%, with a peculiar alkali vs silica pattern: Indeed, first the alkali content increases at increasing SiO_2 from 60 to 65 wt%, then the alkali content decreases at increasing SiO_2 from 65 to 73 wt%. This peculiar pattern is also observed for Vico γ (Fig. 10d; Pereira et al., 2020). Since $^{40}Ar/^{39}Ar$ datings for Vico γ are not available, its age should be constrained by the bracketing Vico β_{top} (406.5 ± 2.4 ka) and Vico δ (399.7 ± 3.0 ka) units. More specifically, the stratigraphic position of TF-114/Vico γ closer to TF-115/Vico β_{top}, would indicate an age closer to 406.5 ± 2.4 ka.

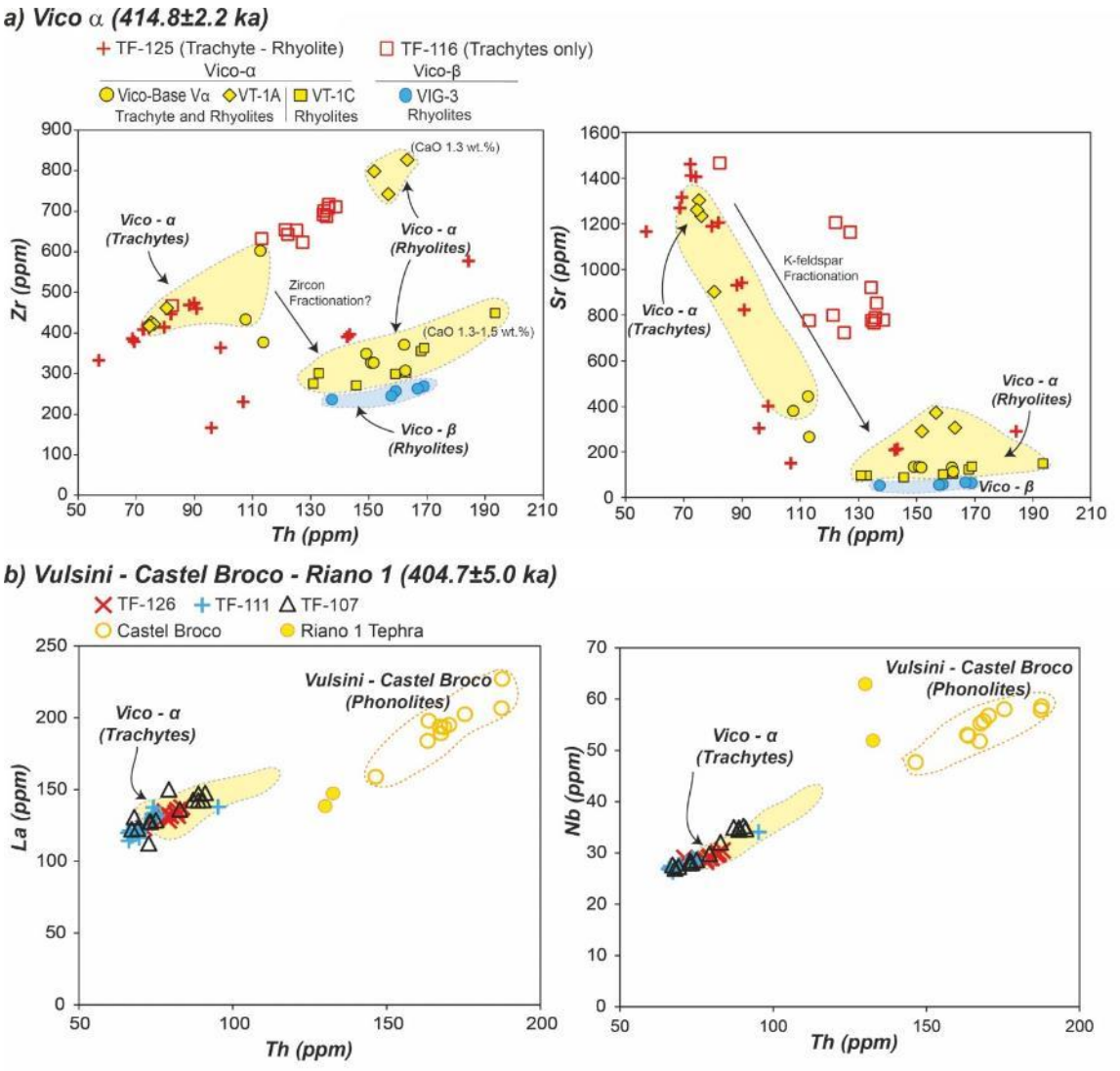

Figure 11: Trace element glass compositions of the Fucino tephra compared to proximal glass data from the Vico and Vulsini volcanoes. **a)** TF-125 and TF-116 compared to the glass compositions of Vico α and Vico β eruption products. Note that in the case of TF-116, only the phonolite-trachyte end-member glasses were analysed, while in proximal settings trace elements were determined only for Vico β rhyolite glasses. **b)** TF-126, TF-111 and TF-107 compared to the Vulsini eruptive products, and specifically the Castel Broco fall deposit. The compositions of the Riano R-1 tephra of unknown origin are also shown.

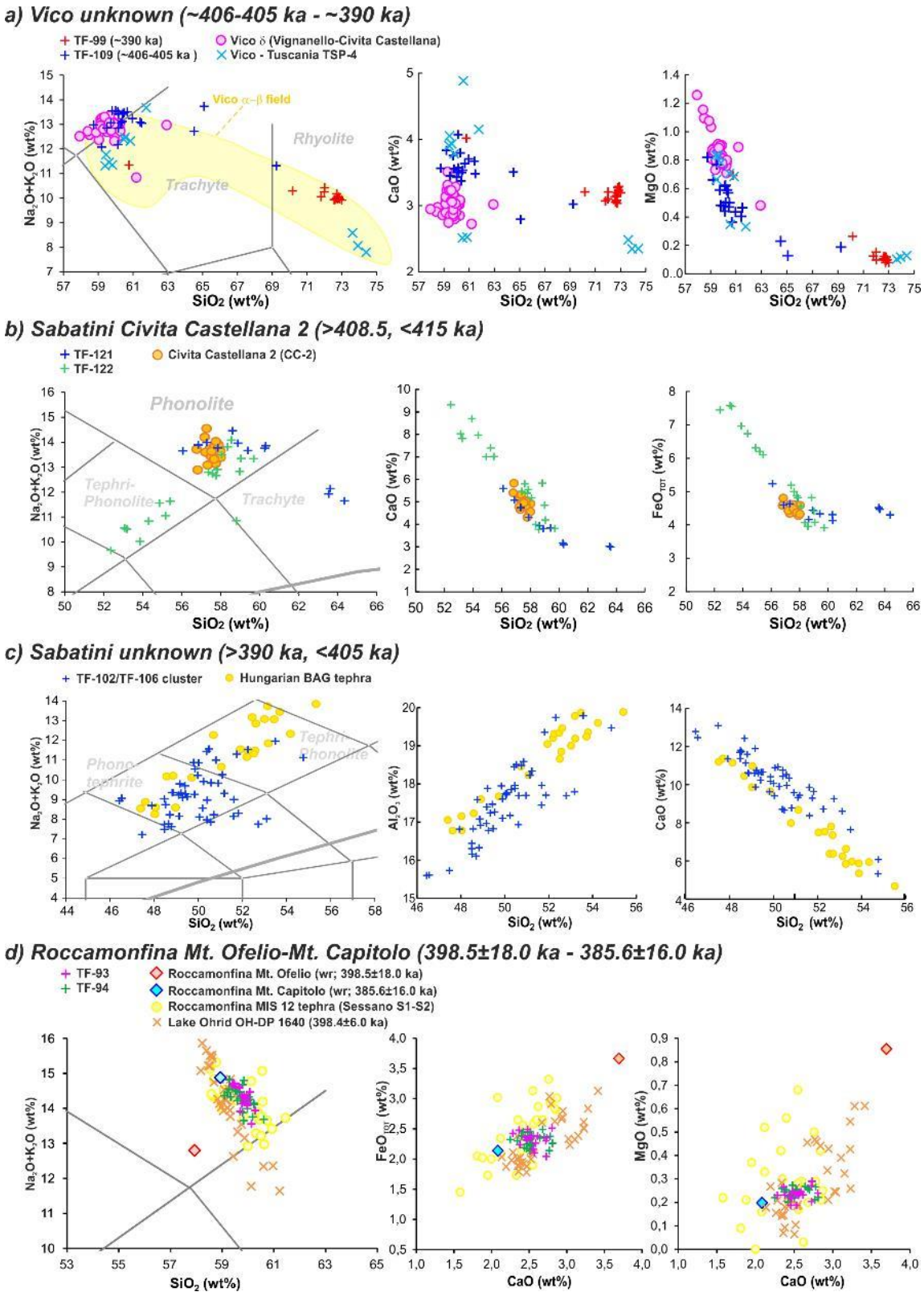

Figure 12. TAS diagram after Le Maitre et al. (2002) and representative bi-plots for the tephra TF-93, TF-94, TF-99, TF-102, TF-103, TF-104, TF-106, TF-109, TF-121 and TF-122 from the F4-F5 record, compared with proximal Vico δ units from Vico

volcano, TSP-4 from Tuscania-San Pietro succession, CC-2 from Civita Castellana succession, the distal Bag tephra from the MIS 10 Hungarian loess, tephra OH-DP-1640 from Lake Ohrid and Sessano-1 and 2 (S1-S2) tephra from Sessano Basin. For comparison, in panel a), the compositional field of the major Vico α and Vico β Plinian eruptions is also shown. Data source: WDS glass composition of TF-93, TF-94, TF-99, TF-102, TF-103, TF-104, TF-106, TF-109, TF-121, TF-122, TF-123, and TSP-4: this study; WDS glass composition and $^{40}Ar/^{39}Ar$ age of Vico δ and CC-2, sampled at Vignanello (VIG) and Civita Castellana (CC), respectively: Pereira et al., 2020; WDS glass composition and modelled age of tephra OH-DP-1640: Leicher et al. (2019); WDS glass composition and of Bag tephra: Pouclet et al. (1999); post-Rio Rava – pre-Brown Leucitic Tuff whole-rock compositions: Rouchon et al. (2008); S1 and S2 SEM-EDS glass composition: Russo Ermolli et al. (2010). $^{40}Ar/^{39}Ar$ ages are recalculated relative to an age of 1.1891 Ma for the Alder Creek sanidine monitor standard (Niespolo et al., 2017), with the uncertainty expressed at 2σ.

TF-99 and TF-109 - TF-99 has a predominantly homogeneous rhyolitic composition (70-73 wt% of SiO_2) with a single trachytic shard (60 wt% SiO_2), while TF-109 is characterised by a heterogeneous trachytic composition (59-65 wt% SiO_2) with a minor rhyolitic component (one shard with ~69 wt% SiO_2; Fig. 12a). As stated in section 5.1.3, the occurrence of a rhyolitic component in these tephra makes their attribution to the Vico volcano quite straightforward, because it is the only known Middle Pleistocene peri-Tyrrhenian volcanic source that produced K-rich rhyolitic tephra. Indeed, in the TAS diagram, both tephra plot within the compositional field of the Vico α and Vico β Plinian eruptions (Fig. 12a).

Considering the stratigraphic position of TF-99 and TF-109 within the F4-F5 record, the most plausible candidate for at least one of these tephra layers would be Vico δ, dated at 399.7 ± 3.0 ka (Pereira et al., 2020). However, neither TF-99 nor TF-109 match Vico δ in composition (Fig. 12a). Although in the TAS diagram TF-109 would seem compatible with Vico δ, suitable bi-plot diagrams show significant differences on several oxides (e.g., CaO content; Fig. 12a). On the other hand, the geochemical composition of TF-109 is consistent with the TSP-4 unit of the Tuscania-San Pietro succession (Fig. 12a). Thus, TF-109/TSP-4 and TF-99 can be only generically attributed to the Vico Period I, their proximal equivalents at Vico not yet identified.

5.2.3. Tephra of Compositional Group-2 (CG-2)

5.2.3.1. Sabatini tephra

TF-102, TF-103, TF-104, TF-106, TF-121, TF-122 and 123 - The geochemical composition of the TF-102/106 and TF-121/122 clusters are quite heterogeneous, with a SiO_2 content ranging from 46 wt% to 55 wt% and from 52 wt% to 64 wt%, respectively (Figs. 12c-b, respectively). TF-123 shows instead a homogenous high-alkali tephriphonolitic composition (Fig. 6).

The TF-102/106 cluster occurs just on top of TF-108, thus constraining its position close to the Centogocce succession time interval (403.4 ± 5 ka - 396.4 ± 5 ka). TF-121/122 and TF-123 occur instead between TF-125 (Vico α, 414.8 ± 2.2 ka; Pereira et al., 2020) and TF-118 (Fontana Ranuccio, 407.0 ± 4.2 ka; Pereira et al., 2018), or the more precisely dated TF-117/PN (408.5 ± 1.2 ka), constraining their ages in the narrow time interval between ~415 ka and ~408 ka. Hence, both the TF-102/106 and TF-121/122 clusters and TF-123 can be attributed to the Southern Sabatini activity (Fig. 3; Sottili et al., 2004, 2010), which was characterised by the emplacement of widespread sub-Plinian to Plinian fall deposits in the time interval ~500-380 kyr (Marra et al., 2014; Sottili et al., 2019). Though no relevant activity is documented in the ~414-402 ka timespan of TF-121/122 and TF-102/106 clusters, recent investigations point to the occurrence of a previously unrecognized Sabatini unit chronologically and geochemically consistent with TF-121/122 (Pereira et al., 2020). Specifically, at Civita Castellana (Fig. 1b), Pereira et al. (2020) described a ~1 m-thick pumice fall unit (CC-2), phonolitic in composition and tentatively ascribed it to Sabatini activity, sandwiched between Vico α (CC-1; 414.8 ± 2.2 ka) and Vico β (CC-3; 406.5 ± 2.4 ka), i.e., a similar stratigraphic position of TF-121/122 within the F4-F5 succession. This unit was also found at San'Abbondio section (Fig. 1b) immediately on top of Vico α (Pereira et al., 2020). Although more variable, in terms of geochemical composition, both TF-121 and TF-122 are compatible with CC-2 phonolitic glass composition (Fig. 12b). Among the two layers, the thickest TF-121 seems to show a higher degree of geochemical similarity, and thus is a good candidate for correlation with CC-2 pumice fall, while the thinner TF-122 could represent a minor eruption slightly proceding CC-2 fall.

In contrast, TF-123, whilst sharing a broadly similar chrono-stratigraphic position to the overlying TF-121/122 deposits, shows no geochemical similarity to the CC-2 pumice fall and thus must be considered the product of a slightly older, unknown Sabatini eruption.

Similarly, the TF-102/106 cluster has no chronological and stratigraphical correlative in the currently determined Sabatini proximal eruption record. This cluster would be instead chronologically consistent with the activity of the Volsci volcanic field and specifically with Pofi Scoria cone and Amafi scoria cone, dated at 394.4 ± 3.5 ka and 395.8 ± 6.1 ka (Marra et al., 2021), respectively, likely equivalent to the Cava Pompi scoria fall (392.7 ± 3.0 ka) and Isoletta I scoria fall (401.7 ± 3.0 ka) (Pereira et al., 2018). However, the lack of any geochemical glass compositional data currently prevents any possible comparison and correlation with TF-102/106.

In contrast, in the ultra-distal setting, the TF-102/106 cluster would be geochemically and chronologically compatible with the so-called Bag Tephra (Fig. 12c), interbedded in Quaternary loess deposits of Hungary and Slovakia (Pouclet et al., 1999; Hum, 2005; Sági et al., 2008). In fact, the Bag Tephra has a phonotephritic-tephriphonolitic glass composition (Pouclet et al., 1999) very similar to that of the TF-102/106 cluster (Fig. 12c). The Bag tephra is commonly found below the so-called Basaharc Lower paleosol of the MIS 9 period (Horváth and Bradák, 2014), thus consistent with the age of TF-102/106. The previous tentative correlation to the Villa Senni eruption (Pouclet et al., 1999) is ruled out by glass geochemistry. More recent petrographic investigations (Sági et al., 2008) point out that the Bag tephra likely represents multiple tephra layers. Therefore, the tephra cluster TF-102/106 would be a good candidate for a correlation with such an important marker of the Hungarian loess. However, at present we can only propose a tentative correlation with either an unknown Sabatini eruption cluster or the Pofi Scoria and Amafi centers of the Volsci volcanic field.

5.2.3.2. Roccamonfina tephra

TF-93 and TF-94 – Both tephra layers are characterised by an almost homogeneous phonolitic composition, with a SiO_2 content of ~59-61 wt% and alkali content ranging between ~13.5 and ~14.5 wt%. Considering their position within the F4-F5 succession, between TF-85 (Villa Senni, 365.8 ± 1.2 ka) and TF-115 (Vico β_{top}, 406.4 ± 2.0 ka), the two tephra can be associated with the

post-Rio Rava/pre-Brown Leucitic Tuff stage (355-440 ka; Rouchon et al., 2008) of Roccamonfina Volcano, and, more specifically, to the activity of the Monte Ofelio-Monte Capitolo centers, dated to 398.5 ± 18.0 ka and 385.6 ± 16.0 ka (recalculated ages from Rouchon et al. (2008)). Although no glass composition is available for these Roccamonfina units, sample RMF6 of Monte Capitolo (398.5 ± 18.0 ka; Rouchon et al., 2008) has a whole rock phonolitic composition, which is consistent with that of the two Fucino tephra (Fig. 12d). The attribution of the two tephra to Roccamonfina is further supported by the analogous composition of two slightly older (i.e., MIS 12) Roccamonfina tephra layers (S1-S2) from the Sessano Basin, southern Italy, located immediately east of this volcano (Russo Ermolli et al., 2010). Furthermore, the OH-DP-1640 tephra from Lake Ohrid (modelled age of 398.4 ± 6.0 ka; Leicher et al., 2019), ascribed to Roccamonfina, could be tentatively correlated with TF-93/94 (Fig. 12d), based on a similar age and geochemical composition (besides minor differences). Therefore, TF-93 and TF-94 can be attributed to the Monte Ofelio-Monte Capitolo centers and, based on good geochemical matching, more likely to the latter. Future higher precision $^{40}Ar/^{39}Ar$ dating of these volcanic units in proximal setting will be of great interest to strengthen the chronology and attribution proposed here.

5.2.3.3. Vulsini tephra

TF-107, TF-111 and TF-126 – In addition to TF-107 and TF-111, likely attributed to the Vulsini activity based on the Cl vs CaO/FeO diagram (Fig. 7c) as discussed above, here we also re-evaluate the TF-126 layer, in light of the new aquired trace element data. Previously, TF-126 was tentatively correlated to the Castel Broco eruption deposit of Vulsini volcano, as well as geochemically matched to the pumice fall pre-Vico α, found immediately below Vico α in the proximal area of Vico Volcano (Pereira et al., 2020).

TF-107 and TF-111 are stratigraphically constrained between the ~365 ka TF-85/Villa Senni tephra and the ~406 ka TF-115/Vico β_{top}. Within the Vulsini volcanic history (e.g., Palladino et al., 2010), the Pumice Fall 0 (PF-0) eruption (399.8 ± 18.0 ka; Turbeville, 1992), here tentatively indentified with with TSP-3 of the Tuscania-San Pietro section, is the only known explosive event geochronologically consistent with both TF-107 and TF-111. Of the two potential distal equivalents of PF-0/TSP-3, TF-

111 shows a good geochemical match with TSP-3 (Fig. 13a). Moreover, TSP-3 occurs below TSP-4 that has been here correlated to TF-109 (Fig. 12a), which support the correlation of TF-111 with PF-0/TSP-3, even if $^{87}Sr/^{86}Sr$ ratios would seem to discount it (Fig. 7).

Regarding the trace element compositions, we notice that both TF-111 and TF-126 share similar levels of incompatible trace element enrichment to the trachytic components of the Vico α deposits, while they strongly differ from Castel Broco (Fig. 11b). This feature, on one hand, would preclude the correlation of TF-126 with Castel Broco and, on the other hand, would also raise doubts over the attribution of TF-111 and TF-126 layers to Vulsini, suggesting instead an origin from Vico. We note, however, that trace element data for Vulsini pyroclastic deposits are currently limited to only one sample from the co-eruptive basal fallout of Castel Broco (Fig. 11b), thus, they may not be fully representative of either the entire compositional spectrum of the Castel Broco eruption products, or even more so, the whole Vulsini eruptive successions. Therefore, to take a conservative approach, while retaining a preferential attribution of TF-111 and TF-126 to the Vulsini district, we cannot fully exclude a Vico source for TF-111/TSP-3 and TF-126/pre-Vico α. Indeed, the unambiguous solution of this issue requires a statistically representative trace element dataset for both Vulsini and Vico products, which is not available yet.

TF-107 shares a similar lithology and major element geochemistry with Riano R-1 tephra (Fig. 13a), here tentatively attributed to the activity of the Vulsini volcanic district (Fig. 7c-II) and dated at 404.7 ± 5.0 ka (Marra et al., 2018). While a correlation is further supported by very similar $^{87}Sr/^{86}Sr$ values (Fig. 8; Table 4), preliminary trace element glass analyses reveal some inconsistency (Fig. 11b).

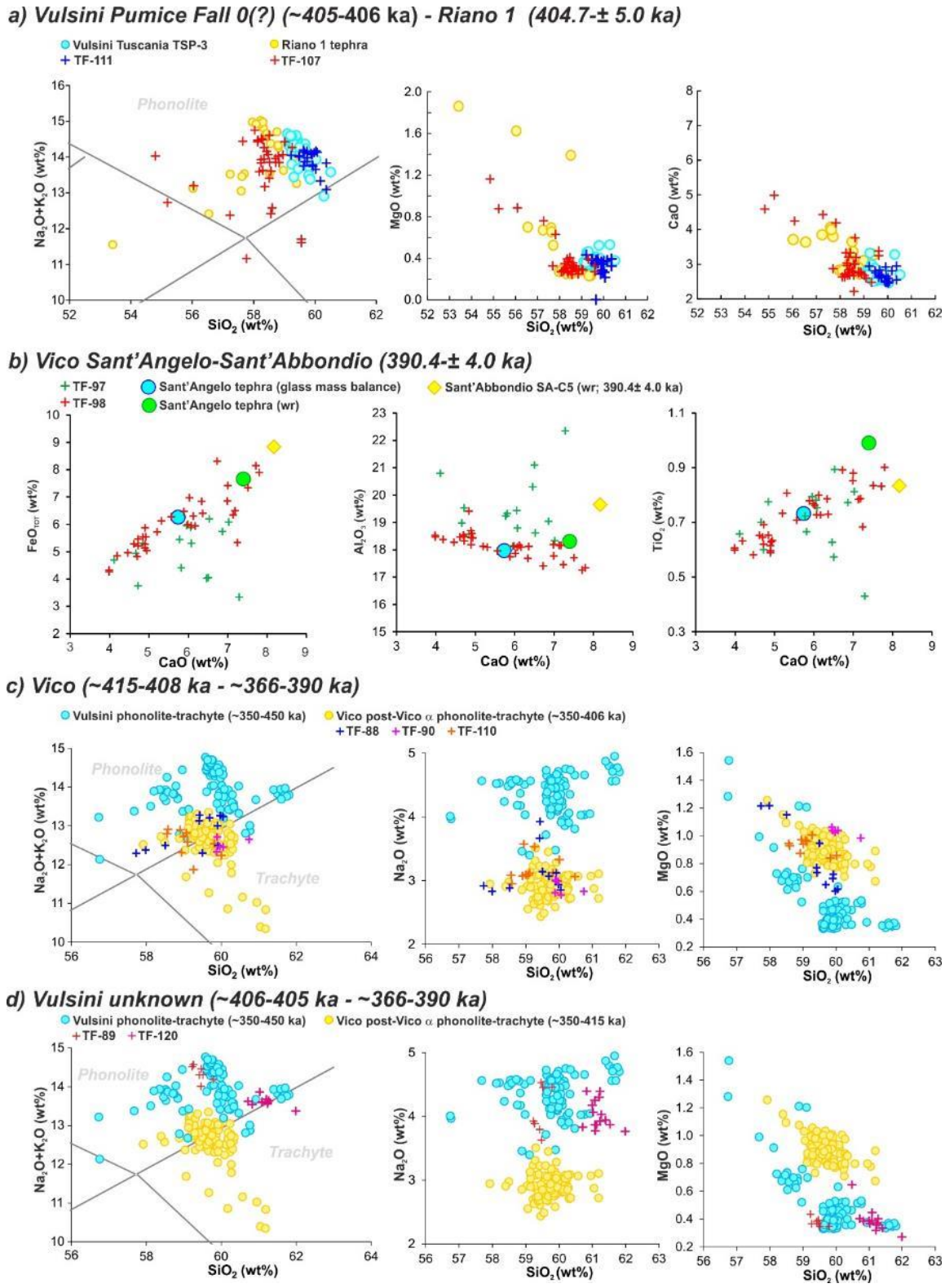

Figure 13. TAS diagram after Le Maitre et al. (2002) and representative bi-plots for the tephra TF-88, TF-89, TF-90, TF-107, TF110, TF-111, TF-120 and TF-124, compared with the proximal Vulsini unit TSP-3 from Tuscania-San Pietro section and

Riano R-1 from the Riano succession (panel **a**), VCO 163 from Vico area, SA C4 and SA C5 from the Sant'Abbondio Fall succession (panel **b**) and with the proximal Vulsini (Casale delle Piane, Castel Broco, TSP-2 and TSP-3 from Tuscania-San Pietro section), and Post-Vico α Vico trachyte-phonolites (Vico β, Vico β_{top}, Vico γ) shown as blue and yellow circles in panels **c)** and **d)**. Data source: WDS glass composition of tephra TF-88, TF-89, TF-90, TF-107, TF-110, TF-111, TF-120, Vulsini (TSP-2, TSP-3) and Riano R-1: this study; VCO 163 whole-rock geochemistry: Perini et al. (2004); SA C4 and SA C5 whole-rock geochemistry and $^{40}Ar/^{39}Ar$ age: Marra et al. (2014); $^{40}Ar/^{39}Ar$ age of R-1: Marra et al. (2018); WDS glass composition of Post-Vico α Vico phonolite-trachytes (Vico β, Vico β_{top}, Vico γ): Pereira et al. (2020). $^{40}Ar/^{39}Ar$ ages are recalculated relative to an age of 1.1891 Ma for the Alder Creek sanidine monitor standard (Niespolo et al., 2017), with the uncertainties expressed at 2σ.

5.2.3.4. Vulsini vs. Vico tephra

TF-88, TF-89, TF-90, TF-96, TF-97, TF-98, TF-110, TF-120, TF-124 – These nine tephra layers are characterised by Cl contents and CaO/FeO ratios consistent with both Vico and Vulsini volcanic sources (Fig. 7c-III).

TF-98 and TF-97 form, together with the rhyolitic tephra TF-99 (unambiguously from Vico; see section 5.2.2.), a stratigraphically strictly related cluster located between TF-85/Villa Senni and TF-116/Vico β. The age of this cluster is therefore bracketed between ~366 ka and ~406 ka. Among the potential Vico equivalents for TF-97 and TF-98, Perini et al. (2004) described the so-called Sant'Angelo tephra, which is stratigraphically constrained between Vico β (406.5 ± 2.4 ka; Pereira et al., 2020) and the Lava di Vico formation (~258 ka), thus chronologically consistent with TF-97 and TF-98, as well as with TF-99, the latter unambiguously attributable to Vico due to its rhyolitic composition (Fig. 12a). However, no glass chemical composition is available for the Sant'Angelo tephra in literature, but only a single whole-rock composition in Perini et al. (2004). Whilst whole rock compositions only allow very limited comparison with glass data, a relatively good geochemical match can be observed between the least evolved end-memember of TF-97/98, and especially of TF-98, and the Sant'Angelo tephra whole-rock composition (Fig. 13b).

On the other hand, the whole rock composition of the Sant'Angelo tephra (Perini et al., 2004) is similar to that of the lowermost unit (i.e., SA-C5) of the Sant'Abbondio lapilli and ash succession of Marra et al. (2014; Fig. 13b), which however yields a quite high loss on ignition, likely reflecting significant alkali loss. Nevertheless, less mobile elements make a tentative correlation of the

Sant'Angelo tephra with SA-C5 still tenable (Fig. 13b). The Sant'Abbondio succession, comprising at least six fallout horizons, occurs in the south-eastern sector of the Vico Volcano, at the boundary of the Vico-Sabatini volcanic domains (Fig. 1b). The base and the top of this succession were $^{40}Ar/^{39}Ar$ dated at 390.4 ± 4.0 ka (lowermost unit SAAS C5) and 380.4 ± 40.0 ka (uppermost unit SAAS C4; wide error associated with biotite dating), and tentatively attributed to the Sabatini activity (Marra et al., 2014). However, considering its chemical affinity with the Sant'Angelo tephra, the Sant'Abbondio lapilli and ash succession can be more likely ascribed to the Vico activity and, possibly, to the Sant'Angelo unit. Thus, transitively, also the TF-99/98 should correlate with Sant'Abbondio units. Unfortunately, Sant'Abbondio units yielded no fresh glass for direct comparison with the potential Fucino equivalents. Therefore, to get an estimation of the interstitial glass composition of Sant'Abbondio/Sant'Angelo unit, based on literature (Perini et al., 2004) and new petrographic observations and mineral composition of the Sant'Abbondio and Sant'Angelo juvenile clasts, we performed a mass balance calculation (SD-1). Notably, according to this calculation, the residual melt of juvenile clasts, having bulk composition, petrographic characters, porphyritic degree, and mineral assemblage featuring the Sant'Angelo/Sant'Abbondio tephra, would be fully consistent with the average glass composition of the TF-98 tephra (Fig. 13b; see also SD-1). Specifically, we found that the bulk composition of Sant'Angelo/Sant'Abbondio tephra is consistent with the average glass composition of TF-98 (49.3 wt%) + Lct (15.9 wt%) + Cpx (12.4 wt%) + bmca (6.5 wt%) + Plg (12.5 wt%) + Ox (3.4 wt%), which substantially matches the textural features and the mineral assemblage observed in Sant'Angelo/Sant'Abbondio SA-C5 tephra. In conclusion, despite the lack of glass compositional data for the proximal counterpart, the correlation of this Vico unit with TF-97-98, and particularly with TF-98, appears quite convincing. As a preliminary tentative attribution, we thus consider the tephra layers TF-97/98, and likely TF-99, as the distal expression of the Sant'Angelo/Sant'Abbondio succession, which may represent the final explosive activity of the Vico Period I (Perini et al., 2004).

TF-88, TF-89, TF-90, TF-96, TF-110, TF-120 and TF-124, though apparently similar in composition and indistinguishable in the CaO/FeO vs diagram (Fig. 7c-III), can be easily attributed either to Vico or Vulsini using the TAS and other simple bivariate diagrams, as shown in Figures 13c-d. Indeed,

the glass geochemistry of the post-Vico α phonolite-trachytes (i.e., the phonolite-trachytes component of Vico β, Vico β_{top} and Vico δ) is quite different from that of the Vulsini phonolite-trachytes spanning a similar time-interval (Figs. 13c-d). Specifically, while TF-88, TF-89 and TF-110 systematically plot within the compositional fields of the post-Vico α phonolite-trachytes (Fig. 13c), TF-90, TF-96, TF-120 and the phonolite component of TF-124 plot in the field of the Vulsini phonolites (Fig. 13d).

As for their potential proximal equivalents, TF-120 stratigraphically occurs between TF-117/Pozzolane Nere (~408 ka) and TF-125/Vico α (~415 ka), i.e., geochronologically roughly consistent with PF-0 (399.8 ± 18.0 ka; Turbeville, 1992), and thus might be considered as an alternative correlative for this Vulsini eruption, other than the above-poposed TF-111. Finally, based on the available geochronological constraints, no specific correlative deposits have been identified in the proximal records for the other Vico (TF-88, TF-89 and TF-110) and Vulsini (TF-90, TF-96, TF-124) distal tephra layers.

5.3. Age model

Based on the direct and indirect (i.e., derived from geochemical fingerprinting) $^{40}Ar/^{39}Ar$ dating of the MIS 11 tephra record, we have developed a Bayesian age-depth model. Only a sub-set of radioisotopic ages (from direct dating or reliable geochemical and/or stratigraphical correlations) with the necessary requisites of both accuracy and precision were selected for this purpose. Specifically, for the investigated interval we selected nine ages from an equivalent number of tephra layers, as shown in Figure 14. The age-depth curve (Fig. 14) shows a remarkable slope change at ~410 ka, indicating that the sedimentation rate was distinctly lower in the first part of the MIS 11 period (~424-410 ka). While this change in sedimentation rate shows no correlation with primary tephra deposition or volcaniclastic input, that is negligible, it coincides with a shift in Ca, from a relatively long and more stable period with higher Ca to a period characterised by large and rapid, millennial-scale variations of Ca (Fig. 15). Ca was addressed to represent lake primary productivity (Giaccio et al., 2019; Mannella et al., 2019) and thus the marked change in sedimentation rate is likely related to changing environmental conditions, a topic which will be addressed elsewhere. Here,

we can only underscore that this change cannot be interpreted as a distortion of the age-depth curve due to age model uncertainty, because it occurs in a stratigraphic interval that is firmly constrained by several radioisotopic ages (Fig. 15).

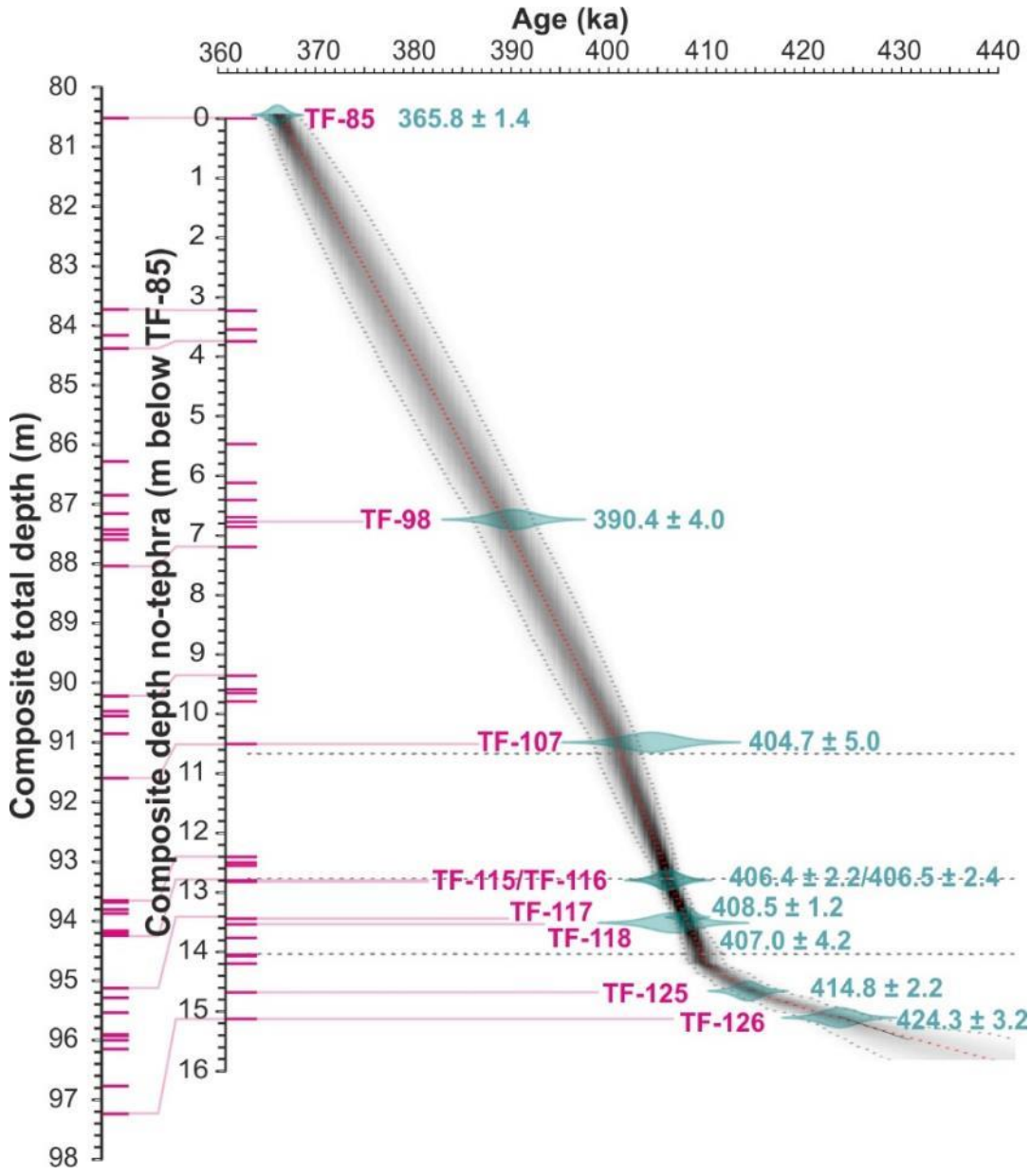

Figure 14. Bayesian age-depth model for the investigated F4-F5 tephra record of the MIS 11 interval.

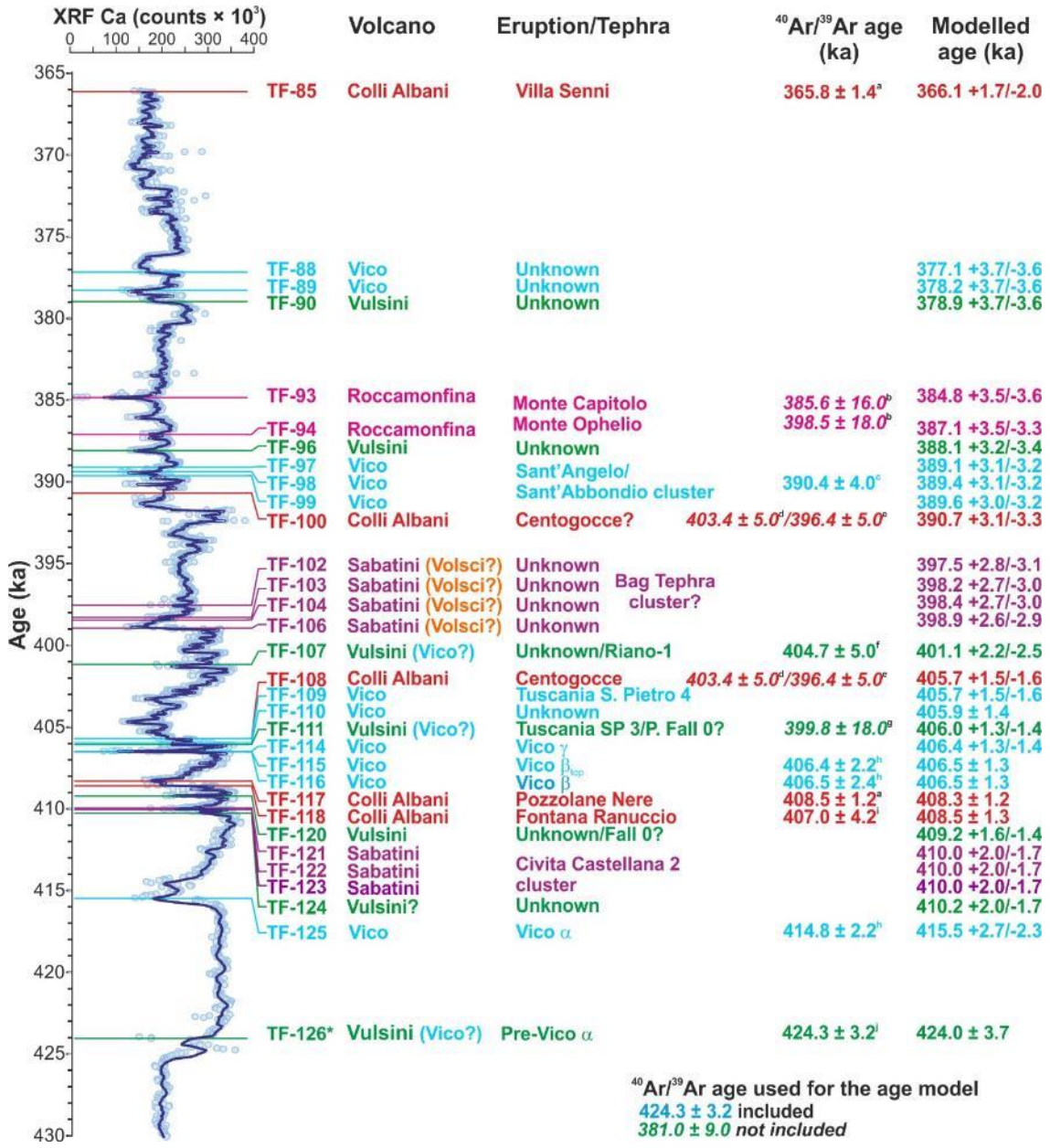

Figure 15. Summary of the volcanic sources, individual correlation and chronology ($^{40}Ar/^{39}Ar$ and modelled ages) of the investigated Fucino F4-F5 tephra record. The MIS 11 temporal series of the calcium content in Fucino lacustrine sediments from F4-F5 core is also shown (XRF data from Giaccio et al., 2019). Ages not used for the age model are reported in italics. Data source: [a] this study; [b] Rouchon et al. (2008); [c] Perini et al. (2004); [d] Marra et al. (2014); [e] Marra et al. (2009); [f] Turbeville (1992); [g] Pereira et al. (2020); [h] Pereira et al. (2018); [i] Giaccio et al. (2019).

The age-depth model allows us to reliably assess the age and climatostratigraphic position of each individual tephra in the F4-F5 MIS 11 section, as shown in Figure 15. Such an integrated

paleoenvironmental-tephra record provides a stratigraphically ordered series of tephra within the framework of the sub-millennial scale paleoclimatic variability of the MIS 11 period, which represents one of the most important features of this kind of integrated record. Indeed, while the chronology is susceptible of improvements through time, the climatostratigraphic position of each tephra is firmly and definitively established here. For instance, the TF-126 tephra is a valuable marker for the onset of a higher productivity interval, likely driven by higher temperature and enhanced nutrients delivery, i.e., typical of interglacial conditions (i.e., MIS 11c; Fig. 15). This specific climatostratigraphic position is independent of the current geochronological (and source) uncertainties of TF-126 tephra and of any possible future improvement in accuracy and precision of the TF-126 dating itself.

5.4. The Fucino MIS 11 tephra record in the framework of central Mediterranean Middle Pleistocene tephrochronology and its relevance for the Quaternary sciences and volcanology

In the framework of the Mediterranean tephrostratigraphy, few relatively continuous sedimentary records span through the Middle Pleistocene (Fig. 1a). The on-land marine succession of Montalbano Jonico, southern Italy (Figs. 1a, 16), records the southern-Italy peri-Tyrrhenian and Vulture volcanic activity at the Early-Middle Pleistocene transition and provides the first evidence for an early onset of the volcanic activity in the Campania Area, at the beginning of the Middle Pleistocene (Petrosino et al., 2015). The radioisotopic geochronological data acquired from Montalbano Jonico also allowed a better constrain of the chronology of the MIS 19 paleoclimatic change (Nomade et al., 2019) and of the cosmogenic nuclide ^{10}Be increase during the Matuyama-Brunhes geomagnetic reversal (Simon et al., 2018).

The Sulmona Basin lacustrine succession, in central Italy (Figs. 1a, 16), represents another rich tephra archive encompassing the Early-Middle Pleistocene transition, which records an intense and frequent activity of the peri-Tyrrhenian volcanism (Giaccio et al., 2013b), poorly documented (or so-far unrecognized) in proximal settings (Marra et al., 2014; Sottili et al., 2019). The Sulmona succession also provided the basis for assembling a robust radiometric chronology for both local and extra-regional MIS 19 paleoclimatic records (Giaccio et al., 2015a; Regattieri et al., 2019) and for constraining the timing of the Matuyama-Brunhes geomagnetic reversal (e.g., Sagnotti et al., 2014).

Furthermore, the Sulmona Basin tephra record spans discontinuously the MIS 15-MIS 10 period (e.g., Giaccio et al., 2013b, 2014; Regattieri et al., 2016), but a comprehensive tephra study for this interval is still pending. Specifically, among several tephra spanning the MIS 11 period (Fig. 16), currently only one has been geochemically characterised (Regattieri et al., 2016). Based on its trachyte-rhyolite composition Regattieri et al. (2016) correlated it to Vico α, but according to the upgraded geochemical dataset obtained by Pereira et al. (2020) for the Vico Period I units, this tephra could be either attributed to Vico α or Vico β (Pereira et al., 2020).

The rich tephra record of the river-lagoon stacked aggradational successions of the Tiber River delta, in central Italy (Figs. 1a, 16), though discontinuous, radioisotopically constrained the timing of the sea-level rise during the last eleven deglaciations (e.g., Marra et al., 2016b; Luberti et al., 2017), including the MIS 11 period (Fig. 16). However, only few tephra layers have been so far geochemically fully characterised (e.g., Pereira et al. 2020), thus limiting the great potential of this succession for tephrochronological purposes.

The deep-sea core KC01B in the Ionian Sea (Fig. 1a) spans continuously the last 1.1 Ma (Lourens, 2004), but detailed tephrostratigraphic investigations are currently available only for the last 200 kyr (Insinga et al., 2014; Fig. 16). A recent detailed tephra and crypto-tephra study of the nearby core ODP Site 964 (Fig. 1) extended this tephrochronological record back to 625 ka (Fig. 16) and resulted in the first reliable synchronization of the marine and terrestrial records during specific intervals of MIS 13 and MIS 10 (Vakhrameeva et al., 2021).

The Mercure, Vallo di Diano and Acerno basins in southern Italy (Figs. 1a, 16), in addition to some known major eruptions from Latium volcanoes, revealed a conspicuous activity of the Roccamonfina Volcano during the MIS 15-MIS 12 period that is still fragmentarily known or currently not yet identified in the near-source volcanic area (Karner et al., 1999; Giaccio et al., 2014; Petrosino et al., 2014a, 2014b). Also located in southern Italy, the San Gregorio Magno lacustrine succession (Fig. 1a) provides a valuable tephra record of the poorly known Middle Pleistocene activity of the Campanian Volcanic Zone, although not extending beyond 250 ka (Petrosino et al., 2019; Fig. 16). Similarly, the Adriatic Sea core PRAD 1-2 (Fig. 1a), extends into the late Middle Pleistocene, reaching ~200 ka (Bourne et al., 2015; Fig. 16).

In the Eastern Mediterranean area, the marine cores KL49, KL51 and LC21 in the Aegean Sea, and the terrestrial (peatland) tephra record of the Tenaghi Philippon Basin (Vakhrameeva et al., 2019) in Greece (Fig. 1a), were used in combination for reconstructing and indirectly dating the explosive activity of the Santorini Volcano during the last 360 kyr (Wulf et al., 2020; Fig. 16). The Tenaghi Philippon archive also documents a MIS 12-MIS 10 tephra record, which was dated climatostratigraphically using the high-resolution pollen profile, allowing a first age estimation of the tephra series of either known or unknown origin (Vakhrameeva et al., 2018; Fig. 16). Finally, the long and continuous tephra record from Lake Ohrid (North Macedonia-Albania; Fig. 1a), mostly from peri-Tyrrhenian potassic volcanic sources, provided important geochronological constraints for developing a robust age model for the outstanding 1.36 Ma-long palaeoclimatic succession, but also for currently unknown volcanic eruptions (Leicher et al., 2019; Wagner et al., 2019; Fig. 16).

In summary, from the above-mentioned Mediterranean Middle Pleistocene tephra records only four long and relatively continuous succesions document in detail the MIS 11 period, i.e., the Sulmona Basin in central Italy, Lake Ohrid in North Macedonia-Albania, the Tenaghi Philippon peatland in Greece and the Ionian Sea core ODP Site 964 (Figs. 1a, 16). However, except the incompletely explored Sulmona record, due to their remote location with respect to the peri-Tyrrhenian volcanoes, the remaining three MIS 11 records document none or only the largest explosive eruptions of the peri-Tyrrhenian potassic volcanic systems, which are the only sources of the tephra found in Fucino Lake record. Specifically, among the Fucino MIS 11 tephra succession, only two tephra layers are found at Lake Ohrid, i.e., (i) Vico α/TF-125/OH-DP 1700.6 and (ii) Roccamonfina Monte Ofelio-Monte Capitolo/TF-96/OH-DP 1640 (Fig. 16), while a third layer, not identified at Fucino, was correlated to an undefined Roccamonfina eruption occurring at onset of the MIS 11 period (Leicher et al., 2019). Due to their greater distance from the peri-Tyrrhenian potassic volcanic sources, the MIS 11 records of Tenaghi Philippon and ODP-964 sites document only few potentially unknown tephra from Neapolitan volcanoes, while the majority are related to the volcanic sources of Santorini, for Tenaghi Philippon, and Santorini, Aeolian Islands and South Aegean Volcanic Arc, for ODP-964 (Vakhrameeva et al., 2018, 2019, 2021). None of the MIS 11 tephra from Tenaghi Philippon or ODP-964 are found in the Fucino record.

In conclusion, the general tephrostratigrapic framework for MIS 11 is far from being satisfactorily developed for a reliable application to Quaternary sciences and volcanology. In this regard, the Fucino MIS 11 record arises as one of the fundamental reference geochemical and chronological datasets for the future development and application of the tephrochronology in the Mediterranean Region, especially for the areas closer to the highly productive tephra sources of peri-Tyrrhenian potassic volcanoes, i.e., that have the potential of capturing part of the activity recorded at Fucino and thus to benefit from its rich tephrochronological record.

5.5. Implications for the peri-Tyrrhenian explosive volcanic history

5.5.1. Distal tephrostratigraphy for elucidating explosive eruption histories: Advantages and limitations

Assessing the issue of the explosive volcanism history using distal archives presents a series of advantages, but also limitations that need to be discussed. The general overview provided in previous sections shows that distal archives often document explosive activity that is hardly traceable to known eruptions or activity period of a specific volcanic source. This highlights the great potential of distal tephrostratigraphy for the assessment of the explosive activity at regional scale (e.g., for the Mediterranean area, Munno and Petrosino, 2007; Paterne et al., 2008; Wulf et al., 2008, 2012; Giaccio et al., 2012, 2014; Leicher et al., 2019). However, several geographical, physical, and time-dependent factors can limit the approach of the distal tephrostratigraphy.

Specifically, the completeness of a distal archive with respect to a given volcano or cluster of volcanoes depends on the (i) relative distance from the volcanic sources, (ii) position with respect to the dominant winds, (iii) magnitude and intensity of the events, (iv) direction of the dispersal axis with respect to the volcano and distal archive location, (v) eruptive dynamics, (vi) variability of the atmospheric circulation pattern during glacial-interglacial and sub-orbital scale climate change (e.g., Bursik, 1998). In turn, the impact of all these factors in limiting the usefulness of the distal tephrostraigraphy depends on the number and geographical distribution of the distal archives documenting the same temporal interval and, more critical, the activity of the same volcanic system. Indeed, a dense network of distal archives distributed across a wide region surrounding a given

volcano, sensibly enhances the possibility of capturing the whole activity of that volcanic system, reducing all the above-mentioned uncertainty and limitating factors, and allowing the construction of a composite record (e.g., Blockley et al., 2014; Lowe et al., 2015; Bronk Ramsey et al., 2015a, 2015b).

As stressed throughout the paper, at present only limited tephrostratigraphic records span the interval documented in this study in detail, and only one (i.e., Lake Ohrid) shares with Fucino some tephra from the peri-Tyrrhenian potassic volcanic sources (Fig. 16). Therefore, the framework of the explosive activity of these volcanic systems obtained using the distal records is likely to be far from complete because of the poorly developed network of tephra records and correlations. Nevertheless, due to its privileged location, we demonstrate that the Fucino paleolake captured most of the known major eruptions and many other unknown explosive events of the peri-Tyrrhenian potassic volcanoes. Therefore, reconstructing the explosive history of the peri-Tyrrhenian potassic volcanoes during the MIS 11 period using the Fucino record alone is fully justified and supported by the data gathered which illustrates that Fucino provides an extremely detailed eruptions record.

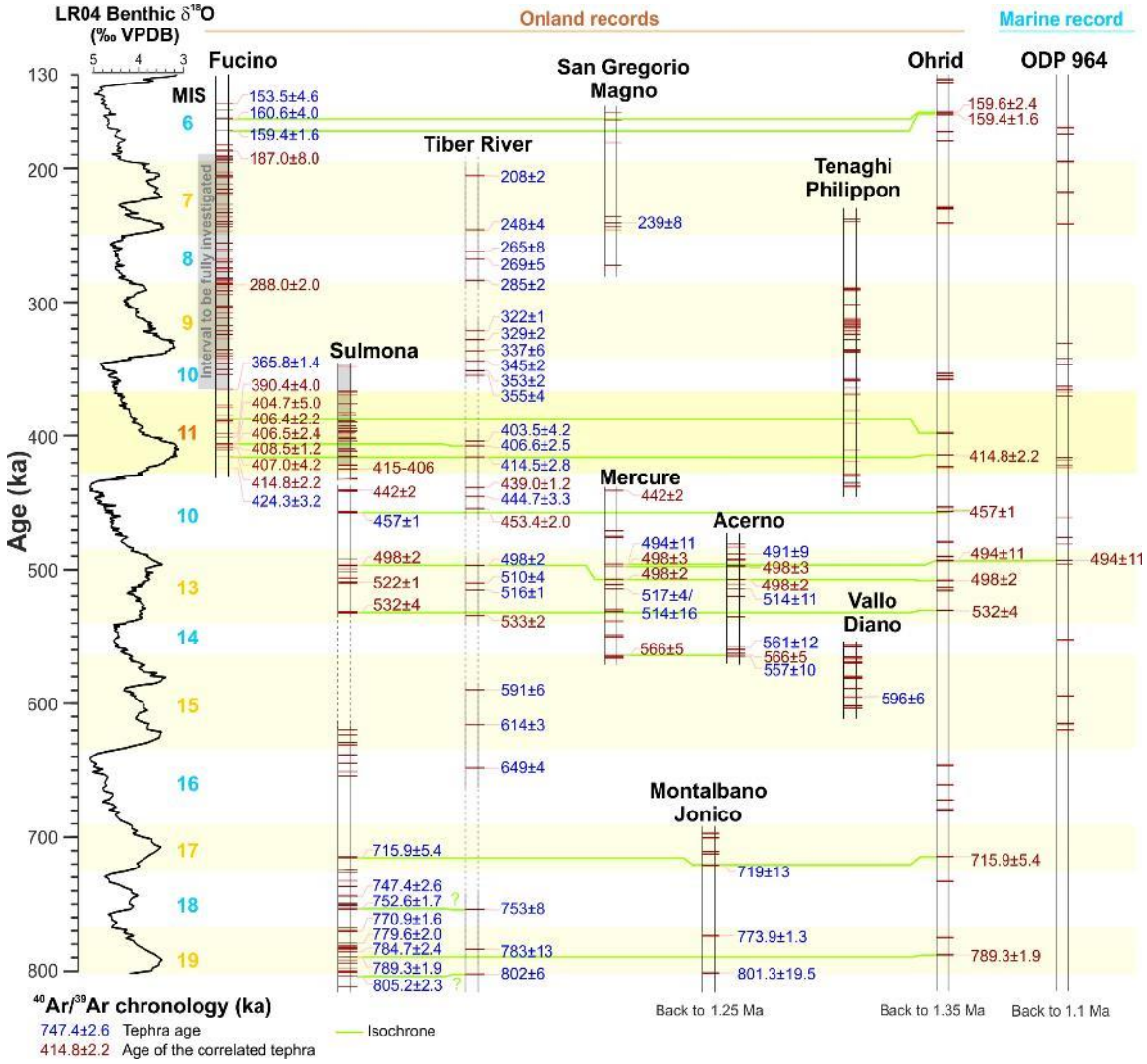

Figure 16. The Fucino MIS 11 tephra record within the framework of the Mediterranen Middle Pleistocene tephrochronological records. Data source: **Fucino**: Giaccio et al. (2017, 2019), Mannella et al (2019), this study; **Sulmona**: Giaccio et al. (2013a, 2013b, 2014, 2015a), Sagnotti et al. (2014), Regattieri et al. (2015, 2019); **Tiber River**: Florindo et al (2007), Villa et al. (2016), Marra et al. (2016a, 2017, 2019, and references therein), Pereira et al. (2020); **Mercure**: Giaccio et al. (2014), Petrosino et al. (2014a); **San Gregorio Magno**: Munno and Petrosino (2007), Petrosino et al. (2019); **Montalbano Jonico**: Petrosino et al. (2015); **Acerno**; Petrosino et al. (2014b); **Vallo di Diano**: Karner et al. (1999); **Tenaghi Philippon**: Vakhrameeva et al. (2018, 2019), Wulf et al. (2020); **Lake Ohrid**: Leicher et al. (2016, 2019), Wagner et al. (2019); **ODP 964**: Vakhrameeva et al. (2021).

5.5.2. The proximal record

In order to compare the distal (Fucino) and proximal records of the peri-Tyrrhenian explosive volcanism of central Italy, we critically review the available geochronological data. The general framework of literature data for the peri-Tyrrhenian volcanic activity encompassing the MIS 11 period, or a slightly wider temporal interval, is provided in Table 6. Though partially and fragmentarily mentioned in previous sections, i.e., when the individual correlations where discussed, in the following section we provide a general overview summarizing the state of the art of the knowledge on the hystory of the peri-Tyrrhenian potassic explosive volcanism.

For the Vulsini Volcanic District, only one direct radioisotopic age determination is available for the studied interval, i.e., the already mentioned Pumice Fall 0 dated at 399.8 ± 18.0 ka (Turbeville, 1992; Table 6). Castel Broco and Casale delle Piane are two others prominent Vulsini eruption units potentially falling in the investigated interval, although lacking direct dating. Recently, Marra et al. (2020a) provided a tentative reconstruction of the eruptive history in this time span, based on xenocryst populations occurring in primary and reworked deposits of the eastern Vulsini (Bolsena-Orvieto and Vulsini Fields activities; Table 6), suggesting that the statistically most significant population age of 425.4 ± 1.6 ka may correspond to that of the Castel Broco eruption.

Table 6. Summary of the literature geochronological data for the peri-Tyrrhenian potassic volcanism of central Italy during the MIS 11, or a slightly wider interval. When possible, i.e., if all the all the required analytical data were published, $^{40}Ar/^{39}Ar$ ages are recalculated relative to an age of 1.1891 Ma for the Alder Creek sanidine or relative to an age of 28.294 Ma for the Fish Canyon sanidine monitor standards (Niespolo et al., 2017), with the uncertainty expressed at 2σ.

Volcanic source	Volcanic phase	Unit/sample	Type of activity/product	K/Ar and $^{40}Ar/^{39}Ar$ age (ka ±2σ)	References
Vulsini	Bolsena	Ponticello Pumices	Pumice fall	352.0±4.0	Nappi et al., 1995
				345.4±2.1	Marra et al., 2020a
	Vulsini Field	Fall 0	Pumice fall	399.8±18.0	Turbeville, 1992
		Castel Broco	Pumice fall-pyroclasti flow	n.d.	
		Piano della Selva	Pyroclastic flow	n.d.	
		Indirect evidence from xenocrysts age populations	undefined	400.5±3.7	Marra et al., 2020a
				411.4±2.4	
				425.4±1.6	
				437.6±2.2	
Vico	Period I	SAAS-bottom	Pumice fall	390.4±4.0	Marra et al., 2014
		VICO δ	Pumice fall	399.7±3.0	

		VICO γ	Pumice fall	n.d.	Pereira et al., 2020
		VICO β_{top}	Pumice fall	406.4±2.0	
		VICO β	Pumice fall	406.5±2.4	
		VICO α	Pumice fall	414.8±2.2	
Sabatini	Southern Sabatini	CC-2	Pumice fall	n.d.	Pereira et al., 2020
		La Rosta	Pumice fall	439.1±1.0	Marra et al., 2020b
		FALL F	Pumice fall	448.5±7.0	Marra et al., 2014
Colli Albani	Villa Senni Eruption Cycle	Madonna degli Angeli succession	Lava dyke	354.5±6.0	Gaeta et al., 2006 and references therein Marra et al 2003
			Lava flow	357.5± 9.0	
			Lava flow	359.5±6.0	
			Lava flow	359.5±8.0	
		Pantano Secco hydromagmatic center	Scoria fall	367.6±2.0	
		Madonna degli Angeli succession	Scoria fall	368.6±2.0	
			Lava flow	369.6±3.0	
		Tufo Lionato	Pyroclastic flow	368.6±4.0	
	Pozzolane Nere Eruption Cycle	Centogocce succession	Lava flow	396.0±5.0	
			Scoria fall	402.3±5.0	
		Pozzolane Nere	Pyroclastic flow	407±2.0	
	Pozzolane Rosse Eruption Cycle	Corcolle succession	Lava flow	439.5±5.0	
			Scoria	440.5±3.0	
		Pozzolane Rosse	Pyroclastic flow	455.5±2.0	
		Vallerano Lava	Lava flow	458.0±8.0	
Volsci volcanic filed		Selva Piana	Lava	362.0±11.0	Boari et al., 2009
		Colle Avarone CA-CGT	Reworked volcanic horizon	360.8±6.5	Marra et al., 2021
		Isoletta III	Scoria fall	363.8±8.0	Pereira et al., 2018
		Isoletta II	Scoria fall	373.7±4.0	
		Valcatora	Lava dyke	379.0±8.0	Boari et al., 2009
		Lademagne II	Reworked volcanic horizon	387.7±5.0	Pereira et al., 2018
		Pofi-Colle La Grotta	Phreatomagmatic deposit	391.5±3.6	Marra et al., 2021
		Giuliano di Roma	Lava	394.6±6.0	Boari et al., 2009
		Pofi Scoria cone	Scoria fall	394.4±3.5	Marra et al., 2021
		Cava Pompi	Scoria fall	392.7±3.0	Pereira et al., 2018
		Arnara Scoria cone	Scoria fall	395.8±6.1	Marra et al., 2021
		Isoletta I	Scoria fall	401.7±3.0	Pereira et al., 2018
		Lademagne I	Scoria fall	404.0±5.0	
		Supino	Phreatomagmatic deposit	407.7±2.6	Marra et al., 2021
		La Tomacella, upper	Pyroclastic rock	410.0±10.0	Boari et al., 2009
		Tecchiena	Lava	416.1±11.0	Boari et al., 2009
		Celleta	Lava	417.1±6.0	
		La Tomacella, lower	Pyroclastic rock	425.2±13.0	
Roccamonfina	Rio Rava-Brown Leucitic Tuff stage	Brown Leucititic Tuff	Pyroclastic flow	343.6±6.0	Scaillet et al., 2008
				358.2±10.0	Rouchon et al., 2008
				385.0±23.0	Luhr and Giannetti, 1987
		Scipicciano 89X	Lava flow	361.7±10.0	

Fontana-radina RMF7	Lava flow	363.7±16.0	Rouchon et al., 2008
SP/R-30	Lava dome	360.0±42.0 (GM)	Giannetti, 2001
		382.0±3.0 (San)	
		390.0±30.0 (San)	
SP/R-31	Effusive	370.8±3.0	
La Frascara RMF4	Lava flow	373.9±18.0	Rouchon et al., 2008
Galluccio RMF3	Lava flow	375.9±16.0	
Monte Casi	Lava dome	370.0±9.0	Radicati di Brozolo et al., 1988
LP/R-247	Effusive	378.9±4.0 (San)	Giannetti, 2001
		399.3±12.0 (San)	
		430.0±6.0 (GM)	
MLT/R-352	Lava flow	374.0±11.0	
MLP/R-69	Lava dome	376.0±16.0	
Monte Capitolo RMF6	Pyroclastic	396.2±16.0	Rouchon et al., 2008
Masseria Robetti	Lava flow	397.0±18.0	Radicati di Brozolo et al., 1988
MLT/R-290	Lava flow	408.4±9.0	Giannetti, 2001
Monte Ofelio RMF12	Pyroclastic	409.4±18.0	Rouchon et al., 2008
MLT/R-351	Lava flow	409.4±10.0	Giannetti, 2001
		415.5±18.0	
LP/R-104	Lava dome	416.6±32.0	
Masseria Robetti	Undefined	421.0±9.0	Radicati di Brozolo et al., 1988
LP/T-247	Lava dome	430.0±6.0	Giannetti, 2001
Rio Rava RMF14	Lava flow	446.0±12.0	Rouchon et al., 2008

GM, goroundmass; San, sanidine.

At Vico Volcano, multiple explosive eruptions of sub-Plinian to Plinian intensity occurred in the investigated interval, which roughly matches the Vico Period I stage (Perini et al., 2004), including Vico α, Vico β, Vico β_{top}, Vico γ, Vico δ and Sant'Angelo tephra (Cioni et al., 1987; Perini et al., 2004; Pereira et al., 2020) (Table 6). The chronology of the Vico Period I has recently been improved by Pereira et al. (2020) who reported new $^{40}Ar/^{39}Ar$ ages for 4 out of the 5 main eruption units recognised in proximal settings (Table 6). In addition, we provided an age constraint for the Sant'Angelo tephra (Perini et al., 2004), based on the proposed correlation to the Sant'Abbondio lapilli and ash succession (390.4 ± 4.0 ka; Marra et al., 2014).

In contrast, no relevant activity is documented at Sabatini Volcanic District during the MIS 11 period. Indeed, the intense explosive activity of the Southern Sabatini stage took place between 500 ka ("Fall A" Plinian eruption) and 439 ka ("La Rosta" Plinian fall; Sottili et al., 2004; Marra et al., 2020b), while the subsequent Bracciano stage started at ~325 ka, thus suggesting a long phase of quiescence extending for more than ~100 kyr. However, the recent attribution of CC-2 pumice fall, which is bracketed between Vico α and Vico β, to the Sabatini activity (Pereira et al., 2020), would partially fill this seemingly long gap in activity. Moreover, as already mentioned in section 3.1., the Strombolian lithological features of the R-2 tephra occurring in the MIS 11 lacustrine succession cropping out near Riano (Fig. 1), laying below the Riano tephra R-1 dated at 404.7 ± 5.0 ka (Marra et al., 2018; Table 6), would also suggest the occurrence of a minor explosive activity of Mts Sabatini during the MIS 11 period.

The 450-350 ka interval at the Colli Albani Volcanic District was characterised by the occurrence of three main eruption cycles, all belonging to the Tuscolano-Artemisio phase of activity: Pozzolane Rosse, Pozzolane Nere and Villa Senni eruption cycles (Freda et al., 1997, 2011; Giordano et al., 2006; Marra et al., 2009; Gaeta et al., 2016; Table 6). Each cycle is characterised by large, caldera-forming eruptions, emplacing up to several tens of km^3 of pyroclastic-flow deposits (De Rita et al., 1988, 1995). The climatic phases were followed by several kyr-long post-caldera phases of activity, characterised by Strombolian and effusive eruptions revealed by numerous scoria cones and lava flows along peri-caldera ring faults, namely the Corcolle, Centogocce and Madonna degli Angeli successions (Giordano et al., 2006; Table 6). The three eruption cycles were separated from each other by ~50 kyr-long quiescent intervals (Marra et al., 2009; Gaeta et al., 2016).

The Volsci Volcanic Field was characterised by diffuse, low-scale, magmatic (Strombolian and subordinate effusive) and phreatomagmatic activities from monogenetic scoria cones and tuff rings (e.g., Cardello et al., 2020; Marra et al., 2021). Several radioisotopic age determinations, encompassing the investigated interval, have been recently acquired (Boari et al., 2009; Nomade et al., 2011; Pereira et al., 2018; Marra et al., 2021; Table 6). It appears that available $^{40}Ar/^{39}Ar$ ages are often grouped in statistically indistinguishable clusters (Table 6), which could be referred to either an individual eruptive event or multiple closely-spaced eruptions. In reconstructing the eruptive

activity, this could lead to overestimate (i.e., multiple dating of the same eruption) or underestimate (i.e., grouping of statistically indistinguishable datings that refer to multiple events) number, frequency, and recurrence of the events. Notwithstanding, the quite distinctive compositional features of the Volsci products (Marra et al., 2021 and references therein), combined with the lack of analysable glass in the dated pyroclastic samples prevents their reliable application for tephrochronological purposes. Therefore, the current data available for the Volsci volcanic field prevent us from assessing the presence of tephra layers from this volcanic system in distal settings (including Fucino) and thus potentially improving its explosive history.

Finally, for the Roccamonfina Volcano, despite the large number of dated products, many of the samples ranging in age from 446 ± 4 ka to 353 ± 5 ka pertain to effusive or poorly defined products (Luhr and Giannetti, 1987; Radicati di Brozolo et al., 1988; Giannetti, 2001; Rouchon et al., 2008) (Table 6). Only the major Brown Leucitic Tuff eruption, and the minor Mt. Capitolo and Mt. Ofelio eruptions document explosive activity in the investigated timespan (Table 6). Moreover, several of these samples were dated by K/Ar method and yielded low precision age estimates, and therefore are scarcely reliable (Table 6). For instance, a previous date on the Brown Leucitic Tuff provided a quite imprecise age of 385 ± 23 ka (Luhr and Giannetti, 1987), and differs quite significantly from more recent age determinations obtained for this eruption (e.g., 358.2 ± 10.0 ka, Rouchon et al., 2008; 343.6 ± 6.0, Scaillet et al., 2008). Finally, a large uncertainty, and unreliability, is reflected by the scattered ages obtained by dating different material from the same sample (e.g., SP/R-30 and LP/R-247; Table 6).

5.5.3. Comparing the proximal and Fucino records of the peri-Tyrrhenian potassic volcanism

The above critical revision of the available literature data for the peri-Tyrrhenian explosive volcanism of central Italy allows a suitable comparison with Fucino MIS 11 tephra record. Overall, the history of the peri-Tyrrhenian explosive volcanism recorded at Fucino appears substantially richer and temporally better resolved with respect to the proximal settings (Fig. 17b). Notably, the Fucino record provides direct evidence for some Vulsini “ghost eruptions” (Marra et al., 2020a). Indeed, the age distribution of xenocrysts extracted from Vulsini pyroclastic units younger than MIS 11 (Marra et

al., 2020a) defines three clusters at 425.4 ± 1.6 ka, 411.4 ± 2.4 ka and 400.5 ± 3.7 ka (Table 6; Fig. 17b) that do not correspond to any exposed products dated so far, which however are in good agreement with the $^{40}Ar/^{39}Ar$ and modelled ages of the Fucino tephra TF-126 (424.0 ± 3.7 ka), TF-120 (409.2 ± 1.6 ka) and TF-107 (401.1 ± 2.5 ka), ascribed to Vulsini (Figs. 15, 17b). This provides further evidence for volcanic activity not yet identified in Vulsini proximal settings.

The Fucino record further refines our knowledge of the early explosive history of Vico Volcano (Pereira et al., 2020). Indeed, except for the missing Vico δ, Fucino documents the whole known activity of Vico Period I and highlights new eruptive events still unrecognised in proximal areas (i.e., TF-99 and TF-109). The age-depth model of Fucino indicates that the previously undated Vico γ eruption occurred around 406.4 ± 1.4 ka (Figs. 15, 17b), i.e., immediately after the Vico β and Vico β_{top} eruption couplet, both with a modelled age of 406.4 ± 1.3 ka. Fucino provides evidence for three distinct tephra layers (i.e., TF-116, TF-115 and TF-114) within a very narrow stratigraphic interval of ~9 cm (Table 2; Fig. 5). They represent three distinct eruptive events of notable intensity occurred in a very short time span and may elude field observations in proximal exposures. Furthermore, while the uppermost fall deposit of the Sant'Abbondio succession, which is here tentatively ascribed to the Vico activity (Sant'Angelo tephra), yielded a poorly constrained age of 380 ± 40 ka (Marra et al., 2014), the Fucino record points out that this eruption cluster likely occurred in a short time span between ~389 ka and ~390 ka (Figs. 15, 17b). Finally, the Fucino record allows us to refine the timing of the early Vico activity, indicating an age of ~377-379 ka for the emplacement of at least two additional, previously unknown, pyroclastic units (Figs. 15, 17b).

Regarding the Sabatini volcanic district, the Fucino dataset improves the knowledge on the history and chronology of the activity, by providing a modelled age of 410.0 ± 2.0 ka for the CC-2 pumice fall (Pereira et al., 2020). Furthermore, Fucino records a cluster of four tephra (TF-102/TF-106) at ~397-400 ka, which may represent the equivalent of the Bag Tephra marker(s) of the Middle Pleistocene Hungarian loess, thus providing the first reliable age and climatostratigraphic position for this stratigraphic marker(s). If confirmed by future investigations, the recognition of this eruption cluster may shed new light on the Sabatini eruption frequency. Indeed, during the whole eruptive history (589 ± 4 ka to 70 ± 3 ka) of the district, the longest dormancy of ~90 kyr has been so far

documented in the time span 438 ± 1 to 329 ± 4 ka (Marra et al., 2020b). The Fucino dataset, showing a previously undetected eruption cluster at 398.9 + 2.6/2.9 ka - 397.5 + 2.8/-3.1 ka, allows us to estimate a maximum quiescence of 68.5 ± 4.1 kyr in the district (i.e., same as the time lapse since the last documented eruption), with implications for hazard assessment in the Roman area. However, at present we cannot exclude that this cluster of eruptions could originate by the Volsci volcanic field (Fig. 15), which documents activity in a comparable timespan (Table 6).

With respect to the known stratigraphic and chronological framework of Colli Albani volcano (Marra et al., 2003, 2009, 2016b; Freda et al., 2006; Giaccio et al., 2009; Gaeta et al., 2011, 2016), the Fucino dataset integrates the chronology of the post-caldera phase that followed the major Pozzolane Nere eruption. Specifically, the last documented eruption of this phase (i.e., Centogocce succession; Fig. 15) occurs at 396.4 ± 5 ka in the Fucino record, which confirms the 30.6 ± 6.4 kyr-long dormancy preceding the onset of the Villa Senni eruption cycle (365.8 ± 1.4 ka), as previously suggested (Gaeta et al., 2016). Such dormancies have relevance in understanding the relationships between the geodynamic/tectonic and magmatic processes (Marra et al., 2004), stress-field and eruptive activity (Marra et al., 2009), as well as in assessing the volcanic hazard in the Roman area (Marra et al., 2016a, 2020b). In particular, the Colli Albani volcano is characterised by a quasi-periodic eruptive behaviour, with average recurrence times of 41 ± 2 kyr for the onset of the main eruptive cycles and average dormancies of 38 ± 2 kyr (Marra et al., 2016a). Notably, the last eruptive cycle started at 41 ± 2 ka and the last eruption occurred at 36 ± 1 ka, thus strongly evidencing a potentially still active (although quiescent) volcanic system.

Finally, the location of the Fucino paleolake NNW of Roccamonfina volcano is less favourable for intercepting the distal products of major (Plinian and Sub-plinian) eruption columns (usually dispersed toward the eastern quadrants at these latitudes), different from co-ignimbrite ash clouds and eruptive plumes from minor explosive events subject to lower altitude winds. Nevertheless, the MIS 11 Fucino dataset improves the chronology, both in term of accuracy and precision, of the post-Rio Rava/pre-Brown Leucitic Tuff stage of the Roccamonfina activity, through the identification of a possible distal equivalent of the Mt. Ofelio-Mt. Capitolo parasitic centers (Rouchon et al., 2008).

Overall, based on the updated chronological data for both proximal volcanic areas and Fucino succession, we obtained the probability density functions for the explosive activity of the peri-Tyrrhenian potassic volcanism during the MIS 11 period (Fig. 17c). By comparing these statistical expressions of the regional explosive volcanism, the proximal record would seem to show a single, monotonous increase of the eruptive frequency between ~410 ka and ~395 ka, followed by a quite homogenous activity during the following 395-365 ka interval. Instead, the better-resolved and richer record derived from Fucino shows a much more complex chronicle. Specifically, the temporal distribution of the peri-Tyrrhenian explosive volcanism is not homogenous and appears significantly clustered, with at least four (or possibly more) ~4-5 kyr-long periods of frequent activity separated by similarly long (5 kyr) periods of declining activity or quiescence. Although intriguing as a feature, here we do not speculate on the possible significance of such cyclicity (e.g., identifying a possible external forcing such as seal level change (Satow et al., 2021), astronomical factors and/or regional tectonics (Marra et al., 2004), as the current analysed record of Fucino is still too short for performing a statistically significant analysis of the frequency distribution of the whole peri-Tyrrhenian potassic explosive activity. We remark that the shape and fluctuation of the reported curve of the temporal distribution (Fig. 17c) does not consider the magnitude and intensity of the events, whereas the actual rate of the erupted volume or mass of magma through time represents an even more important parameter than the mere recurrence interval or frequency of eruptive events. Therefore, further considerations on this key issue are postponed until the complete Fucino tephra record covering the last 430 kyr, or even longer, will be retrieved and fully investigated.

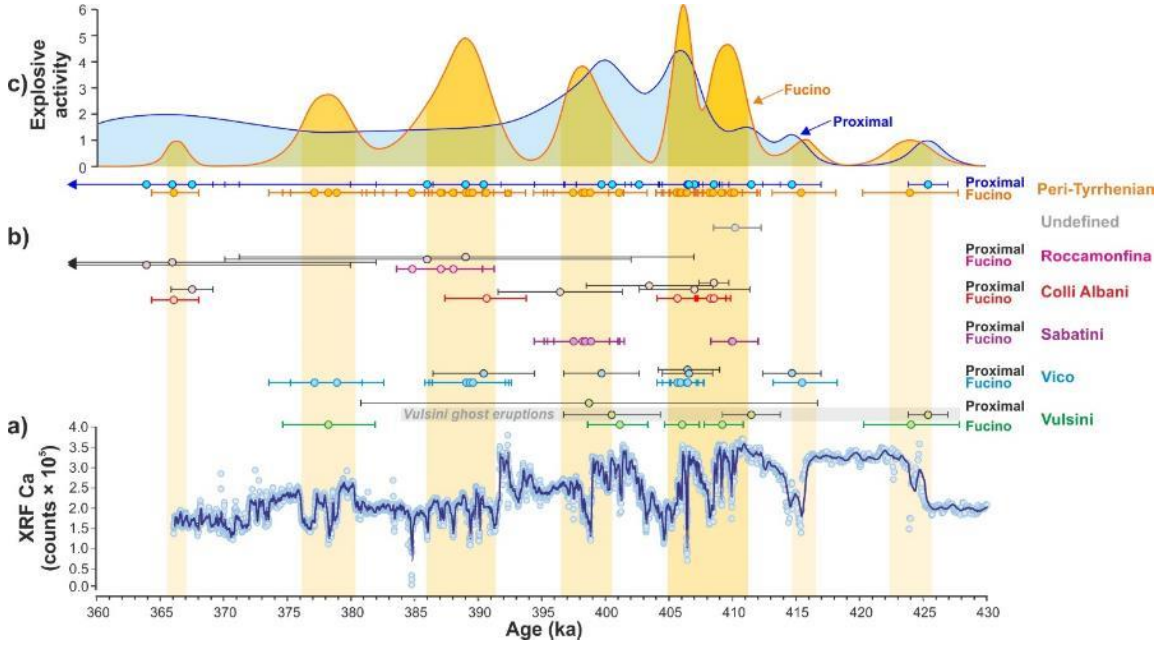

Figure 17. Temporal distribution of the explosive activity of the peri-Tyrrhenian potassic volcanism of central Italy during the 430-360 ka interval, as inferred from the Fucino MIS 11 tephra record and chronological data from proximal volcanic areas. **a)** Temporal series of calcium content of the Fucino lacustrine sediments from F4-F5 core (XRF data from Giaccio et al., 2019). **b)** Comparison between the Fucino and proximal chronological databases from individual peri-Tyrrhenian volcanoes. **c)** Comparison between the probability density functions of the temporal distribution of the peri-Tyrrhenian explosive activity derived from available chronological data from Fucino and proximal volcanic areas. Source for the $^{40}Ar/^{39}Ar$ age of the proximal units: **Vulsini**: Turbeville (1992), Marra et al. (2020a); **Vico**: Marra et al. (2014), Pereira et al. (2020); **Sabatini**: no literature data; **Colli Albani**: Gaeta et al. (2016), Marra et al. (2016a); **Roccamonfina**: Rouchon et al. (2008).

6. Summary and concluding remarks

Here, we have presented a comprehensive review of the state-of-the-art Mediterranean tephrochronology and explosive history of the peri-Tyrrhenian potassic volcanoes during the MIS 11 period. This was achieved in light of new lithostratigraphic, geochemical (major and trace glass composition and multi-phase $^{87}Sr/^{86}Sr$ composition) and geochronological ($^{40}Ar/^{39}Ar$ dating) characterisation of 28 tephra layers from the Fucino F4-F5 succession, as well as of some, potentially equivalent, pyroclastic units collected in proximal areas of the peri-Tyrrhenian potassic volcanoes of central Italy. The integration of these new data with previous investigation from the F4-F5 core, results in a record of 32 tephra layers spanning the 430-365 ka period, thus making Fucino the richest

distal archive for this time interval over the entire Mediterranean region. The resulting dataset allowed us to detect the volcanic sources of most of the newly investigated tephra layers and, in many cases, to recognise the specific equivalent eruption or eruptive phase. A Bayesian age-depth model, based on nine, either directly or geochemically correlated, $^{40}Ar/^{39}Ar$ dated tephra layers yielded a continuously dated record for the Fucino MIS 11 tephra. A synopsis of all the investigated tephra, along with their volcanic sources, corresponding eruptions and related ages is shown in Figure 15. By combining the updated stratigraphic, geochemical, and chronological datasets, we provide an overview of the MIS 11 tephrochronology for the central Mediterranean area (Fig. 16) and even beyond, as shown here by the discovering of a possible equivalent of the Hungarian Bag tephra.

Furthermore, regardless of the limitations of using a single location distal tephra archive to reconstruct past volcanism, the Fucino record clearly documents the eruptive history of the peri-Tyrrhenian explosive volcanoes of central Italy with unprecedented detail and at a higher chronological resolution with respect to available datasets from proximal areas. The improved knowledge of the activity histories of Vulsini, Vico, Sabatini, Colli Albani and Roccamonfina volcanoes, in many cases providing new evidence for previously unidentified eruptions and substantially improving the chronology of the known ones, sets the ground for refining the eruption timing and frequency as well as duration of intervening quiescence periods. This has key implications for hazard assessment as well as for identifying cyclic behaviour of the explosive activity (Fig. 17) linked to still unkown external forcing(s) factors.

Finally, from a wider methodological point of view, the results of this study strengthen and consolidate the relevance of the distal tephra archives as fundamental, integrative records for better reconstructing the behaviour of explosive volcanism, which is crucial for understanding the underlying dynamics and the assessment of the related hazards. This is particularly true in the perspective of future widening of the network of records throughout the regions surrounding Quaternary volcanic areas. Such network will be most valuable for extending the lattice of correlations and for tracing individual tephra layers, which in turn are crucial for both tephrochronological and volcanological purposes. In this perspective, the Fucino Basin, with its long and continuous sedimentary history and strategic position, arises as a cornerstone for the

development and the application of this approach in the Mediterranean region for the Quaternary sciences and volcanology.

Acknowledgments

This article is a contribution of project “FUcino Tephrochronology Unites Quaternary Records (FUTURE)”, supported by the Italian Ministry of Education, University and Research (MIUR, grant PRIN No. 20177TKBXZ_003; G. Zanchetta, coordinator). The Fucino project is co-funded by DFG (German Research Foundation) grant WA 2109/16. $^{40}Ar/^{39}Ar$ dating also received complementary contribution from the CNRS INSU-LEFE 2018-2020 action to S. Nomade. P.G. Albert is supported by a UKRI Future Leaders Fellowship (MR/S035478/1). INGV, OV laboratories have been also financially supported by the EPOS Research Infrastructure through the contribution of the Italian Ministry of University and Research (MUR). An earlier version of the manuscript benefited from useful comments from Roberto Sulpizio and an anonymous reviewer.

References

Albert, P.G., Giaccio, B., Isaia, R., Costa, A., Niespolo, E.M., Nomade, S., Pereira, A., Renne, P.R., Hinchliffe, A., Mark, D.F., Brown, R.J., Smith, V.C., 2019. Evidence for a large-magnitude eruption from Campi Flegrei Caldera (Italy) at 29 ka. Geology. https://doi.org/10.1130/G45805.1.

Albert, P.G., Smith, V.C., Suzuki, T., Tomlinson, E.L., Nakagawa, T., McLean, D., Yamada, M., Staff, R.A., Schlolaut, G., Takemura, T., Nagahashi, Y., Kimura, J., Suigetsu 2006 Project Members, 2018. Constraints on the frequency and dispersal of explosive eruptions at Sambe and Daisen volcanoes (South-West Japan Arc) from the distal Lake Suigetsu record (SG06 core). Earth Science Reviews, 185, 1004-1028. https://doi.org/10.1016/j.earscirev.2018.07.003.

Amato, V., Aucelli, P.P.C., Cesarano, M., Filocamo, F., Leone, N., Petrosino, P., Rosskopf, C.M., Valente, E., Casciello, E., Giralt, S., Jicha, B.R., 2018. Geomorphic response to late Quaternary tectonics in the axial portion of the Southern Apennines (Italy): A case study from the Calore River valley. Earth Surface Processes and Landforms, 43, 2463-2480. https://doi.org/10.1002/esp.4390.

Amato, V., Aucelli, P.P.C., Cesarano, M., Jicha, B., Lebreton, V., Orain, R., Pappone, G., Petrosino, P., Russo Ermolli, E., 2014. Quaternary evolution of the largest intermontane basin of the Molise Apennine (Central Southern Italy). Rendiconti Lincei, 25, 197-216. http://dx.doi.org/10.1007%2Fs12210-014-0324-y.

Belkin, H.E., Rolandi, G., Jackson, J.C., Cannatelli, C., Doherty, A.L., Petrosino, P., De Vivo, B., 2016. Mineralogy and geochemistry of the older (>40 ka) ignimbrites in the Campanian Plain, southern Italy. Journal of Volcanology and Geothermal Research, 323, 1-18. https://doi.org/10.1016/j.jvolgeores.2016.05.002.

Bini, M., Zanchetta, G., Drysdale, R.N., Giaccio, B., Stocchi, P., Vacchi, M., Hellstrom, J.C., Couchoud, I., Monaco, L., Ratti, A., Martini, F., Sarti L., 2020. An end to the Last Interglacial highstand before 120 ka: Relative sea-level evidence from Infreschi Cave (Southern Italy). Quaternary Science Reviews 250, 106658. https://doi.org/10.1016/j.quascirev.2020.106658.

Blaauw, M. & Christen, J.A., 2011. Flexible paleoclimate age-depth models using an autoregressive gamma process. Bayesian Analysis, 6:3, 457-474. https://doi.org/10.1214/11-BA618.

Blockley, S.P.E., Bourne, A.J., Brauer, A., Davies, S.M., Hardiman, M., Harding, P.R., Lane, C.S., MacLeod, A., Matthews, I.P., Pyne-O'Donnel, S.D.F., Rasmussen, S.O., Wulf, S., Zanchetta, G., 2014. Tephrochronology and the extended intimate (integration of ice-core, marine and terrestrial records) event stratigraphy 8-128 ka 2bk. Quaternary Science Reviews, 106, 88-100. https://doi.org/10.1016/j.quascirev.2014.11.002.

Boari, E., Tommasini, S., Laurenzi, M.A., Conticelli, S., 2009. Transition from Ultrapotassic Kamafugitic to Sub-Alkaline Magmas: Sr, Nd, and Pb Isotope, Trace Element and 40Ar-39Ar Age Data from the Middle Latin Valley Volcanic Field, Roman Magmatic Province, Central Italy. Journal of Petrology, 50, 7, 1327-1357. https://doi.org/10.1093/petrology/egp003.

Boncio, P., Lavecchia, G., Pace, B., 2004. Defining a model of 3D seismogenic sources for seismic hazard assessment applications: The case of central Apennines (Italy). Journal of Seismology, 8(3), 407–425. https://doi.org/10.1023/B:JOSE.0000038449.78801.05.

Bourne, A.J., Albert, P.G., Matthews, I.P., Trincardi, F., Wulf, S., Asioli, A., Blockley, S.P.E., Keller, J., Lowe, J.J., 2015. Tephrochronology of core PRAD 1-2 from the Adriatic Sea: insights into Italian explosive volcanism for the period 200-80 ka. Quaternary Science Reviews, 116, 28-43. https://doi.org/10.1016/j.quascirev.2015.03.006.

Bourne, A.J., Lowe, J.J., Trincardi, F., Asioli, A., Blockley, S.P.E., Wulf, S., Matthews, I.P., Piva, A., Vigliotti, L., 2010. Distal tephra record for the last ca 105,000 years from core PRAD 1-2 in the central Adriatic Sea: implications for the marine tephrostratigraphy. Quaternary Science Reviews, 29, 3079-3094. https://doi.org/10.1016/j.quascirev.2010.07.021.

Bronk Ramsey, C., Albert, P.G., Blockley, S.P.E., Hardiman, M., Housley, R.A., Lane, C.S., Lee, S., Matthews, I.P., Smith, V.C., Lowe, J.J., 2015a. Improved age estimates for key Late Quaternary European tephra horizons in the RESET lattice. Quaternary Science Reviews, 118, 18-32. https://doi.org/10.1016/j.quascirev.2014.11.007.

Bronk Ramsey, C., Housley, R.A., Lane, C.S., Smith, V.C., Pollard, A.M., 2015b. The Reset tephra database and associated analytical tools. Quaternary Science Reviews, 118, 33-47. https://doi.org/10.1016/j.quascirev.2014.11.008.

Bursik, M., 1998. Tephra dispersal. In: Gilbert, J.S., Sparks, R.S.J. (eds). The physics of explosive volcanic eruptions. Geological society of London Special Publication, 145, 115-144. https://doi.org/10.1144/GSL.SP.1996.145.01.07.

Cardello, G.L., Consorti, L., Palladino, D.M., Carminati, E., Carlini, M., Doglioni, C., 2020. Tectonically controlled carbonate-seated maar-diatreme volcanoes: The case of the Volsci Volcanic Field, central Italy. Journals of Geodynamics, 139, 101763. https://doi.org/10.1016/j.jog.2020.101763.

Cavinato, G.P., Carusi, C., Dell'Asta, M., Miccadei, E., Piacentini T., 2002. Sedimentary and tectonic evolution of Plio-Pleistocene alluvial and lacustrine deposits of Fucino Basin (central Italy). Sedimentary Geology, 148, 29-59. https://doi.org/10.1016/S0037-0738(01)00209-3.

Centamore, E., Dramis, F., Di Manna, P., Fumanti, F., Milli, S., Rossi, D., Palombo, M.R., Palladino, D.M., Triglia, R., Zanon, V., Chiocchini, M., Didaskalou, P., Potetti, M., Nisio, S., 2010. Note illustrative del Foglio 402 Ceccano. Carta Geologica d'Italia 1:50000. Servizio Geologico d'Italia, Roma (in Italian).

Cioni, R., Sbrana, A., Bertagnini, A., Buonasorte, G., Landi, P., Rossi, U., Salvati, L., 1987. Tephrostratigraphic correlations in the Vulsini, Vico and Sabatini volcanic succession. Periodico di Mineralogia, 56, 137-155.

Cross, J.K., Tomlinson, E.L., Giordano, G., Smith, V.S., De Benedetti, A.A., Roberge, J., Manning, C.J., Wulf, S., Menzies, M.A., 2014. High level triggers for explosive mafic volcanism: Albano Maar, Italy. Lithos, 190-191, 137-153. https://doi.org/10.1016/j.lithos.2013.11.001.

D'Antonio, M., Mariconte, R., Arienzo, I., Mazzeo, F.C., Carandente, A., Perugini, D., Petrelli, M., Corselli, C., Orsi, G., Principato, M.S., Civetta, L., 2016. Combined Sr-Nd isotopic and geochemical fingerprinting as a tool for identifying tephra layers: Application to deep-sea cores from Eastern Mediterranean Sea. Chemical Geology, 443, 121-136. https://doi.org/10.1016/j.chemgeo.2016.09.022.

D'Agostino, N., Jackson, J. A., Dramis, F., Funiciello, R., 2001. Interactions between mantle upwelling, drainage evolution and active normal faulting: an example from the central Apennines (Italy). Geophysical Journal International, 147(2), 475–497. https://doi.org/10.1046/j.1365-246X.2001.00539.x.

de Fontaine, C.S., Kaufman, D.S., Anderson, R.S., Werner, A., Waythomass, C.F., Brown, T.A., 2007. Late Quaternary distal-fall deposits in lacustrine sediments, Kenai Peninsula, Alaska. Quaternary Research, 68, 1, 64-78. https://doi.org/10.1016/j.yqres.2007.03.006.

De Rita, D., Funiciello, R., Parotto, M., 1988. Carta geologica del complesso vulcanico dei Colli Albani (Vulcano Laziale). C.N.R.-Gruppo Nazionale Vulcanologia (in Italian).

De Rita, D., Giordano, G., Rosa, C., Sheridan, M.F., 1995. Volcanic risk at the Alban Hills volcano and numerical simulations. In: Triglia, R. (Ed), The Volcano of the Alban Hills. Tipografia SGS, Rome, pp. 267-283.

De Vivo, B., Rolandi, G., Gans, P.B., Calvert, A., Bohrson, W.A., Spera, F.J., Belkin, H.E., 2001. New constraints on the pyroclastic eruptive history of Campanian volcanic Plain (Italy). Mineralogy and Petrology, 73, 47-65. https://doi.org/10.1007/s007100170010.

Del Carlo, P., Smedile, A., Petrelli, M., Di Roberto, A., 2020. Evidence of an unknown explosive eruption of Mt. Etna volcano (Italy) during the Late Glacial. Journal of Volcanology and Geothermal Research. 402, 106992. https://doi.org/10.1016/j.jvolgeores.2020.106992.

Di Roberto, A., Smedile, A., Del Carlo, P., De Martini, P.M., Iorio, M., Petrelli, M., Pantosti, P., Pinzi, S., Todrani, A., 2018. Tephra and cryptotephra in a ~60,000-year old lacustrine sequence from the Fucino Basin: new insights into the major explosive events in Italy. Bulletin of Volcanology, 80:20. https://doi.org/10.1007/s00445-018-1200-x.

Doglioni, C., Harabaglia, P., Martinelli, G., Mongelli, F., Zito, G., 1996. A geodynamic model of the Southern Apennines accretionary prism. Terra Nova, 8:6, 540-547. https://doi.org/10.1111/j.1365-3121.1996.tb00783.x.

Donato, P., Albert, P.G., Crocitti, M., De Rosa, C., Menzies, M.A., 2016. Tephra layers along the southern Tyrrhenian coast of Italy: Links to the X-5 & X-6 using volcanic glass geochemistry. Journal of Volcanology and Geothermal Research, 317, 30-41. https://doi.org/10.1016/j.jvolgeores.2016.02.023.

Dugmore, A.J., 1989. Icelandic volcanic ash in Scotland. Scottish Geographical Megazine, 105:3, 168-172. https://doi.org/10.1080/14702548908554430.

Dugmore, A.J., Newton, A.J., Smith, K.T., Mairs, K.A., 2013. Tephrochronology and the late Holocene volcanic and flood history of Eyjafjallajökull, Iceland. (2013). Journal of Quaternary Science, 28:3, 237-247. https://doi.org/10.1002/jqs.2608.

Florindo, F., Karner, D.B., Marra, F., Renne, P.R., Roberts A.P., Weaver, R., 2007. Radioisotopic age constraints for Glacial Terminations IX and VII from aggradational sections of the Tiber River delta in Rome, Italy. Earth and Planetary Science Letters 256, 61-80. https://doi.org/10.1016/j.epsl.2007.01.014.

Freda, C., Gaeta, M., Giaccio, B., Marra, F., Palladino, D.M., Scarlato, P., Sottili, G., 2011. CO2-driven large mafic explosive eruptions: the Pozzolane Rosse case study from the Colli Albani Volcanic District (Italy). Bulletin of Volcanology, 73, 241-256.

Freda, C., Gaeta, M., Karner, D.B., Marra, F., Renne, P.R., Taddeucci, J., Scarlato, P., Christensen, J.N., Dallai, L., 2006. Eruptive history and petrologic evolution of the Albano multiple maar (Alban Hills, Central Italy). Bulletin of Volcanology, 68, 567-591. https://doi.org/10.1007/s00445-005-0033-6.

Freda, C., Gaeta, M., Palladino, D.M., Trigila, R., 1997. The Villa Senni eruption (Alban Hills, Central Italy): the role of H2O and CO2 on the magma chamber evolution and on the eruptive scenario. Journal of Volcanology and Geothermal Research, 78 (1-2), 103-120. https://doi.org/10.1016/S0377-0273(97)00007-3.

Funiciello, R., De Rita, D., Sposato, A., Esposito, A., Fabbri, M., Marsili, P., Mazzini, I., Paccara, P., Trigari, A., Capelli, G., Faccenna, C., Fiorentino, A., Mazza, R., Rossetti, F., Sardella, R., Soligo, M., Tuccimei, P., Villa, I.M., 2012. Note Illustrative della Carta Geologica d'Italia alla scala 1:50.000, Foglio 354 "Tarquinia". Presidenza del Consiglio dei Ministri, Agenzia per la Protezione dell'Ambiente e per i servizi Tecnici: Roma, Italy, Servizio Geologico d'Italia, scale 1:50,000 (in press, in Italian).

Gaeta, M., Freda, C., Christensen, J.N., Dallai, L., Marra, F., Karner, D.B., Scarlato, P., 2006. Time-dependent geochemistry of clinopyroxene from the Alban Hills (Central Italy): clues to the source and evolution of ultrapotassic magmas. Lithos 86, 330-346. https://doi.org/10.1016/j.lithos.2005.05.010.

Gaeta, M., Freda, C., Marra F., Arienzo, I., Gozzi, F., Jicha, B., Di Rocco, T., 2016. Paleozoic metasomatism at the origin of Mediterranean ultrapotassic magmas: Constraints from time-dependent geochemistry of Colli Albani volcanic products (Central Italy). Lithos, 244, 151-164. https://doi.org/10.1016/j.lithos.2015.11.034.

Gaeta, M., Freda, C., Marra, F., Di Rocco, T., Gozzi, F., Arienzo, I., Giaccio, B., Scarlato, P., 2011. Petrology of the most recent ultrapotassic magmas from the Roman Province (Central Italy). Lithos, 127, 298-308. https://doi.org/10.1016/j.lithos.2011.08.006.

Galadini, F. & Galli, P., 2000. Active tectonics in the Central Apennines (Italy) - Input Data for Seismic Hazard Assessment. Natural Hazards, 22, 225-270. https://doi.org/10.1023/A:1008149531980.

Gatta, M., Sinopoli, G., Giardini, M., Giaccio, B., Hajdas, I., Pandolfi, L., Bailey, G., Spikins, P., Rolfo, M.F., Sadori, L., 2016. Pollen from Late Pleistocene hyena (Crocuta Crocuta spelaea) coprolites: An interdisciplinary approach from two Italian sites. Review of Palaeobotany and Palynology, 233, 56-66. https://doi.org/10.1016/j.revpalbo.2016.07.005.

Gehrels, M.J., Lowe, D.J., Hazell, Z.J., Newnham, R.M., 2006. A continuous 5300-yr Holocene cryptotephrostratigraphic record from northern New Zealand and impllications for tephrochronlogy and volcanic hazard assessment. The Holocene, 16, 2,

173-187. https://doi.org/10.1191%2F0959683606hl918rp.
Giaccio, B., Arienzo, I., Sottili, G., Castorina, F., Gaeta, M., Nomade, S., Galli, P., Messina, P., 2013a. Isotopic (Sr-Nd) and major element fingerprinting of distal tephras: An application to the Middle-Late Pleistocene markers from the Colli Albani volcano, central Italy. Quaternary Science Reviews, vol. 67, 190-206. https://doi.org/10.1016/j.quascirev.2013.01.028.
Giaccio, B., Castorina, F., Nomade, S., Scardia, G., Voltaggio, M., Sagnotti, L., 2013b. Revised Chronology of the Sulmona Lacustrine Succession, Central Italy. Journal of Quaternary Science, 28, 545-551. https://doi.org/10.1002/jqs.2647.
Giaccio, B., Galli, P., Messina, P., Peronace, E., Scardia, G., Sottili, G., Sposato, A., Chiarini, E., Jicha, B., Silvestri, S., 2012b. Fault and basin depocentre migration over the last 2Ma in the L'Aquila 2009 earthquake region, central Italian Apennines. Quaternary Science Reviews, 56, 69–88. https://doi.org/10.1016/j.quascirev.2012.08.016.
Giaccio, B., Galli, P., Peronace, E., Arienzo I., Nomade, S., Cavinato, G.P., Mancini, M., Messina, P., Sottili, G., 2014. A 560-440 ka tephra record from the Mercure Basin, Southern Italy: volcanological and tephrostratigraphic implications. Journal of Quaternary Science, 29, 232-248. https://doi.org/10.1002/jqs.2696.
Giaccio, B., Leicher, N., Mannella, G., Monaco, L., Regattieri, E., Wagner, B., Zanchetta, G., Gaeta, M., Marra, F., Nomade, S., Palladino, D.M., Pereira, A., Scheidt, S., Sottili, G., Wonik, T., Wulf, S., Zeeden, C., Ariztegui, D., Cavinato, G.P., Dean, R.J., Florindo, F., Leng, M.J., Macrì, P., Niespolo, E., Renne, P.R., Rolf, C., Sadori, L., Thomas, C., Tzedakis, P.C., 2019. Extending the tephra and paleoenvironmental record of the Central Mediterranean back to 430 ka: A new core from Fucino Basin, central Italy. Quaternary Science Reviews, 225, 106003. https://doi.org/10.1016/j.quascirev.2019.106003.
Giaccio, B., Marra, F., Hajdas, I., Karner, D.B., Renne, P.R., Sposato, A., 2009. 40Ar/39Ar and 14C geochronology of the Albano maar deposits: Implications for defining the age and eruptive style of the most recent explosive activity at Colli Albani Volcanic District, Central Italy. Journal of Volcanology and Geothermal Research, 185, 203-213. https://doi.org/10.1016/j.jvolgeores.2009.05.011.
Giaccio, B., Niespolo, E.M., Pereira, A., Nomade, S., Renne, P.R., Albert, P.G., Arienzo, I., Regattieri, E., Wagner, B., Zanchetta, G., Gaeta, M., Galli, P., Mannella, G., Peronace, E., Sottili, G., Florindo, F., Leicher, N., Marra, F., Tomlinson, E.L., 2017. First integrated tephrochronological record for the last ~190 kyr from the Fucino Quaternary lacustrine succession, central Italy. Quaternary Science Reviews, 158, 211-234. https://doi.org/10.1016/j.quascirev.2017.01.004.
Giaccio, B., Nomade, S., Wulf, S., Isaia, R., Sottili, G., Cavuoto, G., Galli, P., Messina, P., Sposato, A., Sulpizio, R., Zanchetta, G., 2012a. The late MIS 5 Mediterranean tephra markers: a reappraisal from peninsular Italy terrestrial records. Quaternary Science Reviews, 56, 31-45. https://doi.org/10.1016/j.quascirev.2012.09.009.
Giaccio, B., Regattieri, E., Zanchetta, G., Nomade, S., Renne, P.R., Sprain, C.J., Drysdale, R.N., Tzedakis, P.C., Messina, P., Scardia, G., Sposato, A., Bassinot, F., 2015a. Duration and dynamics of the best orbital analogue to the present interglacial. Geology, 43, 603-606. https://doi.org/10.1130/G36677.1.
Giaccio, B., Regattieri, E., Zanchetta, G., Wagner, B., Galli, P., Mannella, G., Niespolo, E., Peronace, E., Renne, P.R., Nomade, S., Cavinato, G.P., Messina, P., Sposato, A., Boschi, C., Florindo, F., Marra, F., Sadori, L., 2015b. A key continental archive for the last 2 Ma of climatic history of the central Mediterranean region: A pilot drilling in the Fucino Basin, central Italy. Scientific Drilling, 20, 13-19. https://doi.org/10.5194/sd-20-13-2015.
Giannetti, B. & De Casa, G., 2000. Stratigraphy, chronology, and sedimentology of ignimbrites from the white trachytic tuff, Roccamonfina Volcano, Italy. Journal of Volcanology and Geothermal Research, 96, 3-4, 243-295. https://doi.org/10.1016/S0377-0273(99)00144-4.
Giannetti, B., 1996a. The geology of the Yellow Trachytic Tuff, Roccamonfina Volcano. Journal of Volcanology and Geothermal Research, 71, 1, 53-72. https://doi.org/10.1016/0377-0273(95)00030-5.
Giannetti, B., 1996b. Volcanology of trachytic and associated basaltic pyroclastic deposits at Roccamonfina volcano, Roman Region, Italy. Journal of Volcanology and Geothermal Research, 71, 2-4, 229-248. https://doi.org/10.1016/0377-0273(95)00068-2.
Giannetti, B., 2001. Origin of the calderas and evolution of Roccamonfina volcano (Roman Region, Italy). Journal of Volcanology and Geothermal Research, 106, 301-319. https://doi.org/10.1016/S0377-0273(00)00259-6.
Giordano, G., De Benedetti, A.A., Diana, A., Diano, G., Gaudioso, F., Marasco, F., Miceli, M., Mollo, S., Cas, R.A.F., Funiciello, R., 2006. The Colli Albani mafic caldera (Roma, Italy): Stratigraphy, structure and petrology. Journal of Volcanology and Geothermal Research, 155, 49-80. https://doi.org/10.1016/j.jvolgeores.2006.02.009.
Goldstein, S.L., Denis, P., Oelkers, E.H., Rudnick, R.L., Walter, L.M., 2003. Standards for publication of isotope ratio and chemical data in chemical geology. Chemical Geology, 202, 1-4. https://doi.org/10.1016/j.chemgo.2003.08.003.
Horváth, E. & Bradák, B., 2014. Sárga föld, lősz, lösz: Short historical overview of loess research and litostratigraphy in Hungary. Quaternary International, 319, 1-10. https://doi.org/10.1016/j.quaint.2013.10.066.
Hum, L., 2005. Középső pleisztocén tufithorizontok megjelenése dunaszekcsői és Mórágy környéki löszszelvényekben. Malakológiai Tájékoztató, 23, 131-148 (in Hungarian).
Insinga, D.D., Tamburrino, S., Lirer, F., Vezzoli, L., Barra, M., De Lange, G.J., Tiepolo, M., Vallefuoco, M., Mazzola, S., Sprovieri, M., 2014. Tephrochronology of the astronomically-tuned KC01B deep-sea core, Ionian Sea: insights into the explosive activity of the Central Mediterranean area during the last 200 ka. Quaternary Science Reviews, 85, 63-84. https://doi.org/10.1016/j.quascirev.2013.11.019.
Jochum, K.P., Stoll, B., Herwig, K., Willbold, M., Hofmann, A.W., Amini, M., Aarbug, S., Abouchami, W., Hellebrand, E., Mocek, B., Raczek, I., Stracke, A., Alard, O., Bouman, C., Becker, S., Dücking, M., Brätz, H., Klemd, R., de Bruin, D., Canil, D., Cornell, D., de

Hoog, C.-S., Dalpé, C., Danyushevsky, L., Eisenhauer, A., Gao, Y., Snow, J.E., Groschopf, N., Günther, D., Latkoczy, C., Guillong, M., Hauri, E.K., Höfer, H.E., Lahaye, Y., Horz, K., Jacob, D.E., Kasemann, S.A., Kent, A.J.R., Ludwig, T., Zack, T., Mason, P.R.D., Meixner, A., Rosner, M., Kisawa, K., Nash, P.B., Pfänder, J., Premo, W.R., Sun, W.D., Tiepolo, M., Vannucci, R., Vennemann, T., Wayne, D., Woodhead, J.D., 2006. MPI-DING reference glasses for in situ microanalysis: New reference values for element concentrations and isotope ratios. Geochemistry, Geophysics, Geosystems, 7:2. https://doi.org/10.1029/2005GC001060.

Karner, D.B. & Renne, P.R., 1998. 40Ar/39Ar geochronology of Roman volcanic province tephra in the Tiber River valley: Age calibration of middle Pleistocene sea-level changes. Geological Society of America Bulletin, 110, 6, 740-747. https://doi.org/10.1130/0016-7606(1998)110%3C0740:AAGORV%3E2.3.CO;2.

Karner, D.B., Juvinge, E., Brancaccio, L., Cinque, A., Russo Ermolli, E., Santangelo, L., Bernasconi, S., Lirer, L., 1999. A potential early middle Pleistocene tephrostratotype for the Mediterranean basin: the Vallo Di Diano, Campania, Italy. Global and Planetary Change, 21, 1-15. https://doi.org/10.1016/S0921-8181(99)00004-1.

Keller, J., Ryan, W.B.F., Ninkovich, D., Altherr, R., 1978. Explosive volcanic activity in the Mediterranean over the last 200,000 yr as recorded in deep-sea sediments. Geological Society of America Bulletin, 89, 591-604. https://doi.org/10.1130/0016-7606(1978)89%3C591:EVAITM%3E2.0.CO;2.

Kousis, I., Koutsodendris, A., Peyron, O., Leicher, N., Francke, A., Wagner, B., Giaccio, B., Knipping, M., Pross, J., 2018. Centennial-scale vegetation dynamics and climate variability in SE Europe during Marine Isotope Stage 11 based on a pollen record from Lake Ohrid, Quaternary Science Reviews, 190, 20-38. https://doi.org/10.1016/j.quascirev.2018.04.014.

Kuehn, S.C., Froese, D.G., Shane, P.A.R., INTAV Intercomparison Participants, 2011. The INTAV intercomparison of electron-beam microanalysis of glass by tephrochronology laboratories: Results and recommendations. Quaternary International, 246, 19-47. https://doi.org/10.1016/j.quaint.2011.08.022.

Lane, C.S., Brauer, A., Blockley, S.P.E., Dulski, P., 2013. Volcanic ash reveals time-transgressive abrupt climate change during the Younger Dryas. Geology, 41 (12), 1251-1254. https://doi.org/10.1130/G34867.1.

Larsen, G., Róbertsdóttir, B.G., Oladottir, B.A., Eiríksson, J., 2020. A shift in eruption mode of Hekla volcano, Iceland, 3000 years ago: two-coloured Hekla tephra series, characteriscs, dispersal and age. Journal of Quaternary Sciece, 35, Special Issue 1-2, 143-154. https://doi.org/10.1002/jqs.3164.

Le Maitre, R.W., Streckeisen, A., Zanettin, B., Le Bas, M.J., Bonin, B., Bateman, P., Bellieni, G., Dudek, A., Efremova, S., Keller, J., Lameyre, J., Sabine, P.A., Schmid, R., SØrensen, H., Woolley, A.R., 2002. Igneous Rocks: A Classification and Glossary of Terms. Reccomendation of the International Union of Geological Sciences Subcommission on the Systematics of Igneous Rocks, 2nd Edition. Cambridge University Press, Cambridge. 236 pages.

Lee, J.Y., Marti, K., Severinghaus, J.P., Kawamura, K., Yoo, H.S., Lee, J.B., Kim, J.S., 2006. A redetermination of the isotopic abundances of atmospheric Ar. Geochimica and Cosmochimica Acta, 70, 4507-4512. https://doi.org/10.1016/j.gca.2006.06.1563.

Leicher, N., Giaccio, B., Zanchetta, G., Wagner, B., Francke, A., Palladino, D.M., Sulpizio, R., Albert, P.G., Tomlinson, E.L., 2019. Central Mediterranean explosive volcanism and tephrochronology during the last 630 ka based on the sediment record from Lake Ohrid. Quaternary Science Reviews, 226, 106021. https://doi.org/10.1016/j.quascirev.2019.106021.

Leicher, N., Zanchetta, G., Sulpizio, R., Giaccio, B., Wagner, B., Nomade, S., Francke, A., Del Carlo, P., 2016. First tephrostratigraphic results of the DEEP site record from Lake Ohrid (Macedonia and Albania). Biogeosciences, 13, 2151-2178. https://doi.org/10.5194/bg-13-2151-2016.

Lisiecki, L.E. & Raymo, M.E., 2005. A Pliocene-Pleistocene stack of 57 globally distributed benthic δ18O records. Paleoceanography, 20. https://doi.org/10.1029/2004PA001071.

Lourens, L.J., 2004. Revised tuning of Ocean Drilling Program Site 964 and KC01B (Mediterranean) and implicaions for the d18O, tephra, calcareous nannofossil, and geomagnetic reversal chronologies of the past 1.1 Myr. Paleoceanography and Paleoclimatology, 19, PA3010. https://doi.org/10.1029/2003PA000997.

Lowe, D.J., Bronk Ramsey, C., Housley, R.A., Lane, C.S., Tomlinson, E.L., RESET Team, RESET Associates, 2015. The RESET project: constructing a European tephra lattice refined synchronisation of environmental and archaeological events during the last c. 100 ka. Quaternary Science Reviews, 118, 1-17. https://doi.org/10.1016/j.quascirev.2015.04.006.

Lowe, D.J., 2011. Tephrochronology and its application: A review. Quaternary Geochonology, 6, 107-153. https://doi.org/10.1016/j.quageo.2010.08.003.

Luberti, G.M., Marra, F., Florindo, F., 2017. A review of the stratigraphy of Rome (Italy) according to geochronologically and paleomagnetically constrained aggradational successions, glacio-eustatic forcing and volcano-tectonic processes. Quaternary International, 438, Part B, 40-67. https://doi.org/10.1016/j.quaint.2017.01.044.

Luhr, J.F. & Giannetti, B., 1987. The Brown Leucitic Tuff of Roccamonfina Volcano (Roman Region, Italy). Contributions to Mineralogy and Petrology, 95, 420-436. https://doi.org/10.1007/BF00402203.

Lustrino, M., Duggen, S., Rosenberg, C.L., 2011. The Central-Western Mediterranean: Anomalous igneous activity in an anomalous collisional tectonic setting. Earth-Science Reviews, 104, 1-3, 1-40. https://doi.org/10.1016/j.earscirev.2010.08.002.

Mannella, G., Giaccio, B., Zanchetta, G., Regattieri, E., Niespolo, E.M., Pereira, A., Renne, P.R., Nomade, S., Leicher, N., Perchiazzi, N., Wagner, B., 2019. Paleoenvironmental and paleohydrological variability of mountain areas in the central Mediterranean region: A 190-ka-long chronicle from the independently dated Fucino paleolake record (central Italy). Quaternary Science Reviews, 210, 190-210. https://doi.org/10.1016/j.quascirev.2019.02.032.

Marra, F., Cardello, G.L., Gaeta, M., Jicha, B.R., Montone, P., Niespolo, E.M., Nomade, S., Palladino,

D.M., Pereira, A., De Luca, G., Florindo, F., Frepoli, A., Renne, P.R., Sottili, G., 2021. The Volsci Volcanic Field (central Italy): eruptive history, magma system and implications on continental subduction processes. International Journal of Earth Sciences. https://doi.org/10.1007/s00531-021-01981-6.

Marra, F., Castellano, C., Cucci, L., Florindo, F., Gaeta, M., Jicha, B., Palladino, D.M., Sottili, G., Tertulliani, A., Tolomei, C., 2020b. Monti Sabatini and Colli Albani: the dormant twin volcanoes at the gates of Rome. Scientific Reports 10:8666. https://doi.org/10.1038/s41598-020-65394-2.

Marra, F., Costantini, L., Di Buduo, G.M., Florindo, F., Jicha, B.R., Monaco, L., Palladino, D.M., Sottili, G., 2019. Combined glacio-eustatic forcing and volcano-tectonic uplift: geomorphological and geochronological constraints on the Tiber River terraces in the eastern Vulsini Volcanic District (central Italy). Global and Planetary Change, 182,103009. https://doi.org/10.1016/j.gloplacha.2019.103009.

Marra, F., Freda, C., Scarlato, P., Taddeucci, J., Karner, D.B., Renne, P.R., Gaeta, M., Palladino, D.M., Triglia, R., Cavaretta, G., 2003. Post-caldera activity in the Alban Hills volcanic district (Italy): 40Ar/39Ar geochronology and insights into magma evolution. Bulletin of Volcanology, 65, 227-247. https://doi.org/10.1007/s00445-002-0255-9.

Marra, F., Gaeta, M., Giaccio, B., Jicha, B.R., Palladino, D.M., Polcari, M., Sottili, G., Taddeucci, J., Florindo, F., Stramondo, S., 2016a. Assessing the volcanic hazard for Rome: 40Ar/39Ar and In-SAR constraints on the most recent eruptive acivity and present-day uplift at Colli Albani Volcanic District. Geophysical Research Letters, 43, 6898-6906. https://doi.org/10.1002/2016GL069518.

Marra, F., Jicha, B., Florindo, F., 2017. $^{40}Ar/^{39}Ar$ dating of Glacial Termination VI: constraints to the duration of Marine Isotopic Stage 13. Scientific Reports, 7, 8908. https://doi.org/10.1038/s41598-017-08614-6.

Marra, F., Jicha, B., Palladino, D.M., Gaeta, M., Costantini, L., Di Buduo, G.M., 2020a. $^{40}Ar/^{39}Ar$ single crystal dates from pyroclastic deposits provide a detailed record of the 590-240 ka eruptive period at the Vulsini Volcanic District (central Italy). Journal of Volcanology and Geothermal Research, 398, 106904. https://doi.org/10.1016/j.jvolgeores.2020.106904.

Marra, F., Karner, D.B., Freda, C., Gaeta, M., Renne, P., 2009. Large mafic eruptions at Alban Hills Volcanic District (Central Italy): chronostratigraphy, petrography and eruptive behavior. Journal of Volcanology and Geothermal Research, 179, 217-232. https://doi.org/10.1016/j.jvolgeores.2008.11.009.

Marra, F., Nomade, S., Pereira, A., Petronio, C., Salari, L., Sottili, G., Bahain, J.J., Boschian, G., Di Stefano, G., Falguères, C., Florindo, F., Gaeta, M., Giaccio, B., Masotta, M., 2018. A review of the geological sections and the faunal assemblages of Aurelian Mammal Age of Latium (Italy) in the light of a new chronostratigraphic framework. Quaternary Science Reviews, 181, 173-199. https://doi.org/10.1016/j.quascirev.2017.12.007.

Marra, F., Rohling, E.J., Florindo, F., Jicha, B., Nomade, S., Pereira, A., Renne, P.R., 2016b. Independent $^{40}Ar/^{39}Ar$ and ^{14}C age constraints on the last five glacial terminations from the aggradational successions of the Tiber River, Rome (Italy). Earth and Planetary Science Letters, 449, 105-117. https://doi.org/10.1016/j.epsl.2016.05.037.

Marra, F., Sottili, G., Gaeta, M., Giaccio, B., Jicha, B., Masotta, M., Palladino, D.M., Deocampo, D.M., 2014. Major explosive activity in the Monti Sabatini Volcanic District (central Italy) over the 800-390 ka interval: geochronological-geochemical overview and tephrostratigraphic implications. Quaternary Science Reviews, 94, 74-101. https://doi.org/10.1016/j.quascirev.2014.04.010.

Marra, F., Taddeucci, J., Freda, C., Marzocchi, W., Scarlato, P., 2004. Recurrence of volcanic activity along the Roman Comagmatic Province (Tyrrhenian margin of Italy) and its tectonic significance. Tectonics, 23, TC4013. https://doi.org/10.1029/2003TC001600.

Matthews, I.P., Trincardi, F., Lowe, J.J., Bourne, A.J., MacLeod, A., Abbott, P.M., Andersen, N., Asioli, A., Blockley, S.P.E., Lane, C.S., Oh, Y.A., Satow, C.S., Staff, R.A., Wulf, S., 2015. Developing a robust tephrochronological framework for Late Quaternary marine records in the Southern Adriatic Sea: new data from core station SA03-11. Quaternary Science Reviews, 118, 84-104. https://doi.org/10.1016/j.quascirev.2014.10.009.

Mcmanus, J., Oppo, D., Cullen, J., & Healey, S. 2003. Marine isotope stage 11 (MIS 11): analog for Holocene and future Climate? Earth's climate and orbital eccentricity: the marine isotope stage 11 question, 137, 69-85. https://doi.org/10.1029/137GM06.

Monaco, L., Palladino, D.M., Gaeta, M., Marra, F., Sottili, G., Leicher, N., Mannella, G., Nomade, S., Pereira, A., Regattieri, E., Wagner, B., Zanchetta, G., Albert, P.G., Arienzo, I., D'Antonio, M., Petrosino, P., Manning, C., Giaccio, B. 2021. Mediterranean tephrostratigraphy and peri-Tyrrhenian explosive activity revaluated in light of the 430-365 ka record from Fucino Basin (central Italy). Earth-Science Reviews, 220, 103706. https://doi.org/10.1016/j.earscirev.2021.103706.

Morabito, S., Petrosino, P., Milia, A., Sprovieri, M., Tamburrino, S., 2014. A multidisciplinary approach for reconstructing the stratigraphic framework of the last 40 ka in a bathyal area of eastern Tyrrhenian Sea. Global and Planetary Change, 123, Part A, 121-138. https://doi.org/10.1016/j.gloplacha.2014.10.005.

Munno, R. & Petrosino, P., 2007. The late Quaternary tephrostratigraphical record of the San Gregorio Magno basin (southern Italy). Journal of Quaternary Science, 22, 247-266. https://doi.org/10.1002/jqs.1025.

Nappi, G., Renzulli, A., Santi, P., Gillot, Y.P., 1995. Geological evolution and geochronology of the Vulsini volcanic district (central Italy): Bollettino della Società Geologica Italiana, v. 114, p. 599-613.

Narcisi, B. & Vezzoli, L., 1999. Quaternary stratigraphy of distal tephra layers in the Mediterranean - an overview. Global and Planetary Change, 21, 31-50. https://doi.org/10.1016/S0921-8181(99)00006-5.

Newnham, R.M., Lowe, D.J., Alloway, B.V., 1999. Volcanic hazards in Auckland, New Zealand: a preliminary assessment of the threat posed by central North Island silicic volcanism based on the Quaternary tephrostratigraphical record. Geological Society, London, Special Pubblications, 161, 27-45. https://doi.org/10.1144/GSL.SP.1999.161.01.04.

Niespolo, E.M., Rutte, D., Deino, A.L., Renne, P.R., 2017. Intercalibration and age of the Alder Creek Sanidine

$^{40}Ar/^{39}Ar$ standard. Quaternary Geochronology, 39, 205-213. https://doi.org/10.1016/j.quageo.2016.09.004.

Nomade, S., Bassinot, F., Mariano, M., Simon, Q., Dewilde, F., Maiorano, P., Isguder, G., Blamart, D., Girone, A., Scao, V., Pereira, A., Toti, F., Bertini, A., Combourieu-Nebout, N., Peral, M., Bourlès, D.L., Petrosino, P., Gallicchio, S., Ciaranfi, N., 2019. High-resolution foraminifer stable isotope record of MIS 19 at Montalbano Jonico, southern Italy: A window into Mediterranean climatic variability during a low-eccentricity interglacial. Quaternary Science Reviews, 205, 106-125. https://doi.org/10.1016/j.quascirev.2018.12.008.

Nomade, S., Gauthier, A., Guillou, H., Pastre, J.-F., 2010. $^{40}Ar/^{39}Ar$ temporal framework for the Alleret maar lacustrine sequence (French Massif-Central): Volcanological and paleoclimatic implications. Quaternary Geochronology, 5:1, 20-27. https://doi.org/10.1016/j.quageo.2009.07.001.

Nomade, S., Muttoni, G., Guillou, H., Robin, E., Scardia, G., 2011. First $^{40}Ar/^{39}Ar$ age of the Ceprano man (central Italy). Quaternary Geochronology, 6, 453-457. https://doi.org/10.1016/j.quageo.2011.03.008.

Palladino, D.M., Agosta, E., Freda, C., Spaziani, S., Trigila, R., 1994. Geo-petrographic and volcanological study of Southern Vulsini: the Valentano–Marta–La Rocca sector. Memorie Descrittive della Carta Geologica d'Italia, 49, 255–276.

Palladino, D.M., Simei, S., Sottili, G., Trigila, R., 2010. Integrated approach for the reconstruction of stratigraphy and geology of Quaternary volcanic terrains: an application to the Vulsini Volcanoes (central Italy). In: Groppelli, G., Viereck, e L. (Eds.), Stratigraphy and Geology in Volcanic Areas. Geological Society of America Special Paper, 464, 66–84.

Patacca, E., Scandone, P., Di Luzio, E., Cavinato, G.P., Parotto, M., 2008. Structural architecture of the central Apennines: Interpretation of the CROP 11 seismic profile from the Adriatic coast to the orographic divide. Tectonics, 27, TC3006. https://doi.org/10.1029/2005TC001917.

Paterne, M., Guichard, F., Duplessy, J.C., Siani, G., Sulpizio, R., Labeyrie, J., 2008. A 90,000-200,000 yrs marine tephra record of Italian volcanic activity in the Central Mediterranean Sea. Journal of Volcanology and Geothermal Research, 177, 187-196. https://doi.org/10.1016/j.jvolgeores.2007.11.028.

Paterne, M., Guichard, F., Labeyrie, J., 1988. Explosive activity of the south Italian volcanoes during the past 80,000 years as determined by marine tephrochronology. Journal of Volcanology and Geothermal Research, 34, 153-172. https://doi.org/10.1016/0377-0273(88)90030-3.

Paterne, M., Guichard, F., Labeyrie, J., Gillot, P.Y., Duplessy, J.C., 1986. Tyrrhenian Sea tephrochronology of the oxygen isotope record for the past 60,000 years. Marine Geology, 72, 259-285. https://doi.org/10.1016/0025-3227(86)90123-4.

Peccerillo, A., 2017. Cenozoic Volcanism in the Tyrrhenian Sea Region. In: IAVCEI, Advances in Volcanology, 2 ed. Springer, p. 400.

Pereira, A., Monaco, L., Marra, F., Sébastien, N., Gaeta, M., Leicher, N., Palladino, D.M., Sottili, G., Guillou, H., Scao, V., Giaccio, B., 2020. Tephrochronology of the central Mediterranean MIS 11c interglacial (~425-395 ka): New constraints from the Vico volcano and the Tiber delta, central Italy. Quaternary Science Reviews, 243, 106-470. https://doi.org/10.1016/j.quascirev.2020.106470.

Pereira, A., Nomade, S., Moncel, M.H., Voinchet, P., Bahain, J.J., Biddittu, I., Falgueres, C., Giaccio, B., Manzi, G., Parenti, F., Scardia, G., Scao, V., Sottili, G., Vietti, A., 2018. Integrated geochronology of Acheulian sites from the southern Latium (central Italy): insights on human-environment interaction and the technological innovations during the MIS 11-MIS 10 period. Quaternary Science Reviews, 187, 112-129. https://doi.org/10.1016/j.quascirev.2018.03.021.

Perini, G. & Conticelli, S., 2002. Crystallization conditions of leucite-bearing magmas and their implications on the magmatological evolution of ultrapotassic magmas: the Vico Volcano, central Italy. Mineralogy and petrology, 74, 253-276. https://doi.org/10.1007/s007100200006.

Perini, G., Conticelli, S., Francalanci, L., 1997. Inferences on the volcanic history of the Vico volcano, Roman Magmatic Province, central Italy: stratigraphic, petrographic and geochemical data. Mineralogica et Petrographica Acta, 40, 67-93.

Perini, G., Conticelli, S., Francalanci, L., Davidson, J. P., 2000. The relationship between potassic and calc-alkaline post-orogenic magmatism at Vico volcano, central Italy. Journal of Volcanology and Geothermal Research, 95, 243-268. https://doi.org/10.1016/S0377-0273(99)00123-7.

Perini, G., Francalanci, L., Davidson, J.P., Conticelli, S., 2004. Evolution and Genesis of Magmas from Vico Volcano, Central Italy: Multiple Differentiation Pathways and Variable Parental Magmas. Journal of Petrology, 45:1, 139-182. https://doi.org/10.1093/petrology/egg084.

Perini, G., Teplei III, F.-J., Davidson, J.P., Conticelli, S., 2003. The origin of K-feldspar megacrysts hosted in alkaline potassic rocks from central Italy: a track for low-pressure processes in mafic magmas. Lithos, 66, 223-240. https://doi.org/10.1016/S0024-4937(02)00221-9.

Petrosino, P., Arienzo, I., Mazzeo, F.C., Natale, J., Petrelli, M., Milia, A., Perugini, D., D'Antonio, M., 2019. The San Gregorio Magno lacusrine basin (Campania, southern Italy): improved characterization of the tephrostratigraphic markers based on trace elements and isotopic data. Journal of Quaternary Science, 34, 393-404. https://doi.org/10.1002/jqs.3107.

Petrosino, P., Jicha, B.R., Mazzeo, F.C., Ciaranfi, N., Girone, A., Maiorano, P., 2015. The Montalbano Jonico marine succession: An archive for distal tephra layers at the Early-Middle Pleistocene boundary in southern Italy. Quaternary International, 383, 89-103. https://doi.org/10.1016/j.quaint.2014.10.049.

Petrosino, P., Jicha, B.R., Mazzeo, F.C., Russo Ermolli, E., 2014b. A high-resolution tephrochronological record of MIS 14-12 in the Southern Apennines (Acerno Basin, Italy). Journal of Volcanology and Geothermal Research, 274, 34-50. https://doi.org/10.1016/j.jvolgeores.2014.01.014.

Petrosino, P., Morabito, S., Jicha, B.R., Milia, A., Sprovieri, M., Tamburrino, S., 2016. Multidisciplnary tephrochronological correlation of marker events in the eastern Tyrrhenian Sea between 48 and 105 ka. Journal of Volcanology and Geothermal Research,

315, 79-99. https://doi.org/10.1016/j.jvolgeores.2016.02.001.
Petrosino, P., Russo Ermolli, E., Donato, P., Jich, B., Robustelli, G., Sardella, R., 2014a. Using tephrochornology and palynology to date the MIS 13 lacustrine sediments of the Mercure basin (Southern Apennines - Italy). Italian Journal of Geosciences, 133, 169-186. https://doi.org/10.3301/IJG.2013.22.
Ponomareva, V.V., Portnyagin, M., Davies, S.M., 2015. Tephra without borders: far-reaching clues into past explosive eruptions. Front. Earth Sci. 3 (83). https://doi.org/10.3389/feart.2015.00083.
Pouclet, A., Horvat, E., Gabris, G., Juvignè, E., 1999. The Bag tephra, a widespread tephrochronological marker in Middle Europe: chemical and mineralogical investigations. Bulletin of Volcanology, 60, 265-272. https://doi.org/10.1007/s004450050275.
R Core Team (2017). R: A Language and Environment for Statistical Computing.
Radicati di Brozolo, F., Di Girolamo, P., Turi, B., Oddone, M., 1988. 40Ar-39Ar and K-Ar dating of K-rich rocks from the Roccamonfina Volcano, Roman Comagmatic Region, Italy. Geochmica et Cosmochimica Acta, 52, 1435-1441. https://doi.org/10.1016/0016-7037(88)90213-X.
Regattieri, E., Giaccio, B., Galli, P., Nomade, S., Peronace, E., Messina, P., Sposato, A., Boschi, C., Gemelli, M., 2016. A mmulti-proxy record of MIS 11-12 deglaciation and glacial MIS 12 instability from the Sulmona Basin (central Italy). Quternary Science Reviews, 132, 129-145. https://doi.org/10.1016/j.quascirev.2015.11.015.
Regattieri, E., Giaccio, B., Mannella, G., Zanchetta, G., Nomade, S., Tognarelli, A., Perchiazzi, N., Vogel, H., Boschi, C., Drysdale, R.N., Wagner, B., Gemelli, M., Tzedakis, P., 2019. Frequency and dynamics of millennial-scale variability during marine isotope stage 19: insights from the Sulmona Basin (central Italy). Quaternary Science Reviews, 214, 28-43. https://doi.org/10.1016/j.quascirev.2019.04.024.
Regattieri, E., Giaccio, B., Zanchetta, G., Drysdale, R.N., Galli, P., Nomade, S., Peronace, E., Wulf, S., 2015. Hydrological variability over the Apennines during the Early Last Glacial precession minimum, as revelated by a stable isotope record from Sulmona basin, Central Italy. Journal of Quaternary Science, 30, 19-31. https://doi.org/10.1002/jqs.2755.
Renne, P.R., Balco, G., Ludwig, K.R., Mundil, R., Min, K., 2011. Response to the comment by WH Schwarz et al. on “Joint determination of 40 K decay constants and 40Ar*/40K for the Fish Canyon sanidine standard, and improved accuracy for 40Ar/39Ar geochronology” by PR Renne et al. (2010). Geochimica and Cosmochimica Acta, 75, 5097-5100. https://doi.org/10.1016/j.gca.2011.06.021.
Renne, P.R., Sprain, C.J., Richards, M.A., Self, S., Vanderkluysen, L., Pande, K., 2015. State shift in Deccan volcanism at the Cretaceous Paleogene boundary, possibly induced by impact. Science, 350, 76-78. https://doi.org/10.1126/science.aac7549.
Rolandi, G., Bellucci, F., Heizler, M.T., Belkin, H.E., De Vivo, B., 2003. Tectonic controls on the genesis of ignimbrite from the Campanian Volcanic Zone, southern Italy. Mineralogy and Petrology, 79, 3-31. https://doi.org/10.1007/s00710-003-0014-4.
Rouchon, V., Gillot, P.Y., Quidelleur, X., Chiesa, S., Floris, B., 2008. Temporal evolution of the Roccamonfina volcanic complex (Pleistocene), Central Italy. Journal of Volcanology and Geothermal Research, 177, 500-514. https://doi.org/10.1016/j.jvolgeores.2008.07.016.
Russo Ermolli, E., Aucelli, P.P.C., Di Rollo, A., Mattei, M., Petrosino, P., Porreca, M., Rosskopf, C.M., 2010. An integrated stratigraphical approach to the Middle Pleistocene succession of the Sessano Basin (Molise, Italy). Quaternary International, 225, 114-127. https://doi.org/10.1016/j.quaint.2009.04.008.
Sági, T., Kiss, B., Bradák, B., Harangi, S., 2008. Középső-pleisztocén löszben előforduló vulkáni képződmények Magyarországon: terepi és petrográfiai jellemzők (Middle Pleistocene volcanic sediments in loess in Hungary: field and petrographical characteristics). Földtani Közlöny, 138, 297-310 (in Hungarian with English abstract).
Sagnotti, L., Scardia, G., Giaccio, B., Liddicoat, J.C., Nomade, S., Renne, P.R., Sprain, C.J., 2014. Extreamlly rapid directionl change during Matuyama-Brunhes geomagnetic polarity reversal. Geophysical Journal International, 199, 1110-1124. https://doi.org/10.1093/gji/ggu287.
Satow, C., Gudmundsson, A., Gertisser, R., Ramsey, C. B., Bazargan, M., Pyle, D., Wulf, S., Miles, A., Hardiman, M., 2021. Eruptive activity of the Santorini Volcano controlled by sea-level rise and fall. Nature Geoscience, 14, 586-592. https://doi.org/10.1038/s41561-021-00783-4.
Sbrana, A., Marianelli, P., Pasquini, G., 2018. Volcanology of Ischia (Italy). Journal of Maps, 14, 2. https://doi.org/10.1080/17445647.2018.1498811.
Scaillet, S., Vita-Scaillet, G., Guillou, H., 2008. Oldest human footprints dated by Ar/Ar. Earth and Planestary Science Letters, 275, 320-325. https://doi.org/10.1016/j.epsl.2008.08.026.
Simon, Q., Bourlès, D.L., Thouveny, N., Horng, C.-S., Valet, J.-P., Bassinot, F., Choy, S., 2018. Cosmogenic signature of geomagnetic reversals and excursions from the Réunion event to the Matuyama-Brunhes transition (0.7-2.14 Ma interval). Earth and Planetary Science Letters, 482, 510-524. https://doi.org/10.1016/j.epsl.2017.11.021.
Smith, V.C., Isaia, R., Pearce, N.J.G., 2011. Tephrostratigrapy and glass compositions of post-15 kyr Campi Flegrei eruptions: implications for eruption history and chronostratigraphic markers. Quaternary Science Reviews, 30, 3638-3660. https://doi.org/10.1016/j.quascirev.2011.07.012.
Soligo, M. & Tuccimei, P., 2010. Geochronology of Colli Albani volcano. In: Funicello, R., Giordano, G. (eds). The Colli Albani Volcano. Geological Society of London, Special IAVCEI Publication, 3:99-106.
Sottili, G., Arienzo, I., Castorina, F., Gaeta, M., Giaccio, B., Marra, F., Palladino, D.M., 2019. Time-dependent Sr and Nd isotope variations during the evolution of ultrapotassic Sabatini Volcanic District (Roman Province, Central Italy). Bulletin of Volcanology, 81:67. https://doi.org/10.1007/s00445-019-1324-7.
Sottili, G., Palladino, D.M., Marra, F., Jicha, B., Karner, D.B., Renne, P., 2010. Geochronology of the most recent activity in the Sabatini volcanic district, Roman Province, central Italy. Journal of Volcanology and Geothermal Research, 196, 20-30. https://doi.org/10.1016/j.jvolgeores.2010.07.003.

Sottili, G., Palladino, D.M., Zanon, V., 2004. Plinian activity during the early eruptive history of the Sabatini volcanic district, central Italy. Journal of Volcanology and Geothermal Research, 135, 361-379. https://doi.org/10.1016/j.jvolgeores.2004.03.019.

Tamburrino, S., Insinga, D.D., Sprovieri, M., Petrosino, P., Tiepolo, M., 2012. Major and trace element characterization of tephra layers offshore Pantelleria Island: insights into the last 200 ka of volcanic activity and contribution to the Med- iterranean tephrochronology. Journal of Quaternary Science, 27, 129-140. https://doi.org/10.1002/jqs.1504.

Thirlwall, M.F., 1991. Long-term reproducibility of multicollector Sr and Nd isotope ratio analysis. Chemical Geology, 94:85–104. https://doi.org/10.1016/0168-9622(91)90002-E.

Thorarinsson, 1981a. Greetings from Iceland. Geografiska Annaler: Series A, Physical Geography, 63:3-4, 109-118. https://doi.org/10.1177/0309133307073887.

Thorarinsson, 1981b. Tephra studies and tephrochronology: a historical review with special reference to Iceland. In: S. Self, R.S.J., Sparks (Eds.), Tephra Studies, Reidel, Dordrecht (1981), pp. 1-12. https://doi.org/10.1007/978-94-009-8537-7_1.

Tomlinson, E.L., Albet, P.G., Wulf, S., Brown, R.J., Smith, V.C., Keller, J., Orsi, G., Bourne, A.., Menzes, M.A., 2014. Age and geochemistry of tephra layers from Ischia, Italy: constraints from proximal-distal correlations with Lago Grande di Monticchio. Journal of Vollcanology and Geothermal Research, 287, 22-39. https://doi.org/10.1016/j.jvolgeores.2014.09.006.

Tomlinson, E.L., Arienzo, I., Civetta, L., Wulf, S., Smith, V.C., Hardiman, M., Lane, C.S., Carandente, A., Orsi, G., Rosi, M., Müller, W., Menzies, M.A., 2012. Geochemistry of the Phlegrean Fields (Italy) proximal sources for major Mediterranean tephras: Implications for the dispersal of Plinian and co-ignimbritic components of explosive eruptions. Geochmica et Cosmochimica Acta, 93, 102-128. https://doi.org/10.1016/j.gca.2012.05.043.

Tomlinson, E.L., Smith, V.C., Albert, P.G., Aydar, E., Civetta, L., Cioni, R., çubukçu, E., Gertisser, R., Isaia, R., Menzies, M.A., Orsi, G., Rosi, M., Zanchetta, G., 2015. The major and trace element glass compositions of the productive Mediterranean volcanic sources: tools for correlating distal tephra layers in and around Europe. Quaternary Science Reviews, 118, 48-66. https://doi.org/10.1016/j.quascirev.2014.10.028.

Tomlinson, E.L., Thordarson, T., Muller, W., Thirlwall, M.T., Menzies, M.A., 2010. Microanalysis of tephra by LA-ICP-MS - strategies, advantages and limitations assessed using the Thorsmork ignimbrite (Southern Iceland). Chemical Geology, 279, 73-89. https://doi.org/10.1016/j.chemgeo.2010.09.013.

Turbeville, B.N., 1992. 40Ar/39Ar ages and Stratigraphy of the Latera caldera, Italy. Bulletin of Volcanology, 55, 110-118. https://doi.org/10.1007/BF00301124.

Turbeville, B.N., 1993. Petrology and Petrogenesis of the Latera Caldera, Central Italy. Journal of Petrology, 34:1, 77-123. https://doi.org/10.1093/petrology/34.1.77.

Tzedakis, P.C. 2010. The MIS 11–MIS 1 analogy, southern European vegetation, atmospheric methane and the" early anthropogenic hypothesis". Climate of the Past, 6(2), 131-144. https://doi.org/10.5194/cp-6-131-2010.

Vakhrameeva, P., Koutsodendris, A., Wulf, S., Fletcher, W.J., Appelt, O., Knipping, M., Gertisser, R., Trieloff, M., Pross, J., 2018. The cryptotephra record of the Marine Isotope Stage 12 to 10 interval (460-335 ka) at Tenaghi Philippon, Greece: Exploring chronological markers for the Middle Pleistocene of the Mediterranean reion. Quaternary Science Reviews, 200, 313-333. https://doi.org/10.1016/j.quascirev.2018.09.019.

Vakhrameeva, P., Koutsodendris, A., Wulf, S., Portnyagin, M., Appelt, O., Ludwig, T., Trieloff, M., Pross, J., 2021. Land-sea correlations in the Eastern Mediterranean region over the past c. 800 kyr based on macro- and cryptotephras from ODP Site 964 (Ionian Basin). Quaternary Science Reviews, 255, 106811. https://doi.org/10.1016/j.quascirev.2021.106811.

Vakhrameeva, P., Wulf, S., Koutsodendris, A., Tjallingii, R., Fletcher, W.J., Appet, O., Ludwig, T., Knipping, M., Trieloff, M., Pross, J., 2019. Eastern Mediterranean volcanism during. Marine isotope stages 9 to 7e (335-235 ka): Insights based on cryptotephra layers at Tenaghi Philippon, Greece. Journal of Volcanology and Geothermal Research, 380, 31-47. https://doi.org/10.1016/j.jvolgeores.2019.05.016.

Villa, P., Soriano, S., Grün, R., Marra, F., Nomade, S., Pereira, A., Boschian, G., Pollarolo, L., Fang, F., Bahain, J.J., 2016. The Acheulian and early Middle Paleolithic in Central Italy: Stability and Innovation. PLoS ONE 11, e0160516. https://doi.org/10.1371/journal.pone.0160516.

Wagner, B., Vogel, H., Francke, A., Friederich, T., Donders, T., Lacey, J.H., Leng, M.J., Regattieri, E., Sadori, L., Wilke, T., Zanchetta, G., Albrecht, C., Bertini, A., Combourieu-Nebout, N., Cvetkoska, A., Giaccio, B., Grazhdani, A., Hauffe, T., Holtvoeth, J., Joannin, S., Lagoos, M., Leicher, N., Levkov, Z., Lindhorst, K., Masi, A., Melles, M., Mercuri, A.M., Nomade, S., nowaczyk, N., Panagiotopoulos, K., Peyron, O., reed, J.M., Sagnotti, L., Sinopoli, G., Stellbrink, B., Sulpizio, R., Timmermann, A., Tofilovska, S., Torri, P., Wagner-Cremer, F., Wonik, T., Zhang, X., 2019. Mediterranean winter rainfall in phase with African monsoons during the past 1.36 million years. Nature, 573, 256-260. https://doi.org/10.1038/s41586-019-1529-0.

Washington, H.S., 1906. The Roman comagmatic region. Carnegie Institution of Washington, Publication 57, 199 pp.

Wastergärd, S., 2002. Early to middle Holocenic silicic tephra horizons from Katlavolcanic system, Iceland: new results from the Faroe Islands. Journal of Quaternary Science, 17:8, 723-730. https://doi.org/10.1002/jqs.724.

Wulf, S., Keller, J., Paterne, M., Mingram, J., Lauterbach, S., Opitz, S., Sottili, G., Giaccio, B., Albert, P.G., Satow, C., Tomlinson, E.L., Viccaro, M., Brauer, A., 2012. The 100-133 ka record of Italian explosive volcanism and revised tephrochronology of Lago Grande di Monticchio. Quaternary Sciences Reviws, 58, 104-123. https://doi.org/10.1016/j.quascirev.2012.10.020.

Wulf, S., Keller, J., Satow, C., Gertisser, R., Kraml M., Grant, K.M., Appelt, O., Vakhrameeva, P., Koutsodendris, A., Hardiman, M., Schulz, H., Pross,

J., 2020. Advancing Santorini's tephrostratigraphy: New glass geochemical data and improved marine-terrestrial tephra correlations for the past ~360 kyrs. Earth-Science Reviews, 200, 102964. https://doi.org/10.1016/j.earscirev.2019.102964.

Wulf, S., Kraml, M., Keller, J., 2008. Towards a detailed tephrostratigraphy in the Central Mediterranean: The last 20,000 yrs record of Lago Grande di Monticchio. Journal of Volcanology and Geothermal Research, 177, 118-132. https://doi.org/10.1016/j.jvolgeores.2007.10.009.

Wulf, S., Kraml., M., Brauer, A., Keller, J., Negendank, J.F.W., 2004. Tephrochronology of the 100 ka lacustrine sediment record of Lago Grande di Monticchio (Southern Italy). Quaternary International, 122, 7-30. https://doi.org/10.1016/j.quaint.2004.01.028.

Zanchetta, G., Giaccio, B., Bini, M., Sarti, L., 2018. Tephrostratigraphy of Grotta del Cavallo, Southern Italy: insights of the chronology of Middle to Upper Paleolithic transition in the Mediterranean. Quaternary Science Reviews, 182, 65-77. https://doi.org/10.1016/j.quascirev.2017.12.014.

Chapter IV - Central Mediterranean tephrochronology and explosive volcanism over the 250-170 ka interval (MIS 8-6): a new record from Fucino Basin, central Italy

In this study, 20 Fucino tephra layers covering the 250-170 ka time interval - end of MIS 8, through MIS 7, and beginning of the MIS 6 - are presented and geochemically characterised in terms of major, minor (EPMA-WDS), trace (LA-ICP-MS) elements, Sr-Nd isotope composition, and $^{40}Ar/^{39}Ar$ dating. Furthermore, the geochemical composition of proximal pyroclastic products from Latera Volcanic Complex (LVC, Vulsini Volcanic District), Vico volcano (i.e., Farine Formation unit), and Sabatini Volcanic District (SVD) are presented as well, aiming at providing a reference geochemical dataset for comparison with the Fucino tephra and future investigations in the region. Preliminary results from this study revealed that the Fucino tephra were emplaced by eruptions at Vulsini, Vico, Sabatini, Roccamonfina, Campi Flegrei and Ischia volcanoes. Tephra layers from Fucino Basin were backtracked to known eruptions at LVC (some of the proposed correlations must be corroborated by new $^{40}Ar/^{39}Ar$ age determinations, in progress), SVD, and Roccamonfina volcanic systems, but also to eruptive events at Vico, Ischia and Campi Flegrei volcanoes not documented in proximal settings. Thus, results from this study provide evidence of previously unreported activity at these volcanic districts, with fundamental implications for eruptive histories reconstruction and refinement. The distal-proximal correlations proposed in this case study are preliminary and must be corroborated by further $^{40}Ar/^{39}Ar$ dating of the LVC products (samples irradiated in October 2021; first results in January 2022).

This (unpublished) paper was prepared with the contribution of: L. Monaco (Rome and Prague EPMA data collection and elaboration, LA-ICP-MS data acquisition and interpretation, data elaboration and interpretation, manuscript writing and revision, First Author), N. Leicher (Cologne EPMA data collection and elaboration); B. Giaccio (images preparation, data and manuscript revision); D.M. Palladino (data and manuscript revision); M. Petrelli (LA-ICP-MS data acquisition); I. Arienzo (Sr and Nd isotopes data acquisition); S. Nomade, A. Pereira, and B. Jicha ($^{40}Ar/^{39}Ar$ data aquisition).

ABSTRACT

Tephra layers preserved in lacustrine and marine sedimentary successions provide fundamental integrative information for reconstructing explosive history and dynamics of volcanoes. Central-southern Italy represents an ideal setting for the employment of the tephrostratigraphic method thanks to the coexistence of an intense regional explosive activity from the peri-Tyrrhenian volcanic systems and of several Apennine intermountain Quaternary basins hosting tephras. Among these basins, the Fucino paleolake, with its long and continuous history of Quaternary sediment accumulation, was found to host a rich tephra succession spanning the last 430 kyr at least. Here we present a new detailed investigation of the tephra record from Fucino Basin, spanning the 250-170 ka interval, corresponding to the entire Marine Isotope Stages (MIS) 7 and parts of the MIS 8 and MIS 6. The investigated tephra layers have been characterised in terms of major, minor and trace elements, isotopic composition and $^{40}Ar/^{39}Ar$ ages, which provided the full geochemical and geochronological fingerprint. We integrated the study acquiring glass composition and new high precision $^{40}Ar/^{39}Ar$ ages of selected proximal pyroclastic units from Vulsini, Vico and Sabatini volcanic districts, central Italy, spanning the same temporal interval. The MIS 8-6 Fucino tephra were backtracked to their corresponding volcanic sources, which include Vulsini, Vico, Sabatini, Roccamonfina, Ischia and Campi Flegrei volcanoes. While some of these tephra layers have been correlated to their specific eruption unit, other layers are currently not documented or described in near vent sections, thus highlighting previously unrecognised paroxysmal events at these volcanic systems. The Fucino late MIS 8-early MIS 6 tephra record thus provides new integrative information for reconstructing the explosive history of Italian volcanoes during the investigated interval and the geochronological constrains for the future development of paleoclimatic investigations at local and regional scale.

1. *Introduction*

Unconsolidated volcanic ash layers dispersed over wide regions affirmed as one of the most useful correlative tools for paleoclimatic investigations. Indeed, volcanic ashes, or "tephra" (from the greek word τεφρα; Thorarinsson, 1944), projected into the atmosphere through a sustained eruption column and/or a co-ignimbrite ash cloud during explosive eruptions, are transported and deposited instantaneously over wide regions. In favourable depositional settings, such as lakes or oceans, and occasionally also the sub-aerial environments (e.g., Marciano et al., 2008), tephra deposits can be rapidly buried and preserved and thus used as isochronous horizons that allow synchronization of past natural archives of different environments at several distances from each other's (e.g., Davies et al., 2010). When applicable, the dating of these volcanic ash layers can be obtained via both direct and indirect (i.e., via geochemical correlation with a dated equivalent eruptive unit) radioisotopic methods (e.g., ^{14}C, $^{40}Ar/^{39}Ar$), meaning that they provide ages for the sediments hosting the tephra independently of the orbital tuning. Thanks to this feature, tephra layers have been widely employed to geochronologically constrain or build age models for addressing numerous issues in Quaternary sciences (e.g., Lowe, 2011; Lane et al., 2017), such as paleoclimatic reconstructions (e.g., Lane et al., 2013; Blockley et al., 2014; Kutterolf et al., 2019), archaeology (e.g., Giaccio et al., 2008, 2017a; Lane et al., 2014; Zanchetta et al., 2018; Villa et al., 2020), palaeontology (e.g., Gatta et al., 2016; Marra et al., 2016a, 2018), paleogeographic-tectonic evolution (e.g., Giaccio et al., 2012a; Galli et al., 2017), and past explosive eruptive history reconstruction (e.g., Thorarinsson, 1981a, b; Giaccio et al., 2014; Ponomareva et al., 2015; Albert et al., 2019; Wulf et al., 2020).

However, such a great potential strongly depends on the diagnostic features of the tephra that allow their unambiguous recognition, among which the glass geochemical composition is one of the most powerful. The geochemical fingerprint of a tephra is fundamental also to backtrack the source volcano and the individual eruptive event that emplaced it. This can be achieved by analysis of the glass shards and/or micro-pumices that constitute the tephra (Smith and Westgate, 1968; Hayward, 2011; Lowe et al., 2017; Pearce et al., 2019) and comparison with the glass composition of proximal (i.e., near-vent) pyroclastic deposits of the volcanic systems in the region (e.g., Albert et al., 2013; Tomlinson et al., 2015).

The Mediterranean area (Fig. 1a), with its complex and peculiar geodynamic setting, leading to a diffuse and geochemically various Quaternary magmatism (e.g., Peccerrillo, 2017) and the formation of continental and marine basins acting as fundamental sedimentary traps, arises as an ideal region for the development and the application of tephrochronology, as shown by the large and increasing number of studies (Paterne et al., 1986, 1988, 2008; Wulf et al., 2004, 2008, 2012; Bourne et al., 2010, 2015; Satow et al., 2015; Petrosino et al., 2016; Giaccio et al., 2017a, 2019; Leicher et al., 2019, 2021; Vakhrameeva et al., 2021).

Among the numerous distal tephra archives, the lacustrine succession hosted in Fucino Basin, central Italy (Fig. 1b), has been demonstrated to be one of the most promising and likely the richest Mediterranean Middle Pleistocene tephra record (Giaccio et al., 2017a, 2019; Di Roberto et al., 2018; Del Carlo et al., 2020; Monaco et al., 2021). Here we present a detailed investigation of the tephra succession spanning the 250-170 ka interval from the Fucino lake sediments recovered in the F4-F5 core documenting the last 430 kyr (Giaccio et al., 2019). This includes 20 tephra layers that were geochemically characterised in terms of major, minor, and trace elements of volcanic glass, Sr-Nd isotopes composition, and $^{40}Ar/^{39}Ar$ ages. Furthermore, to improve the reference glass geochemical dataset required for establishing reliable volcanic source identifications and individual correlations of the Fucino tephra with the near-vent volcanic deposits, we also present new glass-analysis of proximal pyroclastic units (Fig. 1b) from the Latera Volcanic Complex (LVC, Vulsini Volcano; Vezzoli et al., 1987; Palladino and Valentine, 1995) and Sabatini Volcanic District (SVD; Sottili et al., 2010), as well as of the Farine Formation Unit of Vico volcano (Sollevanti, 1983), that were all emplaced during the same time interval here considered (i.e., 250-150 kyr). We also present new glass-WDS data of tephra OH-DP-0725 from the million-year-long sequence of Lake Ohrid (North Macedonia-Albania; Leicher et al., 2019, 2021). The Fucino tephra were correlated to paroxysmal events at Vulsini, Vico, Sabatini, Roccamonfina, Ischia and Campi Flegrei volcanoes, and in some cases evidenced eruptions currently undocumented in proximal settings. Thus, combined with the new $^{40}Ar/^{39}Ar$ ages here presented, the results from this study allowed to better refine the explosive history and recurrence time intervals at the peri-Tyrrhenian Quaternary volcanoes, with fundamental implications for hazard assessment at a regional level.

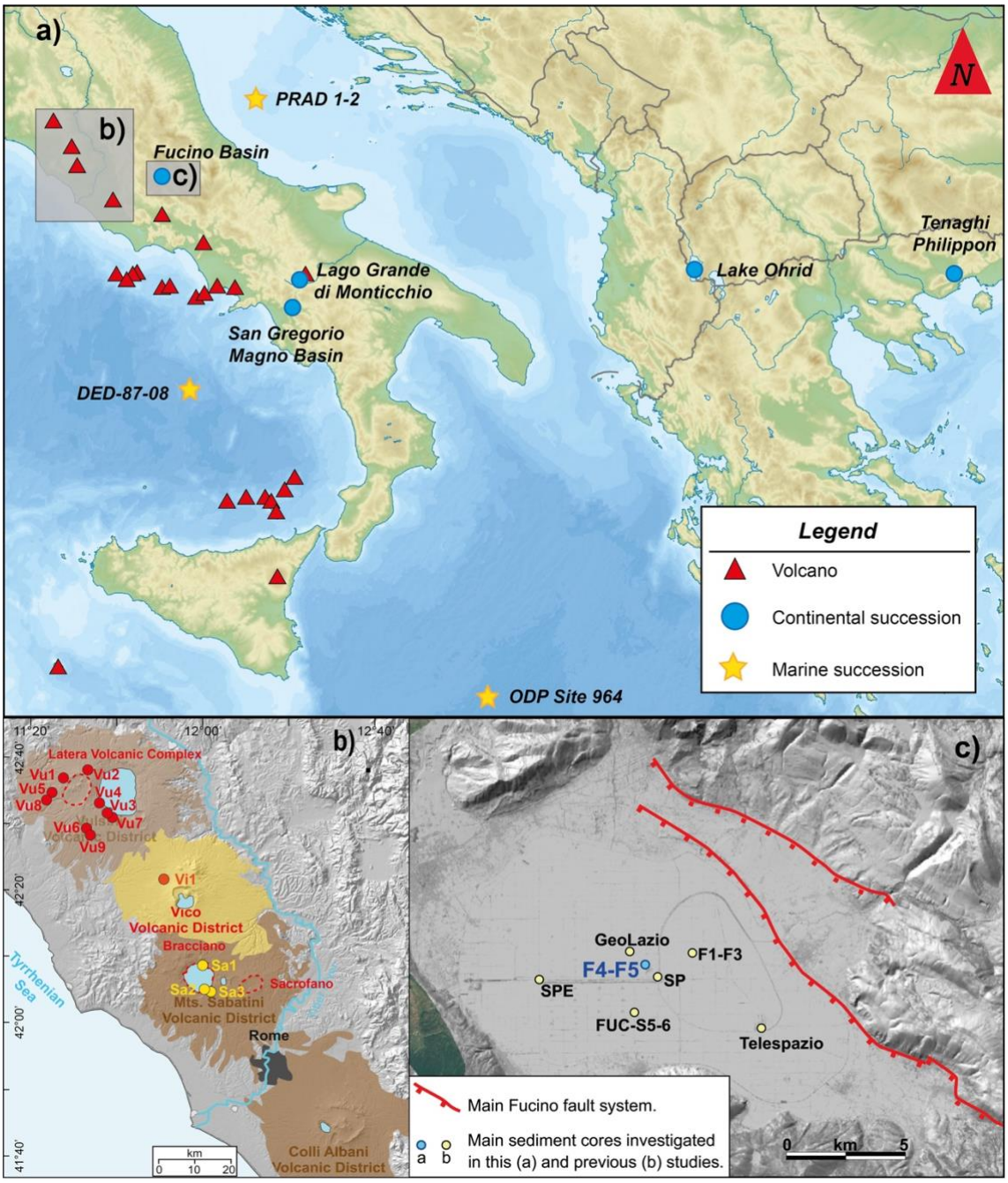

Figure 1. Reference maps. (a) Map of the Central Mediterranean showing location of the Fucino Basin, the continental and insular Quaternary Italian volcanic districts and other sites cited in the text. (b) Location of the Latera Volcanic Complex (LVC), Vico volcano, and Bracciano and Sacrofano (SVD) centres, along with location of the investigated sections. (c) Fucino Plain with location of the F4-F5 core.

2. Geological and tephrochronological setting of the Fucino Basin

The Fucino Basin (midpoint: 42° 00' 00'' N; 013° 30' 00'' E) is one of the largest intermountain Apennine tectonic basins (Fig. 1c) that formed during the extensional stretching of the Apennine chain following the opening of the Tyrrhenian Basin (e.g., Doglioni et al., 1996). Starting from the Late Pliocene-Lower Pleistocene period, extensional tectonics, mainly acting along E-W, NE-SW and NW-SE oriented high-angle normal faults, caused the stretching of the mountain chain (e.g., D'Agostino et al., 2001) and the opening of several intermountain basins, including Fucino (Galadini and Galli, 2000; Boncio et al., 2004; Giaccio et al., 2012b; Amato et al., 2014). The Plio-Quaternary tectonic and sedimentary evolution of the Fucino Basin was driven by the Fucino Fault System (FFS, Galadini and Galli, 2000; Fig. 1c), which depicts a semi-graben architecture with an increasing thickness of the Plio-Quaternary sedimentary infilling of up to ~900 m from west to east toward the depocenter (Cavinato et al., 2002; Patacca et al., 2008). The Fucino Basin was likely characterised by a continuous sedimentation (Giaccio et al., 2017a, 2019; Mannella et al., 2019) since the Plio-Pleistocene and hosted a lake, *Lacus Fucinus*, until the 19th century CE, when it was drained by the Torlonia family.

Two cores were recovered at the F4-F5 drilling site in the central area of the basin (Fig. 1c) and combined in a 98 m-long composite profile. Drilling site selection strategy and recovery procedure are reported in Giaccio et al. (2019). The F4-F5 composite record contains at least 130 tephra (Giaccio et al., 2019; Fig. 2) and was ascribed to the last 430 ka based on correlations with tephra layers from the nearby F1-F3 record, covering the last 190 kyr (Giaccio et al., 2017a), the geochemical fingerprinting of 11 relevant tephra markers and one new direct $^{40}Ar/^{39}Ar$ age determination. Recently, Monaco et al. (2021) provided a detailed geochemical and geochronological characterisation of the succession of 32 tephra layers from the lowermost part of the F4-F5 record, spanning the 430-365 ka time interval or the MIS 11 period (Fig. 2). Tephra layers were backtracked to the Vulsini, Vico, Sabatini, Colli Albani and Roccamonfina volcanic districts, providing integrating information and detailed chronological constraints for explosive activity at these volcanoes.

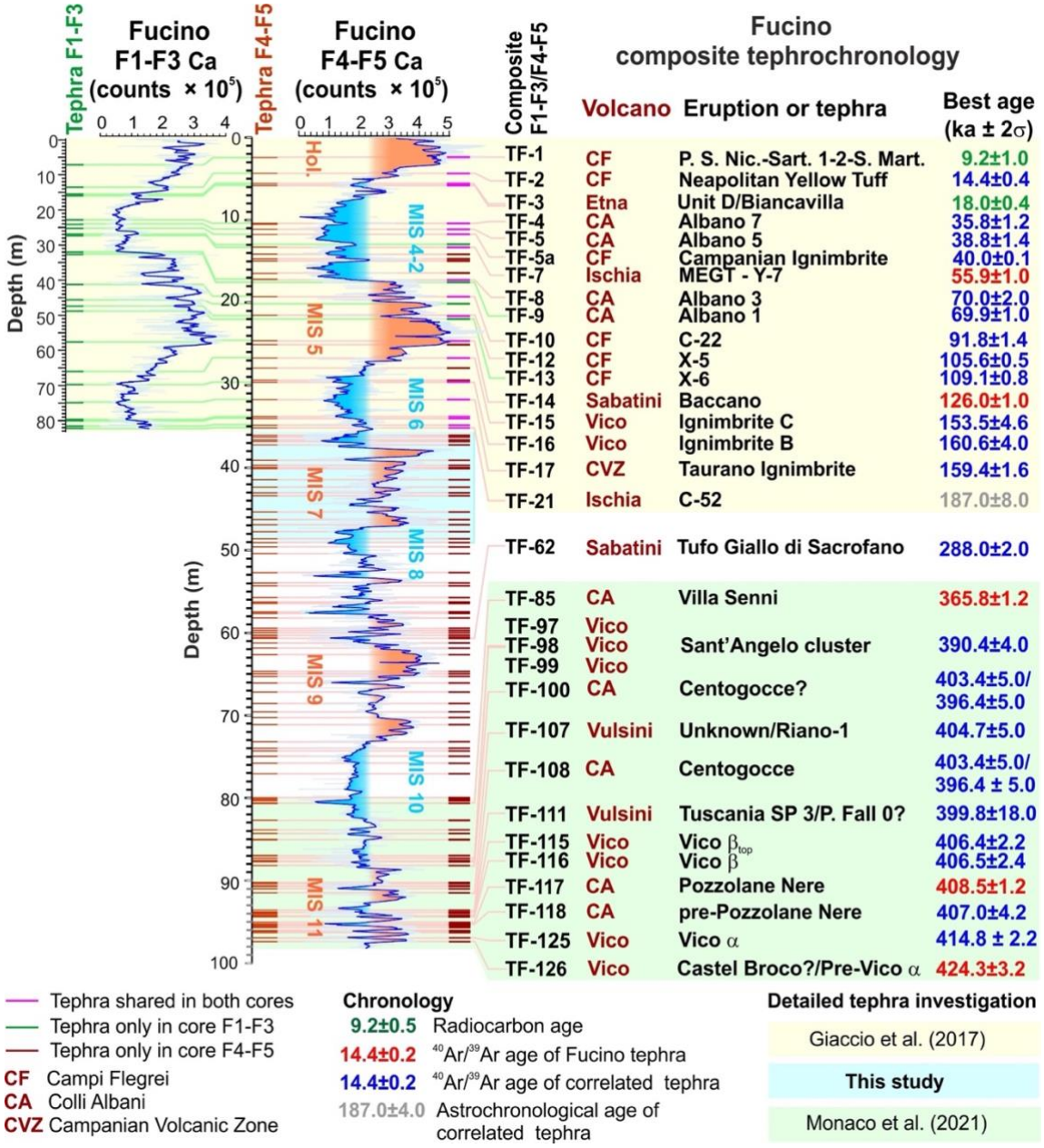

Figure 2. Composite F1-F3/F4-F5 tephra record. Data source: Giaccio et al. (2017a, 2019), Monaco et al. (2021) and references therein.

Table 1. Data summary of the investigated F4-F5 Fucino tephra, along with Ohrid tephra OH-DP-0725 and proximal LVC, Vico and SVD pyroclastic units.

Distal tephra							
Location	**Tephra**	**Core section and depth (cm)**	**Composite Depth (m)**	**Type of analysis**			
				Glass-WDS (EPMA)	**Trace elements (LA-ICP-MS)**	**Sr and Nd isotopes (TIMS)**	**$^{40}Ar/^{39}Ar$**
Fucino Basin (F4-F5)	TF-19[a,b]	F4-23 107.8-111.0	33.79	Yes[1,2]	Yes	Yes	No
	TF-20[a,b]	F5-23 61.50-67.00	34.01	Yes[1,2,3]	Yes	Yes	No
	TF-21[a,b]	F4-24 45.50-48.93	34.83	Yes[1,2,3]	Yes	Yes	No
	TF-21a[b]	F4-24 79.50-81.50	35.15	Yes[3]	No	No	No
	TF-22[a,b]	F5-25 111.5-114.7	36.04	Yes[1,2,3]	No	Yes	Yes
	TF-23[b]	F5-24 130.8-134.3	36.24	Yes[3]	No	No	No
	TF-24[b]	F4-25 66.20-68.50	36.59	Yes[1,2,3]	Yes	No	No
	TF-25[b]	F4-25 78.90-87.70	36.78	Yes[1,2,3]	Yes	No	No
	TF-26[b]	F4-25 127.0-129.0	37.20	Yes[1,2,3]	No	Yes	No
	TF-27[b]	F4-26 136.0-142.0	39.05	Yes[1,2,3]	Yes	Yes	Yes
	TF-28[b]	F4-27 28.00-33.00	39.66	Yes[1,2,3]	No	No	No
	TF-29[b]	F4-27 59.00-60.20	39.94	Yes[2,3]	No	No	No
	TF-30[b]	F5-27 3.000-7.500	40.07	Yes[3]	No	No	No
	TF-31[b]	F4-28 42.00-43.80	41.41	Yes[1,2,3]	No	Yes	No
	TF-32[b]	F4-28 132.0-136.0	42.30	Yes[1,2,3]	Yes	Yes	Yes
	TF-33[b]	F4-29 45.70-47.70	43.00	Yes[3]	No	No	No
	TF-35[b]	F5-29 71.20-71.80	43.70	Yes[3]	No	No	No
	TF-35b[b]	F4-30 79.96-97.45	45.24	Yes[3]	No	No	No
	TF-37[b]	F4-31 20.23-22.76	46.23	Yes[3]	No	No	No
	TF-43[b]	F4-32 149.8-151.5	49.02	Yes[2,3]	No	Yes	No
Lake Ohrid	OH-DP-0725[b,c]	1D-32H-2 1.25-3.75	72.50	Yes[2]	Yes	Yes	No
Proximal volcanic units							
Volcanic system	**Unit**	**Section location**	**Coordinates**				
LVC	Pitigliano[b]	Case Collina quarry	42°38'31''N 11°43'54''E	Yes[2]	Yes	Yes	No
	Onano[b]	Grotte di Castro-Onano road cut Poggio Falchetto-Bonini	42°40'41''N 11°51'10''E 42°35'08''N 11°51'24''E	Yes[1,2]	Yes	Yes	No
	Grotte di Castro[b]	Poggio delle Forche	42°33'11''N 11°53'02''E	Yes[1,2]	Yes	Yes	No
	Sorano[b]	Rio Maggiore road cut	42°37'07''N 11°40'13''E	Yes[1,2]	Yes	Yes	No
	Sovana[b]	Rio Maggiore road cut	42°37'07''N 11°40'13''E	Yes[2]	No	No	No
	Farnese[b]	Arlena di Castro-Tessenanno road cut Rio Maggiore road cut	42°27'46''N 11°48'18''E 42°37'07''N 11°40'13''E	Yes[1,2]	Yes	Yes	Yes
	Stenzano[b]	Rio Maggiore road cut	42°37'07''N 11°40'13''E	Yes[1,2]	No	No	No
	Canino[b]	Monte di Marta Fosso la Nova road cut Pian di Vico	42°32'05''N 11°54'56''E 42°35'54''N 11°38'46''E 42°25'08''N 11°48'41''E	Yes[2]	Yes	Yes	Yes
SVD	TR-CR-2[b]	Trevignano Romano-Centro	42°10'23''N	Yes[2]	Yes	Yes	No
	TR-CR-1[b]	Rapaci	12°14'47''E	Yes[2]	Yes	Yes	No
	Vigna di Valle[b]	Anguillara Sabazia	42°05'29''N 12°16'16''E	Yes[2]	No	Yes	No
	Pizzo Prato[b]	Anguillara Sabazia-Mola Vecchia	42°05'25''N 12°16'55''E	Yes[2]	No	No	No
Vico	Farine Formation	San Martino al Cimino train station	42°22'58''N 12°06'26''E	Yes[2]	No	No	No

[a]: Giaccio et al. (2017a); [b]: this study; [c]: Leicher et al. (2021). EPMA data laboratory information: [1]: Prague; [2]: Rome; [3]: Cologne.

Abbreviations: LVC = Latera Volcanic Complex; SVD = Sabatini Volcanic District.

Table 2. Thickness, lithological and mineralogical features, and TAS classification of the 20 MIS 6-7 F4-F5 Fucino tephra.

Tephra	Thickness (cm)	Composite depth (m)	Core section and depth (cm)	Lithology		Rock type (main)
				Juvenile clasts	Loose crystals	
TF-19	3.20	33.79	F4-23 107.8-111.0	Grey pumice	Kfs>cpx	Ph
TF-20	5.50	34.01	F5-23 61.50-67.00	Grey pumice	Kfs>cpx>bmca	Ph
TF-21	3.43	34.83	F4-24 45.50-48.93	White pumice	Kfs>bmca	Tr
TF-21a	2.00	35.15	F4-24 79.50-81.50	transparent-white – brownish shards and pumice	Kfs>cpx>bmca	Ph-Tr
TF-22	3.20	36.04	F5-24 111.5-114.7	White pumice and grey scoria	Kfs>bmca	Ph-Tph-Lat
TF-23	3.50	36.24	F5-24 130.8-134.3	Transparent shards white pumice	Kfs>plg >bmca>x	Tr
TF-24	2.30	36.59	F4-25 66.20-68.50	White pumice	Kfs>bmca	Ph
TF-25	8.80	36.78	F4-25 78.90-87.70	White pumice	Kfs>bmca	Ph
TF-26	2.00	37.20	F4-25 127.00-129.00	White and grey pumice	Kfs>cpx>bmca	Tr-Ph
TF-27	6.00	39.05	F4-26 136.0-142.0	White pumice	Bmca>kfs	Ph-Tph-Tr-Lat
TF-28	5.00	39.66	F4-27 28.00-33.00 / F5-26 132.27-136.25	White pumice	Bmca>kfs	Ph-Tph-Tr-Lat
TF-29	1.20	39.94	F4-27 59.00-60.20	Grey pumice	Bmca>kfs	Sho-Lat
TF-30	4.50	40.07	F5-27 3.00-7.50 / F4-27 68.99-73.25	White and grey pumice	Kfs>bmca>cpx	Ph-Tr
TF-31	1.80	41.41	F4-28 42.00-43.80	White and grey pumice	Kfs>bmca>cpx	Ph-Tr-Tph-Pht
TF-32	4.00	42.30	F4-28 133.0-134.5	Grey pumice	Kfs>bmca>cpx	Tph-Ph-Tr-Lat
TF-33	2.00	43.00	F4-29 45.75-47.75	white and grey pumice, transparent shards	Kfs>cpx>bmca	Ph
TF-35	0.60	43.70	F5-29 71.20-71.80	White pumice	Kfs>bmca	Tr
TF-35b*	17.5	45.24	F4-30 79.96-97.45	Very few material	No	Ph
TF-37	2.53	46.23	F4-31 20.23-22.76	white and grey pumice, grey-black scoria	Kfs>cpx>bmca	Pht-Tph-Ph-Tr
TF-43	1.70	49.02	F4-32 149.8-151.5	White pumice	Bmca>kfs	Tr

*: Bioturbated layer, real tephra thickness is not quantifiable. Rock type abbreviations: Ph = phonolite; Tr = trachyte; Tph = teprhiphonolite; Pht = phonoteprhite; Lat = latite; Sho = shoshonite. Mineral abbreviations: Kfs = K-feldspar; bmca = black mica; cpx = clinopyroxene.

Table 3. Location, lithological features and TAS classification of the LVC, Vico and SVD investigated proximal units.

Outcrop/ Location	Coordinates	Unit	Sub-unit/ sample	Lithology		Rock type (main)
				Juvenile clasts	Loose crystals	
Case Collina Quarry (Vu1)	42°38'31''N 11°43'54''E	Pitigliano	Tuff	Black scoria	Kfs	Ph-Tr
			Basal pumice fall	White pumice	Kfs	Ph-Tr
Grotte di Castro-Onano road cut (Vu2)	42°40'41''N 11°51'10''E	Onano	Spatter flow	Black spatter	Kfs	Sho
Poggio Falchetto-Bonini (Vu3)	42°35'08''N 11°51'24''E		Lower sillar-mid	Grey and white pumice	Cpx>kfs	Ph-Tph-Pht
			Lower sillar-base	Grey and white pumice	Kfs>bmca>cpx	Ph-Tph
Poggio delle Forche (Vu4)	42°33'11''N 11°53'02''E	Grotte di Castro	Basal fall-top	White pumice	Kfs	Ph-Tr
			Basal fall-base	Dark grey scoria	Cpx	Pht-Te-Trb
Rio Maggiore road cut (Vu5)	42°37'07''N 11°40'13''E	Sorano	Ash flow-main body	White pumice	Kfs>bmca	Ph-Tr
			Ash flow-base	White pumice	Bmca>cpx	Ph-Tr
Rio Maggiore road cut (Vu5)	42°37'07''N 11°40'13''E	Sovana*	Black pumice flow	Black scoria	Kfs>Lc	Ph
			"BUS"	White pumice	Kfs	Ph
Arlena di Castro-Tessennano road cut (Vu6)	42°27'46''N 11°48'18''E	Farnese	Pumice flow	Light grey pumice	Kfs>cpx	Ph
Rio Maggiore road cut (Vu5)	42°37'07''N 11°40'13''E		Pumice fall F	White pumice	Kfs>cpx	Ph
Rio Maggiore road cut (Vu5)	42°37'07''N 11°40'13''E	Stenzano	Pyroclastic flow	White pumice	Kfs>bmca	Tr
Monte di Marta (Vu7)	42°32'05''N 11°54'56''E	Canino	Fall C	White pumice	Kfs>cpx>bmca	Tr
Fosso la Nova road cut (Vu8)	42°35'54''N 11°38'46''E		Upper Flow	Black scoria	Kfs	Tr
Pian di Vico (Vu9)	42°25'08''N 11°48'41''E		Main Flow	Light grey-pink pumice	Kfs>cpx	Tr
			Upper Fall B	White pumice	Kfs>cpx	Tr
			Lower Fall B	White pumice	Kfs>cpx	Tr
Trevignano Romano, Centro Rapaci (Sa1)	42°10'23''N 12°14'47''E	TR-CR-2	TR-CR-2	White pumice	Kfs	Ph
		TR-CR-1	Scoria Fall	Grey scoria	Kfs>cpx	Ph
			Top	White pumice	Kfs>cpx	Ph
			Base	White pumice	Kfs	Ph
Anguillara Sabazia (Sa2)	42°05'29''N 12°16'16''E	Vigna di Valle	Surge-Pumice layer	White pumice	Kfs>cpx	Ph-Lat
			Surge Base	White pumice	Kfs>cpx	Ph
Anguillara Sabazia-Mola Vecchia (Sa3)	42°05'25''N 12°16'55''E	Pizzo Prato	Lower Flow	White pumice	Kfs>cpx	Ph
			Fall Top	White pumice	Kfs>bmca>cpx	Ph-Tr
			Fall Base	White pumice	Kfs>cpx	Ph-Tr
San Martino al Cimino train station (Vi1)	42°22'58''N 12°06'26''E	Farine Formation	Pyroclastic flow	White-brownish pumice	Kfs>cpx>bmca	Ph-Tr

*Sovana ME composition is from Palladino et al., 2014. Rock type abbreviations: Tr = trachyte; Ph = phonolite; Tph = teprhiphonolite; Pht = phonotephrite; Lat = latite; Sho = shoshonite; Te = tephrite; Trb = trachybasalt. Mineral abbreviations: Kfs = K-feldspar; bmca = black mica; cpx = clinopyroxene; Lc = leucite.

3. *Materials and methods*

3.1. Tephra recovering and preparation

This study is focused on the Fucino tephra succession spanning the 250-170 kyr time interval, broadly corresponding to the late MIS 8 and early MIS 6, consisting of 20 layers between the uppermost TF-19 and lowermost TF-43 (Fig. 3; Tables 1 and 2). It is worth mentioning that, due to a methane reservoir, several tephra layers in the interval comprised between TF-33 and TF-43 are affected by dyagenetic glass alteration that prevented and/or limited their geochemical characterisation. Thus, only few (i.e., TF-35, TF-35b, TF-37 and TF-43) of these tephras have been characterised and presented here.

Geochemical and geochronological investigations were also performed on selected near-vent units from Latera Volcanic Complex (LVC), Sabatini Volcanic District (SVD), and Vico volcano. The complete list of the investigated Fucino tephra and near-vent units, along with information of the performed analyses, are reported in Table 1. The main lithological features of the two groups of products are instead summarized in Tables 2 and 3, respectively.

The 20 Fucino tephra layers and 13 proximal LVC (8), Vico (1) and SVD (4) units were all wet sieved with tap water through a series of sieves with decreasing mesh openings. Some Fucino F4-F5 tephra were also pre-treated with HCl (i.e., tephra layers TF-21a, TF-23, TF-35b), sieved at 25 μm (TF-21a, TF-23, TF-33, and TF-35b) and density separated. All fractions were successively oven-dried at 100°C for 1-2 h. Selected fractions of 60-250 μm were mounted on 29 x 49 mm glass slides, embedded in epoxy resin, progressively ground to the desired thickness of 60-100 μm and finally polished to be analysed with the electron microprobe. For trace element analysis, selected samples have been instead embedded in epoxy resin to obtain multi-sample pucks, 1-inch in diameter (Froggatt and Gosson, 1982; Lowe, 2011), and successively polished until fresh sections of the micro-pumices emerged.

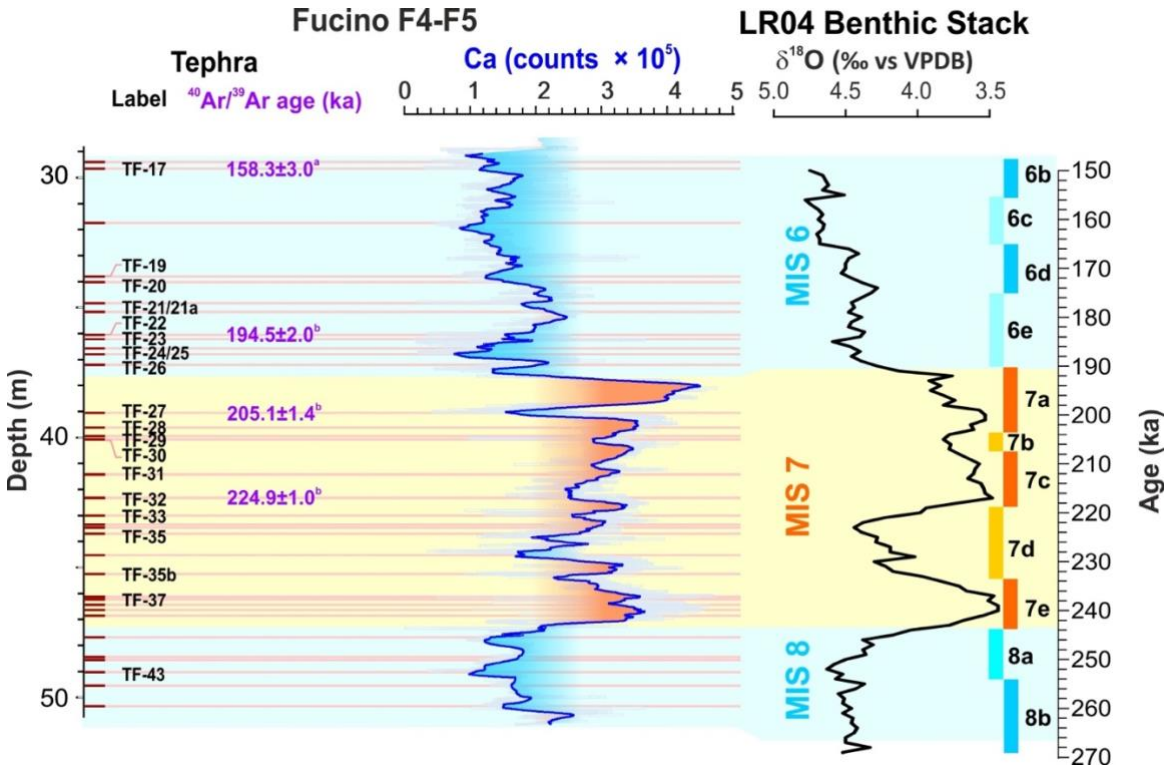

Figure 3. Detailed tephrostratigraphy and Ca counts from XRF scanning (Giaccio et al., 2019) of the investigated MIS 8-MIS 6 interval from Fucino F4-F5 core compared with LR04 Benthic Stack (Lisiecki and Raymo, 2005). The available ([a] Giaccio et al., 2017a) and the new ([b] this study) direct, $^{40}Ar/^{39}Ar$ age determinations of the Fucino dephra are also shown.

3.2. Electron Microprobe

Glass shards and pumice fragments were characterised by single-shard major element chemical analysis using the electron probe micro analyser (EPMA). To achieve a good statistical expression of the tephra composition and their geochemical variability, we aimed at analysing at least 10-15 shards/micro-pumices from each tephra. We successfully achieved this, except for two tephra layers (i.e., TF-29 and TF-35b), due to the incipient alteration of the glass and/or the crypto-tephra nature of the layer that prevented the finding of sufficiently large shard fragments/pumice septa. Analysis was performed at three different institutes, and the specific technical and methodological description of each one is provided below. Comparability of the glass data obtained with the three instruments is guaranteed by analysis of the GOR128-G reference glass secondary standard from Jochum et al. (2006) at all three institutes.

Prague - Analysis was first performed with a Jeol JXA-850F, equipped with five wave dispersive spectrometers (WDS) and installed at the Institute of Petrology and Structural Geology (Charles University, Prague, Czech Republic). The machine operated at 15 kV accelerating voltage, 10 nA beam current and 10 μm defocused beam to limit alkali loss. Element counting times were of 20 s for all elements, except for Na, K, (10 s) and S (30 s). For all measurements, the F content was always below the detection limit of the machine. Standards for calibration were quartz (Si), corundum (Al), rutile (Ti), magnetite (Fe), periclase (Mg), rhodonite (Mn), albite (Na), sanidine (K), diopside (Ca), apatite (P and F), tugtupite (Cl) and anhydrite (S). The secondary standards GOR128-G (Jochum et al., 2006) and CFA47 (Marianelli and Sbrana, 1998) were analysed at the beginning of each microprobe session for a total of one point each to evaluate analysis accuracy.

Rome - Samples were further characterised at the *Istituto di Geologia Ambientale e Geoingegneria* of the Italian National Research Council (IGAG-CNR, Rome, Italy). Major and minor elements quantitative analysis was performed with a CAMECA SX-50 EPMA equipped with five-wavelength dispersive spectrometers (WDS), operating at 15 kV accelerating voltage, 15 nA beam current, 10 μm defocused beam diameter and 20 s element counting time for all elements. Wollastonite (Si and Ca), corundum (Al), periclase (Mg), magnetite (Fe), rutile (Ti), orthoclase (K), jadeite (Na), phlogopite (F), potassium chloride (Cl), barite (S), F-apatite (P) and metals (Mn) were used as internal standards. The Kakanui augite and rhyolite RLS132 from the United States Geological Survey (USGS), and glass secondary standards StHs6/80-G and GOR128-G (Jochum et al., 2006) were measured prior to each analytical run to evaluate the accuracy of the electron-microprobe analysis.

Cologne - A JEOL JXA-8900RL electron microprobe equipped with five-WDS was used for analysis of tephra glass fragments at the University of Cologne (Cologne, Germany). The operation conditions (Leicher et al., 2021) were set to 12 kV accelerating voltage, 6 nA beam current and 5-10 μm beam diameter. Calibration of the machine was performed using the internal reference materials (Lipari glass ID3506, scapolite from the Smithsonian National Museum of Natural History, and all other minerals from the P&H Geostandard Block), while the analytical crystals and counting times were: Lipari glass ID3506 (Si, Al; TAP; 20 s), almandine (Fe; LIF; 30 s), rutile (Ti; PETH; 30 s), rhodonite (Mn; LIF; 30 s), clinopyroxene (Mg; TAP; 30 s), wollastonite (Ca; PETJ; 20 s), albite (Na; TAP; 10 s),

orthoclase (K; TAP; 10 s), apatite (P; PETH; 40 s), scapolite NMNH R6600 (Cl; PETH; 40 s), fluorite (F; TAP; 40 s) and baryte (S; PETJ; 40 s).

Data reduction was carried out using either the ZAF (Prague and Cologne) or PAP (Rome) correction, while data processing was performed in Microsoft Excel. We adopted 93 wt.% as a threshold for the measured totals: analyses with measured totals lower than 93 wt.% were discarded. All compositional data are shown as oxide weight percentages (wt.%) in the *Total Alkali vs Silica* (TAS, Le Maitre et al., 2002; Fig. 4a) and bi-plots diagrams, with total iron (FeO_{tot}) measured as FeO, and normalised to 100 wt.% on a volatile-free (i.e., excluding F, Cl and S) basis for correlation purposes. Mean compositions are reported in Appendix, Table-A1.

3.3. LA-ICP-MS

Trace element compositions have been determined on pumice fragments/glass shards for 8 selected F4-F5 tephra layers displaying the most homogeneous composition, i.e., those with the less variable SiO_2 content (wt.%). Similarly, trace element analysis of glasses from the LVC (6 samples) and SVD (2 samples) proximal units have been also performed to allow direct trace element comparison with the F4-F5 tephra and to provide a reference geochemical dataset for future investigations in the region.

Trace elements have been determined by means of laser ablation-inductively coupled plasma-mass spectrometry (LA-ICP-MS) at the Earth and Physics Department, University of Perugia (Perugia, Italy). The analyses were performed with a Teledyne Photon Machine G2 193 Excimer laser ablation system coupled with a Thermo Fisher Scientific iCAP-Q quadrupole-based ICP-MS (Petrelli et al., 2016). Diameter of the laser beams were 15 and/or 20 μm, depending on glass shards and pumices size, at 8 Hz frequency and 3.5 J/cm^2 energy density at sample surface. The NIST SRM 610 reference material (Pearce et al., 1997) was employed as calibrator, while ^{29}Si was used as internal standard to reduce trace element concentrations from counts per second signals. The USGS BCR2G reference material was analysed as unknown to provide quality control through the analysis (Jochum et al., 2006). All investigated elements showed precision and accuracy better than 10% (Petrelli et al., 2016). Trace element results are presented as biplots diagrams in Figure 5, while the mean

compositions and additional spider diagrams normalized to the primitive mantle (McDonough and Sun, 1995) are reported in the Appendix, Table-A2 and Fig. A1 respectively.

3.4. Sr and Nd isotopes

Strontium (Sr) isotope composition was determined on glass shards and mineral phases (i.e., feldspar, pyroxene and one biotite fraction) from eight selected samples, some representative of fall deposits collected in the proximal outcrops of LVC and SVD volcanoes, others representative of Fucino F4-F5 tephra layers. Neodymium (Nd) isotope composition was measured on glass shards only. The different fractions were handpicked under a binocular microscope, by selecting glass shards among the most homogeneous in colour and visibly poorly affected by secondary alteration. Feldspar and pyroxene crystals were handpicked avoiding those characterised by the presence of glass rinds attached on their surfaces.

Before chemical dissolution, glass shards were acid leached three to five times to reduce the alteration effects as much as possible. Leaching was carried out each time by placing the beakers containing samples and high-purity 6N HCl on a hot plate for 10 min. During each leaching step and after the final leaching, samples were rinsed with Milli-Q® H_2O. Minerals were cleaned with Milli-Q® H_2O for 10 min in an ultrasonic bath. Dissolution was obtained with high-purity HF–HNO_3–HCl mixtures. Sr and Nd were separated from the matrix through conventional ion-exchange procedures. Sr and Nd isotopic compositions were determined in static-mode by thermal ionisation mass spectrometry (TIMS) using a Thermo Finnigan Triton TI® mass spectrometer equipped with one fixed and six adjustable Faraday cups. Average 2σ mean, i.e., the standard error with N = 180, was better than ± 9 x 10^{-6} for Sr, and better than ± 7 x 10^{-6} for Nd measurements. The mean measured values of $^{87}Sr/^{86}Sr$ for the NIST-SRM 987 standard and $^{143}Nd/^{144}Nd$ for the La Jolla standard were 0.710260 ± 0.000021 (2σ, N = 179) and 0.511844 ± 0.000010 (2σ, N = 60), respectively. External reproducibility (2σ) during the period of measurements was calculated according to Goldstein et al. (2003). Measured $^{87}Sr/^{86}Sr$ ratios were normalized for within-run isotopic fractionation to $^{86}Sr/^{88}Sr$ = 0.1194, and $^{146}Nd/^{144}Nd$ = 0.7219. The final, measured isotope ratio values were normalized to the recommended values of the NIST SRM 987 ($^{87}Sr/^{86}Sr$ =0.71025) and La Jolla ($^{143}Nd/^{144}Nd$ = 0.51185)

standards, respectively. Chemistry processing and isotope analysis were performed at the Radiogenic Isotope Laboratory (RIL) of the *Istituto Nazionale di Geofisica e Vulcanologia, Osservatorio Vesuviano*. Full analytical data are reported in Appendix, Table-A3.

3.5. $^{40}Ar/^{39}Ar$ dating

LSCE - The $^{40}Ar/^{39}Ar$ ages were all obtained at the *Laboratoire des Sciences du Climat et de l'Environnement* (CEA, Gif-sur-Yvette, France) dating facility. Fresh and transparent K-rich feldspars were extracted from tephra layers TF-22 (F5-25 111-115), TF-27 (F4-26 136-142) and TF-32 (F4-28 132-136). After being washed in distilled water, three fractions were selected (200-250 μm, 250-350 μm and 350-500 μm). Beside for TF-22, large crystals above 350 μm were found and therefore used for the dating of these tephra layers.

The three pyroclastic units from the LVC (i.e., Farnese, Canino Fall-C and Fall-B) were also prepared for $^{40}Ar/^{39}Ar$ dating at the LSCE (CEA, Gif-sur-Yvette, France) facility. After crushing and sieving, selected K-Feldspar crystals, with a grain size ranging between 1 mm and 630 μm, were handpicked. After being leached with a 7% HF solution and rinsed in distilled water, about 40 crystals without detectable inclusion (i.e., at x40 binocular magnification) were selected for irradiation and loaded in an Al disk.

TF-27, TF-32, Farnese, Canino Fall-C and Fall-B crystals were irradiated for 120 min in the Cd-lined, in core CLICIT facility of the Oregon State University TRIGA reactor (IRR. CO-007). TF-22 crystals were irradiated at the same facility during another irradiation for 120 minutes too (IRR. CO-008). Interference corrections were based on the nucleogenic production ratios given in Balbas et al. (2016). After irradiation, individual crystal for each sample were transferred into a copper 133 pits sample holder placed into a differential vacuum Teledyne Cetac window connected to a home designed compact extraction line. Minerals were fused one by one using a 100W Teledyne Cetac CO_2 laser during 15 s at 2.5 W. Before fusion, each crystal underwent a 10 s long sweeping at 0.3W to remove unwanted gas potentially trapped on the crystals surface and fractures. Extracted gases were firstly purified by a SAES GP 50 cold getter for 90 s and then for 230 s by two hot SAES GP 50 getters. The five Argon isotopes (i.e., ^{40}Ar, ^{39}Ar, ^{38}Ar, ^{37}Ar and ^{36}Ar) were measured using a

multicollector NGX 600 mass spectrometer equipped with 9 ATONA Faraday cups array and an electron multiplier. More technical specifications regarding the NGX 600 ATONA detector array are presented in detail in Cox et al. (2020). ^{40}Ar, ^{39}Ar, ^{38}Ar, and ^{36}Ar isotopes were collected simultaneously while the ^{37}Ar was measured in a second time. In the first run, ^{40}Ar, ^{39}Ar and ^{38}Ar were measured simultaneously on 3 ATONA and ^{36}Ar on the electron multiplier. Following this first run the ^{37}Ar was measured alone using the electron multiplier. Each isotope measurement corresponds to 15 cycles of 20 s integration time. Peak intensity data were reduced using ArArCALC V2.4 (Koppers, 2002). Neutron fluence J factor was calculated using co-irradiated Alder Creek sanidine standard ACs-2 associated to an age of 1.1891 Ma (Niespolo et al., 2017) according to the K total decay constant of Renne et al. (2011), ($\lambda_{e.c.}$ = (0.5757 ± 0.016) × 10^{-10} yr^{-1} and λ_{β^-} = (4.9548 ± 0.013) × 10^{-10} yr^{-1}). To determine the neutron flux for each sample we used at least 12 flux monitor crystals coming from pits framing the samples in each irradiation disk. J-value were 0.00056060 ± 0.00000056 (TF-27, Canino Fall-C); 0.00056040 ± 0.00000056 (TF-32, Farnese, Canino Fall-B) and 0.00055810 ± 0.00000056 (TF-22). To verify the detectors linearity, mass discrimination was monitored by analysis of at least 60 air shots of various beam sizes ranging from 5.0 10^{-3} up to 2.0 10^{-2} V (1 to 4 air shots) are obtained daily. These measurements are done automatically during nightime before and after the unknown measurements. Discrimination is calculated according the $^{40}Ar/^{36}Ar$ ratio of 298.56 (Lee et al., 2006). Procedural blank measurements were achieved after every three unknowns. For typical 5 min time blank backgrounds are between 1.7 10^{-4} V and 2.5 10^{-4} V for ^{40}Ar and 60 to 70 cps for ^{36}Ar (about 1.0 10^{-6} V equivalent).

OSU - K-feldspar phenocrysts were co-irradiated with the 1.1864 Ma Alder Creek sanidine standard (Jicha et al., 2016) at the Oregon State University TRIGA reactor in the Cadmium-Lined In-Core Irradiation Tube. Single crystal fusion analyses were performed at the WiscAr laboratory at the University of Wisconsin-Madison using a 60W CO_2 laser and a Noblesse multi-collector mass spectrometer following Jicha et al. (2016).

Full analytical data from LSCE and OSU facilities for each sample are reported in Appendix, Table-A3.

4. Results

4.1. Major and minor element composition

The analysed 20 Fucino tephra, Ohrid tephra OH-DP-0725 and 13 proximal LVC, Vico, and SVD pyroclastic units are all shown in the *Total Alkali vs Silica* classification diagram (TAS, Le Maitre et al., 2002; Fig. 4a). In this diagram, the 20 Fucino tephra occupy the fields of the high-K series (Appleton, 1972), and can thus be classified as potassic tephrites, phonotephrites, tephriphonolites, phonolites and trachytes, but also as latites and shoshonites (e.g., TF-22, TF-27, and TF-29). In particular, the investigated Fucino tephra are mainly phonolithic and trachytic in composition (Fig. 4a), with variable amounts of alkali contents and ratio, all with $K_2O/Na_2O \geq 1$, except for TF-21 and TF-23 (where $K_2O/Na_2O < 1$).

The 8 LVC units are all characterised by a K_2O content that is always $\geq Na_2O + 2$ wt.%. In the TAS diagram (Fig. 4a) they can be mainly classified as K-phonolites and K-trachytes, but also as potassic tephriphonolites (Onano unit) and tephrites-trachybasalts (Grotte di Castro Basal Fall sub-unit). The 4 SVD units are all phonolitic in composition (Fig. 4a), with similar amounts of K_2O and Na_2O with $K_2O/Na_2O \geq 1$, except for Pizzo Prato unit where K_2O/Na_2O is always > 2-3. The Farine Formation unit from Vico volcano has a fairly homogeneous phonolitic-trachytic composition (Fig. 4a), with 60-62 wt.% SiO_2, 13-15 wt.% alkali sum and mean K_2O/Na_2O ratio of 1.6 ± 0.2 (2 s.d.). Finally, Ohrid tephra OH-DP-0725 is trachytic in composition (Fig. 4a), with $K_2O/Na_2O > 1$ (mean = 1.8 ± 0.1 [2 s.d.]). Leicher et al. (2021) reported both a phonolitic and a rhyolitic component, the latter not observed in the sample analysed in this study.

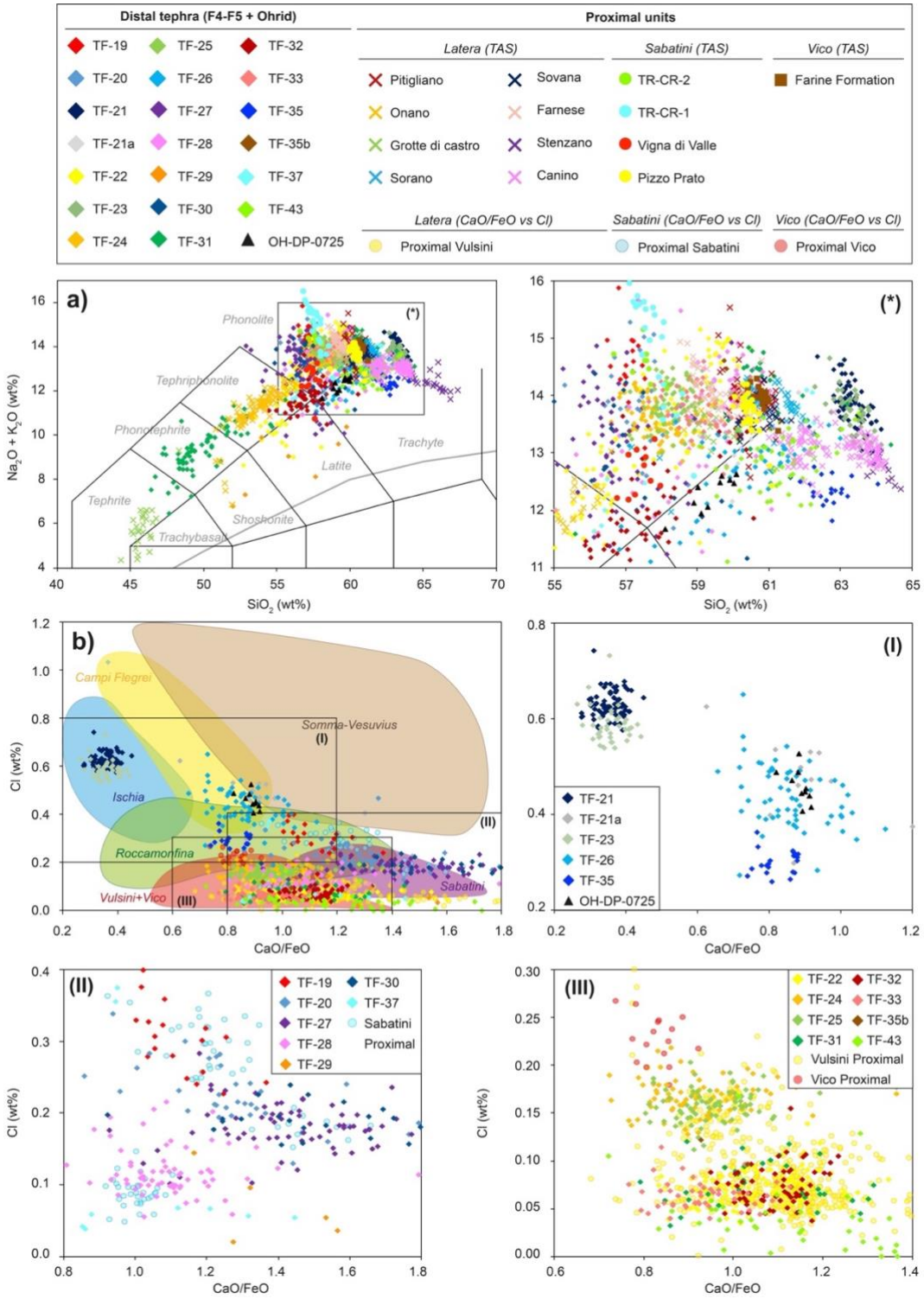

Figure 4. (a) *Total Alkali vs Silica* (TAS; Le Maitre et al., 2002) and (b) CaO/FeO vs Cl (Giaccio et al., 2017a) classification diagrams of the Fucino F4-F5 tephra, along with proximal pyroclastic units of Latera Volcanic Complex (LVC), Vico volcano (Farine Formation unit), and Sabatini Volcanic District (SVD), and Ohrid tephra OH-DP-0725.

4.2. Trace element composition

Out of the 8 Fucino tephra selected for trace element data analysis, all but TF-43 provided a sufficient number of analytical points (i.e., > 10-15) for their characterisation. Instead, all eight selected proximal LVC and SVD units yielded > 10-15 analytical points, thus representative of their geochemical variability.

The Fucino tephra display heterogeneous trace element concentrations (Fig. 5). Tephra layers TF-19, TF-20, TF-27, and TF-32 all display similar variations of Th against other incompatible trace elements (Fig. 5a-b), although with variable Th contents. Indeed, tephra layers TF-19 and TF-20 are more enriched in Th (Th = 140-173 ppm and 122-200 ppm respectively), with respect to TF-27 (58-115 ppm) and TF-32 (49.9-67.8 ppm). Tephra TF-21 is less enriched in Th (74.7-93.4 ppm, amongst the lowest) whilst being more enriched in Zr (869-1113 ppm, Fig. 5a), Nb (98-121 ppm, Fig. 5b) and Ta (4.28-5.27 ppm) respect to all the other tephra. Furthermore, it displays the highest ratios of High Field Strength Elements (HFSE) and Light Rare-Earth Elements (LREE) to Th (e.g., Ta/Th = 0.051-0.068; Nb/Th = 1.165-1.465 [Fig. 5c]; La/Th = 2.218-2.914 [Fig. 5d]; Ce/Th = 4.07-4.97). Phonolitic tephra TF-24 and TF-25 are the most enriched in Th, ranging respectively from 208-285 ppm and 214-264 ppm, compared to all the other tephra having $\leq$ 200 ppm of Th (Fig. 5a-b). TF-24 and TF-25 are also characterised by similar, and basically indistinguishable from one another, ratios of HFSE and LREE to Th (e.g., Nb/Th = 0.236-0.292 for TF-24 and 0.234-0.311 for TF-25 [Fig. 5c]; La/Th = 0.891-0.995 for TF-24 and 0.845-0.977 for TF-25 [Fig. 5d]; Ce/Th = 1.50-1.72 for TF-24 and 1.41-1.59 for TF-25).

The LVC pyroclastic units are characterised by very similar incompatible trace element contents, overlapping with Fucino tephra (Fig. 5a-b). Overall, Th ranges between 55-155 ppm, Zr between 364-899 ppm (Fig. 5a), Nb between 20.9-47.5 ppm (Fig. 5b), and Ta between 0.95-2.96 ppm for the LVC units. Ratios of HFSE and LREE to Th show perfect overlapping with TF-32 and partially with TF-19 and TF-20 (Fig. 5c-d). SVD pyroclastic units show similarly variable incompatible trace elements, with higher Th (i.e., 129-236 ppm) with respect to LVC units, overlapping only with tephra layers TF-19 and TF-20 (Fig. 5a-b). However, when employing ratios of HFSE and LREE to Th, a good overlap is observed also for TF-27 (Fig. 5c-d).

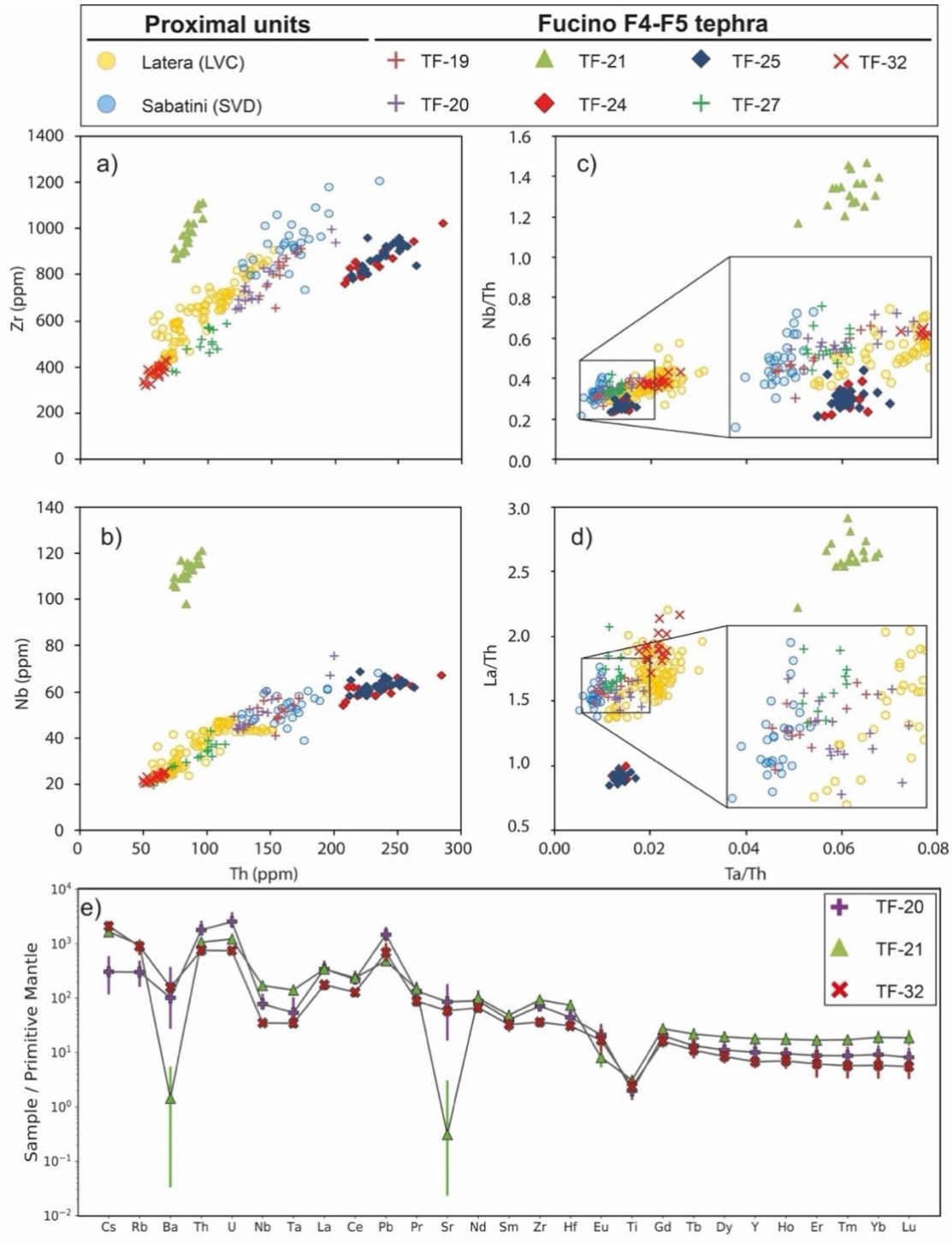

Figure 5. Trace element representative biplot (a to d) and spider (e; normalized to the primitive mantle; McDonough and Sun, 1995) diagrams of the selected Fucino F4-F5 tephra and proximal LVC and SVD pyroclastic units.

4.3. Isotopic composition

$^{87}Sr/^{86}Sr$ ratios (Fig. 6a) of the Fucino F4-F5 tephra range from 0.706233-0.710552, with TF-22 and TF-32 showing values with similar ranges (0.710375-0.710379 [TF-22] and 0.710358-0.710552 [TF-32]). TF-27 shows slightly lower values (0.710132-0.710142), while TF-26 display $^{87}Sr/^{86}Sr$ ranges (0.706233-0.706566) sensibly lower respect to all the other tephra. Samples from the Latera Volcanic Complex (i.e., Pitigliano, Farnese, and Canino Fall-C) range from 0.710081-0.710789, partially overlapping with the Fucino tephra. Sample TR-CR-1 from the Sabatini Volcanic District (SVD), display $^{87}Sr/^{86}Sr$ values (0.710242-0.710263) similar to those of the Fucino and LVC samples. $^{143}Nd/^{144}Nd$ values have been determined for the four Fucino tephra and the Farnese and Fall-C units from LVC (Fig. 6b). LVC units display $^{143}Nd/^{144}Nd$ contents (0.512118 [Farnese]; 0.512105-0.512113 [Fall-C]) similar to all the Fucino tephra (0.512116 [TF-22]; 0.512098 [TF-27]; 0.512118 [TF-32]) but TF-26, which display the highest value among all samples (0.512551).

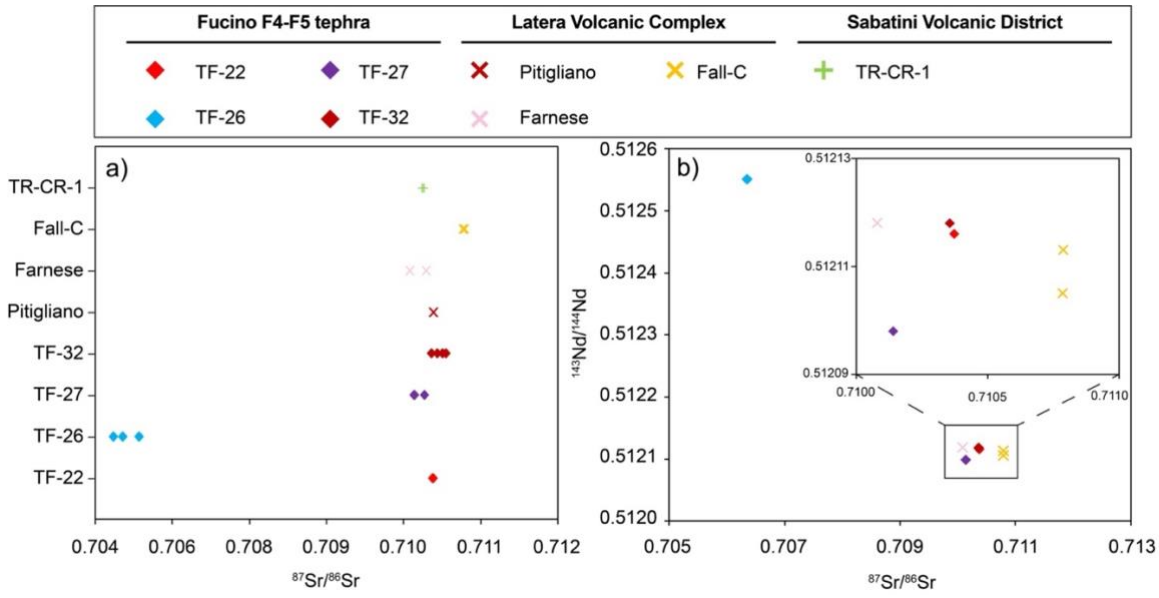

Figure 6. $^{87}Sr/^{86}Sr$ (a) and $^{87}Sr/^{86}Sr$ vs $^{143}Nd/^{144}Nd$ (b) isotopic composition of the selected Fucino F4-F5 tephra and proximal LVC and SVD pyroclastic units.

4.4. $^{40}Ar/^{39}Ar$ ages

LSCE - All individual tephra layer $^{40}Ar/^{39}Ar$ dating results are presented as probability diagrams in Figure 7. Weighted mean age uncertainties are all reported at 2σ, including J uncertainty, and were calculated using Isoplot 4.0 (Ludwig, 2012). For each sample, inverse isochrones have within uncertainties an atmospheric $^{40}Ar/^{36}Ar$ initial intercept suggesting that dated crystals are without detectable excess argon.

TF-22 - The crystals extracted from this tephra layer are small (200-250 μm). Since the presence of xenocrysts can hamper the accuracy of the age, and despite the very small argon beam sizes (2 times the ^{40}Ar blank), we were able to obtain 8 single crystal ages (Fig. 7). Despite the low precision of these ages, we did not detect any obvious older crystals. We improved the precision by fusing two (6 measurements), and four crystals at the same time (6 measurements). All experiments with multiple crystals shared a similar age within uncertainty, which proves that we were not able to detect any significant older crystals within the analytical uncertainties. To obtain a final and more precise age, the remaining crystals were analysed in small populations of 10 to 15 crystals. Including all experiments, we obtained a total of 24 similar ages, allowing to calculate an accurate and precise weighted mean age of 194.5 ± 2.0 ka (MSWD = 0.3, p = 1.0).

TF-27 - A total of 15 individual crystals were dated. Excluding 4 older crystals, a main population constituted by 11 crystals (Fig. 7) allowed to calculate a mean age of 205.1 ± 1.4 ka (MSWD = 1, p = 0.43) for this tephra.

TF-32 - 19 single crystal ages were obtained for this tephra layer. The probability diagram is complex, multimodal with at least 5 modes with crystals as old as 275 ka (Fig 7), indicating potential magma contamination from older xenocrysts entrained during the eruption. The youngest population includes 9 crystals sharing the same age within uncertainties. Using these crystals, we calculated a weighted mean age of 224.9 ± 1.0 ka (MSWD = 0.8, p = 0.60) that we interpret as the age of deposition of this tephra.

Farnese - 15 single crystals were analysed, all of them sharing the same age within uncertainties as shown by the corresponding almost gaussian probability diagram (Fig. 7). Using these crystals, we

calculated a weighted mean age of 235.6 ± 0.6 ka (MSWD = 0.7, p = 0.8) that we interpret as the age of the Farnese eruption.

Canino Fall-B - we analysed 15 single crystals for this sub-unit. Excluding one crystal, that shows an older age and is thus interpreted as a xenocryst, all the 14 remaining ones have the same age within uncertainties (Fig. 7). This main population of crystals, interpreted here as juvenile ones, allows to propose a precise age of 253.8 ± 0.8 ka (MSWD = 1.1, p = 0.4) for the Canino Fall-B sub-unit.

Canino Fall-C - 11 crystals were individually dated for this sub-unit. Like Canino Fall-B, except for one xenocryst with a low $^{40}Ar^*$ dated at 276 ka, all remaining crystals display a similar age within uncertainties (Fig. 7). Using this main and younger population of juvenile crystals we have calculated a weighted mean age of 253.1 ± 0.8 ka (MSWD = 1.4, p = 0.8) for the Canino Fall-C sub-unit. This age is undistinguishable from the one obtained for Canino Fall-B, and the weighted mean age of the Canino eruption, given by Fall-B and Fall-C, is thus 253.4 ± 0.8 ka.

OSU - All individual tephra layer $^{40}Ar/^{39}Ar$ dating results are presented as probability diagrams in Figure 7.

Pitigliano - 33 crystals were individually dated for the Pitigliano unit, yielding a weighted mean age (2σ) of 178.1 ± 0.4 ka (MSWD = 0.70; Fig. 7).

Sovana - 23 crystals were dated for this unit. Of these, 16/23 crystals yielded a weighted mean age of 226.4 ± 0.7 ka (MSWD = 0.38, 2 σ; Fig. 7), while the remaining 7 crystals were interpreted as older xenocrysts.

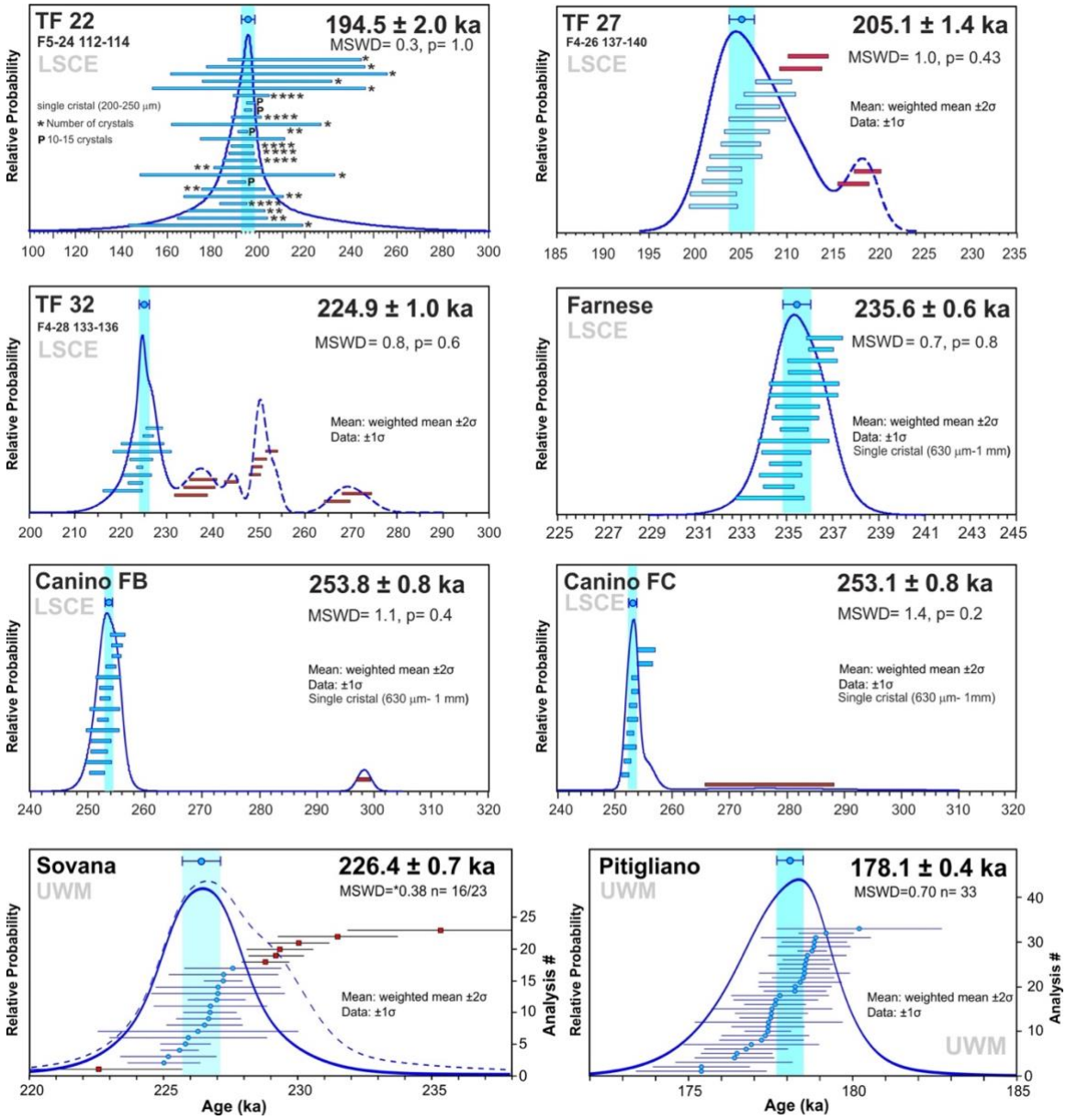

Figure 7. Age probability diagrams of tephra layers TF-22, TF-27, and TF-32, and of proximal LVC pyroclastic units Pitigliano, Onano, Farnese, Canino Fall-B, and Canino Fall-C.

5. Discussion

5.1. Volcanic sources of the Fucino tephra

5.1.1. The active volcanoes over the investigated timespan

Volcanoes belonging to the Quaternary potassic peri-Tyrrhenian volcanic region (Fig. 1b) are the most probable sources of the investigated tephra. Indeed, previous investigations (Giaccio

et al., 2017a, 2019; Di Roberto et al., 2018; Del Carlo et al., 2020; Monaco et al., 2021) showed that all the Fucino tephra documented so far were sourced at these volcanic systems, along with products from Aeolian Islands and Etna volcano. Furthermore, in the time interval here considered, almost all these volcanic systems were active.

At Vulsini (Fig. 1b), between ~250 ka and 160 ka, the Latera volcano (or LVC; Vezzoli et al., 1987) produced several Plinian-fall (Palladino and Agosta, 1997) and pyroclastic flow (Sparks, 1975; Palladino and Valentine, 1995) deposits, some of them associated to caldera-forming eruptions (Palladino et al., 2010). These eruptions include, from the oldest to the youngest, those of Canino, Stenzano, Farnese, Sovana, Sorano, Grotte di Castro, Onano and Pitigliano, whose deposits were investigated in this study.

At Vico volcano (Fig. 1b), after a period of ~50 kyr of prevailing effusive activity (Lago di Vico lava Formation, 305-258 ka, e.g., Perini et al., 2004) that built the stratovolcano, a series of explosive, caldera-forming eruptions (i.e., Ignimbrite A/Farine Formation, Ignimbrite B/Ronciglione Formation, and Ignimbrite C/Sutri Formation; Bertagnini and Sbrana, 1986; Perini et al., 1997; Bear et al., 2009) occurred.

At Sabatini (Fig. 1b), two volcanic areas where simultaneously active, i.e., the Sacrofano (~300-200 ka) and Bracciano (~325-200 ka) calderas (Sottili et al., 2019; Marra et al., 2020), both characterised by major Plinian (e.g., Magliano Romano Plinian Fall; Sottili et al., 2010) and caldera-forming eruptions (e.g., Tufo Giallo di Sacrofano, Tufo di Bracciano, Tufo di Pizzo Prato; Sottili et al., 2010, 2019), and minor strombolian activity and lava flows at parasite cones along the rims of the two calderas.

At Colli Albani, the long Tuscolano-Artemisio Phase (i.e., ~600-355 ka; de Rita et al., 1988), now known as Vulcano Laziale period (Giordano and the CARG Team, 2010), was followed by the Mt. Faete Phase (now Tuscolano-Artemisio-Faete period, 355-180 ka; Giordano and the CARG Team, 2010) that emplaced several lava flows, before switching to the final Late Hydromagmatic Phase (or Via dei Laghi period, 200 ka-quiescent; Giordano and the CARG Team), during which the Ariccia (~200 ka), Nemi (~150 ka) and Albano (~70-36 ka) maars were active (e.g., Marra et al., 2003; Freda et al., 2006; Giaccio et al., 2009; Marra et al., 2016b). Products of the Colli Albani volcano are

generally characterised by K-foiditic compositions, which are not observed for any of the investigated tephra layers, thus allowing us to exclude this volcanic system as a possible source of the F4-F5 tephra.

At Roccamonfina (Fig. 1b), the Upper White Trachytic Tuff (UWTT, ~230 ka; Giannetti and De Casa, 2000) and Yellow Trachytic Tuff (YTT, ~227 ka; Giannetti, 1996) were emplaced, followed by central activity at Mt. Lattani-Mt. Santa Croce latitic scoria cones (170-150 ka; Ruchon et al., 2008).

Finally, in the Campanian Plain (Fig. 1b), explosive activity is documented by a series of deposits, including the Seiano (~290 ka), Moschiano (~185 ka) and Taurano (~157 ka) ignimbrites (De Vivo et al., 2001; Rolandi et al., 2003) and other pyroclastic deposits (i.e., Taurano Layered Tuff Series, 205-183 ka; De Vivo et al., 2001; Belkin et al., 2016). Such an old activity is also documented by tephra deposits in distal settings (e.g., Giaccio et al., 2014; Petrosino et al., 2015; Wagner et al., 2019) with Campanian like-composition, generally ascribed to an unspecified Campanian volcanism (e.g., Wulf et al., 2018), an undefined Neapolitan volcanic area (e.g., Giaccio et al., 2017b) or the so-called Campanian Volcanic Zone (CVZ) of Rolandi et al. (2003). Also, in the Campania area, several Plinian Fall deposits were emplaced by the volcanic island of Ischia (Fig. 1b), the deposits preserved in the Island dating back to 75 ka (e.g., Brown et al., 2008, 2014), but with evidence of an activity as old as at least 150 ka, and up to historical times (e.g., Poli et al., 1987; Sbrana et al., 2018).

5.1.2. Geochemical signatures

Potassic tephrites, phonotephrites, tephriphonolites, phonolites, trachytes, shoshonites and latites (Fig. 4a) are quite common in the peri-Tyrrhenian Quaternary potassic volcanoes (e.g., Peccerillo, 2017). To identify and discriminate the volcanic sources of the Fucino tephra, we employed the Ca/FeO vs Cl classification diagram (Fig. 4b; Giaccio et al., 2017a), which allows distinguishing products with 52-67 wt.% of SiO_2 of the Latium (i.e., Vulsini, Vico and Sabatini), Roccamonfina and Neapolitan (i.e., Ischia, Campi Flegrei and Somma-Vesuvius) volcanoes from each other. A large number of glass-analyses from the Italian Quaternary volcanoes shows a strong consistency and reliability on this discriminating diagram. In Figure 4b, the 20 Fucino tephra can be divided as follow.

Tephra layers TF-21 and TF-23, which are distinguished from all the others by a K_2O/Na_2O ratio < 1, are both characterised by a CaO/FeO ratio of < 0.5 and Cl ranging between 0.54-0.74 wt.%, compatible with products from Ischia volcano (Fig. 4b-I). An origin from Ischia for TF-21 is also suggested by the high ratios of HFSE and LREE to Th (Fig. 5c-d) and was already pointed out by Giaccio et al. (2017a).

Tephra TF-21a and TF-26 have similar CaO/FeO ratios, ranging between 0.6-1.3, and Cl contents (i.e., 0.27-0.63 wt.% and 0.27-0.65 wt.% respectively; Fig. 4b-I) which would suggest a Campi Flegrei origin for both of them.

TF-35 has a less variable CaO/FeO ratio of 0.74-0.88 and Cl content of 0.26-0.36 wt.% (Fig. 4b-I), which is compatible with a Roccamonfina origin.

Tephra layers TF-19, TF-20, TF-27, and TF-30 all have a wider CaO/FeO range, generally ≥ 1 (TF-19 = 1.1 ± 0.2 [2 s.d.]; TF-20 = 1.3 ± 0.4 [2 s.d.]; TF-27 = 1.5 ± 0.4 [2 s.d.]; TF-30 = 1.5 ± 0.5 [2 s.d.]) and Cl contents between 0.01 and 0.47 wt.%, which is compatible with products from Sabatini. Indeed, data of the newly acquired TR-CR-2, TR-CR-1 and Vigna di Valle Sabatini units perfectly overlap with TF-19, TF-20, TF-27, and TF-30 (Fig. 4b-II). TF-28, TF-29 and TF-37 show similarly high Cao/FeO ratios (e.g., TF-28 up to 1.79) and low Cl contents (TF-28 = 0.05-0.21 wt.%; TF-29 = 0.02-0.14 wt.%; TF-37 = 0.04-0.37 wt.%), thus at the intersection between the Sabatini and Vulsini-Vico fields (Fig. 4b-II). Nevertheless, these Cl contents are compatible with that of the Pizzo Prato unit (i.e., 0.05-0.14 wt.%), which extends the field of the Sabatini products (Fig. 4b-II).

Tephra layers TF-22, TF-31, TF-32, TF-33, TF-35b, and TF-43 are all characterised by variable CaO/FeO ratios (overall between 0.70-1.50) and Cl contents generally ≤ 0.10 wt.% (Fig. 4b-III), overlapping with products of the Latera Volcanic Complex (LVC; Vezzoli et al., 1987) here investigated, thus suggesting an origin from this volcano.

Finally, the two phonolitic tephra TF-24 and TF-25 are characterised by very similar CaO/FeO ratios (0.72-1.43 and 0.81-1.37 respectively) and Cl contents (Cl = 0.13-0.22 wt.% and 0.11-0.20 wt.%), which are compatible with products of both Vico and Vulsini volcanoes. However, considering that the investigated LVC products have Cl contents generally ≤ 0.10 wt.% (Fig. 4b-III), we are more inclined to consider Vico as the most possible source of these two tephra layers, which is also

suggested by the peculiar trace element composition of TF-24 and TF-25, which is clearly distinguished from that of the LVC units (Fig. 5).

5.2. Other tephra repositories during Marine Isotope Stages 7 and 6

Only few tephra repositories, both in continental and marine sedimentary environments, covering the same time interval here considered are documented in the literature.

In southern Italy, the lacustrine succession of San Gregorio Magno Basin (Fig. 1a) is described to cover the ~240-15 kyr time interval (Munno and Petrosino, 2007; Petrosino et al., 2019), with the uppermost tephra (i.e., tephra layer S21) correlated to the Neapolitan Yellow Tuff eruption (NYT, 14,190 ± 680 BP; Siani et al., 2004). Tephra layer S5 was correlated by Munno and Petrosino (2007) to the V-2 marine tephra marker of Keller et al. (1978), which has a modelled age of ~170 ka, while tephra S4 was successively $^{40}Ar/^{39}Ar$ dated by Ascione et al. (2013) at 239 ± 8 ka, thus implying that the lowermost three tephra (i.e., S3, S2, and S1) all have an age older than ~240 ka.

In the Adriatic Sea (Fig. 1a), marine core PRAD 1-2 hosts tephra layers dated as far back as ~200 ka (Bourne et al., 2010, 2015). Of these, PRAD-3225 was confidently correlated with Ohrid tephra OH-DP-0624 (Leicher et al., 2016) and Fucino tephra TF-17 by Giaccio et al. (2017a). This leaves only the lowermost two tephra (i.e., PRAD-3586 and PRAD-3666) as potential correlatives for the F4-F5 Fucino tephras here investigated.

In the Tyrrhenian Sea (Fig. 1a), the marine core DED-87-08 spans the 200-90 kyr time interval (Paterne et al., 2008) and hosts several tephra layers ascribed to eruptive activity at Italian volcanoes. Giaccio et al. (2017a) proposed a tentative correlation between either C-52 or C-54 with the Ischia-like tephra TF-21, suggesting that other DED-87-08 tephras might be correlated to the F4-F5 ones. Unfortunately, the lack of glass-WDS analyses for these Tyrrhenian tephras prevent us from any tentative correlation.

The million year-long succession of Lake Ohrid (North Macedonia-Albania; Fig. 1a) hosts a tephra-rich sequence that continuously spans the last 1.36 Myr (Wagner et al., 2019). Leicher et al. (2016, 2019) presented data relative to the last 630 kyr, and reported at least 8 tephra layers, attributed to the CVZ, Pantelleria and Roccamonfina volcanic systems, covering the time interval of ~241-160

kyr, based on Lake Ohrid DEEP site age-depth model (Wagner et al., 2019). Of these tephra layers, OH-DP-0624 was confidently attributed to TF-17 (Giaccio et al., 2017a), which is $^{40}Ar/^{39}Ar$ dated at 158.8 ± 3.0 ka (this study).

In Greece, the peat sequence of Tenaghi Philippon (Fig. 1a) is reported to span the last 1.3 Myr, as far back as the MIS 12 time period (Vakhrameeva et al., 2018; Wulf et al., 2018), but only the cryptotephra record for the last ~460 kyr has been investigated. Vakhrameeva et al. (2019), reported four tephra layers (i.e., TP05-50.05, TP05-50.45, TP05-50.55, and TP05-50.75) the palynological modelled age of which is constrained between 235 and 240 ka. However, these four tephra layers all have a rhyolitic composition of Aegean Arc volcanoes, which is not observed in any of the Fucino tephra presented in this study, thus ruling out any possible correlation candidate from this sequence. Finally, in the Ionian Sea (Fig. 1a), cryptotephra investigations from ODP Site 964 (Vakhrameeva et al., 2021) allowed land-to-sea correlation for the last 800 kyr. Three visible tephra layers, with an orbitally tuned age of ~168 ka (964A-2H-3-78) and ~238 ka (964A-2H-5-59a and 964A-2H-5-59b), were tentatively correlated with tephra from the above-mentioned Lake Ohrid and San Gregorio Magno successions. Of these, tephra layers 964A-2H-3-78 and 964A-2H-5-59a both have a Pantellerite-like composition (Vakhrameeva et al., 2021) which is not observed among the Fucino tephra and can thus be confidently diregarded as potential correlatives. Instead, tephra layer 964A-2H-5-59b has a Campanian like composition that can be tentatively correlated to one of the Fucino tephra. All the other cryptotephras have an orbital age older than 300 ka (Vakhrameeva et al., 2021) and can thus be disregarded as well.

To summarize, potential F4-F5 tephra counterparts could be hosted at San Gregorio Magno, PRAD 1-2, DED-87-08, Lake Ohrid, and ODP Site 964 successions.

5.3. Individual tephra correlation

5.3.1. Correlation of Fucino tephra found in F4-F5 and F1-F3 cores

Tephra layers TF-19, TF-20, TF-21, and TF-22 from the F4-F5 core can be linked to the equivalent tephra from the 190 kyr-long record of the F1-F3 core (Giaccio et al., 2017a), which were attributed to a Latium-undefined source (TF-18/TF-19, TF-20, and TF-22) and Ischia volcano (TF-

21). The latter was also tentatively correlated by Giaccio et al. (2017a) to the marine tephra layers C-52 or C-54 from the Tyrrhenian Sea (Paterne et al., 2008). Direct comparison between the F1-F3 and F4-F5 tephra show consistent geochemical data between the two sets of tephra, corroborating their correlation (Figs. 8, 9, 10).

5.3.2. F4-F5 tephra correlation

5.3.2.1. Tephra from the Vulsini-Latera Volcanic Complex

TF-22 - Onano. This Vulsini tephra (Fig. 4b-III) has a variable geochemical composition, with a silica content ranging from 52 to 61 wt.%, alkali totals between 8-15 wt.%, and alkali ratios (i.e., K_2O/Na_2O) of 1.31-3.94. In the TAS diagram (Fig. 4a) it occupies various compositional fields and can be classified as a potassic tephriphonolite, phonolite, and latite. Sr and Nd isotope ranges indicate a Latium origin (Fig. 6a) as well, corroborating this attribution. Direct comparison with LVC proximal pyroclasts shows a good geochemical matching with Onano unit (Fig. 8a; Palladino and Simei, 2005), which shows similar major and minor element contents. TF-22 is here $^{40}Ar/^{39}Ar$ dated at 194.5 ± 2.0 ka, providing a likely age for the Onano unit. In proximal settings, the Onano deposits are stratigraphically located below the Pitigliano unit (e.g., Nappi et al., 1991; Palladino and Simei, 2005; Palladino et al., 2010), here $^{40}Ar/^{39}Ar$ dated at 177.7 ± 0.4 ka (Fig. 7), thus consistent with the age here determined for TF-22/Onano.

Geochemical comparison of the tephra PRAD-3586 from the Adriatic Sea core PRAD 1-2 (Fig. 1a) with TF-22/Onano shows a good geochemical match (Fig. 8a). This PRAD 1-2 layer was originally correlated with V-2/Sutri Formation (Bourne et al., 2015) dated at 151 ± 3 ka (Laurenzi and Villa, 1987). However, this correlation is stratigraphically and geochronologically inconsistent with the correlation of the younger PRAD-3225 with TF-17/Taurano Ignimbrite dated at 158.3 ± 3.0 ka proposed by Giaccio et al. (2017a), who also correlates the Vico-C/Sutri eruption to the overlying TF-15. Therefore, the correlation of PRAD-3586 with TF-22/Onano appears strongly supported by geochemical data and in agreement with tephrostratigraphical evidence, which places it below PRAD-3225, i.e., the equivalent tephra of TF-17/Taurano Ignimbrite.

In the Tyrrhenian Sea core DED-87-08 (Fig. 1a), Paterne et al. (2008) reported the occurrence of five tephra layers with Roman- and/or Campanian-like composition, with either a High or Low Alkali Ratio (HAR and LAR respectively), with an age comprised between ~205-183 ka. Of these, C-56 occurs just after the end of MIS 7 (~196 ka in Paterne et al., 2008), with an estimated age of 196.4 ka, which is just the same as for TF-22 (194.5 ± 2.0 ka). Unfortunately, Paterne et al. (2008) provided only the mean glass composition for their tephra, preventing us from any detailed correlation.

TF-31 - Grotte di Castro. This tephra occurs in the middle of the period of increasing Ca content correlated to the MIS 7 period (Giaccio et al., 2019; Fig. 3), a climatostratigraphic position that allows to estimate its age at 219.5 ± 1.1 ka (Table 4). This agrees with its stratigraphic position between TF-27 and TF-32, here $^{40}Ar/^{39}Ar$ dated at 205.1 ± 1.4 ka and 224.9 ± 1.0 ka respectively (Fig. 7).

TF-31 also displays a very heterogeneous composition, ranging from tephrites to phonolites-trachytes (Fig. 4a). In particular, this tephra displays a bimodal composition with less evolved tephritic-phonotephritic-tephriphonolitic population and a more evolved phonolitic-trachytic component. It is attributed to the Vulsini volcano based on the CaO/FeO vs Cl diagram (Fig. 4b-III) used for the most evolved composition (i.e., > 52 wt.% SiO_2). Among the LVC proximal pyroclastic units, the Grotte di Castro (GdC) eruption (Colucci et al., 2013) similarly consists of two differently evolved compositions, a tephritic-phonotephritic one and a more evolved phonolitic-trachytic one (Fig. 4a). Comparison between TF-31 and GdC (Fig. 8b) shows a good geochemical match, especially for the more evolved phonolitic-trachytic component. In particular, comparison with literature EMP data from Palladino et al. (2016) shows a fine match with both TF-32 and proximal GdC, although some discrepancies in the alkali content (Fig. 8b) that we ascribe to the high (up to 6 wt.%) Loss On Ignition (L.O.I) measured by these authors. It appears that the proximal GdC deposits analysed here lack the tephriphonolitic component shown by TF-31 and reported in the literature (Palladino et al., 2016), which we attribute to the incompletness of the sampling of the proximal GdC deposits rather than a more complete representation of the geochemical variability of this unit at Fucino Basin.

In terms of stratigraphic and geochronological constraints, GdC is interstatified between the Sovana and Onano eruptions (Palladino et al., 2010; Colucci et al., 2013), here dated at 224.7 ± 0.8 ka and

194.4 ± 2.0 ka, respectively, and thus is in agreement with the climatostratigraphic position of TF-31 and the chronological range of 205.1 ± 1.4 ka to 224.9 ± 1.0 ka available for TF-31.

TF-32 - Sorano. This tephra is immediately below TF-31/GdC and has thus a similar estimated, climatostratigraphic- (Fig. 3) and radioisotopic-based age of ~220 ka. This is confirmed by the highly precise $^{40}Ar/^{39}Ar$ age of 224.9 ± 1.0 ka obtained for TF-32 (Fig. 7). It is characterised by a peculiar composition spanning the tephriphonolite-phonolite-trachyte-latite fields of the TAS diagram (Fig. 4a). Its attribution to the Vulsini volcano (Fig. 4b-III) is also supported by trace element data showing good overlapping with LVC units (Fig. 5). The isotopic composition (Fig. 6) indicates a Latium origin for this tephra as well, with Sr (0.710358-0.710552) and Nd (0.512118) similar to those of the TF-22/Onano tephra (0.710375-0.710379 and 0.512116). By considering the above stratigraphic, geochronological, and geochemical constraints, the Sorano unit, which in proximal settings underlies GdC (e.g., Palladino et al., 2010; Valentine et al., 2019), arises as the best candidate for a correlation with TF-32. However, both major and tarce element composition of the Sorano unit shows differences with TF-32 (Fig. 8c). Furthermore, the previous age of 194 ± 5 (Turbeville, 1992) determined for the Sorano unit sensibly differs from the one of 224.9 ± 1.0 ka calculated for TF-32. Nevertheless, both major and trace element composition of TF-32 is perfectly in line with that of the other LVC proximal units (Figs. 5, 8c), thus allowing us to confidently attribute TF-32 to the LVC. Considering the proposed correlation of the overlying TF-31 with the Grotte di Castro unit, a tentative correlation of TF-32 with Sorano is here proposed. However, new direct $^{40}Ar/^{39}Ar$ dating of the proximal Sorano unit is needed to confirm/reject our tentative correlation of TF-32 with the Sorano unit. Alternatively, TF-32 might correlate to one of the minor events occurred at LVC in the post-Sovana, pre-Sorano time interval (e.g., ignimbrite “c”; Sparks, 1975).

TF-33 - Sovana. TF-33 is positioned in the middle of the MIS 7 period (Fig. 3) and less than one meter below TF-32 and should be thus slightly older than 224.9 ± 1.0 ka. This phonolitic tephra is characterised by a homogeneous composition, with SiO_2 ranging between 57 and 61 wt.% and alkali totals of 12-15 wt.% (Fig. 4a), falling at the boundary with the trachyte field. Based on the CaO/FeO vs Cl diagram (Fig. 4b-III), TF-33 can be attributed to the Vulsini volcano. The LVC unit of Sovana, which in proximal settings underlies the Sorano unit (Palladino and Taddeucci, 1998; Palladino et

al., 2010, 2014; Valentine et al., 2019) and here tentatively correlated to the overlying TF-32, represents the most likely candidate for a correlation with TF-33. Indeed, the comparison with the Sovana unit shows a good geochemical match with TF-33 (Fig. 8b). Here the Sovana unit is $^{40}Ar/^{39}Ar$ dated at 226.4 ± 0.7 ka (Fig. 7), thus slightly older than (and consistent with) the immediately overlying TF-32, here $^{40}Ar/^{39}Ar$ dated at 224.9 ± 1.0 ka (Fig. 7). In proximal settings, the Sovana unit was dated at 215 ± 6.0 ka (Turbeville, 1992), highlithing the possibility that the previous age determinations for some of the Latera units might have been substantially underestimated.

TF-35b - Farnese. This tephra occurs at the end of the first peak of the Ca content, likely corresponding to the MIS 7e sub-stage (Fig. 3), astronomically dated between ~240 and ~230 ka (Lisiecki and Raymo, 2005). For this tephra, due to its crypto-nature, we managed to acquire only 3 analytical points, which are insufficient for expressing the full geochemical variability of the tephra. Nevertheless, the new glass-WDS data allows its attribution to a LVC unit, based on the CaO/FeO vs Cl classification diagram (Fig. 4b-III). Among the remaining investigated LVC units, the only one with a phonolitic composition is Farnese (Fig. 4a; Palladino and Agosta, 1997), to which TF-35b is here tentatively correlated. Comparison with TF-35b show a good, although poorly constrained, geochemical match (Fig. 8d), supporting this correlation. Here the Farnese unit is $^{40}Ar/^{39}Ar$ dated at 235.6 ± 0.6 ka, roughly in agreement within its uncertainties with the age of 242 ± 8 ka previously determined for this unit (Turbeville, 1992). The correlation allows us to transfer the new highly precise $^{40}Ar/^{39}Ar$ age of Farnese to the Fucino succession, thus providing a further age constraint for the interval here investigated. Alternatively, TF-35b might record the deposition from a LVC eruption currently not described in the literature.

TF-43 - Canino. This tephra, the lowermost and oldest investigated in this study, is found towards the end of an interval of low Ca content (Fig. 3) interpreted as the expression of the MIS 8 glacial period (Giaccio et al., 2019) and thus has an estimated climatostratigraphic age of ~250 ka. It is characterised by a quite homogeneous (mainly) trachytic composition, with 59-64 wt.% SiO_2 and 11-14 wt.% alkali totals (Fig. 4a). According to the CaO/FeO vs Cl diagram, this tephra can be attributed to the LVC as well (Fig. 4b-III). Among the LVC units stratigraphically and chronologically compatible with TF-43, both the Stenzano (Taddeucci and Palladino, 2002) and Canino (Palladino and Agosta,

1997; Palladino et al., 2010) units are characterised by a trachytic composition (Fig. 4a). Comparison with these units reveal a good and convincing geochemical match between Canino Fall-C sub-unit and TF-43 (Fig. 8d). Here Canino Fall-C has been dated at 253.1 ± 0.8 ka, virtually indistinguishable from Canino Fall-B (253.8 ± 0.8 ka; Fig. 7), and in agreement with both the climatostratigraphic position of TF-43 and the previously determined $^{40}Ar/^{39}Ar$ age of 253 ± 6.0 ka for this unit (Turbeville, 1992). The correlation of Canino Fall C with TF-43 allows us to transfer its $^{40}Ar/^{39}Ar$ age to the Fucino succession, providing a lower age control point for the interval here investigated.

5.3.2.2. Tephra from Sabatini

TF-19 - Trevignano Romano TR-CR-2. This Fucino tephra occurs in the early part of the period characterised by low Ca content, correlated to the MIS 6 glacial (Fig. 3), and is bracketed between the tephra TF-17 and TF-22, which are respectively $^{40}Ar/^{39}Ar$ dated at 158.8 ± 3.0 ka (Giaccio et al., 2017a) and 194.4 ± 2.0 ka (this study; Fig. 7). This chronostratigraphic position agrees with the modelled age of 181.7 ± 2.4 calculated for TF-19 (Table 4). It also stratigraphically matches the couplet of the geochemically indistingushiable tephra TF-18+TF-19 found in F1-F3 core that was ascribed to an undefined Latium origin (Giaccio et al., 2017a). Here, we correlate TF-19 (and TF-18 of F1-F3 core, not found in F4-F5 core) to the TR-CR-2 unit from Trevignano Romano (Tables 1, 3; Fig. 1), which displays similar major and trace elements composition (Fig. 9a). In proximal settings, TR-CR-2 is stratigraphically located below the deposits of the S. Bernardino Maar (Sottili et al., 2010), which have an inferred age of ≤ 172 ka, consistent with the stratigraphic position of TF-19.

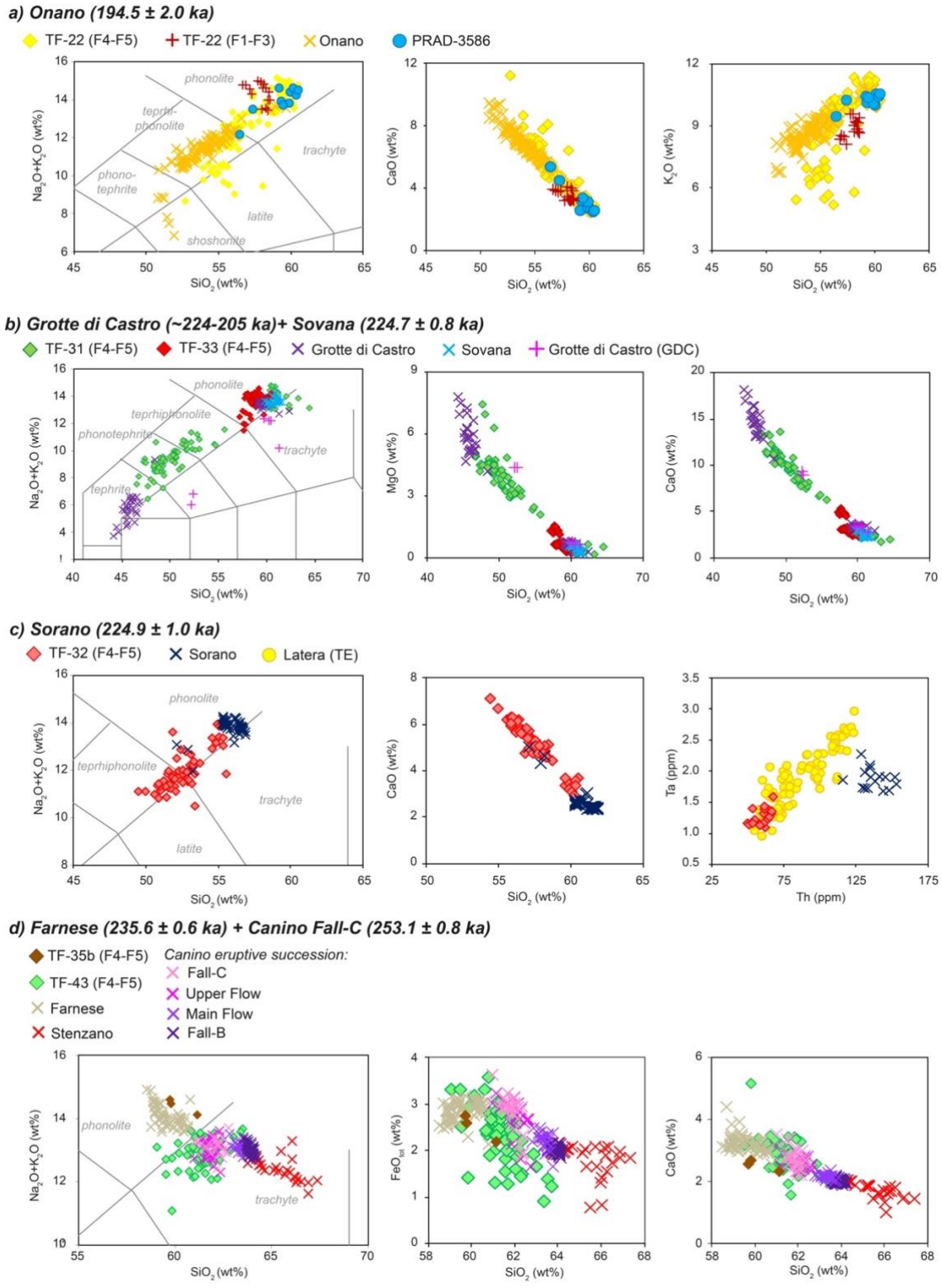

Figure 8. *Total alkali vs silica* (TAS) classification diagram (Le Maitre et al., 2002) and representative major (ME) and trace element (TE) bi-plots for TF-22, TF-31, TF-32, TF-33, TF-35b, and TF-43 from the F4-F5 record compared with proximal Latera Volcanic Complex (LVC) units. Data source: WDS glass composition of TF-22, TF-31, TF-32, TF-33, TF-35b, and TF-

43 (F4-F5), Onano, Grotte di Castro, Sorano, Sovana, Farnese, and Canino (Fall-C, Upper Flow, Main Flow and Fall-B): this study; TF-22 (F1-F3): Giaccio et al. (2017a); PRAD-3586: Bourne et al. (2015); Literature Grotte di castro (GDC): Palladino et al. (2016). Trace element glass composition of TF-32, Sorano and proximal LVC units: this study; $^{40}Ar/^{39}Ar$ age of TF-22, TF-32, Sovana, Farnese, and Fall-C: this study.

TF-20 - Trevignano Romano TR-CR-1. This tephra occurs just ~20 cm below TF-19 (Fig. 3, Table 2) and displays a similar dominantly phonolitic composition (Fig. 4a), with more variable SiO_2 (55-61 wt.%) and Na_2O+K_2O (11-16 wt.%) concentrations. TF-20 was already recognised in core F1-F3 and ascribed to an unspecified Latium volcanic activity (Giaccio et al., 2017a). Based on the similar major and trace element composition, here we correlate TF-20 to the TR-CR-1 unit, which occurs just below TR-CR-2/TF-18+TF-19, (Fig. 9b). Also in this case, the stratigraphic position of TF-20 is perfectly compatible with that of TR-CR-1, which in proximal settings underlies TR-CR-2, in turn overlain by products of the S. Bernardino Maar (≤172 ka; Sottili et al., 2010), and its age can be thus constrained between 158.8 ± 3.0 ka (TF-17; Giaccio et al., 2017a) and 194.4 ± 2.0 ka (TF-22; this study). Indeed, the modelled age calculated for TF-20 is 183.0 ± 2.3 ka (Table 4).

TF-27 - Vigna di Valle. This tephra occurs in a stadial phase of the late MIS 7, likely corresponding to the MIS 7d sub-stage dated at ~205 ka in the LR04 Benthic Stack (Fig. 3), and just below the Iceland Basin geomagnetic excursion (Giaccio et al., 2019). It is characterised by a heterogeneous composition, mainly phonolitic, and in the TAS diagram (Fig. 4a) can be classified as a tephriphonolite-phonolite-latite-trachyte.Comparison with the proximal SVD pyroclastic units shows a convincing geochemical match with the Vigna di Valle unit (Fig. 9c) dated to 194.0 ± 7.0 ka (Sottili et al., 2010), which is replaced by the more precise $^{40}Ar/^{39}Ar$ age of 205.1 ± 1.4 ka obtained here for TF-27 (Fig. 7), which thus substantially reduce the chronological uncertainty for the Vigna di Valle eruption.

TF-28 - Pizzo Prato(?). This tephra occurs in the second half of MIS 7, at the end of a period of high Ca contet likely corresponding to the end of MIS 7c, and thus with an estimated age dated at ~210 ka (Fig. 3). It is characterised by a dominant phonolitic composition (Fig. 4a), with a SiO_2 content of 55-63 wt.% and alkali totals of ~11-16 wt.%. According to the CaO/FeO vs Cl classification diagram, TF-28 plots between the Vulsini+Vico and Sabatini fields, making its attribution to one of these three

potential volcanic sources challenging. However, the newly acquired glass-WDS data from proximal Pizzo Prato unit would perfectly overlap with TF-28, allowing it to be ascribed to the Sabatini volcano (Fig. 4b-II) and to Pizzo Prato unit in particular (Fig. 9d). However, the age of 251 ± 16 ka avialable for the Pizzo Prato unit (Sottili et al., 2010), although associated with a large error, is not compatible with the estimated age of TF-28 (208.8 ± 1.3 ka; Table 4) which occurs less than 1 m below TF-27/Vigna di Valle, dated at 205.1 ± 1.4 ka. This large age discrepancy would thus suggest a correlation with another, currently undocumented, Sabatini unit younger than Pizzo Prato. We thus conservatively propose only a speculative correlation of TF-28 as Pizzo Prato, pending future investigations and new $^{40}Ar/^{39}Ar$ dating of the Pizzo Prato unit.

TF-30 - Sabatini undefined. This tephra is stratigraphically close to the above described TF-28 and thus shares a similar climatostratigraphc position and a modelled age (Fig. 3) of 211.2 ± 1.3 (Table 4). However, its phonolitic composition (Fig. 4a) does not match that of the Pizzo Prato unit (Fig. 9d) or those of other geochronologically compatible known Sabatini units (e.g., Sottili et al., 2019; Marra et al., 2020). Therefore, this tephra is here ascribed to an undefined Sabatini activity.

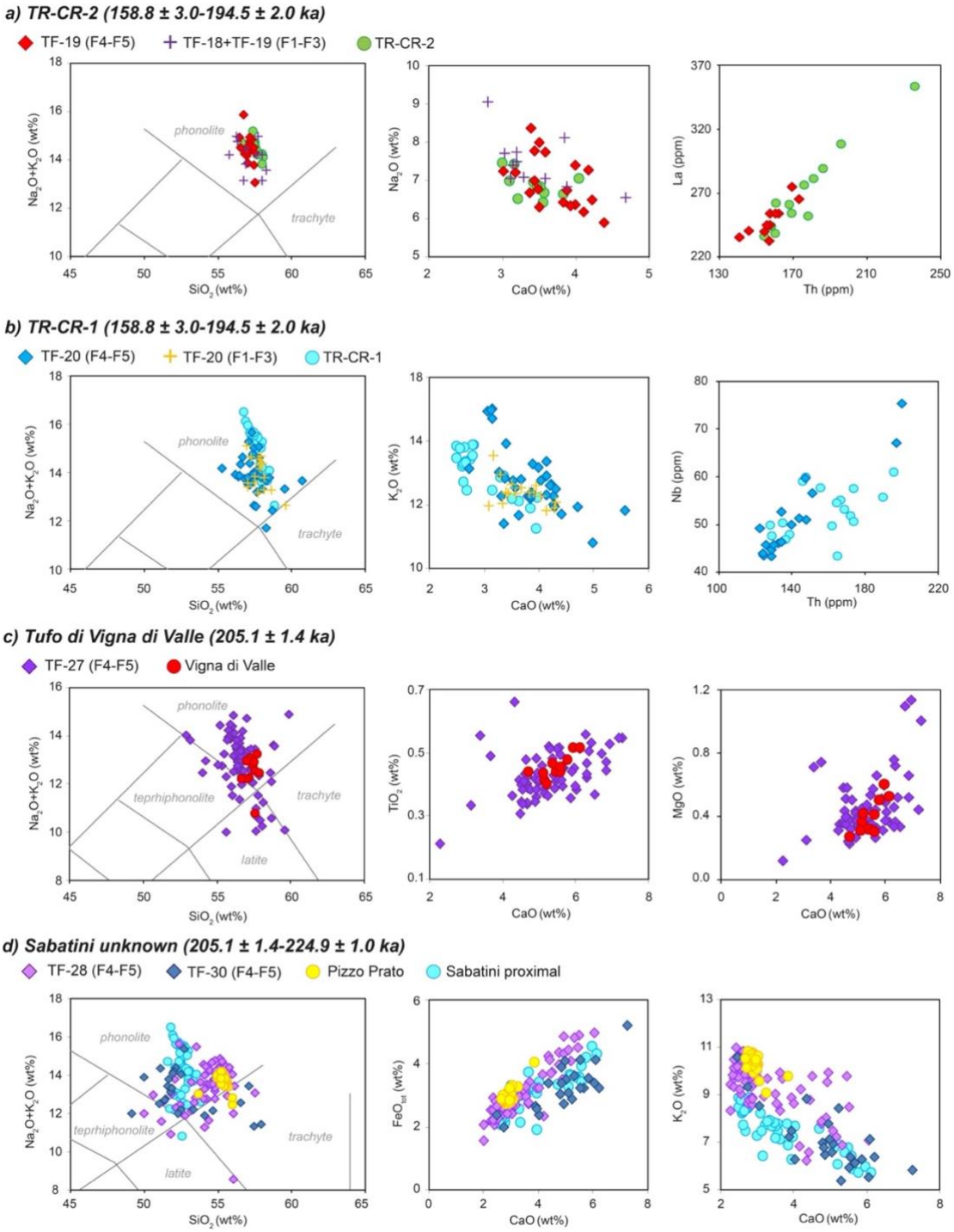

Figure 9. *Total alkali vs silica* (TAS) classification diagram (Le Maitre et al., 2002) and representative major (ME) and trace element (TE) bi-plots for TF-19, TF-20, TF-27, TF-28, and TF-30 from the F4-F5 record compared with proximal Sabatini Volcanic District (SVD) units. Data source: WDS glass composition of TF-19, TF-20, TF-27, TF-28, TF-30 (F4-F5), TR-CR-2, TR-CR-1, Vigna di Valle, and Pizzo Prato: this study; TF-18, TF-19, and TF-20 (F1-F3): Giaccio et al. (2017a); trace element glass composition of TF-19, TF-20 (F4-F5), TR-CR-2, and TR-CR-1: this study; $^{40}Ar/^{39}Ar$ age of TF-27: this study.

5.3.2.3. Tephra from Vico

TF-24 and TF-25 - Vico Unknown. These two closely related tephra layers are climatostratigraphically associated to the early stage of MIS 6 (Fig. 3). They are characterised by a similar and homogeneous phonolitic composition, with SiO_2 ranging between 56-60 wt.% (TF-24) and 57-60 wt.% (TF-25), and alkali totals of 12-15 wt.% (both). According to the CaO/FeO vs Cl discriminating diagram, these two tephras can be either attributed to Vulsini or Vico (Fig. 4b-III). However, the LVC units here investigated show consistent Cl contents, measured in all of the three laboratories (see Table 1), generally < 0.10 wt.%, while TF-24 and TF-25 have a mean Cl content of 0.17 wt.% (± 0.04 wt.% [2 s.d.]) and 0.16 wt.% (0.03 wt.% [2 s.d.]) respectively, suggesting an origin from Vico volcano rather than Latera. Furthermore, trace element biplots highlight a marked difference between these two tephras with respect to the LVC units (Fig. 5), with higher Th contents and thus lower ratios of Th to HFSE and LREE, which are compatible with trace element contents of Vico Period I units (Fig. 10a). TF-24 and TF-25 are located between TF-22 and TF-27, respectively dated at 194.4 ± 2.0 ka and 205.1 ± 1.4 ka, allocating these two tephras between the caldera-forming eruptions of Vico Ignimbrite A (or Farine Formation, ~250 ka; Sollevanti, 1983) and Ignimbrite B (or Ronciglione Formation, 157 ± 3 ka; Laurenzi and Villa, 1987). Indeed, the modelled ages calculated for TF-24 and TF-25 are 196.4 ± 1.9 ka and 197.1 ± 1.9 ka, respectively (Table 4). Comparison with the newly acquired glass-WDS composition of Vico-A/Farine Formation unit (Fig. 10a) shows geochemical similarities with the two Fucino tephra (i.e., similar CaO/FeO ratio), which further supports an origin from Vico volcano. However, no known eruption is reported between the Vico-A and Vico-B Ignimbrites (e.g., Perini et al., 2004), preventing us from any tentative correlation and suggesting that the two Fucino tephra document explosive activity currently undocumented in proximal settings.

On the other hand, we found a good geochemical match between TF-24/TF-25 tephras and the Adriatic tephra PRAD-3666 (Fig. 10a). The layer PRAD-3666 was originally attributed to an undefined Latium volcano (Bourne et al., 2015) and was geochronologically poorly constrained between 181.077-156.346 ka. However, as already discussed above in this paper (see section

5.3.2.1.) and in previous works (Giaccio et al., 2017a) the age model for the Middle Pleistocene section of PRAD 1-2 is biased by erroneous correlation, and thus PRAD-3666 is here poposed as correlative tephra of TF-24 and/or TF-25 tephra. This is also consistent with the above proposed correlation of PRAD-3586 with TF-22/Onano (see section 5.3.2.1).

5.3.2.4. Latium-undefined tephra

TF-29 and TF-37. TF-29, occurring in the late part of the MIS 7 period (Fig. 3), is characterised by a latitic-trachytic composition, with SiO_2 ranging from 55 to 65 wt.% and alkali totals of 9-12 wt.%, while TF-37 has a polymodal composition (Fig. 4a), ranging from phonotephrites to phonolite-trachytes, with increasing alkali totals at increasing SiO_2. The limited number of analytical points obtained for these two tephra layers (9 and 11 respectively) make their attribution to one of the peri-Tyrrhenian volcanic sources more challenging. In the CaO/FeO vs Cl classification diagram (Fig. 4b-II) they plot at the Sabatini and Vulsini+Vico boundary. The low Cl content of TF-29 (0.00-0.14 wt.%, mean of 0.08 wt.%) and TF-37 (0.05-0.37 wt.%, mean of 0.11 wt.%) point out a Latium origin, although the specific source cannot be confidently defined.

5.3.2.5. Tephra from Roccamonfina

TF-35. This tephra is characterised by a fairly homogeneous trachytic composition, with 61-64 wt.% SiO_2, 11-13 wt.% alkali sum, and mean K_2O/Na_2O ratio of 1.63 ± 0.25 (2 s.d.). The relatively high Cl content (up to 0.36 wt.%) and CaO/FeO ratio of 0.74-0.88, suggest a Roccamonfina origin for this tephra. It is located between TF-33/Sovana (224.7 ± 0.8 ka) and TF-35b/Farnese (235.6 ± 0.6 ka), providing a roughly estimated age of 229.3 ± 0.7 ka (Table 4). In proximal settings, deposits of the caldera-forming eruptions of the Upper White Trachytic Tuff (UWTT, Subunit G of Giannetti and De Casa, 2000) and Yellow Trachytic Tuff (YTT) were respectively dated at 234.0 ± 9.0 ka (recalculated age from Giannetti and De Casa, 2000) and 231 ± 6.0 ka (recalculated age from Giannetti, 1996), which are compatible with that estimated for TF-35. Rouchon et al. (2008) provided whole-rock composition of two WTT samples (i.e., RMF96 and RMF11), both trachytic in composition. However, it is not specified by the authors to which sub-units the two samples refer,

preventing us from a detailed correlation with these units, also considering that whole-rock compositions are not directly comparable with glass-WDS data due to the possible crystal contamination. Nevertheless, we suggest that TF-35 might represent one of the two above-mentioned eruptions or an undocumented episode at the end of the UWTT-YTT eruptive period (Fig. 10b). Thus, EPMA glass data for these proximal units is in order for reliable proximal-distal correlations.

At Lake Ohrid (Fig. 1a), Leicher et al. (2019) reported the occurrence of some tephra layers (i.e., OH-DP-1053.5, OH-DP-1053.8, and OH-DP-1055) with mixed Campanian and Roccamonfina-like signature. However, the chronostratigraphic position of these Ohrid tephras at ~240-241 ka rules out any possible correlation with TF-35.

5.3.2.6. Tephra from Ischia

TF-21 and TF-23. These two tephra layers are climatostratiphically placed in the early MIS 6 glacial period, respectively above and below TF-22, here $^{40}Ar/^{39}Ar$ dated at 194.4 ± 2.0 ka. The modelled ages obtained for TF-21 and TF-23 are 187.6 ± 2.2 ka and 195.2 2.0 ka, respectively (Fig. 3; Table 4). Both tephra layers are characterised by a homogeneous trachytic composition (Fig. 4a), with SiO_2 ranging between 62-64 wt.% (TF-21) and 62-65 wt.% (TF-23) and identical alkali totals (~13-15 wt.%). In Giaccio et al. (2017a), TF-21 was tentatively correlated to either the Ischia C-52 or C-54 tephra layers from Tyrrhenian marine core KET 80-04/DED-87-08 of Paterne et al. (2008); however, the lack of individual glass-WDS analyses for these marine tephra (or other KET 80-04/DED-87-08 tephra) still leave a robust correlation open. Nevertheless, the stratigraphic order of Fucino would suggest a correlation of TF-21 to C-52 and of TF-23 to C-54 respectively (Fig. 10c).

5.3.2.7. Tephra from Campi Flegrei

TF-21a and TF-26. Both TF-21a and TF-26 are MIS 6 tephra, precisely positioned in the early stage and at the very onset of this glacial period, respectively, and thus have an estimated age of ~190-200 ka (Fig. 3). For these two tephra layers, we calculated an estimated age of 189.4 ± 2.2 ka (TF-21a) and 198.6 ± 1.8 ka (TF-26). They are characterised by a phonolitic-trachytic composition

(Fig. 4a), with a similar increase of the alkali content at increasing silica, which ranges between 58-62 wt.% (TF-21a) and 56-63 wt.% (TF-26). The relatively high Cl content (TF-21a = 0.23-0.63 wt.%; TF-26 = 0.19-0.65 wt.%) clearly points to a Campanian origin for both tephras, and according to the CaO/FeO vs Cl diagram (Fig. 4b-l) they could be attributed to the Campi Flegrei. The isotopic composition of TF-26 also supports a Campanian origin, based on the low $^{87}Sr/^{86}Sr$ (0.706233-0.706566; Fig. 6a) and simultaneously high $^{143}Nd/^{144}Nd$ ratio (i.e., 0.512551), which are a feature of the Campanian products (Fig. 6b). According to the literature, several Middle Pleistocene Ignimbrites were emplaced in the Campanian Plain (e.g., De Vivo et al., 2001; Rolandi et al., 2003; Belkin et al., 2016), which are ascribed to the so-called Campanian Volcanic Zone (CVZ; Rolandi et al., 2003), dating as far back as 290 ka (i.e., Seiano Ignimbrite; Rolandi et al., 2003). Specifically, in the time interval of 205-183 ka, thus chronologically compatible with TF-21a and TF-26 (Fig. 3), a series of pyroclastic deposits. i.e., the Taurano Layered Tuff Series (De Vivo et al., 2001; Belkin et al., 2016) is documented in proximal settings as well. Unfortunately, no glass-WDS data is available, preventing currently from any tentative correlation.

In the Mediterranean area, Campanian-like tephra layers are reported in several repositories. At Lake Ohrid (Fig. 1a), at least seven tephra with Campanian-Roccamonfina like composition are recorded in the time interval of 241-160 ka (Leicher et al., 2019, 2021). Of these, Ohrid tephra OH-DP-0725 (Leicher et al., 2021; new glass-WDS data presented also in this study) shows a good geochemical match with both TF-21a and TF-26 based on major element composition (Fig. 10d). However, OH-DP-0725 has a modelled age of 174.4 ± 5.2 ka (Leicher et al., 2021), which is geochronologically incompatible with both TF-21a and TF-26. A good geochemical match is also observed between TF-21a and the S7 tephra from San Gregorio Magno Basin (Munno and Petrosino, 2007), which occurs just below tephra S8, which is in turn correlated to OH-DP-0710 (Leicher et al., 2019) dated to 172.3 ± 5.6 ka (Leicher et al., 2021). TF-21a can be thus tentatively correlated with S7, although the age of TF-21a should be slightly older than the modelled age of S8/OH-DP-0710. At DED-87-08 other chronologically compatible Campania-like tephra, such as C-53 and C-55, have been reported by Paterne et al. (2008). Again, the lack of individual glass analyses prevents us from any tentative correlation. Finally, at ODP Site 964 (Vakhrameeva et al., 2021), tephra layer 964A-2H-5-59b has a

Campanian-like composition, although both geochemical (major and minor elements) and geochronological (orbital age of ~238 ka) information rule out a correlation with any of the two Fucino tephras.

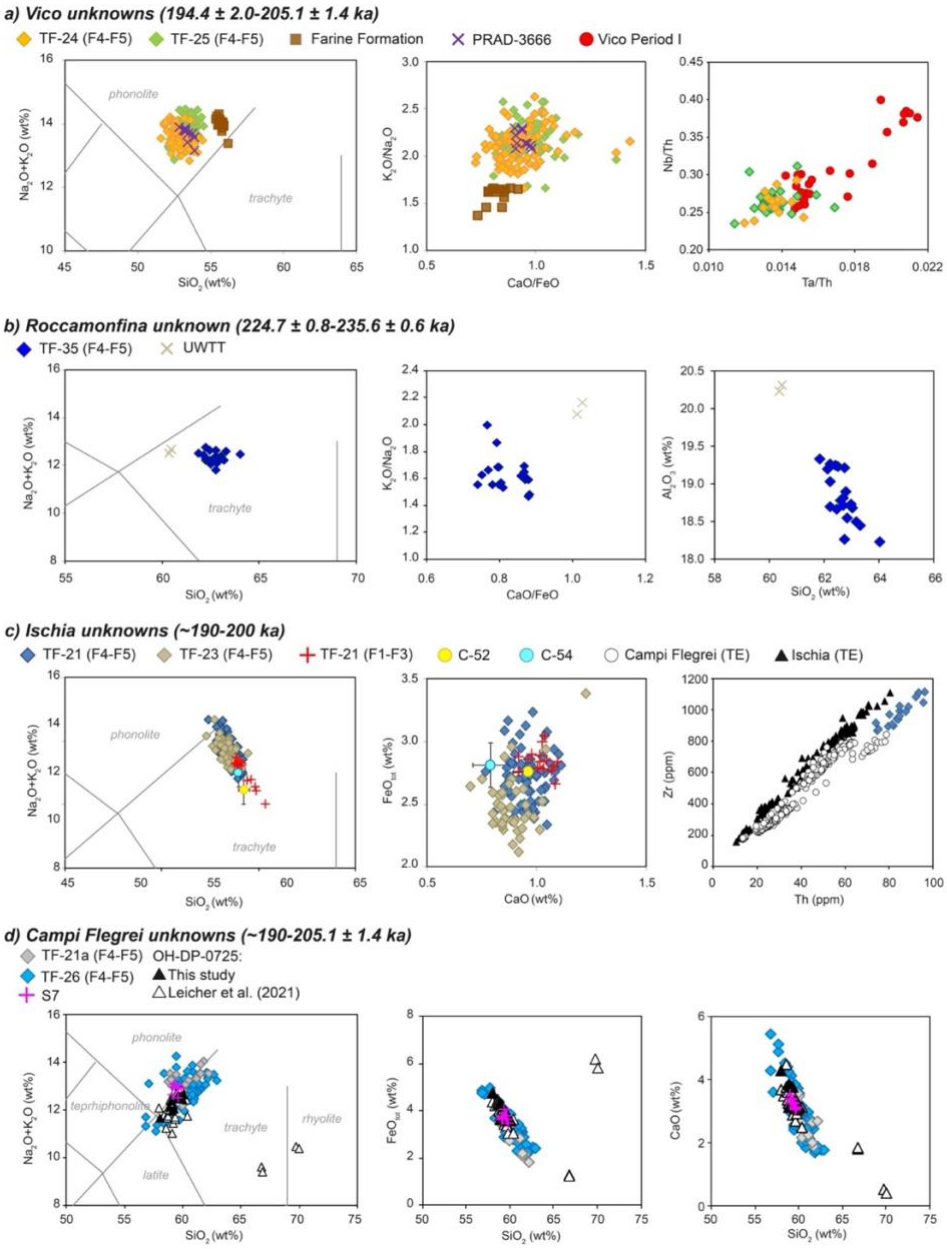

Figure 10. *Total alkali vs silica* (TAS) classification diagram (Le Maitre et al., 2002) and representative major (ME) and trace element (TE) bi-plots for TF-21, TF-21a, TF-23, TF-24, TF-25, TF-26, and TF-35 from the F4-F5 record compared with proximal Vico units (i.e., Farine Formation and Vico Period I), OH-DP-0725 and tephra layers from the literature. Data source: WDS glass composition of TF-21, TF-21a, TF-23, TF-24, TF-25, TF-26, TF-35 (F4-F5), Farine Formation and OH-DP-0725:

this study; TF-21 (F1-F3): Giaccio et al. (2017a); PRAD-3666: Bourne et al. (2015); EDS composition of S7: Munno and Petrosino (2007); WR composition of C-52 and C-54: Paterne et al. (2008); WR composition of UWTT: Rouchon et al. (2008); trace element glass composition of TF-21, TF-24 and TF-25 (F4-F5): this study; trace element glass composition of Vico Period I: Monaco et al. (2021); trace element glass composition of proximal Ischia and Campi Flegrei pyroclastic units: Tomlinson et al. (2012, 2015).

5.4. Peri-Tyrrhenian explosive activity during MIS 6-7 revaluated in light of the Fucino record

In the previous section, we presented geochemical-based correlations between the Fucino F4-F5 tephra with the proximal pyroclastic units from peri-Tyrrhenian Quaternary volcanoes and other tephra layers in distal repositories across the central Mediterranean. A summary of all the proposed correlations is reported in Table 4, while a preliminary age-depth model for the 250-170 ka time interval, based on a simple linear interpolation, is shown in Figure 11. These correlations provide new tie points between the mentioned tephra repositories, as well as new and more precise age constraints based on the presented $^{40}Ar/^{39}Ar$ ages. In particular, in this study we showed two new correlations between the Adriatic Sea PRAD 1-2 and the F4-F5 Fucino tephras (i.e., TF-22=PRAD-3586 and TF-24/TF-25=PRAD-3666) that substantially improve the age model for the lowermost sequence of the PRAD 1-2 core. Specifically, TF-22=PRAD-3586 is here $^{40}Ar/^{39}Ar$ precisely dated at 194.5 ± 2.0 ka, while the modelled ages for TF-24/TF-25=PRAD-3666 is 196.4 ± 1.9-197.1 ± 1.9 ka (Table 4). We also presented a tentative correlation of tephra layer S7 from the San Gregorio Magno Basin succession (Munno and Petrosino, 2007; Petrosino et al., 2019) with the Campanian-like Fucino tephra TF-21a and TF-26, with a modelled age of 189.4 ± 2.2 ka and 198.6 ± 1.8 ka, respectively (Table 4). The former is also geochemically similar to the Ohrid tephra OH-DP-0725, for which here we have provided new glass-WDS analysis, and which has a modelled age of 174.4 ± 5.2 ka (Leicher et al., 2021). Thus, despite the good geochemical match, it is chronologically inconsistent with the age of TF-21a. Unfortunately, no tephra correlation has been determined between the Fucino paleolake sequence and the Tenaghi Philippon (Wulf et al., 2018; Vakhrameeva et al., 2018, 2019) or ODP Site 964 (Vakhrameeva et al., 2021). Currently, the MIS 6-7 tephrostratigraphy at Tenaghi Philippon has not yet been presented, thus, in the future, correlations might emerge between the two tephra repositories.

The F4-F5 sequence presented in this study also allows to better refine the peri-Tyrrhenian eruptive history in the time interval of 250-170 kyr. At Vulsini, the LVC emplaced several fall deposits, some of which (i.e., those belonging to the Canino eruption) are documented at Fucino and allowed to transfer the new high precise $^{40}Ar/^{39}Ar$ ages from the proximal pyroclastic units to the Fucino sequence. Conversely, the Fucino modelled ages provided new chronological constraints for the undated or poorly constrained Vulsini units, such as Grotte di Castro, which is here dated at 219.3 ± 1.5 ka (Table 4; Fig. 11). No previously undocumented LVC tephra has been recognized in the presented interval, although the two Latium-undefined tephra (i.e., TF-29 and TF-37) were not associated to a specific source yet and could be potentially attributed to the LVC after further investigation.

At Sabatini, proximal deposits discontinuously document explosive activity between the eruptions of Vigna di Valle and Pizzo Prato (e.g., Sottili et al., 2019). At Fucino, at least two tephra layers (TF-28 and TF-30) with Sabatini-like composition document explosive activity at ~210 ka (209.0 ± 2.0 ka and 211.0 ± 2.0 ka), which is not currently reported in the literature. The Fucino record also provides a new, more precise $^{40}Ar/^{39}Ar$ age of 205.1 ± 1.4 ka for the poorly dated Vigna di Valle unit, as well as modelled ages for the undated Trevignano Romano TR-CR-1 and TR-CR-2 at 183.0 ± 2.3 ka and 181.7 ± 2.4 ka (Table 4; Fig. 11).

At Vico volcano, a ~90 kyr quiescence interval is reported in the literature between the Vico Ignimbrite A (or Farine Formation, ca. ~250 ka; Sollevanti, 1983) and Ignimbrite B (or Ronciglione Formation, 157 ± 3 ka; Laurenzi and Villa, 1987). However, at Fucino, the two tephra layers TF-24 and TF-25, with a Vico-like geochemical composition, occur in a time interval of 205.1 ± 1.4 (TF-27/Vigna di Valle) and 194.5 ± 2.0 (TF-22/Onano) ka (Table 4; Fig. 11), thus documenting an intra-caldera activity that halves the supposed quiescence period from ~90 kyr to ~45 ka.

In the time interval here considered, only one tephra layer (i.e., TF-35) with a Roccamofina signature is documented. Its modelled age of 229.3 ± 0.7 ka (Table 4; Fig. 11) suggests a possible link with the Upper White Trachytic Tuff eruptive cycle (e.g., Giannetti and De Casa, 2000), but the lack of glass-WDS data in the literature prevented us from a definitive correlation.

At Ischia volcano, proximal deposits outcropping in the SE sector of the island are reported to date as back as > 150 ka (e.g., Poli et al., 1987; Sbrana et al., 2018). Here at Fucino, the two Ischia tephras TF-21 and TF-23, with a modelled age of 187.6 ± 2.2 ka and 195.2 ± 2.0 ka (Table 4; Fig. 11), testify, in agreement with previous tephra study (e.g., Paterne et al., 2008), that the volcanic Island has been active since the most recent Middle Pleistocene period at least.

At Campi Flegrei, field evidence of explosive activity preceding the Campanian Ignimbrite (39.85 ± 0.14 ka; Giaccio et al., 2017b) eruption is quite limited (e.g., Pappalardo et al., 1999; De Vivo et al., 2001; Rolandi et al., 2003; Di Vito et al., 2008; Belkin et al., 2016). However, recent investigations of proximal to medial-distal sections in the Campanian plain allowed the recognition of significant Campi Flegrei explosive activity between 92 and 109 ka, also linking it to widespread tephra, such as X-5, X-6 (Keller et al., 1978) and C-22 (Paterne et al., 1986), which act as relevant markers for the Mediteterranean MIS 5 successions (e.g., Wulf et al., 2012, 2018; Giaccio et al., 2012a; Regattieri et al., 2015; Leicher et al., 2016; Petrosino et al., 2016). At Fucino, two Campi Flegrei-like tephra, i.e., TF-21a and TF-26, document activity at this volcano at ~189-199 ka (Table 4; Fig. 11) and can potentially be correlated to tephra layers occurring at San Gregorio Magno and Lake Ohrid, linking the three sedimentary successions (Table 4; Fig. 11). Furthermore, TF-21a is chronologically consistent with the Moschiano Ignimbrite, dated at 188.0 ± 7.4 ka and attributed to the so-called Campanian Volcanic Zone (CVZ; Rolandi et al., 2003). However, the lack of glass data for this unit prevents us to support a possible correlation.

In conclusion, the MIS 6-8 tephra sequence from Fucino Basin presented here provides new evidence of explosive activity currently undocumented at Vico, Sabatini, and Ischia volcanoes, and confirms previous evidence of major Middle Pleistocene activity at Campi Flegrei Caldera as well. Our record also provides precise chronological constraints for several undated or poorly dated eruptions of the Middle Pleistocene peri-Tyrrhenian volcanoes.

Table 4. Summary of the proposed correlations of the F1-F3 (Giaccio et al., 2017a) and F4-F5 Fucino tephra with tephra layers from other repositories across central-southern Italy and the Mediterranean.

Fucino F1-F3/F4-F5	Direct $^{40}Ar/^{39}Ar$ age (ka)	Correlated $^{40}Ar/^{39}Ar$ age (ka)	Fucino modelled age (ka)	Volcano/Units	PRAD 1-2	Ohrid	San Gregorio Magno
TF-17	158.8±3.0[1]			Vico/Vico-B	PRAD-3225	OH-DP-0624	
TF-18			170.1±2.7	Latium/Unknown			
TF-19			181.7±2.4	Sabatini/TR-CR-2			
TF-20			183.0±2.3	Sabatini/TR-CR-1			
TF-21			187.6±2.2	Ischia/(C-52-C54)			
TF-21a			189.4±2.2	CF/Moschiano Imbrite? CF/Unknown		OH-DP-0725?	S-7
TF-22	194.5±2.0[2]			Vulsini/Onano	PRAD-3586		
TF-23			195.2±2.0	Ischia/Unknown			
TF-24/TF-25			196.4±1.9/ 197.2±1.9	Vico/Unknown	PRAD-3666		
TF-26			198.6±1.8	CF/Unknown			
TF-27	205.1±1.4[2]			Sabatini/Vigna di Valle			
TF-28			208.8±1.3	Sabatini/Pizzo Prato?			
TF-29			210.5±1.3	Latium/Unknown			
TF-30			211.2±1.3	Sabatini/Unknown			
TF-31			219.5±1.1	Vulsini/Grotte di Castro			
TF-32	224.9±1.0[2]			Vulsini/Sorano?			
TF-33		225.8±0.7[2]		Vulsini/Sovana			
TF-35			229.3±0.7	Roccamonfina/UWTT?			
TF-35b		235.6±0.6[2]		Vulsini/Farnese			
TF-37			240.2±0.6	Latium/Unknown			
TF-43		253.1±0.8[2]		Vulsini/Canino			

$^{40}Ar/^{39}Ar$ age data source: [1]: Giaccio et al. (2017a); [2]: this study.

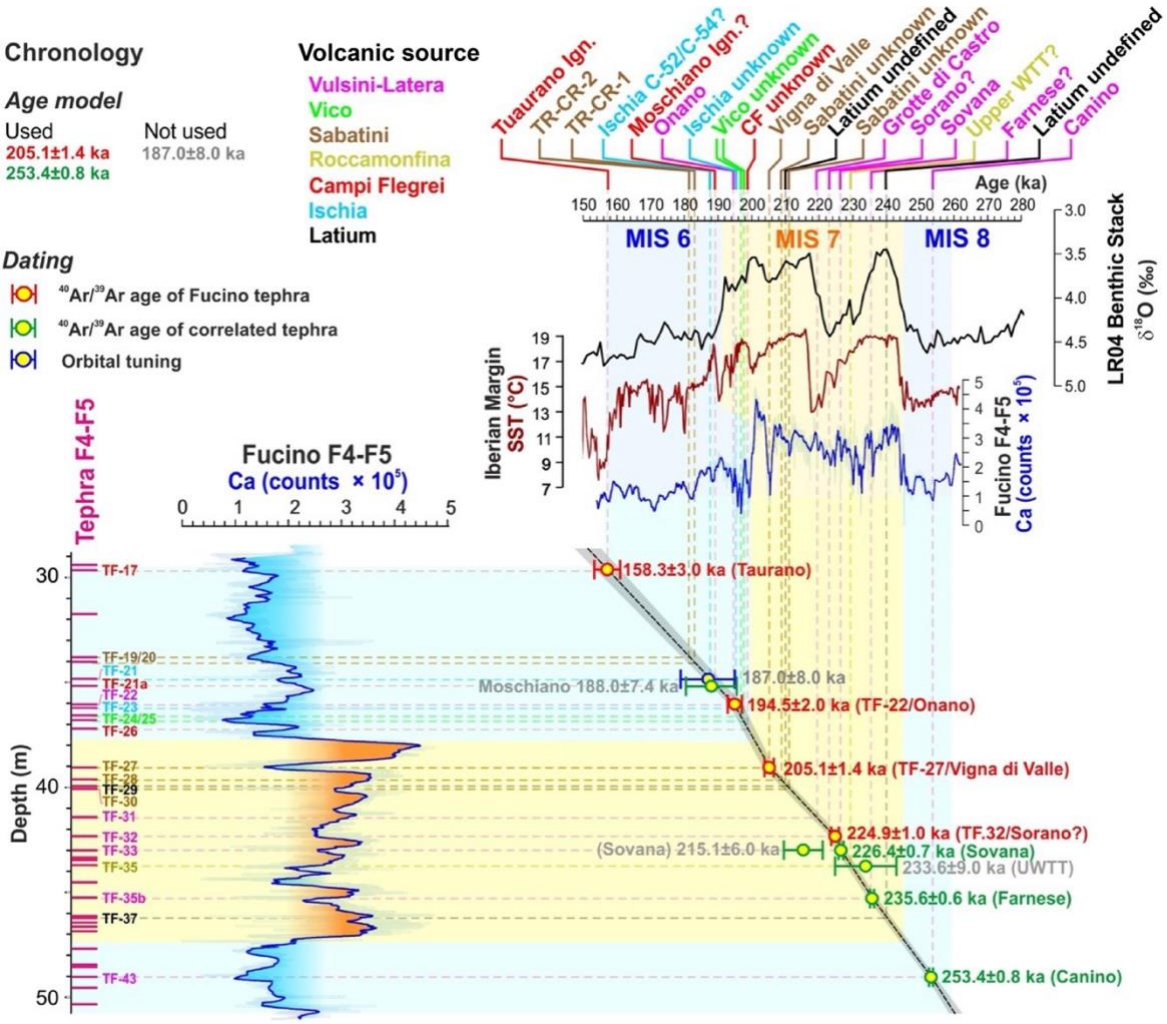

Figure 11. Age depth model of the MIS 6-7 Fucino F4-F5 record, with the proposed tephra correlations. For comparison, the resulting Fucino Ca time-series is shown together with the LR04 Benthic Stack (Lisiecki and Raymo, 2005) and the sea surface temperature (SST) record from the SW Iberian Margin core MD01-2444/43 (Martrat et al., 2007).

6. Summary and Concluding remarks

In this study, we have presented a new tephra record from Fucino Basin, central Italy, spanning the ~250-170 ka time interval, corresponding to the late Marine Isotope Stage (MIS) 8 and early MIS 6. Twenty Fucino tephra layers recognised in this time-interval, one tephra from Ohrid Lake succession, and thirteen selected pyroclastic units from near vent sections of Latera Volcanic Complex (LVC, Vulsini Volcanic District), Vico volcano, and Sabatini Volcanic District (SVD) have been characterised in terms of their major, minor (EPMA) and trace elements (LA-ICP-MS) glass

composition, Sr-Nd isotopic (TIMS) ratios, and seven of them by $^{40}Ar/^{39}Ar$ dating. The obtained results provide new relevant data for both refining the history of the peri-Tyrrhenian explosive volcanism during the 250-180 ka interval and for the MIS 8-6 Mediterranean tephrostratigraphy.

The combination of the new direct $^{40}Ar/^{39}Ar$ ages acquired in this study for LVC units with the ages of Fucino tephra, both direct $^{40}Ar/^{39}Ar$ and modelled, correlated to LVC units, provide a new, comprehensive chronological dataset for the whole succession of the main LVC units (Onano, Grotte di Castro, Sorano, Sovana, Farnese and Canino), which substantially improves the previous chronological framework and thus the reconstruction of the eruptive history of this volcano. In this regard, we highlight that some of the new $^{40}Ar/^{39}Ar$ ages here determined for the Latera units differ from the ages previously determined for the same units (e.g., Sovana, Farnese), whilst others (e.g., Canino) agree. This discrepancy should be further examinated, as precise $^{40}Ar/^{39}Ar$ ages of the proximal units are fundamental for reliable proximal-distal correlations. The Fucino tephrostratigraphical record also provides the first ages for the previously undated Trevignano Romano eruptions TR-CR-1 and TR-CR-2, SVD, and likely an improved age for the Upper White Trachytic Tuff of the Roccamonfina volcano. Finally, the Fucino record also evidences currently undocumented or poorly known explosive activity at Vico, Sabatini, Ischia and Campi Flegrei volcanoes, providing new fundamental insights into the eruptive history of these volcanic systems, also relevant for future hazard assessment.

Regarding the development of the Mediterranean tephrochronology general knowledge, there is a significant paucity of records spanning the MIS 8-6 interval. Some potential correlative layers have been found only in the Adriatic Sea core PRAD 1-2, the San Gregorio Magno Basin, southern Italy, and Lake Ohrid, North Macedonia-Albania. With this regard, the rich and detailed Fucino record can provide a reference dataset for future tephra studies in the Mediterranean region of this poorly investigated period. Finally, the high-precision $^{40}Ar/^{39}Ar$ dating acquired in this study provides the basis for the assemblage of high-resolution paleoevironmental and paleoclimatic records anchored to a robust radioisotopic-based chronology, allowing to explore the timing and dynamics of past climate changes independently of any assumption of the orbital tuning.

Acknowledgments

R. Jedlička and M. Racek are thanked for providing valuable technical assistance during EPMA analysis at Prague University. This article is a contribution to project "FUcino Tephrochronology Unites Quaternary Records (FUTURE)", financed by the Italian Research Ministry (MUR, PRIN 2017, grant 20177TKBXZ_003, project "FUTURE, G. Zanchetta, coordinator), issued to BG, DP and GZ. The Fucino project is co-funded by DFG (German Research Foundation) grant WA 2109/16. $^{40}Ar/^{39}Ar$ dating also received complementary contribution from the CNRS INSU-LEFE 2018-2020 action to S. Nomade. The INGV-OV laboratories have been also financially supported by the EPOS Research Infrastructure through the contribution of the Italian Ministry of University and Research (MUR).

References

Albert, P.G., Giaccio, B., Isaia, R., Costa, A., Niespolo, E.M., Nomade, S., Pereira, A., Renne, P.R., Hinchliffe, A., Mark, D.F., Brown, R.J., Smith, V.C., 2019. Evidence for a large-magnitude eruption from Campi Flegrei Caldera (Italy) at 29 ka. *Geology.* **47** (7), 595-599. https://doi.org/10.1130/G45805.1.

Albert, P.G., Tomlinson, E.L., Lane, C.S., Wulf, S., Smith, V.C., Coltelli, M., Keller, J., Lo Castro, D., Manning, C.J., Müller, W., Menzies, M.A., 2013. Late glacial explosive activity on Mount Etna: Implications for proximal-distal tephra correlations and the synchronisation of Mediterranean archives. *J. Volcanol. Geotherm. Res.* **265**, 9-26. https://doi.org/10.1016/j.jvolgeores.2013.07.010.

Amato, V., Aucelli, P.P.C., Cesarano, M., Jicha, B., Lebreton, V., Orain, R., Pappone, G., Petrosino, P., Russo Ermolli, E., 2014. Quaternary evolution of the largest intermontane basin of the Molise Apennine (Central Southern Italy). *Rend. Fis. Acc. Lincei* **25**, 197-216. https://doi.org/10.1007/s12210-014-0324-y.

Appleton, J.D., 1972. Petrogenesis of Potassium-rich Lavas from the Roccamonfina Volcano, Roman Region, Italy. *J. Petrol.* **13** (3), 425-456. https://doi.org/10.1093/petrology/13.3.425.

Ascione, A., Mazzoli, S., Petrosino, P., Valente, E., 2013. A decoupled kinematic model for active normal faults: Insights from the 1980, Ms = 6.9 Irpinia earthquake, southern Italy. *Geol. Soc. Amer. Bull.* **125** (7-8), 1239-1259. https://doi.org/10.1130/B30814.1.

Balbas, A., Koppers, A.A.P., Kent, D.V., Konrad, K., Clark, P.U., 2016. Identification of the short-lived Santa Rosa geomagnetic excursion in lavas on Floreana Island (Galapagos) by $^{40}Ar/^{39}Ar$ geochronology. *Geology* **44** (5), 359-362 (2016). https://doi.org/10.1130/G37569.1.

Bear, A.N., Cas, R.A.F., Giordano, G., 2009. The implications of spatter, pumice and lithic clast rich proximal co-ignimbrite lag breccias on the dynamics of caldera forming eruptions: The 151 ka Sutri eruption, Vico Volcano, Central Italy. *J. Volcanol. Geotherm. Res.* **181** (1-2), 1-24. https://doi.org/10.1016/j.jvolgeores.2008.11.032.

Belkin, H.E., Rolandi, G., Jackson, J.C., Cannatelli, C., Doherty, A.L., Petrosino, P., De Vivo, B., 2016. Mineralogy and geochemistry of the older (>40 ka) ignimbrites in the Campanian Plain, southern Italy. *J. Volcanol. Geotherm. Res.* **323**, 1-18. https://doi.org/10.1016/j.jvolgeores.2016.05.002.

Bertagnini, A. & Sbrana, A., 1986. Il volcano di Vico: stratigrafia del complesso vulcanico e sequenze eruttive delle formazioni piroclastiche (in Italian). *Mem. Soc. Geol. It.* **35**, 699-713.

Blockley, S.P.E., Bourne, A.J., Brauer, A., Davies, S.M., Hardiman, M., Harding, P.R., Lane, C.S., MacLeod, A., Matthews, I.P., Pyne-O'Donnel, S.D.F., Rasmussen, S.O., Wulf, S., Zanchetta, G., 2014. Tephrochronology and the extended intimate (integration of ice-core, marine and terrestrial records) event stratigraphy 8-128 ka 2bk. *Quat. Sci. Rev.* **106**, 88-100. https://doi.org/10.1016/j.quascirev.2014.11.002.

Boari, E., Tommasini, S., Laurenzi, M.A., Conticelli, S., 2009. Transition from Ultrapotassic Kamafugitic to Sub-Alkaline Magmas: Sr, Nd, and Pb Isotope, Trace Element and ^{40}Ar-^{39}Ar Age Data from the Middle Latin Valley Volcanic Field, Roman Magmatic Province, Central Italy. *J. Petrol.* **50** (7), 1327-1357. https://doi.org/10.1093/petrology/egp003.

Boncio, P., Lavecchia, G., Pace, B., 2004. Defining a model of 3D seismogenic sources for seismic hazard assessment applications: The case of central Apennines (Italy). *J. Seismol.* **8** (3), 407–425. https://doi.org/10.1023/B:JOSE.0000038449.78801.05.

Bourne, A.J., Albert, P.G., Matthews, I.P., Trincardi, F., Wulf, S., Asioli, A., Blockley, S.P.E., Keller, J., Lowe, J.J., 2015. Tephrochrunology of core PRAD 1-2 from the Adriatic Sea: insights into Italian explosive volcanism for the period 200-80 ka. *Quat. Sci. Rev.* **116**, 28-43. https://doi.org/10.1016/j.quascirev.2015.03.006.

Bourne, A.J., Lowe, J.J., Trincardi, F., Asioli, A., Blockley, S.P.E., Wulf, S., Matthews, I.P., Piva, A., Vigliotti, L., 2010. Distal tephra record for the last ca 105,000 years from core PRAD 1-2 in the central Adriatic Sea: implications for the marine tephrostratigraphy. *Quat. Sci. Rev.* **29**, 3079-3094. https://doi.org/10.1016/j.quascirev.2010.07.021.

Brown, R.J., Civetta, L., Arienzo, I., D'Antonio, M., Moretti, R., Orsi, G., Tomlinson, E.L., Albert, P.G., Menzies, M.A., 2014. Geochemical and isotopic insights into the assembly, evolution and disruption of a magmatic plumbing system before and after cataclysmic caldera-collapse eruption at Ischia volcano (Italy). *Contirb. Mineral. Petrol.* **168**: 1035. https://doi.org/10.1007/s00410-014-1035-1.

Brown, R.J., Orsi, G., de Vita, S., 2008. New insights into Late Pleistocene explosive volcanic activity and caldera formation on Ischia. *Bull. Volcanol.* **70**, 583-603. https://doi.org/10.1007/s00445-007-0155-0.

Cavinato, G.P., Carusi, C., Dell'Asta, M., Miccadei, E., Piacentini T., 2002. Sedimentary and tectonic evolution of Plio-Pleistocene alluvial and lacustrine deposits of Fucino Basin (central Italy). *Sediment. Geol.* **148**, 29-59. https://doi.org/10.1016/S0037-0738(01)00209-3.

Cox, S.E., Hemming, S.R., Tootell, D., 2020 The Isotopx NGX and ATONA Faraday amplifiers. *Geochronology* **2**, 231-243. https://doi.org/10.5194/gchron-2-231-2020.

Colucci, S., Palladino, D.M., Mulukutla, G.K., Proussevitch, A.A., 2013. 3-D Reconstruction of ash vesicularity: insights into the origin of ash-rich explosive eruptions. J. *Volcanol. Geotherm. Res.* **255**, 98-107. https://doi.org/10.1016/j.jvolgeores.2013.02.002.

D'Agostino, N., Jackson, J. A., Dramis, F., Funiciello, R., 2001. Interactions between mantle upwelling, drainage evolution and active normal faulting: an example from the central Apennines (Italy). *Geophys. J. Inter.* **147** (2), 475–497. https://doi.org/10.1046/j.1365-246X.2001.00539.x.

Davies, S.M., Wastegård, S., Abbott, P.M., Barbante, C., Bigler, M., Johnsen, S.J., Rasmussen, T.L., Steffensen, J.P., Svensson, A., 2010. Tracing volcanic events in the NGRIP ice-core and synchronising North Atlantic marine records during the last glacial period. *Earth Planet. Sci. Lett.* **294** (1-2), 69-79. https://doi.org/10.1016/j.epsl.2010.03.004.

de Rita, D., Funiciello, R., Parotto, M., 1988. Carta geologica del complesso vulcanico dei Colli Albani

(Vulcano Laziale) (in Italian). C.N.R.-Gruppo Nazionale Vulcanologia.

De Vivo, B., Rolandi, G., Gans, P.B., Calvert, A., Bohrson, W.A., Spera, F.J., Belkin, H.E., 2001. New constraints on the pyroclastic eruptive history of Campanian volcanic Plain (Italy). *Mineral. Petrol*. **73**, 47-65. https://doi.org/10.1007/s007100170010.

Del Carlo, P., Smedile, A., Petrelli, M., Di Roberto, A., 2020. Evidence of an unknown explosive eruption of Mt. Etna volcano (Italy) during the Late Glacial. *J. Volcanol. Geotherm. Res.* **402**, 106992. https://doi.org/10.1016/j.jvolgeores.2020.106992.

Di Roberto, A., Smedile, A., Del Carlo, P., De Martini, P.M., Iorio, M., Petrelli, M., Pantosti, P., Pinzi, S., Todrani, A., 2018. Tephra and cryptotephra in a ~60,000-year old lacustrine sequence from the Fucino Basin: new insights into the major explosive events in Italy. *Bull. Volcanol.* **80**:20. https://doi.org/10.1007/s00445-018-1200-x.

Di Vito, M.A., Sulpizio, R., Zanchetta, G., D'Orazio M., 2008 The late Pleistocene pyroclastic deposits of the Campanian Plain: New insights into the explosive activity of the Neapolitan volcanoes. *J. Volcanol. Geotherm. Res.* **177**, 19-48. https://doi.org/10.1016/j.jvolgeores.2007.11.019.

Doglioni, C., Harabaglia, P., Martinelli, G., Mongelli, F., Zito, G., 1996. A geodynamic model of the Southern Apennines accretionary prism. *Terra Nova* **8** (6), 540-547. https://doi.org/10.1111/j.1365-3121.1996.tb00783.x.

Freda, C., Gaeta, M., Karner, D.B., Marra, F., Renne, P.R., Taddeucci, J., Scarlato, P., Christensen, J.N., Dallai, L., 2006. Eruptive history and petrologic evolution of the Albano multiple maar (Alban Hills, Central Italy). *Bull. Volcanol*. **68**, 567-591. https://doi.org/10.1007/s00445-005-0033-6.

Froggat, P.C. & Gosson, G.J., 1982. Techniques for the preparation of tephra samples for mineral and chemical analysis and radiometric dating. *Geology Department, Victoria University of Wellington Publication* 23, 1-12.

Galadini, F. & Galli, P., 2000. Active tectonics in the Central Apennines (Italy) - Input Data for Seismic Hazard Assessment. *Nat. Haz.* **22**, 225-270. https://doi.org/10.1023/A:1008149531980.

Galli, P., Giaccio, B., Messina, P., Peronace, E., Amato, V., Naso, G., Nomade, S., Pereira, A., Piscitelli, S., Bellanova, J., Billi, A., Blamart, D., Galderisi, A., Giocoli, A., Stabile, T., Thil, F., 2017. Middle to Late Pleistocene activity of the Matese fault system (southern Apennines, Italy). *Tectonophysics* **699**, 61-81. https://doi.org/10.1016/j.tecto.2017.01.007.

Gatta, M., Sinopoli, G., Giardini, M., Giaccio, B., Hajdas, I., Pandolfi, L., Bailey, G., Spikins, P., Rolfo, M.F., Sadori, L., 2016. Pollen from Late Pleistocene hyena (Crocuta Crocuta spelaea) coprolites: An interdisciplinary approach from two Italian sites. *Rev. Palaeobot. Palynol.* **233**, 56-66. https://doi.org/10.1016/j.revpalbo.2016.07.005**.**

Giaccio, B., Galli, P., Messina, P., Peronace, E., Scardia, G., Sottili, G., Sposato, A., Chiarini, E., Jicha, B., Silvestri, S., 2012a. Fault and basin depocentre migration over the last 2Ma in the L'Aquila 2009 earthquake region, central Italian Apennines. *Quat. Sci. Rev.* **56**, 69–88. https://doi.org/10.1016/j.quascirev.2012.08.016.

Giaccio, B., Galli, P., Peronace, E., Arienzo I., Nomade, S., Cavinato, G.P., Mancini, M., Messina, P., Sottili, G., 2014. A 560-440 ka tephra record from the Mercure Basin, Southern Italy: volcanological and tephrostratigraphic implications. *J. Quat. Sci.* **29**, 232-248. https://doi.org/10.1002/jqs.2696.

Giaccio, B., Haydas, I., Isaia, R., Deino, A., Nomade, S., 2017b. High-precision ^{14}C and $^{40}Ar/^{39}Ar$ dating of Campanian Ignimbrite (Y-5) reconciles the time-scales of climatic cultural processes at 40 ka. *Sci. Rep.* **7**, 45940. https://doi.org/10.1038/srep45940.

Giaccio, B., Leicher, N., Mannella, G., Monaco, L., Regattieri, E., Wagner, B., Zanchetta, G., Gaeta, M., Marra, F., Nomade, S., Palladino, D.M., Pereira, A., Scheidt, S., Sottili, G., Wonik, T., Wulf, S., Zeeden, C., Ariztegui, D., Cavinato, G.P., Dean, R.J., Florindo, F., Leng, M.J., Macrì, P., Niespolo, E., Renne, P.R., Rolf, C., Sadori, L., Thomas, C., Tzedakis, P.C., 2019. Extending the tephra and paleoenvironmental record of the Central Mediterranean back to 430 ka: A new core from Fucino Basin, central Italy. *Quat. Sci. Rev.* **225**, 106003. https://doi.org/10.1016/j.quascirev.2019.106003.

Giaccio, B., Marra, F., Hajdas, I., Karner, D.B., Renne, P.R., Sposato, A., 2009. $^{40}Ar/^{39}Ar$ and ^{14}C geochronology of the Albano maar deposits: Implications for defining the age and eruptive style of the most recent explosive activity at Colli Albani Volcanic District, Central Italy. *J. Volcanol. Geotherm. Res.* **185**, 203-213. https://doi.org/10.1016/j.jvolgeores.2009.05.011.

Giaccio, B., Niespolo, E.M., Pereira, A., Nomade, S., Renne, P.R., Albert, P.G., Arienzo, I., Regattieri, E., Wagner, B., Zanchetta, G., Gaeta, M., Galli, P., Mannella, G., Peronace, E., Sottili, G., Florindo, F., Leicher, N., Marra, F., Tomlinson, E.L., 2017a. First integrated tephrochronological record for the last ~190 kyr from the Fucino Quaternary lacustrine succession, central Italy. *Quat. Sci. Rev.* **158**, 211-234. https://doi.org/10.1016/j.quascirev.2017.01.004.

Giaccio, B., Nomade, S., Wulf, S., Isaia, R., Sottili, G., Cavuoto, G., Galli, P., Messina, P., Sposato, A., Sulpizio, R., Zanchetta, G., 2012b. The late MIS 5 Mediterranean tephra markers: a reappraisal from peninsular Italy terrestrial records. *Quat. Sci. Rev.* **56**, 31-45. https://doi.org/10.1016/j.quascirev.2012.09.009.

Giaccio, B., Isaia, R., Fedele, F.G., Di Canzio, E., Hoffecker, J., Ronchitelli, A., Sinitsyn, A.A., Anikovich, M., Lisitsyn, S.N., Popov, V.V., 2008. The Campanian Ignimbrite and Codola tephra layers: Two temporal/stratigraphic markers for the Early Upper Palaeolithic in southern Italy and eastern Europe. *J. Volcanol. Geotherm. Res.* **177** (1), 208-226. https://doi.org/10.1016/j.jvolgeores.2007.10.007.

Giannetti, B. & De Casa, G., 2000. Stratigraphy, chronology, and sedimentology of ignimbrites from the white trachytic tuff, Roccamonfina Volcano, Italy. *J. Volcanol. Geotherm. Res.* **96**, 3-4, 243-295. https://doi.org/10.1016/S0377-0273(99)00144-4.

Giannetti, B., 1996. The geology of the Yellow Trachytic Tuff, Roccamonfina Volcano. *J. Volcanol. Geotherm. Res.* **71** (1), 53-72. https://doi.org/10.1016/0377-0273(95)00030-5.

Giordano, G. & the CARG Team, 2010. Stratigraphy, volcano tectonics and evolution of the Colli Albani volcanic field. In: Funicello, R. & Giordano, G. (Eds.): The Colli Albani volcano. *Spec. Pub. IAVCEI* **3**, 43-97, *Geol. Soc., Lond.* (2010).

Giraudi, C. & Giaccio, B., 2015. Middle Pleistocene glaciations in the Apennines, Italy: new chronological data and preservation of the glacial record. *Geol. Soc.*

Lond. Spec. Pub. **433**, 161-178. https://doi.org/10.1144/SP433.1.

Giraudi, C., Bodrato, G., Ricci Lucchi, M., Cipriani, N., Villa, M.I., Giaccio, B., Zuppi, G.M., 2011. Middle and late Pleistocene glaciations in the Campo Felice Basin (central Apennines, Italy). *Quat. Res.* **75** (1), 219-230. https://doi.org/10.1016/j.yqres.2010.06.006.

Goldstein, S.L., Denis, P., Oelkers, E.H., Rudnick, R.L., Walter, L.M., 2003. Standards for publication of isotope ratio and chemical data in chemical geology. *Chem. Geol.* **202**, 1-4. https://doi.org/10.1016/j.chemgeo.2003.08.003.

Hayward, C., 2011. High spatial resolution electron probe microanalysis of tephras and melt inclusion without beam-induced chemical modification. *The Holocene* **22** (1), 119-125. https://doi.org/10.1177%2F0959683611409777.

Jicha, B.R., Singer, B.S., Sobol, P., 2016. Re-evaluation of the ages of $^{40}Ar/^{39}Ar$ sanidine standards and supereruptions in the western U.S. using a Noblesse multi-collector mass spectrometer. *Chem. Geol.* **431**, 54-66. https://doi.org/10.1016/j.chemgeo.2016.03.024.

Jochum, K.P., Stoll, B., Herwig, K., Willbold, M., Hofmann, A.W., Amini, M., Aarbug, S., Abouchami, W., Hellebrand, E., Mocek, B., Raczek, I., Stracke, A., Alard, O., Bouman, C., Becker, S., Dücking, M., Brätz, H., Klemd, R., de Bruin, D., Canil, D., Cornell, D., de Hoog, C.-S., Dalpé, C., Danyushevsky, L., Eisenhauer, A., Gao, Y., Snow, J.E., Groschopf, N., Günther, D., Latkoczy, C., Guillong, M., Hauri, E.K., Höfer, H.E., Lahaye, Y., Horz, K., Jacob, D.E., Kasemann, S.A., Kent, A.J.R., Ludwig, T., Zack, T., Mason, P.R.D., Meixner, A., Rosner, M., Kisawa, K., Nash, P.B., Pfänder, J., Premo, W.R., Sun, W.D., Tiepolo, M., Vannucci, R., Vennemann, T., Wayne, D., Woodhead, J.D., 2006. MPI-DING reference glasses for in situ microanalysis: New reference values for element concentrations and isotope ratios. *Geochem. Geophys.* **7**:2. https://doi.org/10.1029/2005GC001060.

Keller, J., Ryan, W.B.F., Ninkovich, D., Altherr, R., 1978. Explosive volcanic activity in the Mediterranean over the last 200,000 yr as recorded in deep-sea sediments. *Geol. Soc. Am. Bull.* **89**, 591-604. https://doi.org/10.1130/0016-7606(1978)89%3C591:EVAITM%3E2.0.CO;2.

Koppers, A.A.P., 2002. ArArCALC e software for $^{40}Ar/^{39}Ar$ age calculations. *Comput. Geosci.* **28**, 605-619. https://doi.org/10.1016/S0098-3004(01)00095-4.

Kutterolf, S., Schindlbeck, J.C., Jegen, M., Freundt, A., Straub, S.M., 2019. Milankovitch frequencies in tephra records at volcanic arcs: The relation of kyr-scale cyclic variations in volcanism to global climatic changes. *Quat. Sci. Rev.* **204**, 1-16. https://doi.org/10.1016/j.quascirev.2018.11.004.

Lane, C.S., Brauer, A., Blockley, S.P.E., Dulski, P., 2013. Volcanic ash reveals time-transgressive abrupt climate change during the Younger Dryas. *Geology* **41** (12), 1251-1254. https://doi.org/10.1130/G34867.1.

Lane, C.S., Cullen, V.L., White, D., Bramham.Law, C.W.F., Smith, V.C., 2014. Cryptotephra as a dating and correlation tool in archaeology. *J. Archaeol. Sci.* **42**, 42-50. https://doi.org/10.1016/j.jas.2013.10.033.

Lane, C.S., Lowe, D.J., Blockley, S.P.E., Suzuki, T., Smith, V.C., 2017. Advancing tephrochronology as a global dating tool: Applications in volcanology, archaeology and palaeoclimatic research. *Quat. Geochronol.* **40**, 1-7. https://doi.org/10.1016/j.quageo.2017.04.003.

Laurenzi, M.A. & Villa, I.M., 1987. $^{40}Ar/^{39}Ar$ chronostratigraphy of Vico ignimbrites. *Period. Mineral.* **56**, 285-293.

Le Maitre, R.W., Streckeisen, A., Zanettin, B., Le Bas, M.J., Bonin, B., Bateman, P., Bellieni, G., Dudek, A., Efremova, S., Keller, J., Lameyre, J., Sabine, P.A., Schmid, R., SØrensen, H., Woolley, A.R., 2002. Igneous Rocks: A Classification and Glossary of Terms. Reccomendation of the International Union of Geological Sciences Subcommission on the Systematics of Igneous Rocks, 2nd Edition. Cambridge University Press, Cambridge. 236 pages.

Lee, J.Y., Marti, K., Severinghaus, J.P., Kawamura, K., Yoo, H.S., Lee, J.B., Kim, J.S., 2006. A redetermination of the isotopic abundances of atmospheric Ar. *Geochim. Cosmochim. Acta* **70** (17), 4507-4512. https://doi.org/10.1016/j.gca.2006.06.1563.

Leicher, Giaccio, B., Zanchetta, G., Sulpizio, R., Albert, P.G., Tomlinson, E.L., Lagos, M., Francke, A., Wagner, B., 2021. Lake Ohrid's tephrochronological dataset reveals 1.36 Ma of Mediterranean explosive volcanic activity. *Sci. Data* **8**, 231. https://doi.org/10.1038/s41597-021-01013-7.

Leicher, N., Giaccio, B., Zanchetta, G., Wagner, B., Francke, A., Palladino, D.M., Sulpizio, R., Albert, P.G., Tomlinson, E.L., 2019. Central Mediterranean explosive volcanism and tephrochronology during the last 630 ka based on the sediment record from Laker Ohrid, *Quat. Sci. Rev.* **226**, 106021. https://doi.org/10.1016/j.quascirev.2019.106021.

Leicher, N., Zanchetta, G., Sulpizio, R., Giaccio, B., Wagner, B., Nomade, S., Francke, A., Del Carlo, P., 2016. First tephrostratigraphic results of the DEEP site record from Lake Ohrid (Macedonia and Albania). *Biogeosciences* **13**, 2151-2178. https://doi.org/10.5194/bg-13-2151-2016.

Lisiecki, L.E. & Raymo, M.E., 2005. A Pliocene-Pleistocene stack of 57 globally distributed benthic d18O records. *Palaeoceanogr. Palaeoclimatol.* **20** (1), PA1003. https://doi.org/10.1029/2004PA001071.

Lowe, D.J., 2011. Tephrochronology and its application: A review. *Quat. Geochronol.* **6**, 107-153. https://doi.org/10.1016/j.quageo.2010.08.003.

Lowe, D.J., Pearce, N.J.G., Jorgensen, M.A., Kuhen, S., Tyron, C.A., Hayward, C.L., 2017. Correlating tephras and cryptotephras using glass compositional analyses and numerical and statistical methods: Review and evaluation. *Quat. Sci. Rev.* **175**, 1-44. https://doi.org/10.1016/j.quascirev.2017.08.003.

Ludwig, K.R., 2012. User's Manual for Isoplot Version 3.75-4.15: A Geochronological Toolkit for Microsoft Excel. *Berkley Geochronological Centre Special Publication* **5**.

Mannella, G., Giaccio, B., Zanchetta, G., Regattieri, E., Niespolo, E.M., Pereira, A., Renne, P.R., Nomade, S., Leicher, N., Perchiazzi, N., Wagner, B., 2019. Paleoenvironmental and paleohydrological variability of mountain areas in the central Mediterranean region: A 190-ka-long chronicle from the independently dated Fucino paleolake record (central Italy). *Quat. Sci. Rev.* **210**, 190-210. https://doi.org/10.1016/j.quascirev.2019.02.032.

Marianelli, P. & Sbrana, A. Risultati di misure standard di minerali e di vetri naturali in microanalisi a dispersione di energia (In Italian). *Atti Soc. Tosc. Sci. Nat. Resid. Pisa, Mem. Serie A* **105**, 57-63 (1998).

Marra F., Freda C., Scarlato P., Taddeucci J., Karner D.B., Renne P.R., Gaeta M., Palladino D.M., Trigila R., Cavarretta G., 2003. Post-caldera activity in the Alban Hills volcanic district (Italy): $^{40}Ar/^{39}Ar$ geochronology and insights into magma evolution. *Bull. Volcanol.* **65**, 227-247. https://doi.org/10.1007/s00445-002-0255-9.

Marra, F., Castellano, C., Cucci, L., Florindo, F., Gaeta, M., Jicha, B., Palladino, D.M., Sottili, G., Tertulliani, A., Tolomei, C., 2020. Monti Sabatini and Colli Albani: the dormant twin volcanoes at the gates of Rome. *Sci. Rep.* **10**:8666. https://doi.org10.1038/s41598-02-65394-2.

Marra, F., Ceruleo, P., Jicha, B., Pandolfi, L., Petronio, C., Salari, L., Giaccio, B., Sottili, G., 2016a. Chronostratigraphic constraints on Middle Pleistocene faunal assemblages and Acheulian industries from the Cretone lacustrine basin, central Italy. *J. Quat. Sci.* **31** (7), 641-658. https://doi.org/10.1002/jqs.2889.

Marra, F., Gaeta, M., Giaccio, B., Jicha, B.R., Palladino, D.M., Polcari, M., Sottili, G., Taddeucci, J., Florindo, F., Stramondo, S., 2016b. Assessing the volcanic hazard for Rome: $^{40}Ar/^{39}Ar$ and In-SAR constraints on the most recent eruptive activity and present-day uplift at Colli Albani Volcanic District. *Geophys. Res. Lett.* **43**, 6898-6906. https://doi.org/10.1002/2016GL069518.

Marra, F., Nomade, S., Pereira, A., Petronio, C., Salari, L., Sottili, G., Bahain, J.J., Boschian, G., Di Stefano, G., Falguères, C., Florindo, F., Gaeta, M., Giaccio, B., Masotta, M., 2018. A review of the geological sections and the faunal assemblages of Aurelian Mammal Age of Latium (Italy) in the light of a new chronostratigraphic framework. *Quat. Sci. Rev.* **181**, 173-199. https://doi.org/10.1016/j.quascirev.2017.12.007.

Martrat, B., Grimalt, J.O., Shackleton, N.J., de Abreu, L., Hutterli, M.A., Stocker, T.F., 2007. Four climate cycles of recurring deep and surface water destabilizations on the Iberian margin. *Science* **317**, 502-507. https://doi.org/10.1126/science.1139994.

McDonough, W.F. & Sun, S.-s., 1995. The composition of the Earth. *Chem. Geol.* **120** (3-4), 223-253. https://doi.org/10.1016/0009-2541(94)00140-4.

Monaco, L., Palladino, D.M., Gaeta, M., Marra, F., Sottili, G., Leicher, N., Mannella, G., Nomade, S., Pereira, A., Regattieri, E., Wagner, B., Zanchetta, G., Albert, P.G., Arienzo, I., D'Antonio, M., Petrosino, P., Manning, C., Giaccio, B., 2021. Mediterranean tephrostratigraphy and peri-Tyrrhenian explosive activity revaluated in light of the 430-365 ka record from Fucino Basin (central Italy). *Earth Sci. Rev.* **220**, 103706. https://doi.org/10.1016/j.earscirev.2021.103706.

Munno, R. & Petrosino, P., 2007. The late Quaternary tephrostratigraphical record of the San Gregorio Magno basin (southern Italy). *J. Quat. Sci*. **22**, 247-266. https://doi.org/10.1002/jqs.1025.

Nappi, G., Renzulli, A., Santi, P., 1991. Evidence of incremental growth in the Vulsinian calderas (central Italy). *J. Volcanol. Geotherm. Res.* **47** (1-2), 13–31. https://doi.org/10.1016/0377-0273(91)90098-K.

Niespolo, E.M., Rutte, D., Deino, A.L., Renne, P.R., 2017. Intercalibration and age of the Alder Creek Sanidine $^{40}Ar/^{39}Ar$ standard. *Quat. Geochronol.* **39**, 205-213. https://doi.org/10.1016/j.quageo.2016.09.004.

Palladino, D.M. & Agosta, E., 1997. Pumice fall deposits of the Western Vulsini Volcanoes (Central Italy). *J. Volcanol. Geotherm. Res.* **78** (1-2), 77-102. https://doi.org/10.1016/S0377-0273(96)00107-2.

Palladino, D.M. & Simei, S., 2005. Eruptive dynamics and caldera-collapse during the Onano eruption, Vulsini, Italy. *Bull. Volcanol.* **67**, 423-440. https://doi.org/10.1007/s00445-004-0385-3.

Palladino, D.M. & Taddeucci, J., 1998. The basal ash deposit of the Sovana Eruption (Vulsini Volcanoes, central Italy): the product of a dilute pyroclastic density current. J*. Volcanol. Geotherm. Res.* **87** (1-4), 233-254. https://doi.org/10.1016/S0377-0273(98)00095-X.

Palladino, D.M. & Valentine, G.A., 1995. Coarse-tail vertical and lateral grading in pyroclastic flow deposits of the Latera Volcanic COmples (Vulsini, central Italy): origin and implications for flow dynamics. *J. Volcanol. Geotherm. Res.* **69** (3-4), 343-364. https://doi.org/10.1016/0377-0273(95)00036-4.

Palladino, D.M., Gaeta, M., Giaccio, B., Sottili, G., 2014. On the anatomy of magma chamber and caldera collapse: the example of trachyphonolite explosive eruptions of the Roman province (Central Italy). *J. Volcanol. Geotherm. Res.* **281**, 12-26. https://doi.org/10.1016/j.jvolgeores.2014.05.020.

Palladino, D.M., Simei, S., Sottili, G., Trigila, R., 2010. Integrated approach for the reconstruction of stratigraphy and geology of Quaternary volcanic terrains: an application to the Vulsini Volcanoes (central Italy). In: Groppelli, G., Viereck, e L. (Eds.), Stratigraphy and Geology in Volcanic Areas. *Geol. Soc. Am. Spec. Pap.* **464**, 66–84.

Palladino, D.M., Simei, S., Triglia, R., 2016. Note Illustrative della Carta geologica d'Italia alla scala 1:50.000, foglio 344 Tuscania, *ISPRA-Servizio Geologico d'Italia* (In Italian). https://www.isprambiente.gov.it/Media/carg/note_illustrative/344_Tuscania.pdf.

Pappalardo, L., Civetta, L., D'Antonio, M., Deino, A., Di Vito, M., Orsi, G., Carandente, A., de Vita, S., Isaia, R., Piochi, M., 1999. Chemical and Sr-isotopical evolution of the Phlegrean magmatic system before the Campanain Ignimbrite and the Neapolitan Yellow Tuff eruptions. *J. Volcanol. Geotherm. Res.* **91** (2-4), 141-166. https://doi.org/10.1016/S0377-0273(99)00033-5.

Patacca, E., Scandone, P., Di Luzio, E., Cavinato, G.P., Parotto, M., 2008. Structural architecture of the central Apennines: Interpretation of the CROP 11 seismic profile from the Adriatic coast to the orographic divide. *Tectonics* **27**, TC3006. https://doi.org/10.1029/2005TC001917.

Paterne, M., Guichard, F., Duplessy, J.C., Siani, G., Sulpizio, R., Labeyrie, J., 2008. A 90,000-200,000 yrs marine tephra record of Italian volcanic activity in the Central Mediterranean Sea. J. *Volcanol. Geotherm. Res.* **177**, 187-196. https://doi.org/10.1016/j.jvolgeores.2007.11.028.

Paterne, M., Guichard, F., Labeyrie, J., 1988. Explosive activity of the south Italian volcanoes during the past 80,000 years as determined by marine tephrochronology. *J. Volcanol. Geotherm. Res.* **34**, 153-172. https://doi.org/10.1016/0377-0273(88)90030-3.

Paterne, M., Guichard, F., Labeyrie, J., Gillot, P.Y., Duplessy, J.C., 1986. Tyrrhenian Sea tephrochronology of the oxygen isotope record for the past 60,000 years. *Mar. Geol.* **72**, 259-285. https://doi.org/10.1016/0025-3227(86)90123-4.

Paterne, M., 1985. Reconstruction de l'activité explosive des volcans de l'Italie du Sud par tephrochronologie marine. (In French). Thèse Doctorat-Etat, Université Paris-Sud Orsay.

Pearce, N.J.G., Alloway, B., Wickham, C., 2019. Correlating weathered, microphenocryst-rich, intermediate tephra: An approach combining bulk and single shard analyses from the Lepué Tephra, Chile and Argentina. *Quat. Internat.* **500**, 71-82. https://doi.org/10.1016/j.quaint.2019.01.017.

Pearce, NJ.G., Perkins, W.T., Westgate, J.A., Gorton, M.P., Jackson, S.E., Neal, C.R., Chenery, S.P., 1997. A Compilation of New and Published Major and Trace Element Data for NIST SRM 610 and NIST SRM 612 Glass Reference Materials. *Geostand. Newslett.* **21** (1), 115-144. https://doi.org/10.1111/j.1751-908X.1997.tb00538.x.

Peccerillo, A., 2017. Cenozoic Volcanism in the Tyrrhenian Sea Region. In: IAVCEI, Advances in Volcanology, 2 ed. Springer, p. 400.

Perini, G., Conticelli, S., Francalanci, L., 1997. Inferences on the volcanic history of the Vico volcano, Roman Magmatic Province, central Italy: stratigraphic, petrographic and geochemical data. *Mineral. Petrograph. Acta* **40**, 67-93.

Perini, G., Francalanci, L., Davidson, J.P., Conticelli, S., 2004. Evolution and Genesis of Magmas from Vico Volcano, Central Italy: Multiple Differentiation Pathways and Variable Parental Magmas. *J. Petrol.* **45** (1), 139-182. https://doi.org/10.1093/petrology/egg084.

Petrelli, M., Laeger, K., Perugini, D., 2016. High spatial resolution trace element determination of geological samples by laser ablation quadrupole plasma mass spectrometry: implications for glass analysis in volcanic products. *Geosci. J.* **20** (851-863. https://doi.org/10.1007/s12303-016-0007-z.

Petrosino, P., Arienzo, I., Mazzeo, F.C., Natale, J., Petrelli, M., Milia, A., Perugini, D., D'Antonio, M., 2019. The San Gregorio Magno lacusrine basin (Campania, southern Italy): improved characterization of the tephrostratigraphic markers based on trace elements and isotopic data. *J. Quat. Sci.* **34**, 393-404. https://doi.org/10.1002/jqs.3107.

Petrosino, P., Jicha, B.R., Mazzeo, F.C., Ciaranfi, N., Girone, A., Maiorano, P., 2015. The Montalbano Jonico marine succession: An archive for distal tephra layers at the Early-Middle Pleistocene boundary in southern Italy. *Quat. Int*. **383**, 89-103. https://doi.org/10.1016/j.quaint.2014.10.049.

Petrosino, P., Morabito, S., Jicha, B.R., Milia, A., Sprovieri, M., Tamburrino, S., 2016. Multidisciplnary tephrochronological correlation of marker events in the eastern Tyrrhenian Sea between 48 and 105 ka. *J. Volcanol. Geotherm. Res.* **315**, 79-99. https://doi.org/10.1016/j.jvolgeores.2016.02.001.

Poli, S., Chiesa, S., Gillot, P.-Y., Gregnanin, A., Guichard, F., 1987. Chemistry versus time in the volcanic complex of Ischia (Gulf of Naples, Italy): evidence of successive magmatic cycles. *Contrib. Mineral. Petrol.* **95**, 322-335.

Ponomareva, V.V., Portnyagin, M., Davies, S.M., 2015. Tephra without borders: far-reaching clues into past explosive eruptions. *Front. Earth Sci.* **3** (83). https://doi.org/10.3389/feart.2015.00083.

Regattieri, E., Giaccio, B., Zanchetta, G., Drysdale, R.N., Galli, P., Nomade, S., Peronace, E., Wulf, S., 2015. Hydrological variability over the Apennines during the Early Last Glacial precession minimum, as revelated by a stable isotope record from Sulmona basin, Central Italy. J. *Quat. Sci.* **30**, 19-31. https://doi.org/10.1002/jqs.2755.

Renne, P.R., Balco, G., Ludwig, K.R., Mundil, R., Min, K., 2011. Response to the comment by WH Schwarz et al. on "Joint determination of 40 K decay constants and $^{40}Ar^*/^{40}K$ for the Fish Canyon sanidine standard, and improved accuracy for $^{40}Ar/^{39}Ar$ geochronology" by PR Renne et al. (2010). *Geochim. Cosmochim. Acta* **75**, 5097-5100.

Rolandi, G., Bellucci, F., Heizler, M.T., Belkin, H.E., De Vivo, B., 2003. Tectonic controls on the genesis of ignimbrite from the Campanian Volcanic Zone, southern Italy. *Mineral. Petrol.* **79**, 3-31. https://doi.org/10.1007/s00710-003-0014-4.

Rouchon, V., Gillot, P.Y., Quidelleur, X., Chiesa, S., Floris, B., 2008. Temporal evolution of the Roccamonfina volcanic complex (Pleistocene), Central Italy. *J. Volcanol. Geotherm. Res.* **177**, 500-514. https://doi.org/10.1016/j.jvolgeores.2008.07.016.

Satow, C., Tomlinson, E.L., Grant, K.M., Albert, P.G., Smith, V.C., Manning, C.J., Ottolini, L., Wulf, S., Rohling, E.J., Lowe, J.J., Blockley, S.P.E., Menzies, M.A., 2015. A new contribution to the Late Quaternary tephrostratigraphy of the Mediterranean: Aegean Sea core LC21. *Quat. Sci. Rev.* **117**, 96-112. https://doi.org/10.1016/j.quascirev.2015.04.005.

Sbrana, A., Marianelli, P., Pasquini, G., 2018. Volcanology of Ischia. *J. Maps* **14** (2) 494-503. https://doi.org/10.1080/17445647.2018.1498811.

Siani, G., Sulpizio, R., Paterne, M., Sbrana, A., 2004. Tephrostratigraphy study for the last 18,000 14C years in a deep-sea sediment sequence for the South Adriatic. Quaternary Science Reviews, 23, 2485-2500. https://doi.org/10.1016/j.quascirev.2004.06.004.

Smith, D.G.W. & Westgate, J.A., 1968. Electron probe technique for characterising pyroclastic deposits. *Earth Planet. Sci. Lett.* **5**, 313-319. https://doi.org/10.1016/S0012-821X(68)80058-5.

Sollevanti, F., 1983. Geologic, volcanologic, and tectonic setting of the Vico-Cimino area, Italy. *J. Volcanol. Geotherm. Res.* **17** (1-4), 203-217. https://doi.org/10.1016/0377-0273(83)90068-9.

Sottili, G., Arienzo, I., Castorina, F., Gaeta, M., Giaccio, B., Marra, F., Palladino, D.M., 2019. Time-dependent Sr and Nd isotope variations during the evolution of ultrapotassic Sabatini Volcanic District (Roman Province, Central Italy). *Bull. Volcanol.* **81**:67. https://doi.org/10.1007/s00445-019-1324-7.

Sottili, G., Palladino, D.M., Marra, F., Jicha, B., Karner, D.B., Renne, P., 2010. Geochronology of the most recent activity in the Sabatini volcanic district, Roman Province, central Italy. *J. Volcanol. Geotherm. Res.* **196**, 20-30. https://doi.org/10.1016/j.jvolgeores.2010.07.003.

Sparks, R. S. J., 1975. Stratigraphy and geology of the ignimbrites of Vulsini volcano, central Italy. *Geologische Rundschau* **64**, 497-523. https://doi.org/10.1007/BF01820680.

Taddeucci, J. & Palladino, D.M., 2002. Particle size-density relationships in pyroclastic deposits: inferences from emplacement processes. *Bull. Volcanol.* **64**, 273-284. https://doi.org/10.1007/s00445-002-0205-6.

Thorarinsson, S., 1944. Tefrokronologiska Studier På Island. Pjórsárdalur Och Dess Förödelse.

Geografiska Annaler **26** (1-2), 1-217. https://doi.org/10.1080/20014422.1944.11880727.

Thorarinsson, S., 1981a. Greetings from Iceland. Geografiska Annaler: Series A, Physical Geography, 63:3-4, 109-118.

Thorarinsson, S., 1981b. Tephra studies and tephrochronology: a historical review with special reference to Iceland. In: S. Self, R.S.J., Sparks (Eds.), Tephra Studies, Reidel, Dordrecht (1981), pp. 1-12. https://doi.org/10.1007/978-94-009-8537-1_1.

Tomlinson, E.L., Arienzo, I., Civetta, L., Wulf, S., Smith, V.C., Hardiman, M., Lane, C.S., Carandente, A., Orsi, G., Rosi, M., Müller, W., Menzies, M.A., 2012. Geochemistry of the Phlegrean Fields (Italy) proximal sources for major Mediterranean tephras: Implications for the dispersal of Plinian and co-ignimbritic components of explosive eruptions. *Geochim. Cosmochim. Acta* **93**, 102-128. https://doi.org/10.1016/j.gca.2012.05.043.

Tomlinson, E.L., Smith, V.C., Albert, P.G., Aydar, E., Civetta, L., Cioni, R., çubukçu, E., Gertisser, R., Isaia, R., Menzies, M.A., Orsi, G., Rosi, M., Zanchetta, G., 2015. The major and trace element glass compositions of the productive Mediterranean volcanic sources: tools for correlating distal tephra layers in and around Europe. *Quat. Sci. Rev.* **118**, 48-66. https://doi.org/10.1016/j.quascirev.2014.10.028.

Turbeville, B.N., 1992. $^{40}Ar/^{39}Ar$ ages and Stratigraphy of the Latera caldera, Italy. *Bull. Volcanol.* **55**, 110-118. https://doi.org/10.1007/BF00301124.

Vakhrameeva, P., Koutsodendris, A., Wulf, S., Fletcher, W.J., Appelt, O., Knipping, M., Gertisser, R., Trieloff, M., Pross, J., 2018. The cryptotephra record of the Marine Isotope Stage 12 to 10 interval (460-335 ka) at Tenaghi Philippon, Greece: Exploring chronological markers for the Middle Pleistocene of the Mediterranean region. *Quat. Sci. Rev.* **200**, 313-333. https://doi.org/10.1016/j.quascirev.2018.09.019.

Vakhrameeva, P., Koutsodendris, A., Wulf, S., Portnyagin, M., Appelt, O., Ludwig, T., Trieloff, M., Pross, J., 2021. Land-sea correlations in the Eastern Mediterranean region over the past c. 800 kyr based on macro- and cryptotephras from ODP Site 964 (Ionian Basin). *Quat. Sci. Rev.* **255**, 106811. https://doi.org/10.1016/j.quascirev.2021.106811.

Vakhrameeva, P., Wulf, S., Koutsodendris, A., Tjallingii, R., Fletcher, W.J., Appet, O., Ludwig, T., Knipping, M., Trieloff, M., Pross, J., 2019. Eastern Mediterranean volcanism during Marine isotope stages 9 to 7e (335-235 ka): Insights based on cryptotephra layers at Tenaghi Philippon, Greece. *J. Volcanol. Geotherm. Res.* **380**, 31-47. https://doi.org/10.1016/j.jvolgeores.2019.05.016.

Valentine, G.A., Palladino, D.M., DiemKaye, K., Fletcher, C., 2019. Lithic-rich and lithic-poor ignimbrites and their basal deposits: Sovana and Sorano formations (Latera caldera, Italy). *Bull. Volcanol.* **81**, 29. https://doi.org/10.1007/s00445-019-1288-7.

Vezzoli, L., Conticelli, S., Innocenti, F., Landi, P., Manetti, P., Palladino, D. M., Triglia, R., 1987. Stratigraphy of the Latera Volcanic Complex: a proposal for a new nomenclature. Periodico di Mineralogia, 56, 89-110.

Villa, P., Soriano, S., Pollarolo, L., Smiriglio, C., Gaeta, M., D'Orazio, M., Conforti, J., Tozzi, C., 2020. Neandertals on the beach: Use of marine resources at Grotta dei Moscerini (Latium, Italy). *PLoS ONE* **15** (1), e0226690. https://doi.org/10.1371/journal.pone.0226690.

Wagner, B., Vogel, H., Francke, A., Friederich, T., Donders, T., Lacey, J.H., Leng, M.J., Regattieri, E., Sadori, L., Wilke, T., Zanchetta, G., Albrecht, C., Bertini, A., Combourieu-Nebout, N., Cvetkoska, A., Giaccio, B., Grazhdani, A., Hauffe, T., Holtvoeth, J., Joannin, S., Lagoos, M., Leicher, N., Levkov, Z., Lindhorst, K., Masi, A., Melles, M., Mercuri, A.M., Nomade, S., Nowaczyk, N., Panagiotopoulos, K., Peyron, O., reed, J.M., Sagnotti, L., Sinopoli, G., Stellbrink, B., Sulpizio, R., Timmermann, A., Tofilovska, S., Torri, P., Wagner-Cremer, F., Wonik, T., Zhang, X., 2019. Mediterranean winter rainfall in phase with African monsoons during the past 1.36 million years. *Nature* **573**, 256-260. https://doi.org/10.1038/s41586-019-1529-0.

Wulf, S., Hardiman, M.J., Staff, R.A., Koutsodendris, A., Appelt, O., Blockley, S.P.E., Lowe, J.J., Manning, C.J., Ottolini, L., Schmitt, A.K., Smith, V.C., Tomlinson, E.L., Vakhrameeva, P., Knipping, M., Kotthoff, U., Milner, A.M., Müller, U.C., Christanis, K., Kalaitzidis, S., Tzedakis, P.C., Schmiedl, G., Pross, J., 2018. The Marine isotope stage 1-5 cryptotephra record of Tenaghi Philippon, Greece: Towards a detailed tephrostratigraphic framework for the Eastern Mediterranean region. *Quat. Sci. Rev.* **186**, 236-262. https://doi.org/10.1016/j.quascirev.2018.03.011.

Wulf, S., Keller, J., Paterne, M., Mingram, J., Lauterbach, S., Opitz, S., Sottili, G., Giaccio, B., Albert, P.G., Satow, C., Tomlinson, E.L., Viccaro, M., Brauer, A., 2012. The 100-133 ka record of Italian explosive volcanism and revised tephrochronology of Lago Grande di Monticchio. *Quat. Sci. Rev.* **58**, 104-123. https://doi.org/10.1016/j.quascirev.2012.10.020.

Wulf, S., Keller, J., Satow, C., Gertisser, R., Kraml M., Grant, K.M., Appelt, O., Vakhrameeva, P., Koutsodendris, A., Hardiman, M., Schulz, H., Pross, J., 2020. Advancing Santorini's tephrostratigraphy: New glass geochemical data and improved marine-terrestrial tephra correlations for the past ~360 kyrs. *Earth Sci. Rev.* **200**, 102964. https://doi.org/10.1016/j.earscirev.2019.102964.

Wulf, S., Kraml., M., Brauer, A., Keller, J., Negendank, J.F.W., 2004. Tephrochronology of the 100 ka lacustrine sediment record of Lago Grande di Monticchio (Southern Italy). *Quat. Int*. **122**, 7-30. https://doi.org/10.1016/j.quaint.2004.01.028.

Wulf, S., Kraml, M., Keller, J., 2008. Towards a detailed tephrostratigraphy in the Central Mediterranean: The last 20,000 yrs record of Lago Grande di Monticchio. J. *Volcanol. Geotherm. Res.* **177**, 118-132. https://doi.org/10.1016/j.jvolgeores.2007.10.009.

Zanchetta, G., Giaccio, B., Bini, M., Sarti, L., 2018. Tephrostratigraphy of Grotta del Cavallo, Southern Italy: insights of the chronology of Middle to Upper Paleolithic transition in the Mediterranean. *Quat. Sci. Rev.* **182**, 65-77. https://doi.org/10.1016/j.quascirev.2017.12.014.

Appendix.

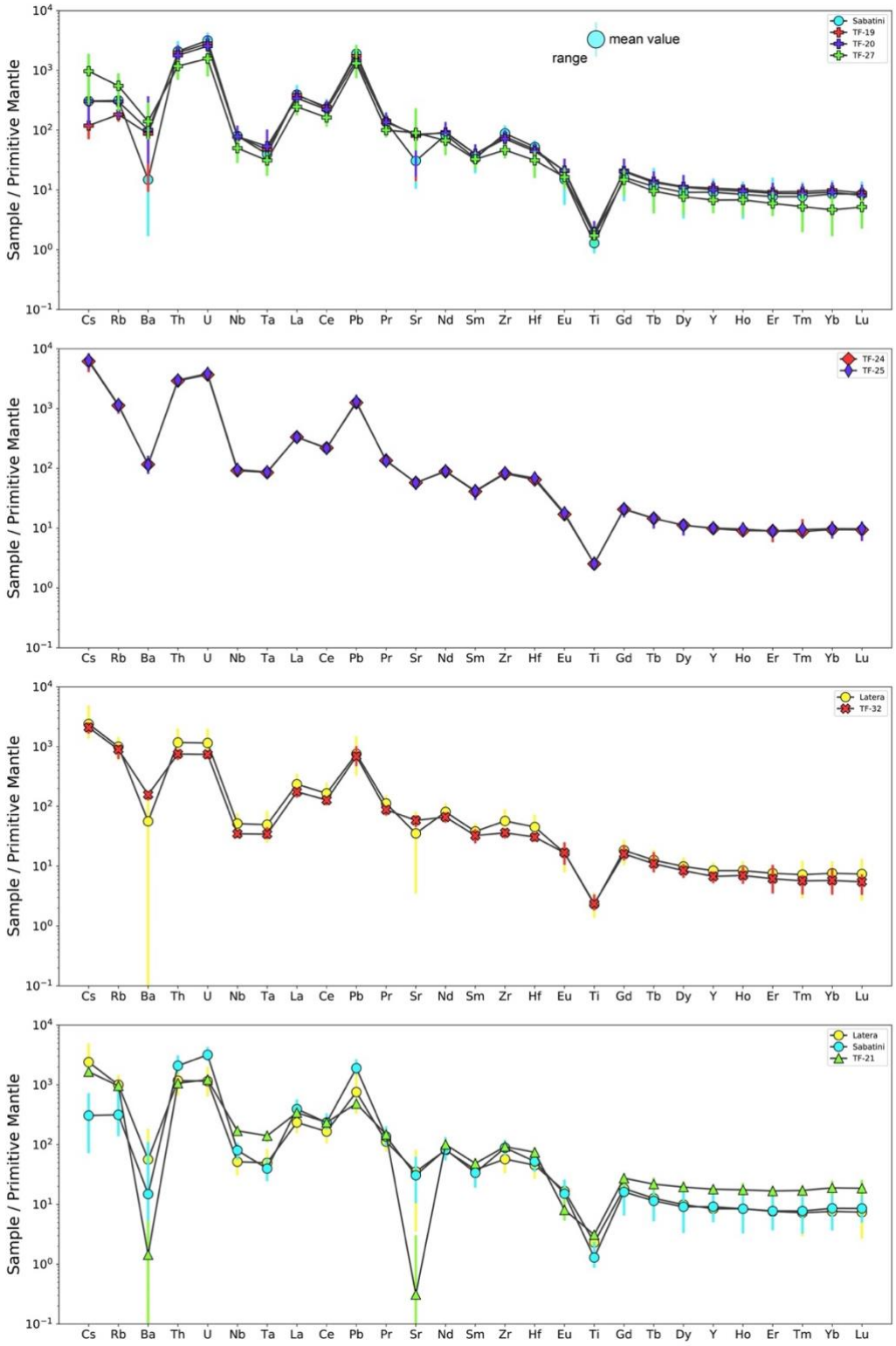

Figure A1. Spider diagrams (normalized to the primitive mantle; McDonough and Sun, 1995) of the investigated Fucino F4-F5 tephra compared with LVC and SVD proximal pyroclastic units.

Table-A1. Major and minor element mean composition (normalised to 100 wt.%), standard deviation (2 s.d.) and number of analyses (n.) for the investigated F4-F5 Fucino tephra, Ohird tephra OH-DP-0725, and proximal LVC, SVD and Vico units.

Tephra	TF-19			TF-20			TF-21			TF-21a			TF-22		
Oxide (wt.%)	Mean	2 s.d.	n.	Mean	2 s.d.	n.	Mean	2 s.d.	n.	Mean	2 s.d.	n.	Mean	2 s.d.	n.
SiO_2	57.11	0.60	19	57.51	1.95	34	63.39	0.75	72	60.32	2.27	15	57.31	3.83	102
TiO_2	0.44	0.20		0.48	0.31		0.63	0.06		0.55	0.13		0.60	0.18	
Al_2O_3	20.50	0.92		20.71	1.17		17.86	0.64		19.26	0.97		18.78	1.19	
FeO_{tot}	3.31	0.56		3.07	1.13		2.73	0.40		2.94	1.25		4.34	2.46	
MnO	0.27	0.10		0.22	0.13		0.28	0.12		0.16	0.19		0.17	0.13	
MgO	0.18	0.08		0.26	0.17		0.32	0.04		0.54	0.33		1.07	1.04	
CaO	3.70	0.76		3.85	1.18		0.96	0.15		2.80	1.07		4.76	3.36	
Na_2O	6.97	1.34		6.11	1.31		7.49	0.77		5.32	0.91		3.44	1.05	
K_2O	7.50	1.14		7.75	2.01		6.28	0.44		7.97	1.42		9.33	3.36	
P_2O_5	0.03	0.03		0.03	0.04		0.05	0.08		0.13	0.14		0.20	0.24	
F	0.80	0.66		0.62	0.72		0.33	0.39		0.20	0.28		0.15	0.41	
Cl	0.31	0.10		0.23	0.12		0.63	0.05		0.44	0.02		0.07	0.04	
SO3	0.10	0.21		0.09	0.14		0.07	0.09		0.05	0.06		0.24	0.15	
Tot*	100	-		100	-		100	-		100	-		100	-	
Na_2O+K_2O	14.47	1.14		13.86	1.63		13.77	0.87		13.30	0.91		12.77	3.23	
K_2O/Na_2O	1.09	0.32		1.29	0.55		0.84	0.11		1.52	0.57		2.78	1.21	
CaO/FeO	1.12	0.20		1.28	0.41		0.36	0.07		0.98	0.45		1.08	0.26	
Tephra	**TF-23**			**TF-24**			**TF-25**			**TF-26**			**TF-27**		
Oxide (wt.%)	**Mean**	**2 s.d.**	**n.**	**Mean**	**2 s.d.**	**n.**	**Mean**	**2 s.d.**	**n.**	**Mean**	**2 s.d.**	**n.**	**Mean**	**2 s.d.**	**n.**
SiO_2	63.32	0.84	42	57.88	1.15	79	58.38	1.04	81	60.23	2.72	61	56.69	2.56	69
TiO_2	0.55	0.12		0.51	0.07		0.52	0.08		0.50	0.18		0.44	0.18	
Al_2O_3	18.46	0.64		19.73	1.05		18.81	0.91		19.20	1.12		20.27	1.46	
FeO_{tot}	2.47	0.61		3.79	0.43		3.81	0.48		3.34	1.34		3.66	1.07	
MnO	0.26	0.12		0.15	0.15		0.14	0.16		0.15	0.14		0.21	0.18	
MgO	0.28	0.09		0.75	0.16		0.78	0.16		0.77	0.71		0.45	0.37	
CaO	0.90	0.22		3.52	0.87		3.64	0.73		2.92	1.73		5.31	1.89	
Na_2O	7.51	0.57		4.39	0.58		4.36	0.54		5.19	0.91		6.06	2.19	
K_2O	6.19	0.47		9.17	0.65		9.44	0.71		7.56	0.93		6.80	3.32	
P_2O_5	0.06	0.08		0.11	0.08		0.11	0.06		0.15	0.18		0.11	0.15	
F	0.32	0.41		0.38	0.53		0.42	0.63		0.14	0.36		0.62	0.75	
Cl	0.58	0.22		0.17	0.04		0.16	0.03		0.43	0.14		0.18	0.07	
SO3	0.07	0.09		0.19	0.14		0.20	0.15		0.18	0.19		0.34	0.63	
Tot	100	-		100	-		100	-		100	-		100	-	
Na_2O+K_2O	13.70	0.66		13.56	0.66		13.81	0.72		12.75	1.39		12.86	2.44	
K_2O/Na_2O	0.83	0.10		2.10	0.37		2.17	0.35		1.47	0.30		1.20	1.04	
CaO/FeO	0.37	0.24		0.93	0.24		0.96	0.18		0.86	0.20		1.46	0.42	

*: this is the total normalized to 100% excluding volatiles (F, Cl, SO3) from the sum.

Table-A1. Continued.

Tephra	TF-28			TF-29			TF-30			TF-31			TF-32		
Oxide (wt.%)	Mean	2 s.d.	n.	Mean	2 s.d.	n.	Mean	2 s.d.	n.	Mean	2 s.d.	n.	Mean	2 s.d.	n.
SiO_2	59.37	2.85	73	60.42	4.86	9	57.87	4.66	24	53.03	10.55	94	57.58	2.86	59
TiO_2	0.43	0.12		0.52	0.38		0.47	0.16		0.73	0.39		0.58	0.15	
Al_2O_3	19.82	1.17		19.06	4.07		19.75	2.46		17.66	2.75		18.40	0.74	
FeO_{tot}	2.95	1.56		3.64	2.50		3.27	1.38		6.17	4.84		4.64	1.54	
MnO	0.14	0.11		0.10	0.22		0.19	0.13		0.15	0.09		0.13	0.07	
MgO	0.47	0.59		0.57	0.72		0.41	0.42		3.14	3.96		1.34	0.80	
CaO	3.26	2.02		5.10	1.88		4.89	2.28		8.10	7.71		5.09	1.93	
Na_2O	4.17	1.54		4.93	2.06		5.94	2.69		2.63	1.93		2.98	0.61	
K_2O	9.31	2.13		5.55	2.09		7.11	2.54		7.96	3.29		8.98	1.35	
P_2O_5	0.09	0.15		0.11	0.18		0.10	0.14		0.43	0.48		0.28	0.21	
F	0.18	0.46		0.43	0.52		0.64	0.67		0.18	0.42		0.12	0.30	
Cl	0.12	0.07		0.08	0.12		0.17	0.13		0.06	0.04		0.07	0.04	
SO3	0.22	0.20		0.13	0.24		0.35	0.58		0.25	0.23		0.35	0.33	
Tot	100	-		100	-		100	-		100	-		100	-	
Na_2O+K_2O	13.48	2.21		10.48	2.03		13.05	2.14		10.59	4.80		11.97	1.67	
K_2O/Na_2O	2.33	1.15		1.23	1.29		1.32	1.18		3.25	1.63		3.04	0.60	
CaO/FeO	1.10	0.28		1.50	0.72		1.50	0.51		1.26	0.46		1.10	0.14	
Tephra	**TF-33**			**TF-35**			**TF-35b**			**TF-37**			**TF-43**		
Oxide (wt.%)	**Mean**	**2 s.d.**	**n.**	**Mean**	**2 s.d.**	**n.**	**Mean**	**2 s.d.**	**n.**	**Mean**	**2 s.d.**	**n.**	**Mean**	**2 s.d.**	**n.**
SiO_2	59.02	1.25	48	62.71	0.97	20	60.24	1.59	3	57.62	8.18	11	61.37	2.00	51
TiO_2	0.49	0.08		0.35	0.08		0.43	0.09		0.56	0.39		0.40	0.15	
Al_2O_3	19.96	0.64		18.83	0.68		19.37	0.05		18.51	1.10		19.34	1.43	
FeO_{tot}	3.07	0.74		2.76	0.31		2.51	0.57		4.41	4.15		2.30	1.26	
MnO	0.14	0.18		0.13	0.15		0.15	0.16		0.09	0.15		0.07	0.13	
MgO	0.57	0.27		0.52	0.10		0.31	0.18		1.46	2.31		0.53	0.61	
CaO	2.84	0.48		2.26	0.26		2.52	0.34		4.69	4.75		2.83	1.13	
Na_2O	3.81	0.84		4.71	0.49		3.94	0.53		3.11	1.60		3.59	1.26	
K_2O	9.99	0.84		7.63	0.44		10.45	1.02		9.23	3.20		9.27	1.71	
P_2O_5	0.10	0.09		0.10	0.06		0.07	0.08		0.32	0.36		0.30	0.41	
F	0.28	0.58		0.13	0.28		0.29	0.23		0.21	0.39		0.11	0.27	
Cl	0.06	0.03		0.30	0.05		0.11	0.03		0.11	0.25		0.04	0.08	
SO3	0.20	0.14		0.03	0.07		0.24	0.19		0.20	0.30		0.14	0.22	
Tot	100	-		100	-		100	-		100	-		100	-	
Na_2O+K_2O	13.80	0.74		12.34	0.44		14.40	0.50		12.34	2.96		12.87	0.99	
K_2O/Na_2O	2.66	0.69		1.63	0.25		2.67	0.62		3.14	1.88		2.68	1.18	
CaO/FeO	0.93	0.17		0.82	0.10		1.01	0.14		1.08	0.40		1.32	0.97	

Table-A1. Continued.

Unit	OH-DP-0725			TR-CR-2			TR-CR-1			Vigna di Valle			Pizzo Prato		
Oxide (wt.%)	Mean	2 s.d.	n.	Mean	2 s.d.	n.	Mean	2 s.d.	n.	Mean	2 s.d.	n.	Mean	2 s.d.	n.
SiO_2	59.38	1.24	10	57.63	0.86	11	57.74	1.03	23	57.45	0.72	11	60.42	0.74	34
TiO_2	0.6	0.09		0.34	0.05		0.26	0.22		0.45	0.07		0.44	0.06	
Al_2O_3	18.92	0.87		20.57	0.43		21.31	1.43		19.70	0.54		18.93	0.29	
FeO_{tot}	3.94	0.81		3.06	0.31		2.37	0.90		3.71	0.84		2.93	0.46	
MnO	0.18	0.07		0.28	0.10		0.22	0.10		0.28	0.10		0.17	0.07	
MgO	0.99	0.39		0.22	0.09		0.14	0.13		0.39	0.21		0.47	0.17	
CaO	3.49	0.81		3.45	0.63		2.99	0.99		5.48	0.82		2.94	0.40	
Na_2O	4.37	0.33		6.87	0.66		6.97	0.97		6.09	0.84		3.34	0.39	
K_2O	7.92	0.44		7.56	0.90		7.99	1.45		6.38	1.19		10.31	0.74	
P_2O_5	0.21	0.09		0.02	0.03		0.02	0.04		0.07	0.07		0.06	0.07	
F	0.18	0.12		0.97	0.34		0.92	0.41		0.76	0.21		0.31	0.25	
Cl	0.46	0.07		0.29	0.09		0.29	0.08		0.18	0.03		0.09	0.04	
SO3	0.11	0.08		0.09	0.08		0.07	0.08		0.26	0.09		0.14	0.09	
Tot	100	-		100	-		100	-		100	-		100	-	
Na_2O+K_2O	12.29	0.65		14.44	0.72		14.95	1.92		12.47	1.36		13.64	0.74	
K_2O/Na_2O	1.81	0.13		1.10	0.20		1.15	0.24		1.05	0.26		3.10	0.49	
CaO/FeO	0.89	0.06		1.13	0.18		1.28	0.42		1.49	0.19		1.01	0.09	
Unit	Farine Formation			Pitigliano			Onano			Grotte di castro			Sorano		
Oxide (wt.%)	Mean	2 s.d.	n.	Mean	2 s.d.	n.	Mean	2 s.d.	n.	Mean	2 s.d.	n.	Mean	2 s.d.	n.
SiO_2	60.80	0.43	16	60.47	0.80	67	54.15	3.52	115	51.84	14.22	49	60.85	1.89	50
TiO_2	0.43	0.06		0.51	0.05		0.71	0.17		0.85	0.75		0.41	0.11	
Al_2O_3	19.15	0.18		19.35	0.58		18.69	0.61		17.15	3.51		19.53	0.76	
FeO_{tot}	2.75	0.19		2.48	0.28		5.73	1.81		7.12	7.01		2.28	0.85	
MnO	0.17	0.06		0.16	0.08		0.17	0.05		0.18	0.08		0.16	0.07	
MgO	0.42	0.06		0.34	0.08		2.07	1.13		3.62	5.42		0.27	0.38	
CaO	2.28	0.16		2.72	0.64		6.67	2.45		9.76	11.52		2.66	1.07	
Na_2O	5.42	0.37		3.81	0.65		2.84	1.34		2.40	1.31		4.20	0.94	
K_2O	8.55	0.53		10.13	0.78		8.54	2.85		6.59	6.65		9.62	0.61	
P_2O_5	0.06	0.05		0.04	0.05		0.45	0.25		0.48	0.66		0.03	0.08	
F	0.15	0.18		0.12	0.35		0.04	0.22		0.07	0.25		0.27	0.42	
Cl	0.23	0.05		0.08	0.06		0.06	0.03		0.06	0.04		0.10	0.04	
SO3	0.13	0.07		0.16	0.07		0.42	0.27		0.11	0.21		0.16	0.12	
Tot	100	-		100	-		100	-		100	-		100	-	
Na_2O+K_2O	13.96	0.42		13.94	0.89		11.38	2.16		8.99	7.87		13.82	0.77	
K_2O/Na_2O	1.58	0.18		2.68	0.53		3.13	1.13		2.60	1.53		2.34	0.81	
CaO/FeO	0.83	0.09		1.10	0.23		1.16	0.13		1.29	0.51		1.17	0.21	

Table-A1. Continued.

Unit	Sovana			Farnese			Stenzano			Canino		
Oxide (wt.%)	Mean	2 s.d.	n.	Mean	2 s.d.	n.	Mean	2 s.d.	n.	Mean	2 s.d.	n.
SiO_2	60.78	0.92	24	59.61	1.25	57	65.40	2.09	28	63.02	1.90	124
TiO_2	0.52	0.07		0.51	0.12		0.32	0.27		0.34	0.10	
Al_2O_3	19.04	0.41		19.24	1.02		17.87	1.14		18.28	0.44	
FeO_{tot}	2.78	0.73		2.85	0.44		1.83	0.72		2.37	0.88	
MnO	0.18	0.09		0.15	0.07		0.17	0.12		0.17	0.10	
MgO	0.42	0.28		0.30	0.15		0.22	0.22		0.39	0.35	
CaO	2.56	0.53		3.24	0.56		1.76	0.54		2.31	0.74	
Na_2O	4.11	1.07		3.97	0.90		4.95	0.97		3.96	1.48	
K_2O	9.55	0.77		10.10	0.77		7.47	1.51		9.09	1.59	
P_2O_5	0.06	0.09		0.04	0.05		0.02	0.03		0.07	0.10	
F	0.27	0.18		0.12	0.31		0.33	0.52		0.21	0.25	
Cl	0.06	0.05		0.07	0.04		0.16	0.14		0.12	0.09	
SO3	0.19	0.11		0.22	0.22		0.08	0.14		0.14	0.13	
Tot	100	-		100	-		100	-		100	-	
Na_2O+K_2O	13.66	0.53		14.07	0.66		12.42	0.72		13.06	0.46	
K_2O/Na_2O	2.38	0.84		2.58	0.67		1.54	0.60		2.44	1.59	
CaO/FeO	0.93	0.10		1.14	0.20		0.99	0.43		0.99	0.25	

Table-A2. Trace elements mean composition, standard deviation (2 s.d.) and number of analysis (n.) for the selected F4-F5 Fucino tephra and proximal LVC and SVD units.

Tephra/Unit	TF-19			TF-20			TF-21			TF-24			TF-25		
TE (ppm)	Mean	2 s.d.	n.	Mean	2 s.d.	n.	Mean	2 s.d.	n.	Mean	2 s.d.	n.	Mean	2 s.d.	n.
Li	179.7	62.5	11	163.2	48.4	17	74.6	16.6	18	314.3	59.1	18	332.2	50.3	29
Be	38.8	8.9		36.1	10.5		21.8	6.0		39.2	10.9		38.0	6.5	
V	125.3	34.7		121.7	54.3		35.6	5.4		113.1	14.3		116.0	18.1	
Ga	25.1	4.1		23.2	4.9		28.4	4.5		23.9	2.8		24.4	2.8	
Rb	109.8	26.9		180.5	98.0		576.1	32.2		675.1	131.6		693.0	134.5	
Sr	1610.5	2205.9		1702.1	1453.8		6.2	26.3		1145.8	208.4		1146.8	222.4	
Y	46.5	6.3		43.4	14.8		77.3	14.2		42.6	7.1		43.2	4.8	
Zr	812.0	157.9		751.1	196.9		974.2	155.0		857.8	137.8		880.8	103.2	
Nb	51.7	9.7		51.3	17.8		111.9	11.0		60.6	6.5		62.9	5.2	
Cs	2.5	1.2		6.4	5.2		34.8	4.8		129.7	33.0		134.5	27.4	
Ba	575.5	997.9		668.9	1158.2		9.5	17.2		767.0	146.6		755.6	190.2	
La	249.1	25.7		222.3	65.4		221.8	36.7		216.1	33.4		215.2	17.8	
Ce	409.5	38.1		372.2	117.6		394.9	53.3		367.6	46.5		362.3	29.4	
Pr	36.5	5.4		34.4	12.7		37.4	5.7		34.3	6.1		33.8	3.2	
Nd	115.8	21.8		111.7	44.7		125.5	23.4		111.0	15.3		112.7	12.3	
Sm	16.2	4.1		16.3	6.7		19.7	3.7		16.7	2.9		17.0	3.2	
Eu	3.2	1.1		3.2	1.3		1.2	0.4		2.6	0.6		2.7	0.4	
Gd	11.4	3.4		11.0	5.9		14.9	2.9		11.2	2.2		11.4	2.1	
Tb	1.4	0.4		1.3	0.7		2.2	0.5		1.4	0.3		1.4	0.3	
Dy	7.6	2.0		7.5	3.4		13.1	2.5		7.6	2.0		7.5	1.6	
Ho	1.5	0.3		1.4	0.5		2.6	0.6		1.4	0.3		1.4	0.2	
Er	4.1	0.9		3.8	1.6		7.4	1.5		3.9	1.1		3.9	0.7	
Tm	0.6	0.1		0.6	0.2		1.2	0.2		0.6	0.2		0.6	0.1	
Yb	4.4	1.0		4.0	1.5		8.4	2.2		4.2	1.2		4.3	1.1	
Lu	0.6	0.1		0.5	0.2		1.3	0.4		0.6	0.1		0.7	0.2	
Hf	13.5	2.7		12.5	3.9		21.0	4.1		18.3	3.6		19.4	3.0	
Ta	1.7	0.7		2.0	1.2		5.2	1.0		3.2	0.5		3.2	0.5	
Pb	260.2	73.6		220.2	68.7		72.8	13.7		188.6	18.4		195.1	38.6	
Th	157.3	18.4		142.0	46.1		84.7	13.6		232.0	39.9		237.5	27.2	
U	57.0	13.9		51.8	17.8		24.8	3.3		74.9	8.9		77.9	5.6	

Table-A2. Continued.

Tephra/Unit	TF-27			TF-32			Pitigliano Fall			Onano Lower			Grotte di Castro Upper		
TE (ppm)	**Mean**	**2 s.d.**	**n.**	**Mean**	**2 s.d.**	**n.**	**Mean**	**2 s.d.**	**n.**	**Mean**	**2 s.d.**	**n.**	**Mean**	**2 s.d.**	**n.**
Li	112.3	45.9	14	83.3	12.0	18	108.4	12.0	20	71.5	14.2	17	84.0	33.9	17
Be	22.7	11.0		13.8	2.7		26.9	6.2		17.5	4.9		18.6	5.8	
V	122.0	42.2		111.9	67.0		79.1	8.4		166.4	46.6		95.4	24.1	
Ga	25.4	5.1		20.8	3.3		21.9	3.3		19.3	2.4		20.0	3.6	
Rb	331.5	184.8		538.3	128.0		512.1	37.2		516.9	90.1		675.4	163.3	
Sr	1797.9	1947.3		1163.8	224.9		525.7	106.8		1336.5	263.8		1071.5	445.7	
Y	29.1	9.9		29.1	5.0		41.9	5.3		32.8	3.8		32.2	8.0	
Zr	488.9	145.8		381.5	62.4		679.4	83.9		398.0	51.9		480.5	125.4	
Nb	33.0	11.6		23.0	3.0		44.8	4.7		22.4	2.5		26.0	6.7	
Cs	20.4	15.2		44.0	8.5		35.9	3.1		34.3	4.2		56.9	15.0	
Ba	924.1	764.9		1039.1	129.1		41.6	40.9		968.7	162.2		784.2	531.8	
La	159.7	44.8		114.3	15.7		178.1	20.4		119.2	14.2		132.6	49.7	
Ce	273.0	74.2		214.2	22.8		331.7	33.7		228.7	25.3		225.3	56.8	
Pr	25.5	5.9		22.4	3.7		33.4	3.8		24.9	3.2		25.2	7.7	
Nd	83.8	27.2		83.1	12.4		117.5	14.4		91.8	11.7		91.0	29.7	
Sm	13.3	3.7		13.2	2.6		17.7	2.8		15.4	2.7		14.3	4.6	
Eu	2.5	1.0		2.6	0.9		3.0	0.6		2.9	0.6		2.6	0.8	
Gd	8.0	3.5		8.7	2.1		11.8	2.0		9.7	1.2		9.4	3.6	
Tb	0.9	0.4		1.1	0.4		1.4	0.2		1.2	0.3		1.2	0.4	
Dy	5.2	2.7		5.7	1.5		7.9	1.4		6.2	1.2		6.2	1.9	
Ho	1.0	0.4		1.0	0.3		1.5	0.3		1.1	0.3		1.2	0.3	
Er	2.6	1.1		2.7	1.1		3.7	0.8		3.1	0.8		3.2	1.4	
Tm	0.4	0.2		0.4	0.1		0.6	0.2		0.4	0.1		0.4	0.1	
Yb	2.1	1.6		2.6	1.1		3.7	1.3		2.8	0.8		3.0	1.5	
Lu	0.4	0.2		0.4	0.1		0.6	0.2		0.4	0.2		0.4	0.2	
Hf	8.9	3.8		8.7	1.4		14.0	2.2		9.0	1.8		10.5	3.1	
Ta	1.2	0.4		1.3	0.3		2.4	0.5		1.2	0.3		1.5	0.5	
Pb	196.9	137.8		103.5	42.9		133.1	20.8		71.0	15.2		88.1	23.6	
Th	93.8	31.7		60.0	11.1		112.1	14.9		64.2	10.7		78.9	27.4	
U	32.0	12.3		15.1	2.7		29.5	3.2		15.7	2.2		18.9	6.5	

Table-A2. Continued.

Tephra/Unit	Sorano Base			Farnese Fall			Canino Fall-C			TR-CR-2			TR-CR-1		
TE (ppm)	**Mean**	**2 s.d.**	**n.**	**Mean**	**2 s.d.**	**n.**	**Mean**	**2 s.d.**	**n.**	**Mean**	**2 s.d.**	**n.**	**Mean**	**2 s.d.**	**n.**
Li	154.2	29.7	16	91.5	26.2	17	108.5	32.8	15	203.5	46.4	12	209.7	41.3	18
Be	30.3	6.4		22.6	6.8		19.1	6.8		44.4	12.8		43.3	8.9	
V	65.2	27.1		90.9	26.2		48.2	11.4		115.9	40.8		81.0	32.7	
Ga	25.4	3.1		20.9	4.5		20.8	4.8		27.5	3.3		28.0	5.4	
Rb	727.0	82.9		541.5	118.8		652.6	71.1		165.1	126.2		204.8	162.5	
Sr	128.7	96.4		632.6	224.9		504.6	181.2		622.5	554.2		603.6	568.6	
Y	39.3	4.6		34.1	8.7		37.0	6.2		47.8	15.4		33.8	20.2	
Zr	812.0	99.8		655.6	143.8		571.4	58.7		955.2	276.7		913.4	171.2	
Nb	43.1	1.6		37.7	6.1		28.2	4.2		52.9	15.4		52.8	10.0	
Cs	77.6	13.7		40.9	26.2		61.8	9.6		4.2	5.9		8.0	7.6	
Ba	46.1	116.5		184.4	175.8		210.2	141.6		175.4	392.7		43.6	74.9	
La	196.7	24.6		152.4	35.9		130.5	21.4		271.2	67.2		244.6	48.3	
Ce	342.4	46.2		282.4	73.6		243.8	43.1		423.6	109.3		372.4	80.1	
Pr	32.1	4.9		28.7	8.1		26.1	4.4		38.3	10.2		32.2	9.7	
Nd	105.2	13.8		102.4	31.4		95.1	15.9		119.4	37.2		93.8	32.4	
Sm	14.4	2.7		15.2	5.0		15.6	3.4		16.2	5.2		12.1	5.9	
Eu	1.9	0.6		2.5	0.7		2.4	0.6		2.8	1.0		2.0	1.4	
Gd	8.8	2.5		9.8	3.9		10.3	2.6		11.3	6.0		7.2	5.1	
Tb	1.2	0.4		1.2	0.5		1.3	0.4		1.5	0.7		0.9	0.5	
Dy	6.5	1.7		6.2	1.3		7.0	1.5		7.9	3.0		5.0	3.7	
Ho	1.3	0.2		1.2	0.3		1.3	0.3		1.6	0.5		1.0	0.7	
Er	3.6	0.7		3.1	0.8		3.3	0.9		4.2	2.3		2.9	2.2	
Tm	0.6	0.2		0.5	0.2		0.5	0.2		0.6	0.3		0.5	0.3	
Yb	4.0	1.0		3.3	1.3		3.3	1.0		4.7	1.9		3.2	2.1	
Lu	0.6	0.2		0.5	0.2		0.5	0.2		0.7	0.3		0.5	0.3	
Hf	17.2	2.1		13.2	3.9		13.2	2.0		15.5	4.6		14.4	3.4	
Ta	1.9	0.3		2.0	0.5		1.8	0.4		1.5	0.7		1.5	0.3	
Pb	159.8	33.7		129.8	43.3		96.8	33.4		272.5	56.0		294.6	72.7	
Th	137.4	19.4		91.5	28.0		73.0	15.0		176.9	44.9		158.5	39.9	
U	35.1	4.3		22.5	6.8		17.5	4.6		64.2	15.0		64.6	10.8	

Table-A3. $^{87}Sr/^{86}Sr$, $^{143}Nd/^{144}Nd$, and $^{40}Ar/^{39}Ar$ values of the investigated Fucino tephra and proximal SVD and LVC pyroclastic units.

Tephra/Unit	$^{87}Sr/^{86}Sr$		$^{143}Nd/^{144}Nd$		$^{40}Ar/^{39}Ar$ (ka)	
	Value	Error	Value	Error	Value	Error
TF-22	0.710375 0.710378 0.710379	± 0.00002 ± 0.00002 ± 0.00002	0.512116	± 0.00002	194.5	± 2.0
TF-26	0.706233 0.706352 0.706566	± 0.00002 ± 0.00002 ± 0.00002	0.512551	± 0.00002	-	-
TF-27	0.710132 0.710142 0.710270	± 0.00002 ± 0.00002 ± 0.00002	0.512098	± 0.00002	205.1	± 1.4
TF-32	0.710358 0.710438 0.710504 0.710552	± 0.00002 ± 0.00002 ± 0.00002 ± 0.00002	0.512118	± 0.00002	224.9	± 1.0
TR-CR-1	0.710242 0.710263	± 0.00002 ± 0.00002	-	-	-	-
Pitigliano	0.710385 0.710392	± 0.00002 ± 0.00002	-	-	177.7	± 0.4
Sovana	-	-	-	-	225.8	± 0.7
Farnese	0.710081 0.710292	± 0.00002 ± 0.00002	0.512118	± 0.00002	235.6	± 0.6
Canino (Fall-C)	0.710765 0.710788 0.710789	± 0.00002 ± 0.00002 ± 0.00002	0.512105 0.512113	± 0.00002 ± 0.00002	253.1	± 0.8
Canino (Fall-B)	-	-	-	-	253.8	± 0.8

Chapter V - Linking the Mediterranean MIS 5 tephra markers to the Campi Flegrei 109-92 ka explosive activity (southern Italy) and refining the chronology of the MIS 5c-d millennial-scale climate variability

In this study, proximal to medial-distal sub-aerial occurrences of tephra fall deposits from the Campanian region are presented. Pyroclastic units have been characterised in terms of their major, minor (EPMA-WDS), trace (LA-ICP-MS) elements glass composition, Sr and Nd isotopic ratios, and by $^{40}Ar/^{39}Ar$ dating. Results revealed that these fall deposits, emplaced in the narrow time interval of ~90-110 ka, show all Campi Flegrei-like compositions. Data from this study allowed for the first time to backtrack the proximal to medial-distal occurrences of the C-22, TM-24a, TM-24b, X-5, and X-6 tephra layers. These represent key marker horizons in the Mediterranean region during the MIS 5 period and, although associated to the Campanian Volcanic Zone (CVZ) based on their Campanian-like composition, their proximal counterparts were never documented in near-vent deposits. Thus, results from this study represent an important step forward in the development of the Mediterranean tephra lattice and provide a full reference geochemical dataset for future investigations. Furthermore, results from this study set the basis for reassessing the Campi Flegrei volcanic history, and the related hazard, on a long-term perspective. Finally, the new high-precise $^{40}Ar/^{39}Ar$ dating of these units provide new fundamental temporal constraints for refining and consolidating, on a larger regional scale, the timing and duration of the millennial and sub-millennial scale climatic oscillations of the MIS 5d-c period. This paper was submitted to *Global and Planetary Change* journal (GLOPLACHA-D-21-00513; accepted for publication following minor revisions) and was prepared with the contribution of: L. Monaco (field investigations, EPMA data acquisition and elaboration, data interpretation, manuscript writing and revision, First author); B. Giaccio, D.M. Palladino, R. Sulpizio, G. Zanchetta, M. di Vito, R. Isaia, P. Petrosino, I. Arienzo, M. D'Antonio, S. Conticelli (field investigations, manuscript writing and revision, Sr-Nd isotope data acquisition); G. Sottili, A. Fabbrizio, A. Costa (manuscript writing and revision); S. Nomade, A. Pereira ($^{40}Ar/^{39}Ar$ age determination); P.G. Albert (LA-ICP-MS data acquisition).

ABSTRACT

Explosive activity preceding the ~40 ka Campanian Ignimbrite (CI) eruption in the Neapolitan volcanic area, Southern Italy, has long been speculated based on the occurrences of widespread tephra layers, with a Campanian geochemical signature, such as the C-22, X-5, and X-6, preserved in Mediterranean Marine Isotope Stage (MIS) 5 sedimentary records. However, previous studies of pre-CI pyroclastic units occurring in close proximity of the Neapolitan volcanoes, including Campi Flegrei, Somma-Vesuvius, Ischia and Procida islands, did not allow a conclusive identification of the near-source equivalents of these tephra markers. Here we present a comprehensive characterisation of four pyroclastic units from the Campanian Plain, comprising major and trace element glass compositions, Sr-Nd isotopes and $^{40}Ar/^{39}Ar$ dating. Our data allowed the identification of the medial equivalents of the MIS 5 tephra markers, including the widespread C-22, X-5, and X-6 tephra, and their assignment to previously undocumented Campi Flegrei activity between 109-92 ka. In addition to substantially extending Campi Flegrei explosive activity deeper in time, and thus providing the basis for a revaluation of its history, our findings provide new precise radioisotopic dating to better constrain the chronology of the millennial scale climatic oscillations of the MIS 5c-d in the Mediterranean area and possibly on a larger scale.

1. *Introduction*

Near-vent volcanic successions provide fundamental information for reconstructing the eruption history and dynamics of volcanoes. Proximal exposures, however, often provide only fragmentary records of the past activity of a volcanic system, since deposits of older explosive events can be eroded, not preserved or, more commonly, covered by products of younger eruptions. In contrast, tephra layers preserved in sedimentary successions located far away from the volcanic source and characterised by a continuous sediment accumulation history, can provide detailed and undisturbed records of explosive eruptions for a given volcano, including events that are poorly represented or missing in near-vent sections (e.g., Paterne et al., 1988; Monaco et al., 2021).

This also applies to the Neapolitan volcanic area (Campania, southern Italy), including Campi Flegrei, Ischia, Procida and Somma-Vesuvius (Fig. 1b), where the intense Late Pleistocene explosive activity (e.g., Peccerillo, 2017 and reference therein) made the earliest pyroclastic products barely accessible in proximal settings. However, these activities are instead documented in distal sedimentary archives. Indeed, since the first distal marine discoveries of Keller et al. (1978), several occurrences of widespread tephra layers with a Campanian geochemical signature embedded within Marine Isotope Stage 5 (MIS 5) sedimentary successions suggested the occurrence of a major explosive activity that, however, had never been documented in proximal sections of the Neapolitan volcanoes. Among them, the C-22 (Paterne et al., 1986), X-5 and X-6 (Keller et al., 1978) tephra layers have been traced widely across the central Mediterranean area in several terrestrial (e.g., Wulf et al., 2004, 2012, 2018; Marciano et al., 2008; Sulpizio et al., 2010; Giaccio et al., 2012, 2017a; Lucchi et al., 2013; Regattieri et al., 2015; Donato et al., 2016; Leicher et al., 2016; Zanchetta et al., 2018; Petrosino et al., 2019) and marine (e.g., Paterne et al., 1986, 1988, 2008; Bourne et al., 2010, 2015; Insinga et al., 2014; Iorio et al., 2014; Petrosino et al., 2016) sedimentary archives. Moreover, at least two additional tephras, occurring between the C-22 and X-5 markers, with a similar Neapolitan geochemical signature, are also found in Mediterranean MIS 5 records (Giaccio et al., 2012, 2017a; Wulf et al., 2012; Leicher et al., 2016; Petrosino et al., 2016; Table 1).

Over the last decades, these widespread tephra layers have been used as remarkable marker horizons for dating, synchronizing, and correlating MIS 5 Mediterranean sedimentary successions,

the chronologies of which would have otherwise been poorly determined. With this regard, tephra markers from Neapolitan volcanoes arise as pivotal stratigraphic and chronological tools for paleoclimatic and archaeological investigations at the regional scale (e.g., Wulf et al., 2012, 2018; Bourne et al., 2015; Regattieri et al., 2015; Leicher et al., 2016; Petrosino et al., 2016; Giaccio et al., 2017a; Zanchetta et al., 2018).

Despite their great chronological importance, the lack of near-vent counterparts has left the specific volcanic source of these marker layers still undetermined, leading authors to ascribe them either to an unspecified Campanian volcanism (e.g., Wulf et al., 2012), or to an undefined Neapolitan volcanic area (e.g., Giaccio et al., 2017a) or to the so-called "Campanian Volcanic Zone" (CVZ; Rolandi et al., 2003) (e.g., Munno and Petrosino, 2007). Furthermore, in terms of tephrochronological applications, precise and accurate radioisotopic ages are currently available only for two of these markers (i.e., X-5 and X-6), and their full geochemical characterization (i.e., major, trace elements, and Sr-Nd composition) in near-vent outcrops is still pending. Such remaining uncertainties on their origins and incompleteness of their geochronological and geochemical characterization, prevent their use for any volcanological purposes and limit their tephrochronological potential.

In order to fill the knowledge gap about these tephra markers and exploit their full potential for both volcanological and tephrochronological perspectives, we acquired stratigraphic, geochemical, and geochronological data for five medial-distal (30-60 km from the vent) pyroclastic units, preceding the Campanian Ignimbrite (CI) eruption, outcropping around the eastern rim of the Campanian Plain (Fig. 1b). Four of these units (Maddaloni, Montemaoro, Cancello and Santa Lucia; Fig. 1b) were previously described (Di Vito et al., 2008), while a fifth one (i.e., Triflisco) is recognised as a distinct, younger event in this study (Fig. 1b). The new chemical, isotopic and geochronological data acquired in this study allowed confidently to correlate the five medial-distal fall units to the widespread X-6, X-5, TM-24b/POP-2a, TM-24a/POP2 and C-22 marker tephra (Table 1), attributing them to the 109-92 ka Campi Flegrei explosive activity. Our findings thus extend back in time the explosive history of the Campi Flegrei volcanic field and provide new precise dating for refining the chronology of the millennial-scale climatic oscillations of the MIS 5c-d in the Mediterranean area.

Table 1. Main Mediterranean tephrostratigraphic records documenting the occurrence of the MIS 5 Neapolitan-like tephra.

Site/area	Ionian Sea	Tyrrhenian Sea	Lago Grande di Monticchio	Sulmona Basin	Fucino Basin
Reference	Keller et al. (1978)	Paterne et al. (1986, 1988); Petrosino et al. (2016)	Wulf et al. (2004, 2012)	Giaccio et al. (2012); Regattieri et al. (2015, 2017)	Giaccio et al. (2017a)
MIS 5 tephra markers		C-22	TM-23-11	POP-1	TF-10
		CET1-crypto 12/14	TM-24a	POP-2	
		CET1-crypto 15	TM-24b	POP-2A	TF-11
	X-5	C-27	TM-25	POP-3	TF-12
	X-6	C-31	TM-27	POP-4	TF-13

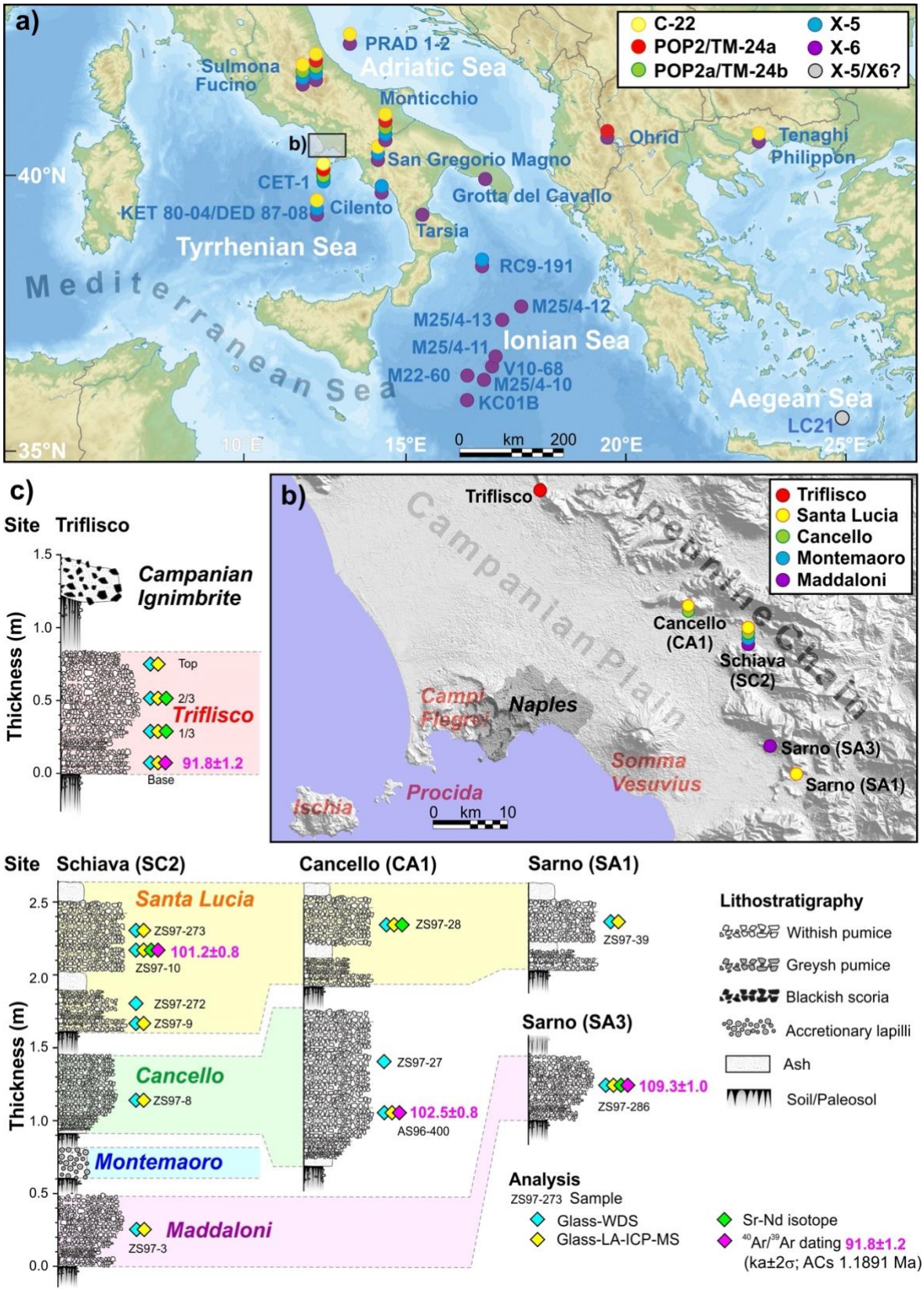
a)
C-22
POP2/TM-24a
POP2a/TM-24b
X-5
X-6
X-5/X6?
PRAD 1-2
Sulmona
Fucino
Adriatic Sea
Monticchio
b)
Ohrid
Tenaghi
Philippon
San Gregorio Magno
40°N
CET-1
Grotta del Cavallo
KET 80-04/DED 87-08
Cilento
Tarsia
Tyrrhenian Sea
RC9-191
M25/4-12
M25/4-13
Ionian Sea
M25/4-11
V10-68
M22-60
M25/4-10
KC01B
Aegean Sea
LC21
35°N
10°E
15°E
0 km 200
20°E
25°E
c)
Site Triflisco
Campanian Ignimbrite
Thickness (m)
Top
2/3
Triflisco
1/3
91.8±1.2
Base
b)
Triflisco
Santa Lucia
Cancello
Montemaoro
Maddaloni
Campanian Plain
Apennine Chain
Cancello (CA1)
Schiava (SC2)
Campi Flegrei
Naples
Somma Vesuvius
Sarno (SA3)
Sarno (SA1)
Procida
Ischia
0 km 10
Site Schiava (SC2)
Cancello (CA1)
Sarno (SA1)
Santa Lucia
ZS97-273
101.2±0.8
ZS97-10
ZS97-272
ZS97-9
ZS97-28
ZS97-39
Cancello
ZS97-8
ZS97-27
102.5±0.8
AS96-400
Sarno (SA3)
109.3±1.0
ZS97-286
Montemaoro
Maddaloni
ZS97-3
Lithostratigraphy
Withish pumice
Greysh pumice
Blackish scoria
Accretionary lapilli
Ash
Soil/Paleosol
Analysis
ZS97-273 Sample
Glass-WDS
Glass-LA-ICP-MS
Sr-Nd isotope
40Ar/39Ar dating 91.8±1.2
(ka±2σ; ACs 1.1891 Ma)

Figure 1. Reference maps and stratigraphic logs of the investigated sections. a) Central Mediterranean sedimentary successions containing the MIS 5 tephra markers investigated in this study. b) Digital Elevation Map (DEM) of the Campanian Plain with location of the Neapolitan volcanoes and the investigated pyroclastic successions (Cancello-SEMAC Quarry, CA1; Schiava-Masseria Montemaoro Quarry, SC2; Sarno-Tre Valloni, SA1; Sarno-Pian della Colla, SA3). c) Stratigraphic logs of the investigated pyroclastic units showing the distribution of the analysed samples and the type of the performed analysis.

2. Geological setting: The Neapolitan volcanoes

The Neapolitan volcanoes comprise Campi Flegrei, Ischia and Procida islands and Somma-Vesuvius (Fig. 1). The Campi Flegrei volcanic field was the site of the most intense activity among the four Neapolitan volcanoes, as well as in the whole Mediterranean area. Three main eruptions occurred in this volcanic area, i.e., the Campanian Ignimbrite (CI; 39.85 ± 0.14 ka; Giaccio et al., 2017b), the Masseria del Monte Tuff (MdMT; 29.3 ± 0.7 ka; Albert et al., 2015, 2019), and the Neapolitan Yellow Tuff (NYT; 14.5 ± 0.4 ka; Deino et al., 2004; Galli et al., 2017) caldera-forming eruptions. Overall, while there is quite satisfactory knowledge on the activity occurred in-between and after these three main events, especially that following the NYT (e.g., Smith et al., 2011), the eruptive history preceding the CI is still poorly resolved, being documented only by deposits sporadically exposed outside the caldera and dated back to ~80 ka (e.g., Pappalardo et al., 1999; Scarpati et al., 2013). Far from the Campi Flegrei volcanic area, several pyroclastic units documenting explosive activity in the Campania region can be dated as back as 290 ka (De Vivo et al., 2001; Rolandi et al., 2003). This older activity is however referred to the so-called Campanian Volcanic Zone (Rolandi et al., 2003), i.e., a hypothesized diffuse, regional volcanism not related to the present Campi Flegrei source area.

Volcanic activity at Ischia Island, off the Naples gulf (Fig. 1b), is documented as back as 150 ka, which is the age of the oldest exposed deposits, and up to historical times (e.g., Poli et al., 1987). The activity of Ischia is subdivided in five stages (i.e., >150-75 ka; 75-55 ka; 55-33 ka; 28-12 ka; 12 ka-1302 CE), characterised by different eruptive styles and types of products (e.g., Poli et al., 1987; Brown et al., 2008). The third stage of activity (55-33 ka) included several explosive events, following the largest 55 ka Monte Epomeo Green Tuff eruption (MEGT; Poli et al., 1987), recognized in the

Mediterranean region as the Y-7 tephra marker horizon (e.g., Tomlinson et al., 2014), although this attribution has been recently questioned (D'Antonio et al., 2021).

The Island of Procida, located between Ischia Island and Campi Flegrei (Fig. 1b), was active over a period of ~60 kyr, between ~80 ka and 23,624 ± 330 cal yr BP (e.g., De Astis et al., 2004; Morabito et al., 2014). Its activity originated from five eruptive centres, i.e, Vivara, Terra Murata, Pozzo Vecchio, Fiumicello, and Solchiaro (Rosi et al., 1988a, 1988b) and is documented by pyroclastic deposits and lava dome interbedded with Campi Flegrei and Ischia units, which acts as stratigraphic, chronological markers (e.g., Morabito et al., 2014).

The Somma-Vesuvius stratovolcano, east of the Naples metropolitan area (Fig. 1b), has completely grown on the products of the CI eruption (e.g., Santacroce and Sbrana, 2003), and thus it is younger than 40 ka. Its activity is subdivided in three main stages: (i) the pre-Mercato eruption stage (ca. 35-9 ka), (ii) the stage between Mercato and the infamous AD 79 Pompeii eruption (ca. 9 ka-79 CE) and (iii) the stage following the Pompeii eruption until present (i.e., last historical eruption of 1944 CE). These three stages differ from one another in terms of either the frequency of the related inter-Plinian eruptive episodes (e.g., Andronico and Cioni, 2002) or the silica undersaturation degree, both increasing over the time (Santacroce et al., 2008).

3. Methods

3.1. Sample selection

For the present study, we used samples collected from 4 eruptive units out of the 14 pre-CI eruption deposits recognised by Di Vito et al. (2008) in the Campanian Plain (Fig. 1b). They are, from bottom to top, SC2-a (hereafter Maddaloni), SC2-b (hereafter Montemaoro), CA1-a (hereafter Cancello), and Santa Lucia (Table 2; Fig. 1c). However, new analysis for the Montemaoro unit was not possible due to unavailability of the sample previously collected by Di Vito et al. (2008) and the inaccessibility of the outcrop during the new field investigations. The list of the investigated units is integrated with the fall deposit outcropping near the Triflisco village, at the edge of the Campanian Plain, here labelled Triflisco (Fig. 1b-c). Moreover, the isotopic characterisation has been performed

also on samples CIL1 and CIL2 from the Cilento Coast being representative for the X5 and X6 stratigraphic markers (Giaccio et al., 2012).

Table 1. Location and data summary of the investigated units.

Units	Locality	Sample source	Coordinates	Sample/sub-units	Analysis			
					Major elements (EMPA)	Trace elements (LA-ICP-MS)	Sr-Nd isotopes	$^{40}Ar/^{39}Ar$ age
Triflisco	Triflisco	This study	41°08'14'' N 14°15'12'' E	TRIF-Top	Y	Y	-	-
				TRIF-2/3	Y	Y	Y	-
				TRIF-1/3	Y	Y	Y	-
				TRIF-Base	Y	Y	-	Y
Santa Lucia (Santa Lucia)	Schiava, Masseria Montemaoro Quarry (SC2)	Di Vito et al. (2008)	40°56'39'' N 14°33'56'' E	ZS97-9	Y	Y	-	-
				ZS97-10	Y	Y	Y	Y
				ZS97-272	Y	Y	-	-
				ZS97-273	Y	Y	-	-
	Cancello, SEMAC Quarry (CA1)		40°59'11'' N 14°29'27'' E	ZS97-28	Y	Y	Y	-
	Sarno, Tre Valloni (SA1)		40°49'03'' N 14°38'06'' E	ZS97-39	Y	Y	-	-
Cancello (CA1-a)	Cancello, SEMAC Quarry (CA1)	Di Vito et al. (2008)	40°59'11'' N 14°29'27'' E	ZS97-27	Y	-	-	-
				AS96-400	Y	Y	-	Y
	Schiava, Masseria Montemaoro Quarry (SC2)		40°56'39'' N 14°33'56'' E	ZS97-8	Y	Y	-	-
Montemaoro (SC2-b)	Schiava, Masseria Montemaoro-Quarry (SC2)	Di Vito et al. (2008)	40°56'39'' N 14°33'56'' E	SC2-b	-	-	-	-
Maddaloni (SC2-a)	Schiava, Masseria Montemaoro-Quarry (SC2)	Di Vito et al. (2008)	40°56'39'' N 14°33'56'' E	ZS97-3	Y	Y	-	-
	Sarno, Pian della Colla (SA3)		40°48'44'' N 14°39'31'' E	ZS97-286	Y	Y	Y	Y
CIL1	Cilento Cost	Giaccio et al. (2012)	40°03'24''N 15°17'02''E	CIL1	Y[1]	-	Y	-
CIL2				CIL2	Y[1]	-	Y	-

"Y": type of analysis performed on the sample. "-": type analysis not performed on the sample. Literature data source: [1] = Giaccio et al. (2012).

3.2. Volcanic glass characterisation

3.2.1. Sample preparation

The samples selected for the major and trace glass composition (Fig. 1c; Table 2) were wet sieved with tap water through a series of sieves with decreasing mesh openings. All fractions were successively oven-dried at 100°C until completely dry. For major element analysis, selected fractions of 60-250 μm were mounted on 29 x 49 mm glass slides, embedded in epoxy resin, progressively ground to a thickness of 60-100 μm and finally polished to be analysed with the electron microprobe.

For trace element analysis, selected samples were embedded in epoxy resin and successively polished.

3.2.2. Electron probe micro analyser (EPMA)

Glass shards and (micro-)pumice fragments were analysed by single-shard major element chemical analysis using the electron probe micro analyser (EPMA). Analysis was first performed with a Jeol JXA-850F equipped with five wave dispersive spectrometers (WDS), installed at the Institute of Petrology and Structural Geology, Charles University of Prague (Prague, Czech Republic). The machine operated at 15 kV accelerating voltage, 10 nA beam current and 10 μm defocused beam to limit alkali loss. Element counting times were of 20 s for all elements, except for Na, K, and S, for which counting times of 10 s (Na and K) and 30 s (S) were employed respectively. For all measurements, the F content was always below the detection limit of the machine. Standards for calibration were quartz (Si), corundum (Al), rutile (Ti), magnetite (Fe), periclase (Mg), rhodonite (Mn), albite (Na), sanidine (K), diopside (Ca), apatite (P and F), tugtupite (Cl) and anhydrite (S). The secondary standards GOR128-G (Jochum et al., 2006) and CFA47 (Marianelli and Sbrana, 1998) were analysed at the beginning of each microprobe session for a total of one point each to evaluate analysis accuracy.

Further WDS analyses were carried out at the Dipartimento di Scienze della Terra, Università degli Studi di Firenze (Florence, Italy), with a Jeol Superprobe JXA-8230 equipped with five-WDS spectrometers. Operating conditions were set to 15 kV accelerating voltage, 10 nA beam current and 10 μm defocused beam diameter to limit Na mobilisation. Element counting times were 15 s for all elements except for Na (10s), F (20s), S (30s), Mn, P and Cl (40s). Albite (Si and Na), ilmenite (Ti and Fe), plagioclase (Al), bustamite (Mn), olivine (Mg), diopside (Ca), sanidine (K), apatite (P), fluorite (F), tugtupite (Cl) and celestine (S) were used as internal standards. The accuracy of the measurements was assessed using the glass secondary standards GOR128-G, ATHO-G and StHs6/80-G (Jochum et al., 2006), Lipari ID3506 (Kuehn et al., 2011), Scapolite NMNH, and CFA47 (Marianelli and Sbrana, 1998).

For both analytical facilities, the ZAF method was used for matrix effect correction. We adopted 93 wt% as a threshold for the measured totals. All compositional data are shown as oxide weight percentages (wt%) in the TAS and bi-plots diagrams, with total iron measured as FeO, and normalised to 100% on a volatile-free basis for correlation purposes. Collected data and secondary standards measurements are all reported in Supplementary Materials-1.

3.2.3. Laser Ablation Inductively Coupled Plasma Mass Spectrometry (LA-ICP-MS)

Trace element analyses were conducted on volcanic glasses from the Triflisco, Santa Lucia, Cancello, and Maddaloni units. The analyses were performed using an Agilent 8900 triple quadrupole ICP-MS (ICP-QQQ) coupled to a Resonetics 193nm ArF excimer laser-ablation device at the Department of Earth Sciences, Royal Holloway, University of London. Full analytical procedures used for volcanic glass analysis follow those reported in Tomlinson et al. (2010). Crater sizes of 20, 25 and 34 µm were used depending on the sample vesicularity and/or size of glass surfaces available for analysis. The repetition rate was 5 Hz, with a count time of 40 s on the sample, and 40 s on the gas blank to allow the subtraction of the background signal. Typically, blocks of eight glass shards and one MPI-DING reference glass were bracketed by the NIST612 glass adopted as the calibration standard. The internal standard applied was ^{29}Si (determined by EMP-WDS analysis). In addition, MPI-DING reference glasses were used to monitor analytical accuracy (Jochum et al., 2006). LA-ICP-MS data reduction was performed in Microsoft Excel, as outlined in Tomlinson et al. (2010). Accuracies of LA-ICP-MS analyses of the MPI-DING reference glasses, ATHO-G and StHs6/80-G, were typically ≤ 5% for the majority of elements measured. Tephra and standard measurements are all provided in Supplementary Materials-1. Data averages reported in the text are accompanied by a ± 2 standard deviation (2 s.d.), whilst error bars in the plots are typically smaller than the data symbols.

3.2.4. Sr and Nd isotopes

^{87}Sr/^{86}Sr and ^{143}Nd/^{144}Nd isotope ratios have been determined on two samples from the Santa Lucia and one from Maddaloni units (i.e., ZS97-10 and ZS97-28, and ZS97-286 respectively)

previously investigated by Di Vito et al. (2008), on two samples from the Triflisco unit (i.e., TRIF 1/3 and TRIF 2/3) and on the CIL1 and CIL2 units from the Cilento Coast (Giaccio et al. 2012; Fig. 1c; Table 2). Measurements have been performed either on the glasses (pumices) and/or crystals (pyroxene or feldspar). $^{143}Nd/^{144}Nd$ measurement were performed on the glass fraction of samples from Triflisco, Santa Lucia (ZS97-10) and Maddaloni (ZS97-286) units. The different fractions were handpicked under a binocular microscope. Among all the available glass shards/pumices the most homogeneous in colour, and visibly poorly affected by secondary alteration, were selected for isotope analyses. Feldspar and pyroxene crystals were handpicked avoiding those characterised by the presence of glass rinds attached on their surfaces.

Before chemical dissolution, glass shards/pumices were acid leached three to five times to reduce as much as possible the alteration effects. The leaching procedure was prolonged until the acid solution became light-yellow in colour. Leaching was carried out each time by placing the beakers containing samples and high purity 6N HCl on a hot plate for 10 min. During each leaching step and after the final leaching, samples were rinsed with Milli-Q® H_2O. Feldspar and pyroxene were cleaned with Milli-Q® H_2O for 10 min. in an ultrasonic bath. Dissolution was obtained with high-purity HF–HNO_3–HCl mixtures. Sr and Nd were separated from the matrix through conventional ion-exchange procedures. Sr and Nd isotopic compositions were determined in a static mode by thermal ionisation mass spectrometry (TIMS) using a Thermo Finnigan Triton TI® mass spectrometer equipped with one fixed and six adjustable Faraday cups. Average 2σ mean, i.e., the standard error with N = 180, was better than ± $9x10^{-6}$ for Sr, and better than ± $7x10^{-6}$ for Nd measurements. The mean measured values of $^{87}Sr/^{86}Sr$ for the NIST-SRM 987 standard and $^{143}Nd/^{144}Nd$ for the La Jolla standard were 0.710261 ± 0.000021 (2σ, N = 169) and 0.511845 ± 0.000010 (2σ, N = 55), respectively; external reproducibility (2σ) during the period of measurements was calculated according to Goldstein et al. (2003). Measured $^{87}Sr/^{86}Sr$ ratios were normalized for within-run isotopic fractionation to $^{86}Sr/^{88}Sr$ = 0.1194, and $^{146}Nd/^{144}Nd$ = 0.7219. The final, measured isotope ratio values were normalized to the recommended values of the NIST SRM 987 ($^{87}Sr/^{86}Sr$ =0.71025) and La Jolla ($^{143}Nd/^{144}Nd$ = 0.51185) standards, respectively. Chemistry processing and isotope analyses were performed at the

Radiogenic Isotope Laboratory (RIL) of the Istituto Nazionale di Geofisica e Vulcanologia, Osservatorio Vesuviano, and the full analytical dataset is reported in Supplementary Materials-2.

3.2.5. $^{40}Ar/^{39}Ar$ dating

The $^{40}Ar/^{39}Ar$ ages were obtained at the Laboratoire des Sciences du Climat et de l'Environnement (CEA, CNRS UMR 8212, Gif-sur-Yvette, France) dating facility. Fresh and transparent K-rich feldspars were extracted from Triflisco, Santa Lucia, Cancello and Maddaloni samples. After being washed in distilled water, transparent K-feldspars (500-630 μm) without any visible inclusions were handpicked under a binocular and used for dating these four pyroclastic units. Between 20 and 30 crystals for each sample were irradiated in the Cd-lined, in core CLICIT facility of the Oregon State University TRIGA reactor for 2 h (IRR. CO-007) for Triflisco and 1 h in the same reactor (IRR. CO-009) for Santa Lucia, Cancello, and Maddaloni. Interference corrections were based on the nucleogenic production ratios given in Balbas et al. (2016). After irradiation, individual crystal for each tephra layers were transferred into a copper 133 pits sample holder placed into a differential vacuum Teledyne Cetac window connected to a home designed compact extraction line. Minerals were fused one by one using a 100W Teledyne Cetac CO_2 laser during 15s at 2.5 W. Before fusion, each crystal underwent a 10s long sweeping at 0.3W to remove unwanted gas potentially trapped on the crystals surface and fractures. Extracted gases were firstly purified by a SAES GP 50 cold getter for 90s and then for 230s by two hot SAES GP 50 getters. The five Argon isotopes (i.e., ^{40}Ar, ^{39}Ar, ^{38}Ar, ^{37}Ar and ^{36}Ar) were measured using a multicollector NGX 600 mass spectrometer equipped with 9 ATONA® amplifiers array and an electron multiplier. More technical specifications regarding the NGX 600 ATONA detector array are presented in detail in Cox et al. (2020). ^{40}Ar, ^{39}Ar, ^{38}Ar, and ^{36}Ar isotopes were collected simultaneously while the ^{37}Ar was measured in a second time. In the first run, ^{40}Ar, ^{39}Ar and ^{38}Ar were measured simultaneously on 3 ATONA® amplifiers and ^{36}Ar on the electron multiplier. Following this first run the ^{37}Ar was measured alone using the electron multiplier. Each isotope measurement corresponds to 15 cycles of 20-seconds integration time. Peak intensity data were reduced using ArArCALC V2.4 (Koppers, 2002). Neutron fluence J factor was calculated using co-irradiated Alder Creek sanidine standard ACs-2 associated to an age of 1.1891

Ma (Niespolo et al., 2017) according to the K total decay constant of Renne et al. (2011) ($\lambda_{e.c.}$ = (0.5757 ± 0.016) × 10^{-10} yr^{-1} and λ_{β^-} = (4.9548 ± 0.013) × 10^{-10} yr^{-1})). To determine the neutron flux for each sample we used at least 6 flux monitor crystals coming from pits framing the samples in each irradiation disk. J-values are of 0.00056080 ± 0.00000062 (Triflisco [Base]); 0.00028350 ± 0.00000023 (Santa Lucia [ZS97-10); 0.00028340 ± 0.00000028 (Cancello [AS96-400]); 0.00028340 ± 0.00000020 (Maddaloni [ZS97-286]). To verify the detectors linearity, mass discrimination was monitored by analysis of at least 60 air shots of various beam sizes ranging from 5.0 10^{-3} up to 2.0 10^{-2} V (1 to 4 air shots). About 15 air shots analyses are performed every day. These measurements are done automatically during the nights before and after the unknown measurements. Discrimination is calculated according the $^{40}Ar/^{36}Ar$ ratio of 298.56 (Lee et al., 2006). Procedural blank measurements were achieved after every two to three unknowns. For typical 5 min time blank backgrounds are between 2.5 and 4.0 10^{-4} V for ^{40}Ar and 60 to 90 cps for ^{36}Ar (about 1.0-1.3 10^{-6} V equivalent). Full analytical data for each sample can be found in Supplementary Materials-3.

4. Results

4.1. Stratigraphy

Most samples investigated in this study refer to the pyroclastic units already described in Di Vito et al. (2008), to which the reader is referred for the lithostratigraphic details. They generally consist in dm-thick fallout deposits made up of either pumice lapilli or coarse ash (Fig. 1c). At the site “Schiava” (SC2 in Fig. 1b) all the four previously investigated units, i.e., Maddaloni, Montemaoro, Cancello and Santa Lucia, occur as distinct eruptive units separated by either paleosols, epiclastic deposits or unconformity bounding surfaces.

The newly recognised Triflisco unit (Fig. 1b), consists in an 80 cm-thick fallout deposit made up of moderately sorted, white-pinkish and well-vesicular pumice lapilli (max Φ 3 cm) with intervening coarse ash layers. Accidental lithics are scant (Fig. 1c). The Triflisco unit overlies a paleosol and at the top, in turn, it is capped by a thick reddish paleosol on which lays a greyish pyroclastic flow deposit that we attribute to the CI (Fig. 1c). Thus, our interpretation differs from previous ones that

correlated the pumice fall at this locality to the CI Plinian fall exposed elsewhere (Civetta et al., 1997; Fanara et al., 2015).

4.2. Major and minor element volcanic glass chemistry

All samples analysed in this study have a dominant composition overlapping the boundary between phonolite and trachyte fields (Fig. 2a) of the *Total alkali vs Silica* (TAS, Le Maitre et al., 2002) classification diagram. Mean compositions are reported at 2 σ (2 standard deviation) error.

Triflisco unit. It is made up by four sub-units (Fig. 1c) with a relatively homogeneous composition. The majority of the data straddle the boundary between trachyte and phonolite fields (SiO_2 content of 59.5 ± 0.9 wt%, and alkali sum of 12.8 ± 1.0 wt%), depicting a trend within the trachyte field with decreasing alkali negatively correlated with a small increase in silica; Fig. 2a-b). The CaO/FeO values are < 1 (0.8 ± 0.1) and the Cl content is 0.6 ± 0.1 wt% for all sub-units (Fig. 2c). Glasses display a High Alkali Ratio (HAR), with K_2O/Na_2O generally > 2 and up to 3.08 (Fig. 2d). There is no appreciable chemical variation from the lowermost (Triflisco Base) to the uppermost (Triflisco Top) sub-units.

Santa Lucia unit. The glass of this unit, analysed in six samples (Fig. 1c; Table 2), is characterised by the most heterogeneous composition among those analysed, although mainly phonolitic, with a mean SiO_2 content of 59.0 ± 2 wt%, and an alkali sum of 12.8 ± 1 wt% (Fig. 2a-b). The CaO/FeO ratio is ≤ 1 (mean of 0.9 ± 0.1) and the Cl content is medium-high (0.6 ± 0.1 wt%; Fig. 2c). Santa Lucia glasses display a HAR typically ≥ 2, with a mean K_2O/Na_2O ratio of 2.1 ± 0.5 (Fig. 2d).

Cancello unit. Glasses from this unit are phonolitic-trachytic in composition, with a SiO_2 content of 60.9 ± 1.3 wt%, a mean alkali sum of 13.1 ± 0.9 wt% (Fig. 2a-b) and a HAR of 2.2 ± 0.6 (Fig. 2d). The CaO/FeO ratio ranges between 0.7 and 1.0 and the Cl content between 0.5 and 0.7 wt% (Fig. 2c).

Montemaoro unit. As stated in the previous section, it was not possible to acquire new data for this unit. Thus, for the purpose of this study, we rely on the available glass-EDS data from Di Vito et al. (2008). The Montemaoro unit is mainly trachytic in composition with some points straddling the boundary with the phonolite field, with silica and alkali sum content of c.a. 61 wt% and 13 wt%,

respectively (Fig. 2a-b). The glasses display a HAR, up to 2.5, with a CaO/FeO ratio of c.a. 0.7 (Fig. 2d), while Cl content was not determined.

Maddaloni unit. The glass of this unit, collected from the former SC2 and SA3 sections (Fig. 1; Table 2), is characterised by a homogeneous SiO_2 content (mean 61.6 ± 0.5 wt%), with an alkali sum of 13.7 ± 0.6 wt% (Fig. 2a-b). Respect to all the above-mentioned samples, Maddaloni glasses predominantly display a Low Alkali Ratio (LAR), with K_2O/Na_2O typically ≤ 1.5 (0.9 ± 0.1; Fig. 2d), due to an almost equal content of K_2O and Na_2O of ca. 7 wt%. In addition to a lower K_2O/Na_2O ratio, with respect to the other analysed units, the glass of the Maddaloni pumices has noticeably lower CaO/FeO ratios (0.5 ± 0.1), whilst the Cl content is appreciably higher, up to 1.1 wt% (Fig. 2c).

4.3. Trace element volcanic glass chemistry

The Triflisco eruption unit contains HAR glasses that are fairly homogeneous in terms of their incompatible trace element contents (e.g., Th = 29.9 ± 2.9 ppm [Fig. 2e-f]; Nb = 59.2 ± 4.0 ppm [Fig. 2e]; Zr = 327 ± 31 ppm [Fig. 2f]) and ratios of other High Field Strength elements (HFSE) to Th remaining constant (e.g., Nb/Th = 2.0 ± 0.1; Zr/Th = 10.9 ± 0.5). Light Rare Earth Elements (LREE) are enriched relatively to the Heavy Rare Earth Elements (HREE) with La/Yb = 27.9 ± 3.7.

The HAR Santa Lucia eruption products in the SC2, CA1 and SA1 sections (see Table 2) are compositionally consistent and fairly homogeneous (e.g., Th = 27.1 ± 3.1 ppm; Nb = 55.8 ± 4.5 ppm [Fig. 2e]; Zr = 306 ± 29 ppm [Fig. 2f]; Rb = 307 ± 25 ppm; La = 77.9 ± 6.0 ppm) with constant HFSE/Th ratios (Nb/Th = 2.1 ± 0.1; Zr/Th = 11.3 ± 0.5) and displaying LREE enrichment relatively to HREE (La/Yb = 27.7 ± 3.1).

The Cancello unit displays HAR glasses that are fairly homogeneous in composition (e.g., Th = 26.7 ± 3.0 ppm; Nb = 56.1 ± 7.0 ppm [Fig. 2e]; Zr = 316 ± 34 ppm [Fig. 2f]; La = 81.4 ± 8.3 ppm), with minor variation relating to a single less enriched analysis. HFSE to Th ratios remain constant within the Cancello glasses (Nb/Th = 2.1 ± 0.2; Zr/Th = 11.8 ± 0.4), and LREE are enriched relative to the HREE where La/Yb = 27.6 ± 3.4.

The LAR Maddaloni tephra shows variable incompatible trace element glasses compositions (e.g., Th = 84-114 ppm; Nb = 169-231 ppm [Fig. 2e]; Zr = 1037-1319 ppm [Fig. 2f]) and displays far greater

levels of enrichment relative to the above mentioned HAR units (i.e., Triflisco, Santa Lucia and Cancello; Fig. 2e-f). HFSE/Th values remain constant within these glasses (Nb/Th = 2.1 ± 0.1; Zr/Th = 11.8 ± 0.4) and are entirely consistent with the HAR samples from Triflisco, Santa Lucia and Cancello deposits (Fig. 2e-f).

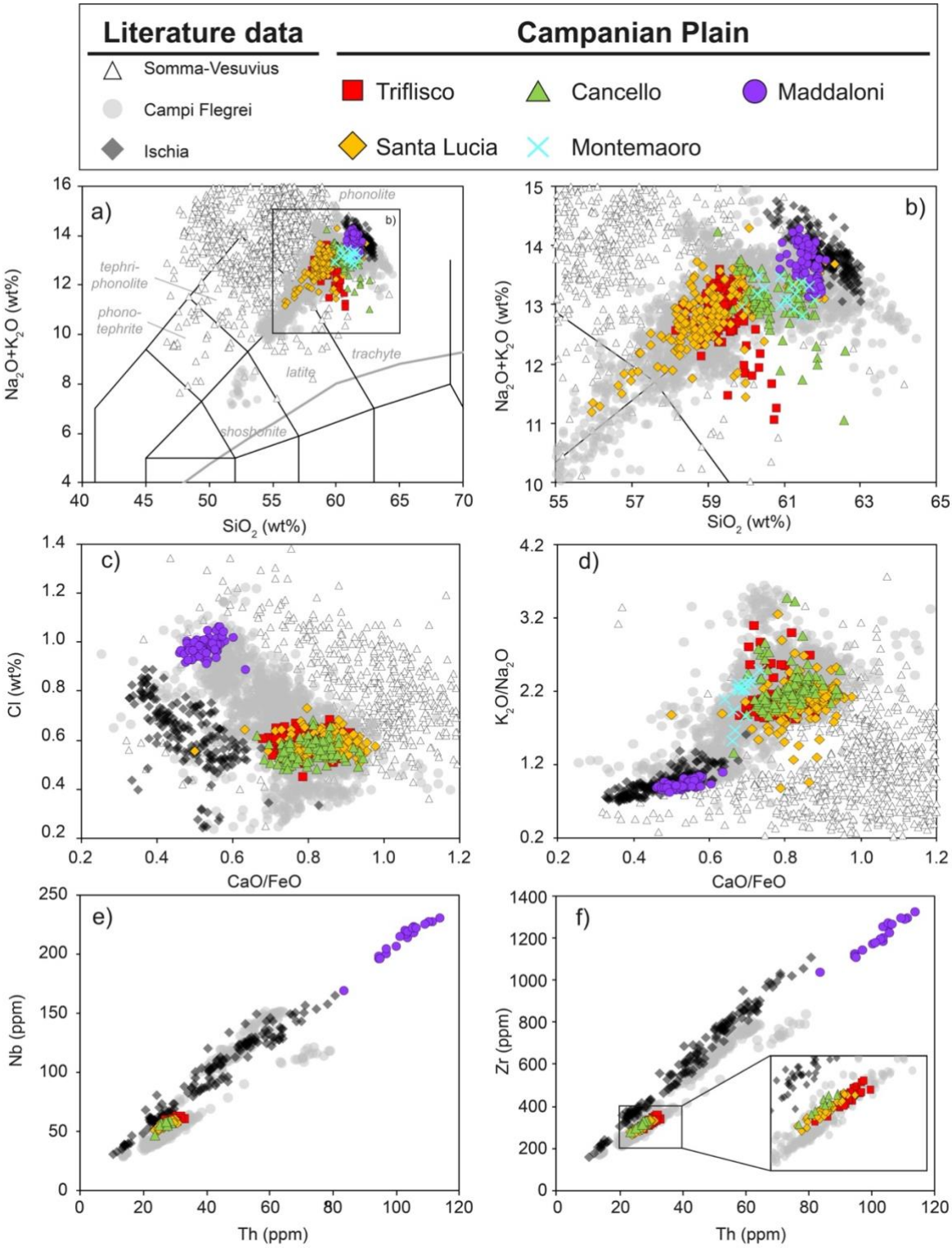

Figure 2. Major and trace element compositions of the investigated medial Campanian Plain units in comparison with literature data of Ischia and Campi Flegrei volcanic systems. (a, b) *Total alkali vs silica* (TAS; Le Maitre et al., 2002), (c) CaO/FeO vs Cl classification diagram (Giaccio et al., 2017a), (d) CaO/FeO vs K_2O/Na_2O, (e) Th vs Nb (ppm) and (f) Th vs Zr (ppm). Glass-

WDS data source: Triflisco, Santa Lucia, Cancello and Maddaloni medial Campanian Plain units: this study; Somma-Vesuvius: Santacroce et al. (2008); Ischia: Tomlinson et al. (2014); Campi Flegrei: Smith et al. (2011, 2016), Tomlinson et al. (2012). Trace elements data source: Triflisco, Santa Lucia, Cancello and Maddaloni medial Campanian Plain units: this study; Ischia: Tomlinson et al. (2014); Campi Flegrei (Tomlinson et al., 2012).

4.4. Sr and Nd isotopes

Whilst the $^{143}Nd/^{144}Nd$ isotopic ratios are homogeneous within the analytical error (c.a. 0.51250), the $^{87}Sr/^{86}Sr$ ratios (Fig. 3a) range from 0.70687 and 0.70780 (glass from sample ZS97-286). The highest value is possibly due to post-depositional alteration of the glass as suggested by the Sr isotope composition of the embedded feldspar. Samples from Triflisco and Santa Lucia display similar and lower Sr isotope composition (c.a. 0.7069) with respect to sample from Maddaloni unit. CIL1 and CIL2 are characterized by Sr isotope ratios (from ca. 0.7071 to 0.7072) similar to that of the Maddaloni feldspar (from c.a. 0.7071). Figure 3 displays the variations in terms of Sr-Nd isotope ratios compared with literature data.

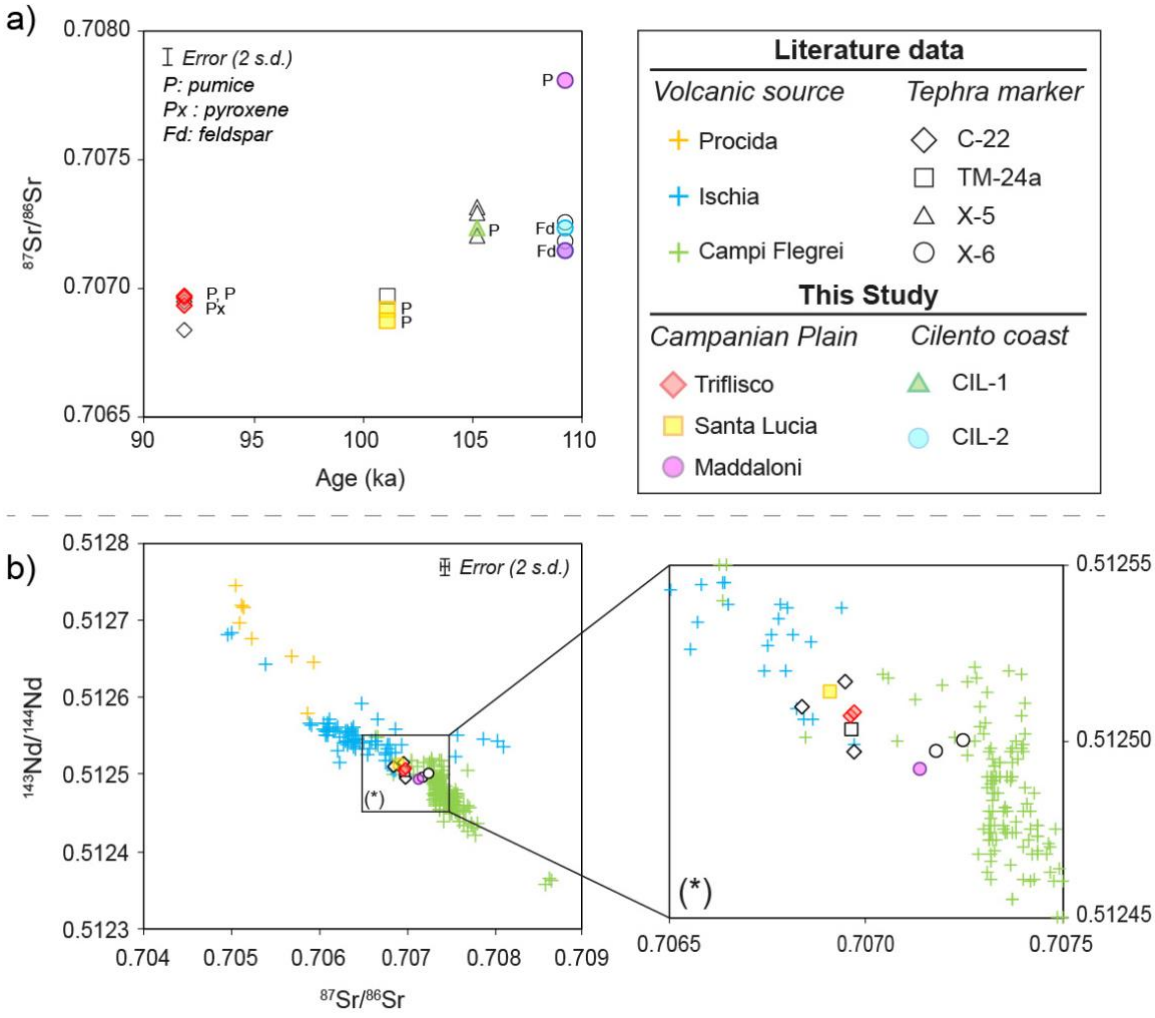

Figure 3. Sr and Nd isotope ratios determined for the Triflisco, Santa Lucia and Maddaloni units from the Campanian Plain and CIL-1 and CIL-2 tephra from the Cilento coast. In panel b the Sr isotope composition of the feldspar from the Maddaloni sample has been associated to the Nd isotope composition of its glass fraction, being the glass possibly affected by post depositional alteration. This latter did not modify the $^{143}Nd/^{144}Nd$, because the Nd is a less fluid mobile element. Tephra layers literature data source: **C-22**: POP-1 (Giaccio et al., 2012), TF-10 (Giaccio et al., 2017a), S14 (Petrosino et al., 2019); **TM-24a:** POP-2A (Giaccio et al., 2012); **X-5**: TF-12 (Giaccio et al., 2017a), S11 (Petrosino et al., 2019); **X-6** = TF-13 (Giaccio et al., 2017a), S10 (Petrosino et al., 2019). Literature data for Ischia, Procida and Campi Flegrei proximal deposits: Arienzo et al. (2009, 2010, 2015, 2016), Brown et al. (2014), Casalini et al. (2018), D'Antonio et al. (2007, 2013), Di Renzo et al. (2011), Pabst et al. (2008), Pelullo et al. (2020), Tonarini et al. (2009).

4.5. $^{40}Ar/^{39}Ar$ ages

All $^{40}Ar/^{39}Ar$ results for individual tephra layers are presented as probability diagrams (Fig. 4). Weighted mean age uncertainties are all reported at 2σ, including J uncertainty and were calculated using Isoplot 4.0 (Ludwig, 2001). For each sample, inverse isochrones have an atmospheric $^{40}Ar/^{36}Ar$ initial intercept with uncertainties suggesting that dated crystals are without detectable excess argon. Full inverse isochrones dataset can be found in Supplementary Materials-3.

Triflisco (TRIF-Base) - 13 single crystals were individually dated. Eleven out of thirteen crystals analysed gave a similar age within uncertainties (Fig. 4a). The two other older crystals, one sanidine (~104 ka, red bar in Fig. 4) and one plagioclase (~404 ka, not showed in Fig. 4; see Supplementary Materials-3) according to their Ca/K ratio, are interpreted as xenocrysts. The main population of crystal interpreted as juvenile allows to calculate a weighted mean age of 91.8 ± 1.2 ka (MSWD = 1.20, p = 0.27).

Santa Lucia (ZS97-10) - A total of 14 individual sanidine crystals were dated. The probability diagram is simple (Fig. 4b) with one mode allowing to calculate a meaningful and precise weighted mean age of 101.2 ± 0.8 ka (MSWD = 0.59, p = 0.87).

Cancello (AS96-400) - The probability diagram displays one single mode with no xenocrystal contamination (Fig. 4c). These crystals are interpreted as juvenile ones (12 crystals), allowing to calculate a precise weighted mean age of 102.5 ± 0.8 ka (MSWD = 0.58, p = 0.85).

Maddaloni (ZS97-286) - 14 crystals were dated individually. All gave within uncertainty the same age resulting in a gaussian probability diagram (Fig. 4d). Using this very homogenous crystal population we calculated a weighted mean age of 109.3 ± 1.0 ka (MSWD = 0.43, p = 0.96).

While for Maddaloni we obtained the $^{40}Ar/^{39}Ar$ age of 109.3 ± 1.0 ka, the overlying Montemaoro unit, which was not resampled or re-analysed in this work, was not dated.

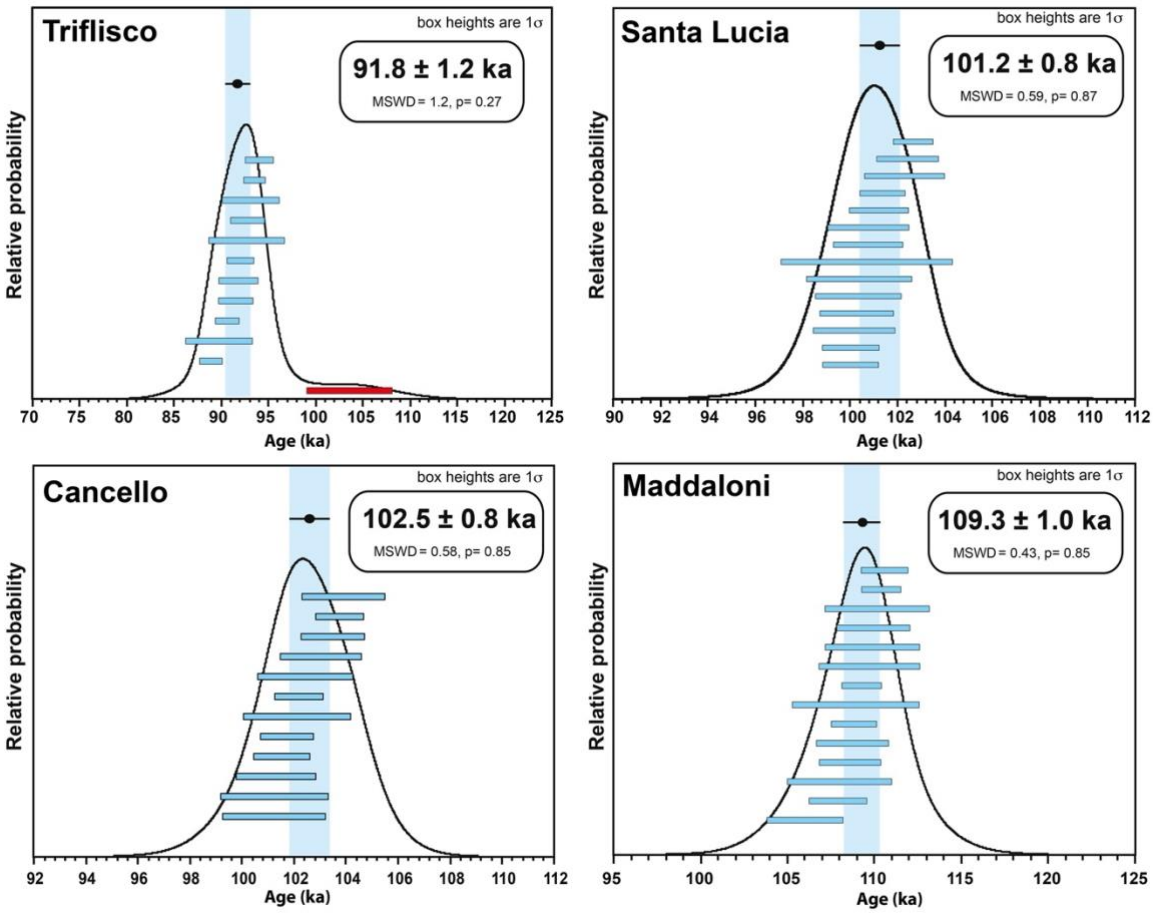

Figure. 4. Age probability diagrams for the Triflisco, Santa Lucia, Cancello and Maddaloni units. The light-blue and red horizontal bars are the single crystal ages with the uncertainty expressed at 1σ. Whilst the light-blue bars are included in the weighted mean age (vertical light-blue bars, 2σ uncertainty), the red ones are not included because statistically different and thus interpreted as ages of xenocrystatls.

5. Discussion

5.1. Volcanic source of the Campanian Plain Units

All the investigated pyroclastic fall units occur in a range of 30-35 km to 55-60 km in the eastern quadrants from the Neapolitan volcanoes, including Campi Flegrei, Ischia, Procida and Somma-Vesuvius (Fig. 1b). Somma-Vesuvius can be reasonably excluded as a potential source since its oldest known activity is younger than Campanian Ignimbrite (i.e., < 40 ka; Santacroce et al., 2008) and thus incompatible with the 109-92 ka chronology obtained here for the Campanian Plain units. Also, in terms of glass chemical composition, the Somma-Vesuvius products appear

incompatible due to the higher alkali sum at similar SiO_2 content (Fig. 2a-b), and the significantly higher CaO/FeO at same Cl content and alkali ratio (Fig. 2c-d). Procida island can also be excluded based on the Sr-Nd isotope compositions, which are clearly different from those of the Campanian Plain units (Fig. 3a-b). Among the two remaining potential sources for the investigated units (i.e., Campi Flegrei and Ischia), based on the lithostratigraphic and geochemical characteristics, as already argued by Di Vito et al. (2008), the Campi Flegrei volcanic area is the most probable. In terms of major element glass composition, although Campi Flegrei and Ischia products partially overlap, each of the two volcanic sources show distinctive features in terms of oxide concentrations and ratios (Fig. 2a-d). This applies to four out of the five investigated units (i.e., Triflisco, Santa Lucia, Cancello, and Montemaoro), which unambiguously plot in the compositional field of the Campi Flegrei glass because of the higher K_2O/Na_2O and CaO/FeO values with respect to the Ischia products (Fig. 2b-c). Trace elements glass compositions also support the attribution of the Triflisco, Santa Lucia and Cancello units to the Campi Flegrei, for instance all these units show enrichment in Zr that is diagnostic of the Campi Flegrei products and is slightly lower than that of the products typically erupted at Ischia (Fig. 2f).

Owing to its distinctive K_2O/Na_2O and CaO/FeO values, which are lower than those of the most common Campi Flegrei products (Fig. 2c-d), the source attribution of the Maddaloni unit is not so straightforward. Indeed, CaO/FeO and K_2O/Na_2O ratios of Maddaloni unit partly overlap with those of Ischia (Fig. 2b-c). However, using the CaO/FeO vs. Cl diagram, the glass composition of Maddaloni unit falls out of the Ischia field and within the Campi Flegrei one, though, sporadically, the Campi Flegrei compositions can overrun the typical Ischia one (Fig. 2c). Indeed, such chemical characteristics, i.e., LAR trachyte-phonolite with relatively low CaO/FeO ratio, are also found in Campi Flegrei products (e.g., Tomlinson et al., 2012), notably in the CI (Smith et al., 2016) and some minor Campi Flegrei eruptions following the NYT caldera-forming eruption (e.g., Averno 2, Fondi di Baia, Monte Nuovo; Smith et al., 2011). Likewise, the Maddaloni unit can be attributed to the Campi Flegrei and ascribed to this less common, LHR trachyte-phonolite compositional group of this volcanic area. Incompatible trace element enrichment of the Maddaloni glasses exceeds that currently recognised in the known products of Campi Flegrei and Ischia (Fig. 2e-f) making their use

again less conclusive. However, the lower Zr/Th ratios observed in the Maddaloni glasses are seemingly more akin to those of Campi Flegrei, rather than to the higher values typically observed in the eruptive products of Ischia spanning a period of intense explosive volcanism at ~40-80 ka (Tomlinson et al., 2014). More convincing, and seemingly definitive, evidence to confirm Campi Flegrei as the source for the Maddaloni unit, is provided by isotope data. Indeed, the Sr- and Nd-isotope compositions for the Maddaloni samples are positioned well within the field of the Campi Flegrei (Fig. 3a-b).

In summary, the volcanological and sedimentological constraints, the acquired major and trace elements glass composition, the geochronological and Sr- and Nd-isotope data consistently indicate that Campi Flegrei is the most probable source for all the five investigated Campanian Plain units. This significantly extends back in time the known explosive activity of this volcanic field, previously documented only up to ca. 80 ka (Scarpati et al., 2013), or as far back as 290 ka (CVZ; De Vivo et al., 2001; Rolandi et al., 2003). Regardless the precise vent location, our data point to a frequent activity that took place within the Campi Flegrei volcanic area. Specifically, we recognised five eruptions that, based on their lithological features in medial settings, can be likely considered of Plinian intensity and magnitude. These occurred across approximately a 17 kyr time-window, with recurrence times of a few thousands of years and in one case are barely more than 1 kyr (e.g., time elapsed between the 102.5 ± 0.8 ka Cancello and the 101.2 ± 0.8 ka Santa Lucia eruptions). Consequently, the period of 109-92 ka was characterized by a high frequency of moderate to large explosive eruptions, i.e., an eruptive behaviour that has not been recognised within the more recent (i.e., post-CI) activity of the Campi Flegrei volcano.

5.2. Tephra correlations

To correlate the investigated units of the Campanian Plain with MIS 5 Mediterranean tephra markers, we refer to the Central Mediterranean tephrostratigraphic successions spanning this interval that (i) record in stratigraphic order most MIS 5 tephra markers, (ii) have a good geochemical characterization of all tephra, (iii) have a good radioisotopic or stratigraphic chronology, and (iv) have

a good expression of the MIS 5 climate variability, which enable a reliable assessment of the tephra climato-stratigraphic position.

These requisites are fully or partially met by (i) the rich tephrostratigraphic record of the Lago Grande di Monticchio, southern Italy (Fig. 1a), located ca. 120 km east of the Neapolitan volcanoes – thus in an ideal position for recording their explosive activity (Wulf et al., 2004, 2012) – and (ii) the Popoli MIS 5 succession, in Sulmona Basin (Fig. 1a), where MIS 5 tephra were dated by $^{40}Ar/^{39}Ar$ method (Giaccio et al., 2012; Regattieri et al., 2017), allowing a direct, unambiguous comparison with the $^{40}Ar/^{39}Ar$ chronology here obtained for the investigated Campanian Plain units.

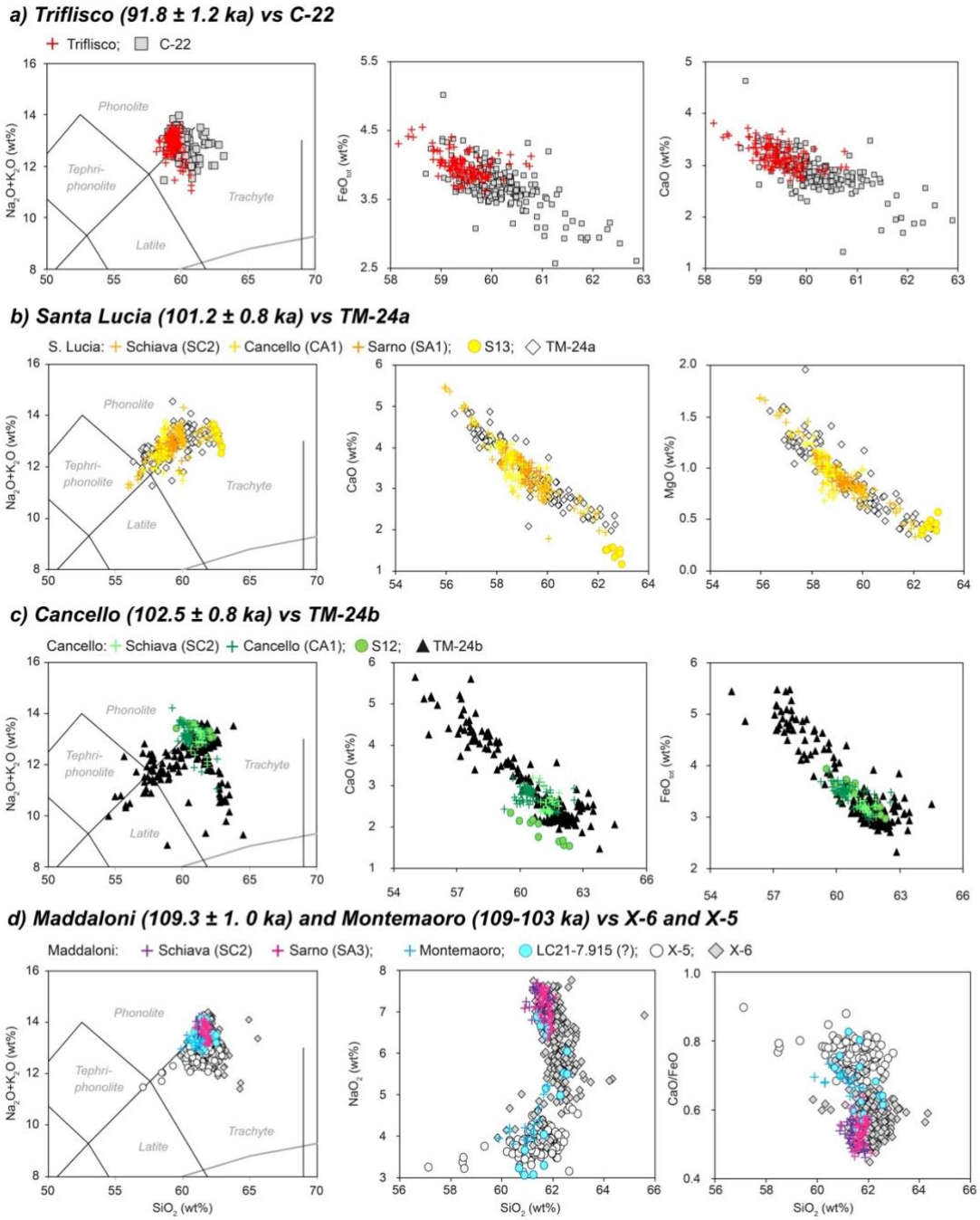

Figure 5. Major element bi-plots and ratios of Triflisco, Santa Lucia, Cancello, Montemaoro and Maddaloni units from the Campanian Plain in comparison with literature data. Literature EDS data source: SC2-b (Di Vito et al., 2008), S13, S12 (Munno and Petrosino, 2007). Literature glass-WDS data source: C-22 marker = TM-23-11 (Wulf et al., 2004), POP-1 (Giaccio et al., 2012), PRAD-2525 (Bourne et al., 2015), TF-10 (Giaccio et al., 2017a), TP05-25.195 (Wulf et al., 2018); TM-24a marker = TM-24a (Wulf et al., 2012), POP-2 (Regattieri et al., 2015); TM-24b marker = TM-24b (Wulf et al., 2012), POP-2A (Giaccio et al., 2012), OH-DP-0404 (Leicher et al., 2016), TF-11 (Giaccio et al., 2017a); X-5 marker = TM-25 (Wulf et al., 2012), POP-3, CIL-1 (Giaccio et al., 2012), LeS1 (Donato et al., 2016), TF-12 (Giaccio et al., 2017a), LC21-7.915 (Satow et al., 2015); X-6

marker = TM-27 (Wulf et al., 2012, 2018), CIL-2 (Giaccio et al., 2012), I-9 (Insinga et al., 2014), POP-4 (Regattieri et al., 2015), PRAD-2812 (Bourne et al., 2015), OH-DP-0435 (Leicher et al., 2016), Tarsia, LeS2 (Donato et al., 2016), TF-13 (Giaccio et al., 2017a), TP05-27.915 (Wulf et al., 2018), Cavallo-G (Zanchetta et al., 2018).

Triflisco - Both $^{40}Ar/^{39}Ar$ chronology and major elements (Fig. 5a) glass composition of Triflisco unit (91.8 ± 1.4 ka) are fully consistent with those of the Sulmona tephra POP1 (92.1 ± 4.6 ka; Giaccio et al., 2012) that, in turn, was correlated to the Monticchio tephra TM-23-11 (Giaccio et al., 2012; Fig. 5a), dated at 95.18 ± 4.76 ka (Wulf et al., 2012). POP1/TM-23-11 was also correlated to the widespread C-22 tephra marker (Giaccio et al., 2012) of the Tyrrhenian Sea tephra series (Paterne et al., 1986, 1988). The correlation of Triflisco with POP1//TM-23-11/C-22 is supported also by incompatible trace element contents plotted against Th (Fig. 6a). Furthermore, $^{87}Sr/^{86}Sr$ isotope ratios of Triflisco perfectly match literature values for the POP1/TM-23-11/C-22 tephra layers/markers (Fig. 3a), strengthening this correlation.

The POP1/TM-23-11/C-22 was also identified in Fucino succession, as layer TF-10 (Giaccio et al., 2017a), and in San Gregorio Magno basin, as layer S14, (Munno and Petrosino, 2007; Petrosino et al. 2019; Fig. 1a). The C-22 was also correlated to the 11 cm- thick tephra layer CET1-10/14 in the Tyrrhenian core CET-1 (Petrosino et al., 2016). This marker was also identified in the marine core PRAD 1-2, in the Adriatic Sea, as layer PRAD-2517 (Giaccio et al., 2012; Bourne et al., 2015). Finally, in the peatland succession of Tenaghi Philippon, in Greece (Figs. 1a, 7), recent cryptotephra investigations by Wulf et al. (2018) allowed the correlation of the C-22 marker with tephra layer TP05-25.195 (Fig. 5a).

Santa Lucia – Both major (Fig. 5b) and trace (Fig. 6a) element compositions, as well as the chronology of Santa Lucia unit are compatible with TM-24a tephra of Monticchio, to which the Sulmona tephra POP2 was also correlated (Giaccio et al., 2012; Fig. 7). The Monticchio varve-supported age for TM-24a is 102.0 ± 5.7 ka (Wulf et al, 2012; Monticchio chronology MON-2014, Sabine Wulf, personal communication 2017), whereas the modelled age of POP2 is 102.0 ± 2.4 ka (Regattieri et al., 2015). In Sulmona paleo-hydrological record, POP2 falls in the early stage of a period of increasing precipitation correlated to the Greenland Interstadial 23, which in reference records (e.g., Corchia Cave, North Greenland Ice Core Project members et al., 2004; Drysdale et

al., 2007) starts about 102-103 ka, thus in agreement with the estimated age of POP2/TM-24a. Here Santa Lucia unit is precisely $^{40}Ar/^{39}Ar$ dated at 101.2 ± 0.8 ka (Fig. 4b), supporting this correlation. $^{87}Sr/^{86}Sr$ isotope ratios determined on Santa Lucia samples show values similar to those obtained for Triflisco/C-22 tephra layer/marker (Fig. 3a), but they can be discriminated based on the higher HFSE (e.g., Th, U) contents of the Triflisco/C-22 glasses than the Santa Lucia ones, thus preventing erroneous correlations (Fig. 6a).

At Fucino Basin (Figs. 1a, 7), tephra layer TF-11, located immediately below tephra layer TF-10/C-22, was correlated by Giaccio et al. (2017a) to the Monticchio tephra POP2/TM-24a (Fig. 7). The same marker horizon was also recognized in Lake Ohrid (North Macedonia-Albania; Figs, 1a, 7) as layer OH-DP-0404 (Leicher et al., 2016). The crypto-tephra CET1 12-13-14 in the Tyrrhenian core CET1 (Fig. 1a) also has major element composition compatible with TM-24a/POP2 (Petrosino et al., 2016), thus representing the unique so far known occurrence of Santa Lucia unit in the marine realm. Finally, at San Gregorio Magno (Munno and Petrosino, 2007; Petrosino et al., 2019), tephra layer S13, underlying tephra layer S14/C-22, would be stratigraphically well suited to be a potential candidate for the TM-24a/Santa Lucia unit (Fig. 7). However, EDS-glass chemical composition supports only partially this correlation (Fig. 5b), and WDS-glass composition should be acquired on purpose.

Cancello – The Cancello pumice fall occurs below Santa Lucia unit=TM-24a/POP2 (Di Vito et al., 2008; Fig. 1b), thus indicating POP2a (Giaccio et al., 2012) and TM-24b (Wulf et al., 2012), which respectively underlay POP2 and TM-24a, as the best candidates for correlation to this unit (Fig. 7). Major element biplots confirm this correlation (Fig. 5c), also supported by trace element comparison (Fig. 6a). In particular, with respect to the Santa Lucia unit, the Cancello unit appears to extend to lower Th contents (Figs. 2f, 6a), which allows discriminating these two tephra markers. At Monticchio, TM-24b is varve-dated at 103.1 ± 5.7 ka (Wulf et al., 2012; MON-2014), while in Sulmona Basin a modelled age of 103.3 ± 1.4 ka was obtained for POP2a (Regattieri et al., 2015), in agreement with the more precise age of 102.5 ± 0.8 ka here measured for the Cancello unit (Fig. 4c). In summary, the correlation of Cancello unit to POP2a/TM-24b is fully supported by all the geochemical and geochronological data.

At San Gregorio Magno (Munno and Petrosino, 2007; Petrosino et al., 2019), the tephra layer S12 is stratigraphically well suited for being a good correlation candidate for POP2a/TM-24b (Fig. 7). The geochemical correlation of S12 with Cancello unit, based on the available EDS-glass composition, is quite convincing (Fig. 5c), but more compelling WDS data would be required. Finally, the crypto-tephra CET1-15 in the Tyrrhenian core CET1 (Fig. 1a) is stratigraphically (Fig. 7) and compositionally consistent with TM-24b/POP2b (Petrosino et al., 2016).

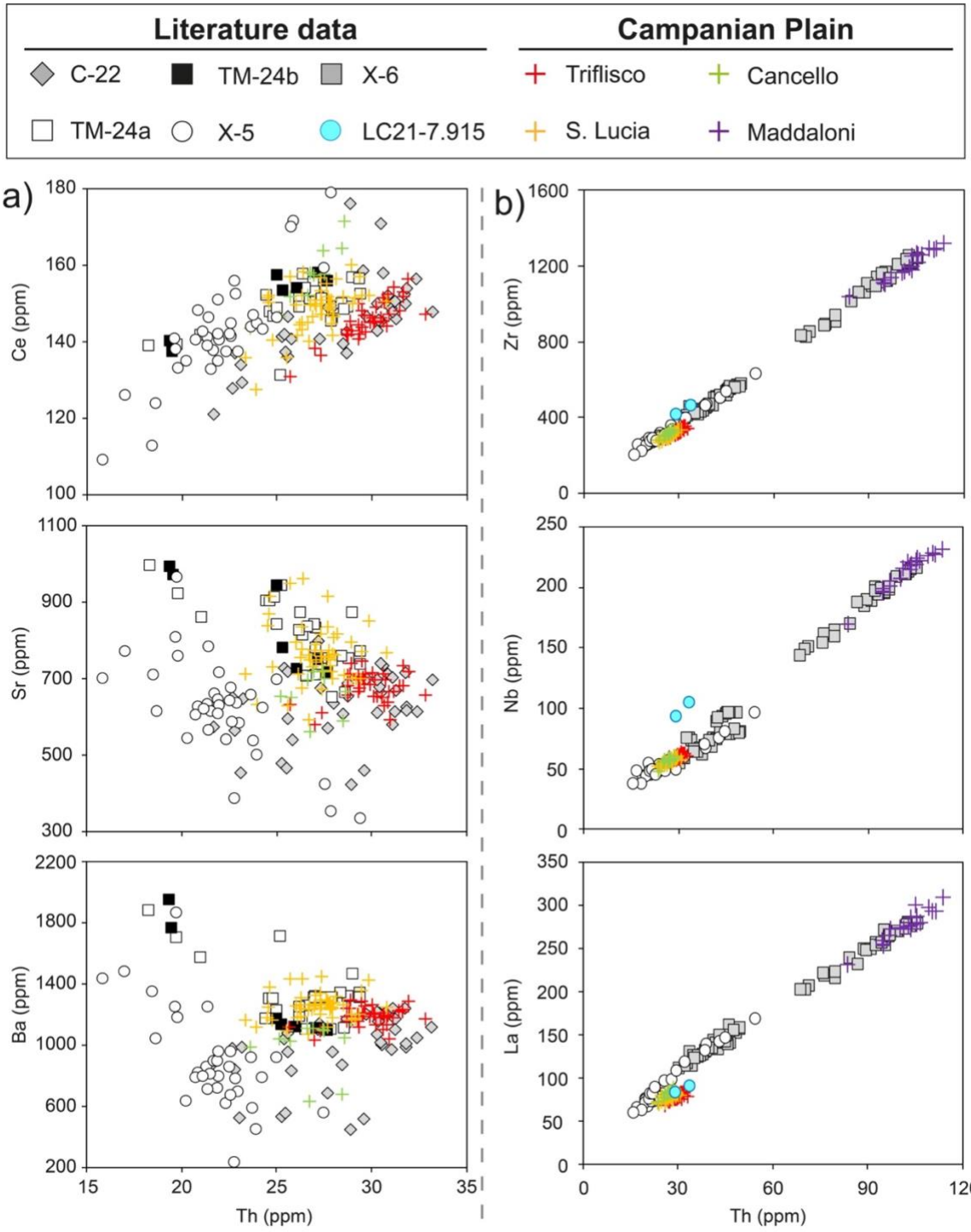

Figure 6. Incompatible trace element patterns against Th for the Triflisco, Santa Lucia, Cancello and Maddaloni units in comparison with literature data. Literature data source: C-22 = TM-23-11, PRAD 2525 (Bourne et al., 2015), S14 (Petrosino et al., 2019); TM-24a = TM-24a (Wulf et al., 2012); TM-24b = TM-24b (Wulf et al., 2012); X-5 = TM-25 (Wulf et al., 2012), POP-3 (Giaccio et al., 2012), LC21-7.915 (Satow et al., 2015), LeS1 (Donato et al., 2016), TF-12 (Giaccio et al., 2017a), S11

(Petrosino et al., 2019); X-6 = TM-27, PRAD 2812 (Bourne et al., 2015), LeS2 (Donato et al., 2016), TF-13 (Giaccio et al., 2017a), S10 (Petrosino et al., 2019).

Maddaloni and Montemaoro – At Masseria Montemaoro quarry (site SC2; Fig. 1c), these two, stratigraphically superimposed units underlie the Cancello unit (Fig. 1c). The $^{40}Ar/^{39}Ar$ age of 109.3 ± 1.0 ka determined for Maddaloni unit is virtually indistinguishable from that of 109.1 ± 0.8 ka, obtained for the Sulmona tephra layer POP4 (Regattieri et al., 2017), which was correlated to the X-6 tephra marker (Regattieri et al., 2015), corresponding to the Monticchio TM-27 (Wulf et al., 2012). Consistent with this chronological information, the major (Fig. 5d) and trace (Fig. 6b) elements composition of the Maddaloni unit well match the most evolved term of POP4/TM-27 tephra layer/marker and those of the other X-6 equivalent layers in distal archives through the central Mediterranean area (Fig. 1a). Sr-Nd isotope values obtained from the Maddaloni unit are consistent with those of CIL-2/X-6 tephra layer/marker from the Cilento coast and other X-6 occurrences (Fig. 3a-b), thus further supporting its correlation with the X-6 marker. Moreover, major and trace elements glass compositions are extremely distinctive (e.g., different alkali ratio and Cl content, incompatible trace element patterns), and we thus highly recommend the employment of these geochemical tracers as a correlation tool for the X-6 tephra (Figs. 5d, 6b; Supplementary Materials-1). All geochemical and chronological data thus corroborate Maddaloni as the most proximal equivalent of the X-6 tephra marker.

The Ionian X-6 tephra marker (Keller et al., 1978), and its other marine and terrestrial equivalents, is the most widespread MIS 5 Campi Flegrei tephra (Figs. 1a, 7), while considering the whole Campi Flegrei record, in terms of dispersal area it is second only to the CI (e.g., Costa et al., 2012). It has been recognised in a series of sedimentary successions in the central Mediterranean area (Figs. 1a, 7), including the Ionian Sea (I-9, Insinga et al., 2014), Tyrhhenian Sea (C-31, Paterne et al., 2008), Adriatic Sea (PRAD-2812, Bourne et al. 2015), Fucino Basin (TF-13, Giaccio et al., 2017a), Cilento Coast (Giaccio et al., 2012; Donato et al., 2016), San Gregorio Magno Basin (S10, Petrosino et al., 2019), Valle del Crati (Tarsia, Donato et al., 2016), Grotta del Cavallo Palaeolithic site (Unit G,

Zanchetta et al., 2018), Lake Ohrid (OH-DP-0435, Leicher et al., 2016), and Tenaghi Philippon (TP05-27.915, Wulf et al., 2018).

Regarding Montemaoro unit, its stratigraphic position between Maddaloni/X-6 and Cancello/TM-24b, which chronologically constrains it between ~109 ka and ~103 ka, makes it the best candidate for the terrestrial counterpart of the Ionian Sea marker X-5, which lays immediately above the X-6 (Keller et al., 1978). The X-5 is equivalent to tephra layer TM-25 in the Lago Grande di Monticchio succession, dated at 105.6 ± 0.5 ka (recalculated with ACs at 1.1891 Ma; Tyrrhenian Sea; Petrosino et al., 2015), or POP3 $^{40}Ar/^{39}Ar$ dated at 105.8 ± 1.3 ka (Sulmona Basin; Giaccio et al., 2012). Although it was not possible to acquire new major (glass-WDS) and/or trace element data, the available glass-EDS composition for the Montemaoro unit supports this correlation (Fig. 5d). Consequently, we suggest that the Montemaoro unit is the most likely proximal counterpart of the X-5, based on the chronological and stratigraphical constraints provided in this study and the existing chemical data. Future discovery of a new field exposure of Montemaoro would allow further verification of this correlation.

Although less dispersed, the X-5 marker, like the X-6, was reported in several stratigraphic successions (Figs. 1a, 7), including the Fucino Basin (TF-12, Giaccio et al., 2017a), Cilento Coast (CIL1, Giaccio et al., 2012; LeS1, Donato et al., 2016), San Gregorio Magno Basin (S11, Petrosino et al., 2019), and as the lowermost tephra layer in CET1 core (i.e., CET1-18, Petrosino et al., 2015), $^{40}Ar/^{39}Ar$ dated at 105.18 ± 0.5 ka (2σ analytical uncertainty).

A potential correlative for either the X-6 or X-5 marker was also recognised at the remote site of marine core LC21 (Satow et al., 2015), in the Aegean Sea (Fig. 1a). Specifically, the crypto-tephra LC21-7.915, whose base was dated at 104.1 ± 2.2 ka, according to the LC21 age model (Satow et al., 2015), presents two geochemical compositions indicating both Santorini and Campanian sources. The Campanian component is in turn represented by two glass HAR and LAR trachyte-phonolite populations, which are compatible with X-5 and X-6 compositions, respectively (Fig. 5d). Moreover, in terms of trace element composition, the few available data appear quite consistent with both markers (Fig. 6b). However, both the age and climatostratigraphic position of the crypto-tephra LC21-7.915 make the X-5 the most probable correlative. Indeed, LC21-7.915 precisely marks the

onset of the sapropel S4 deposition, at the base of which in the Tyrrhenian Sea records the tephra X-5/C-27 is also found (Fig. 8; Paterne et al., 2008; Regattieri et al., 2015). Therefore, we are inclined to consider the X-5 as the most likely correlative for the HAR component of the Campanian portion of LC21-7.915 crypto-tephra, though the co-presence of the LAR component would require a plausible explanation.

Overall, the correlations of the investigated Campanian Plain units with the five distal tephra markers are well supported by several lines of consistent, independent evidence, including their stratigraphic order, geochronology, and geochemistry (major and trace elements, and the Sr-Nd isotopes). However, in some cases, the geochemical variability of the investigated Campanian Plain units is less wide than the corresponding distal tephra. This is especially true for Cancello and Maddalloni units, the composition of which covers only a part of the wider variability observed in distal settings (Figs. 5c-d, 6b). This is not surprising, as the occurrence of the analysed medial-distal units is relatively scant with respect to the distal ones, and thus could be not representative of the complete eruptive sequence and geochemical variability. This would suggest that not all the eruptive phases or sub-units, e.g., pyroclastic flow or fall, of Cancello and Maddaloni units reached the distance of 30-40 km, at which the investigated sections are located (Fig. 1b) or had dispersal axes not compatible with pumice deposition in these localities.

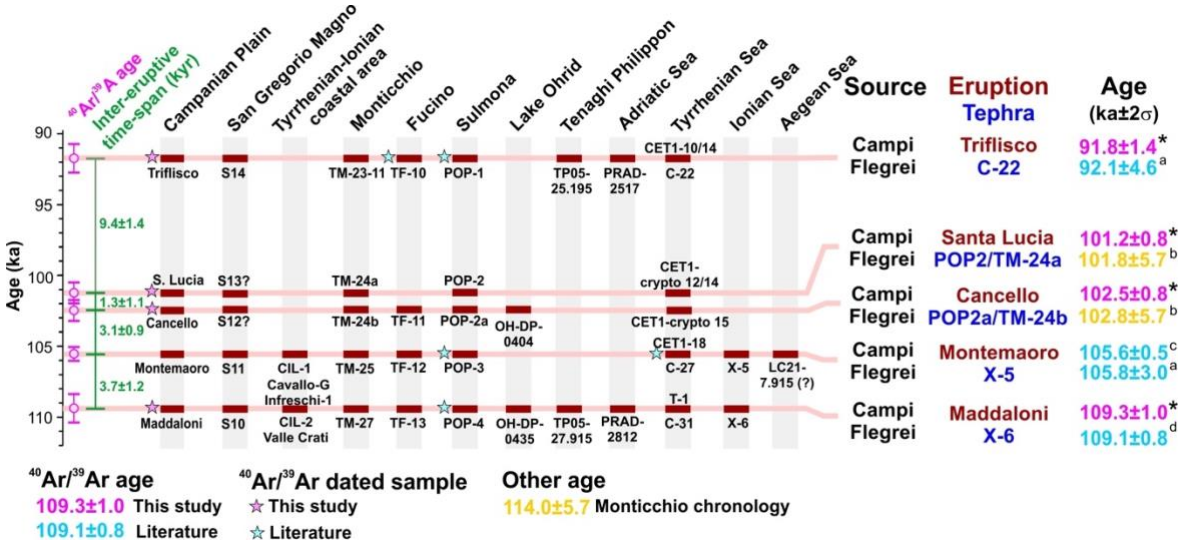

Figure 7. Age and occurrences of the C-22, POP2/TM-24a, POP2a/TM-24b, X-5, and X-6 tephra markers in terrestrial and marine sedimentary environments through the Mediterranean region. $^{40}Ar/^{39}Ar$ ages are according to ACs at 1.1891 Ma and FCs at 28.294 Ma. * This study, [a] Giaccio et al. (2012); [b] Wulf et al. (2012); [c] Petrosino et al. (2016); [d] Regattieri et al. (2015).

5.3. Implications for the chronology of the millennial-scale climatic oscillations of the MIS 5c-d

The great relevance of some of the investigated tephra layers as fundamental chronological and stratigraphic markers for the Mediterranean MIS 5c-d high frequency climatic variability was widely acknowledged and discussed in previous papers (e.g., Giaccio et al., 2012; Regattieri et al., 2015). However, the acquisition of new high-precision $^{40}Ar/^{39}Ar$ ages for two previously undated tephra (Cancello/TM-24b and Santa Lucia/TM-24a tephra layers/markers), the substantial improvement in accuracy of the Triflisco/C-22 unit, as well as the acquisition of new high-resolution records containing these tephra markers (e.g., Tenaghi Philippon; Wulf et al., 2018), give us the opportunity to discuss the implications of these new data from a palaeoclimatological perspective, in particular on the timing and spatial synchronicity of MIS 5c-d climatic variability.

For this purpose, we consider the records endowed with suitable resolution and good expression of the millennial scale climate oscillations of the MIS 5d-c, which can be reasonably correlated to the succession of stadial and interstadial events documented in the reference record of the Greenland ice (e.g., North Greenland Ice Core Project members et al., 2004). These are (i) the Lago Grande di Monticchio pollen profile, Southern Italy (e.g., Brauer et al., 2007; Wulf et al., 2012), (ii) the isotope series of Sulmona Basin, Central Italy (Regattieri et al., 2015, 2017), (iii) the Tenaghi Philippon pollen record, in Greece (Milner et al., 2012, 2013, 2016), and (iv) the pollen record of Lake Ohrid, North Macedonia-Albania (Sinopoli et al., 2018; Figs. 1a, 8). For the sapropel stratigraphy, we also consider the Tyrrhenian Sea record of the core KET 8004 (Paterne et al., 2008), which contains three out of the five markers (Fig. 8), and the Aegean Sea core LC21, likely containing the X-5 layer (Satow et al., 2015; Fig. 8).

So far, Monticchio and Sulmona are the only Mediterranean records containing all the five MIS 5d-c tephra from Campi Flegrei (Fig. 8), whereas Tenaghi Philippon and Ohrid contain only two markers,

i.e., Maddaloni/X-6 and Triflisco/C-22, and Maddaloni/X-6 and Santa Lucia/TM-24a, respectively (Fig. 8; Table 3).

The Maddaloni/X-6 unit, the most common tephra in the considered records (Fig. 7), occurs at the very end of a short interstadial pulsation, likely corresponding to Greenland Interstadial (GI) 25_a. It precedes the onset of the first marked stadial oscillation of the MIS 5 period, the Greenland Stadial (GS) 25_a, corresponding to the North Atlantic cold event C24 (e.g., Shackleton et al., 2004; Fig. 8). The temporal offset, i.e., the difference between the radioisotopic $^{40}Ar/^{39}Ar$ age of Maddaloni/X-6 tephra and the age reported in the various paleoclimatic records (Δt in Fig. 8), is small, reaching the maximum value of ca. 1 kyr in the Monticchio record (Fig. 8; Table 3). However, assuming that the inferred position of Maddaloni/X-6 tephra layer/marker in the Greenland isotope record is correct, then, the age of the end of the GI-25_a, 110.6 ka, according to GICC05 (Rasmussen et al., 2014), should be approximately 1.3 kyr younger (Fig. 8). On the contrary, Sardinian stalagmite evidence suggests instead that the GI-25_b ended at 110.5 ka (Columbu et al., 2017), which is fully consistent with the GICC05 chronology.

The Montemaoro/X-5 tephra occurs in the middle of an interstadial oscillation correlated to the GI-24 (e.g., Regattieri et al., 2015). More precisely, Montemaoro/X-5 tephra occurs close to a very brief stadial pulsation within the GI-24 that is quite evident in all the considered records and that likely corresponds to the short GS-24.2 (Fig. 8). The Δt, relative to the Montemaoro/X-5 tephra, is of ca. 1 kyr in all records, except Monticchio, in which it is negligible (Fig. 8; Table 3). In the Tyrrhenian Sea, and likely in the Aegean Sea, the Montemaoro/X-5 also represents an excellent marker for the Sapropel S4, which is in turn correlated to the GI-24.1 (Regattieri et al., 2015; Fig. 8).

The Cancello and Santa Lucia tephra layers form an interesting couplet of temporally closely related tephra, which mark the onset of an interstadial and the ensuing stadial phase, likely corresponding to the GI-23.2 and the GS-23.2, respectively (Fig. 8). In all the considered records, the negligible Δt relative to this couple of tephra evidences a good agreement between the $^{40}Ar/^{39}Ar$ chronology and the age models of the records (Fig. 8).

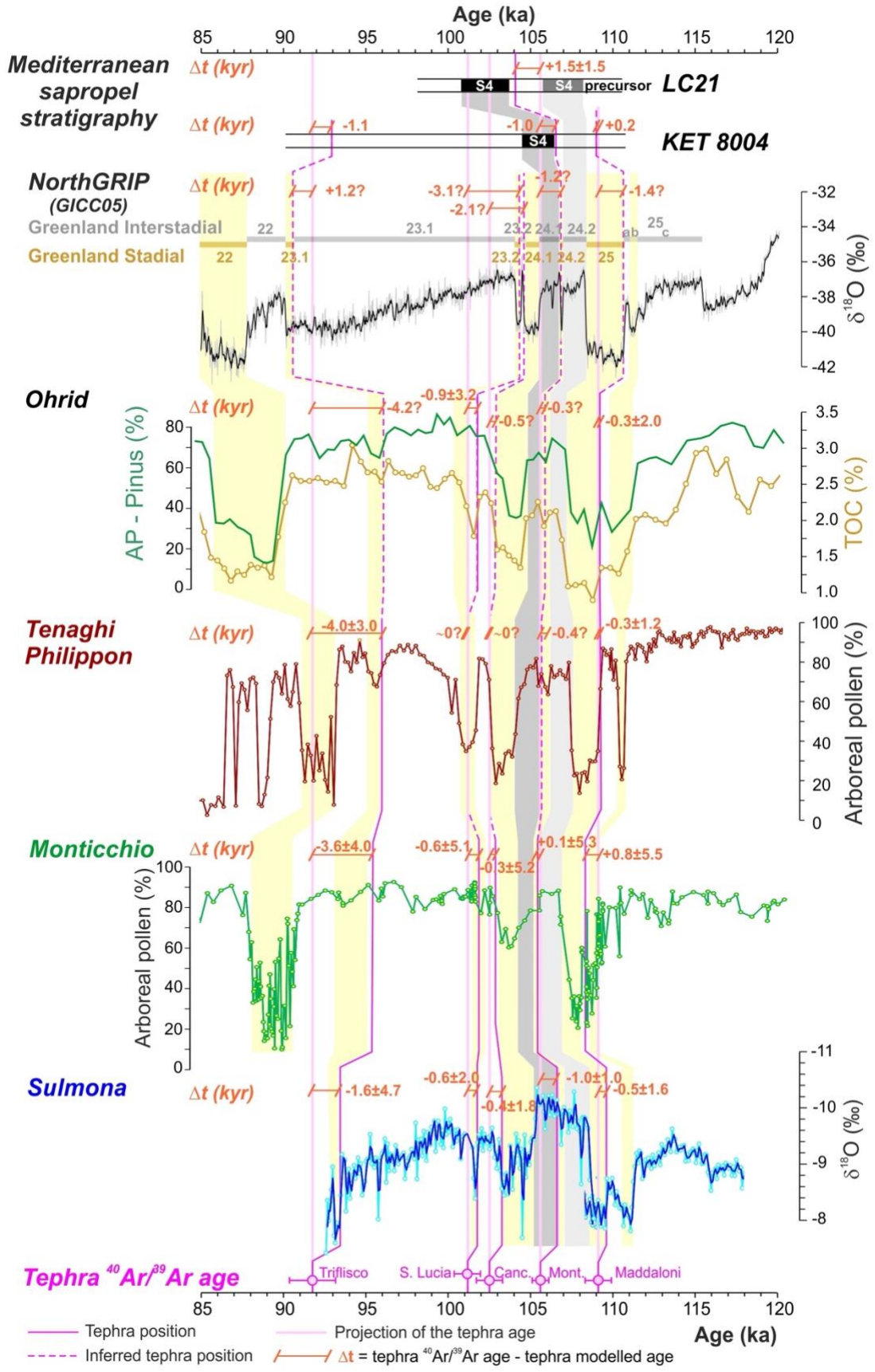
Age (ka)
85 90 95 100 105 110 115 120
Mediterranean sapropel stratigraphy
Δt (kyr)
+1.5±1.5
S4
S4 precursor
LC21
Δt (kyr)
-1.1
-1.0
+0.2
S4
KET 8004
NorthGRIP (GICC05)
Δt (kyr)
+1.2?
-3.1?
-2.1?
-1.2?
-1.4?
Greenland Interstadial
22 23.1 23.2 24.1 24.2 ab 25c
Greenland Stadial
22 23.1 23.2 24.1 24.2 25
-32 -34 -36 -38 -40 -42
δ18O (‰)
Ohrid
Δt (kyr)
-4.2?
-0.9±3.2
-0.5?
-0.3?
-0.3±2.0
AP - Pinus (%)
80 60 40 20 0
3.5 3.0 2.5 2.0 1.5 1.0
TOC (%)
Tenaghi Philippon
Δt (kyr)
-4.0±3.0
~0?
~0?
-0.4?
-0.3±1.2
100 80 60 40 20 0
Arboreal pollen (%)
Monticchio
Δt (kyr)
-3.6±4.0
-0.6±5.1
-0.3±5.2
+0.1±5.3
+0.8±5.5
Arboreal pollen (%)
100 80 60 40 20 0
Sulmona
Δt (kyr)
-1.6±4.7
-0.6±2.0
-0.4±1.8
-1.0±1.0
-0.5±1.6
-11 -10 -9 -8
δ18O (‰)
Tephra 40Ar/39Ar age
Triflisco
S. Lucia
Canc.
Mont.
Maddaloni
85 90 95 100 105 110 115 120
Age (ka)
Tephra position
Projection of the tephra age
Inferred tephra position
Δt = tephra 40Ar/39Ar age - tephra modelled age

Figure 8. Chronological offset between $^{40}Ar/^{39}Ar$ and modelled tephra age in selected high-resolution Mediterranean records containing the here investigated tephra and showing the millennial-scale climatic oscillations of the MIS 5d-c, compared to Greenland ice succession of stadial-interstadial events (Rasmussen et al., 2014). The Mediterranean sapropel stratigraphy from the Tyrrhenian Sea core KET 8004 (Paterne et al., 2008) and Aegean Sea core LC21 (Satow et al., 2015), is also shown. The sapropel nomenclature is according to Ziegler et al. (2010). Data source: Lake Ohrid Arboreal pollen minus *Pinus* (AP – Pinus) and total organic carbon (TOC): Sinopoli et al. (2018), Wagner et al., (2017, 2019); Tenaghi Philippon pollen record: Milner et al. (2012, 2013, 2016); Monticchio pollen record; Brauer et al. (2007); Sulmona isotope record, Regattieri et al (2015).

Finally, the Triflisco/C-22 tephra occurs at the beginning of a stadial event that interrupts a relatively long interstadial period, likely corresponding to the GS-23.1, which occurs at the end of the long-term cooling period featuring the GI-23.1 (Fig. 8). Noteworthy, the Δt relative to this tephra is quite long for the Monticchio and Tenaghi Philippon pollen records, reaching the considerable value of ca. 4 kyr (Fig. 8). The Δt is instead quite negligible for the NorthGRIP record (~1.2 kyr), provided that the inferred climatostratigraphic position of Triflisco/C-22 in the Greenland record is correct.

In summary, the Δt is relatively little for most of the climatic events, for which the Campi Flegrei MIS 5 tephra act as fundamental markers, and generally do not exceed the uncertainty associated to both $^{40}Ar/^{39}Ar$ ages and the age models of the respective paleoclimatic records (Table 3). However, the event associated with the Triflisco/C-22 represents a notable exception, for which the Δt can exceed the uncertainty associated to the $^{40}Ar/^{39}Ar$ dating of Triflisco/C-22 and of the paleoclimatic record age models (Figs. 7, 8; Table 3). With this regard, we emphasize that such wide Δt cannot be explained invoking an uncertainty of the tephra position within the records, as, at least for Monticchio and Tenaghi Philippon, where the Δt is -3.6 ± 4.0 kyr and -4.0 ± 3.0 kyr (Table 3), it is not relayed on an inference, this being based on undisputable stratigraphic evidence (Fig. 8).

Overall, the investigated tephra can be considered good stratigraphic markers of some of the stadial-interstadial events, as well as of the very short sub-stadial and sub-interstadial oscillations that punctuated the MIS 5c-d climatic variability (Table 3), whose chronology can greatly benefit from the high precision $^{40}Ar/^{39}Ar$ dating of the Campi Flegrei eruption products.

Table 3. Detailed climatostratigraphic position of the Campi Flegrei units with respect to the millennial to sub-millennial scale MIS 5 paleoclimatic events - expressed as Greenland stadial-interstadial successions (Rasmussen et al., 2014) - as recorded in reference archives of the central Mediterranean area (Figs. 1, 7 and 8). The temporal offset, i.e., the difference between the radioisotopic $^{40}Ar/^{39}Ar$ age of Campi Flegrei tephra and the age of the corresponding distal tephra, as reported in the various paleoclimatic records, is also shown. Data source: Sulmona: Regattieri et al. (2015, 2017); Monticchio: Wulf et al. (2012), Regattieri et al. (2015); Ohrid: Leicher et al. (2021); Tenaghi-Philippon: Wulf et al. (2018); LC21: Satow et al. (2015).

Campanian Plain	**Sulmona**	**Monticchio**	**Ohrid**	**Tenaghi-Philippon**	**LC21**	**Correlated event**
Tephra $^{40}Ar/^{39}Ar$ age (ka±2σ)	Tephra Age±2σ ka Δt±2σ kyr	Tephra Age±2σ ka Δt±2σ kyr	Tephra Age±2σ ka Δt±2σ kyr	Tephra Age±2σ ka Δt±2σ kyr	Tephra Age±2σ ka Δt±2σ kyr	
Triflisco 91.8±1.4	POP1 93.4±4.5 -1.6±4.7	TM-23-11 95.4±3.8 -3.6±4.0		TP05-25.195 95.8±2.6 -4.0±3.0		Onset GS-23.1
Santa Lucia 101.2±0.8	POP2 101.8±1.8 -0.6±2.0	TM-24a 101.8±5.0 -0.6±5.1	OH-DP-0404 102.1±3.1 -0.9±3.2			Middle GS-23.2
Cancello 102.5±0.8	POP2a 102.9±1.5 -0.4±1.7	TM-24b 102.8±5.1 -0.3±5.2				Onset GI-23.2
Montemaoro 105.6±0.5	POP3 106.6±1.0 -1.0±1.0	TM-25 105.5±5.3 0.1±5.3			LC21-7.915 (?) 104.0±2.0 1.5±1.5	End GS-24.2 - base sapropel S4
Maddaloni 109.1±0.8	POP4 109.6±1.4 -0.5±1.6	TM-27 108.3±5.4 0.8±5.5	OH-DP-0435 109.4±1.8 -0.3±2.0	TP05-27.915 109.4±0.9 -0.3±1.2		Onset GS-25 - End GI-25a

6. *Conclusions*

In this study, we presented a wide dataset (i.e., stratigraphy, major, minor, and trace elements, Sr-Nd isotopic composition and $^{40}Ar/^{39}Ar$ ages) required for a full characterization of four pumice fall deposits, named Triflisco, Santa Lucia, Cancello, and Maddaloni, occurring in the Campanian Plain, 30 to 60 km east of the Campi Flegrei volcanic field, and stratigraphically laying below the CI (~40 ka). Based on these data, these units are here attributed to a previously unknown 109-92 ka explosive activity at Campi Flegrei volcano and correlated with the widespread C-22, TM-24a/POP-2, TM-24b/POP-2a and X-6 tephra markers, respectively. Furthermore, the chronological and stratigraphic constraints provided in this study, and a review of previous EDS data, allow us also to propose the correlation of a fifth unit (i.e., Montemaoro) with the X-5 marine tephra marker as well. Our data confidently allow us to trace the volcanic source of these fundamental Mediterranean marker horizons, so far only hypothesized. This extends the activity history of the Campi Flegrei

volcano back ~110 ka at least, setting the groundwork for a reassessment of the volcanic history, and related hazards, and confirming the Campi Flegrei volcano as one of the Europe's most productive sources of widespread and disruptive ash fall events. The Maddaloni/X-6, given its wide dispersal area, clearly arises from one of the largest explosive events through the whole Campi Flegrei eruptive history and demands further volcanological investigations.

The new high-precision $^{40}Ar/^{39}Ar$ dating of the investigated units provide new fundamental temporal constraints for refining and consolidating the chronology of MIS 5d-c period, characterised by a marked millennial- to sub-millennial scale climatic variability, well documented in Mediterranean archives. Specifically, the ages obtained for the Cancello and Santa Lucia tephra markers provide two new chronological constraints for the climatic oscillations likely corresponding to the Greenland interstadial GI-23.2 and Greenland stadial GS-23.2. Furthermore, the improved precision of the age for Triflisco would imply a substantial extension of the duration of the interstadial period corresponding to the GI-23.1 up to 92 ka, i.e., ~4 kyr later than the ~96 ka age reported for the GI-23.1 in several reference Mediterranean records. (Fig. 8). A reappraisal of the related chronologies is thus required.

Future research development on the eruptive history and long-term hazard assessment at Campi Flegrei, as well as paleoclimatic and archaeological investigations in central Mediterranean, will greatly benefit from the geochemical and geochronological dataset provided in this contribution. Given the strong geochemical similarities of the HAR Triflisco/C-22, Santa Lucia/TM-24a, and Cancello/TM-24b units, we encourage caution to avoid potentially misleading correlations based solely on major elements. Therefore, especially when a specific tephra layer occurrence lacks bracketing tephra units, we recommend integrating major element data with trace element and Sr-Nd isotope analysis, as they proved to be the best discriminating tool for these tephra deposits.

Acknowledgments

R. Jedlička and M. Racek, E. Braschi and A. Orlando, are thanked for providing valuable technical assistance during EPMA analysis at Prague and Florence Universities respectively. Field activities of L.M. were financially supported by “Sapienza” University, “Bando di Avvio alla Ricerca”, protocol N° AR120172AD35B81D (responsible: L.M.). G.S. received funding by “Sapienza” University, Fondi di Ateneo-Progetti Medi (protocol N° RM11715C82384428). Financial support was provided by the Competitive fund of the Italian Research Ministry (MUR, PRIN 2017, grant 20177TKBXZ_003, project “FUTURE, G. Zanchetta, coordinator), issued to BG, DP and GZ. The INGV-OV laboratories have been also financially supported by the EPOS Research Infrastructure through the contribution of the Italian Ministry of University and Research (MUR). P.G.A. is funded through a UK Research and Innovation (UKRI) Future Leaders Fellowship (MR/S035478/1). An earlier version of the manuscript benefited from useful comments from R. Cioni and Sabine Wulf. Ioan Seghedi (IG “SSS” AR) and an anonymous reviewer provided thoughtful and constructive comments that improved the manuscript.

References

Albert, P.G., Giaccio, B., Isaia, R., Costa, A., Niespolo, E.M., Nomade, S., Pereira, A., Renne, P.R., Hinchliffe, A., Mark, D.F., Brown, R.J., Smith, V.C., 2019. Evidence for a large-magnitude eruption from Campi Flegrei Caldera (Italy) at 29 ka. *Geology.* **47** (7), 595-599. https://doi.org/10.1130/G45805.1.

Albert, P.G., Hardiman, M., Keller, J., Tomlinson, E.L., Smith, V.C., Bourne, A.J., Wulf, S., Zanchetta, G., Sulpizio, R., Müller, U.C., Pross, J., Ottolini, L., Matthews, I.P., Blockley, S.P.E., Menzies, M.A., 2015. Revisiting the Y-3 stratigraphic marker: a new diagnostic glass geochemistry, age estimate, and details on its climatostratigraphical context. *Quat. Sci. Rev.* **118**, 105-121. https://doi.org/10.1016/j.quascirev.2014.04.002.

Arienzo, I., Civetta, L., Heumann, A., Wörner, G., Orsi, G., 2009. Isotopic evidence for open system processes within the Campanian Ignimbrite (Campi Flegrei-Italy) magma chamber. *Bull. Volcanol.* **71**, 285-300. https://doi.org/10.1007/s00445-008-0223-0.

Arienzo, I., D'Antonio, M., Di Renzo, V., Tonarini, S., Minolfi, G., Orsi, G., Carandente, A., Belviso, P., Civetta, L., 2015. Isotopic microanalysis sheds light on the magmatic endmembers feeding volcanic eruptions: The Astroni 6 case study (Campi Flegrei, Italy). *J. Volcanol. Geotherm. Res.* **304**, 24–37. https://doi.org/10.1016/j.jvolgeores.2015.08.003.

Arienzo, I., Mazzeo, F.C., Moretti, R., Cavallo, A., D'Antonio, M., 2016. Open-system magma evolution and fluid transfer at Campi Flegrei caldera (Southern Italy) during the past 5 ka as revealed by geochemical and isotopic data: the archetype of Nisida eruption. Chem. Geol. **427**, 109-124. https://doi.org/10.1016/j.chemgeo.2016.02.007.

Arienzo, I., Moretti, R., Civetta, L., Orsi, G., Papale, P., 2010. The feeding system of the Agnano-Monte Spina eruption Campi Flegrei, Italy): dragging the past into present activity and future scenarios. *Chem. Geol.* **270** (1-4), 135-147. https://doi.org/10.1016/j.chemgeo.2009.11.012.

Balbas, A., Koppers, A.A.P., Kent, D.V., Konrad, K., Clark, P.U., 2016. Identification of the short-lived Santa Rosa geomagnetic excursion in lavas on Floreana Island (Galapagos) by $^{40}Ar/^{39}Ar$ geochronology. *Geology* **44** (5), 359-362 (2016). https://doi.org/10.1130/G37569.1.

Bourne, A.J., Albert, P.G., Matthews, I.P., Trincardi, F., Wulf, S., Asioli, A., Blockley, S.P.E., Keller, J., Lowe, J.J., 2015. Tephrochrunology of core PRAD 1-2 from the Adriatic Sea: insights into Italian explosive volcanism for the period 200-80 ka. *Quat. Sci. Rev.* **116**, 28-43. https://doi.org/10.1016/j.quascirev.2015.03.006.

Bourne, A.J., Lowe, J.J., Trincardi, F., Asioli, A., Blockley, S.P.E., Wulf, S., Matthews, I.P., Piva, A., Vigliotti, L., 2010. Distal tephra record for the last ca 105,000 years from core PRAD 1-2 in the central Adriatic Sea: implications for the marine tephrostratigraphy. *Quat. Sc. Rev.* **29**, 3079-3094. https://doi.org/10.1016/j.quascirev.2010.07.021.

Brauer, A., Allen, J.R.M., Mingram, J., Dulski, P., Wulf, S., Huntley, B., 2007. Evidence for the last interglacial chronology and environmental change from Southern Europe. *PNAS* **104** (2), 450-455. https://doi.org/10.1073/pnas.0603321104.

Brown, R.J., Civetta, L., Arienzo, I., D'Antonio, M., Moretti, R., Orsi, G., Tomlinson, E.L., Albert, P.G., Menzies, M.A., 2014. Geochemical and isotopic insights into the assembly, evolution and disruption of a magmatic plumbing system before and after cataclysmic caldera-collapse eruption at Ischia volcano (Italy). *Contirb. Mineral. Petrol.* **168**: 1035. https://doi.org/10.1007/s00410-014-1035-1.

Brown, R.J., Orsi, G., de Vita, S., 2008. New insights into Late Pleistocene explosive volcanic activity and caldera formation on Ischia. *Bull. Volcanol.* **70**, 583-603. https://doi.org/10.1007/s00445-007-0155-0.

Casalini, M., Heumann, A., Marchionni, S., Conticelli, S., Avanzinelli, R., Tommasini, S., 2018. Inverse modelling to unravel the radiogenic isotope signature of mantle sources from evolved magmas: the case-study of Ischia volcano. *Ital. J. Geosci.* **137**, pp. 00. https://doi.org/:103301/IJG.2018.05.

Cioni, R., Bertagnini, A., Santacroce, R., Andronico, D., 2008. Explosive activity and eruption scenarios at Somma-Vesuvius (Italy): Towards a new classification scheme. Journal of Volcanology and Geothermal Research, 178 (3), 331-346. https://doi.org/10.1016/j.jvolgeores.2008.04.024.

Civetta, L., Orsi, G., Pappalardo, L., Fisher, R.V., Heiken, G., Ort, M., 1997. Geochemical zoning, mingling, eruptive dynamics and depositional processes - the Campanian Ignimbrite, Campi Flegrei, Italy. *J. Volcanol. Geotherm. Res.* **75** (3-4), 183-219. https://doi.org/10.1016/S0377-0273(96)00027-3.

Columbu, A., Drysdale, R., Capron, E., Woodhead, J., De Waele, J., Sanna, L., Hellstrom, J., Bajo, P., 2017. Early last glacial intra-interstadial climate variability recorded in Sardinian speleothem. *Quat. Sci. Rev.* **169**, 391-397. https://doi.org/10.1016/j.quascirev.2017.05.007.

Costa, A., Folch, A., Macedonio, G., Giaccio, B., Isaia, R., Smith, V.R., 2012. Quantifying volcanic ash dispersal and impact of the Campanian Ignimbrite super-eruption. *Geophys. Res. Lett.* **39**, p. L101310. https://doi.org/10.1029/2012GL051605.

Cox, S.E., Hemming, S.R., Tootell, D., 2020 The Isotopx NGX and ATONA Faraday amplifiers. *Geochronology* **2**, 231-243. https://doi.org/10.5194/gchron-2-231-2020.

D'Antonio, M., Arienzo, I., Brown, R.J., Petrosino, P., Pelullo, C., Giaccio, B., 2021. Petrography and mineral chemistry of Monte Epomeo Green Tuff, Ischia Island, South Italy: Constraints for identification of the Y-7 tephrostratigraphic marker in distal sequences of the Central Mediterranean. *Minerals* **11**, 955. https://doi.org/10.3390/min11090955.

D'Antonio, M., Tonarini, S., Arienzo, I., CIvetta, L., Dallai, L., Moretti, R., Orsi, G., Andria, M., Trecalli, A., 2013. Mantle and crustal processes in the magmatism of the Campania region: inferences from mineralogy, geochemistry, and Sr-Nd-O isotopes of young hybrid volcanics of the Ischia island (South Italy). *Contrib. Mineral. Petrol.* **165**, 1173-1194. https://doi.org/10.1007/s00410-013-0853-x.

D'Antonio, M., Tonarini, S., Arienzo, I., Civetta, L., Di Renzo, V., 2007. Components and processes in the magma genesis of the Phlegrean Volcanic District, southern Italy. In: Beccaluva, L., Bianchini, G., Wilson, M. (eds.) Cenozoic Volcanism in the Mediterranean Area. *Geol. Soc. Am. Special Paper* **418**, 203-220.

De Astis, G., Pappalardo, L., Piochi, M., 2004. Procida volcanic history: new insights into the evolution of the

Phlegrean Volcanic District (Campania region, Italy). *Bull. Volcanol.* **66**, 622-641. https://doi.org/10.1007/s00445-004-0345-y.

De Vivo, B., Rolandi, G., Gans, P.B., Calvert, A., Bohrson, W.A., Spera, F.J., Belkin, H.E., 2001. New constraints on the pyroclastic eruptive history of Campanian volcanic Plain (Italy). *Mineral. Petrol*. **73**, 47-65. https://doi.org/10.1007/s007100170010.

Deino, A.L., Orsi, G., de Vita, S., Piochi, M., 2004. The age of the Neapolitan Yellow Tuff caldera-forming eruption (Campi Flegrei Caldera - Italy) assessed by $^{40}Ar/^{39}Ar$ dating method. *J. Volcanol. Geotherm. Res.* **133** (1-4), 157-170. https://doi.org/10.1016/S0377-0273(03)00396-2.

Di Renzo, V., Arienzo, I., Civetta, L., D'Antonio, M., Tonarini, S., Di Vito, M.A., Orsi, G., 2011. The magmatic feeding system of the Campi Flegrei caldera: Architecture and temporal evolution. *Chem. Geol.* **281** (3-4), 227-241. https://doi.org/10.1016/j.chemgeo.2010.12.010.

Di Vito, M.A., Sulpizio, R., Zanchetta, G., D'Orazio M., 2008 The late Pleistocene pyroclastic deposits of the Campanian Plain: New insights into the explosive activity of the Neapolitan volcanoes. *J. Volcanol. Geotherm. Res.* **177**, 19-48. https://doi.org/10.1016/j.jvolgeores.2007.11.019.

Donato, P., Albert, P.G., Crocitti, M., De Rosa, C., Menzies, M.A., 2016. Tephra layers along the southern Tyrrhenian coast of Italy: Links to the X-5 & X-6 using volcanic glass geochemistry. J. *Volcanol. Geotherm. Res.* **317**, 30-41. https://doi.org/10.1016/j.jvolgeores.2016.02.023.

Drysdale, R., Zanchetta, G., Hellstrom, J.C., Fallick, A.E., McDonald, J., Catwright, I., 2007. Stalagmite evidence for the precise timing of North Atlantic cold events during the early last glacial. *Geology* **35** (1), 77-80. https://doi.org/10.1130/G23161A.1.

Fanara, S., Botcharnikov, R.E., Palladino, D.M., Adams, F., Buddensieck, J., Mulch, A., Behrens, H., 2015. Volatiles in magma related to Campanian Ignimbrite eruption: Experiments vs natural findings. *Am. Min.* **100** (10), 2284-2297. https://doi.org/10.2138/am-2015-5033.

Galli, P., Giaccio, B., Messina, P., Peronace, E., Amato, V., Naso, G., Nomade, S., Pereira, A., Piscitelli, S., Bellanova, J., Billi, A., Blamart, D., Galderisi, A., Giocoli, A., Stabile, T., Thil, F., 2017. Middle to Late Pleistocene activity of the Matese fault system (southern Apennines, Italy). *Tectonophysics* **699**, 61-81. https://doi.org/10.1016/j.tecto.2017.01.007.

Giaccio, B., Haydas, I., Isaia, R., Deino, A., Nomade, S., 2017b. High-precision ^{14}C and $^{40}Ar/^{39}Ar$ dating of Campanian Ignimbrite (Y-5) reconciles the time-scales of climatic cultural processes at 40 ka. *Sci. Rep.* **7**, 45940. https://doi.org/10.1038/srep45940.

Giaccio, B., Niespolo, E.M., Pereira, A., Nomade, S., Renne, P.R., Albert, P.G., Arienzo, I., Regattieri, E., Wagner, B., Zanchetta, G., Gaeta, M., Galli, P., Mannella, G., Peronace, E., Sottili, G., Florindo, F., Leicher, N., Marra, F., Tomlinson, E.L., 2017a. First integrated tephrochronological record for the last ~190 kyr from the Fucino Quaternary lacustrine succession, central Italy. *Quat. Sci. Rev.* **158**, 211-234. https://doi.org/10.1016/j.quascirev.2017.01.004.

Giaccio, B., Nomade, S., Wulf, S., Isaia, R., Sottili, G., Cavuoto, G., Galli, P., Messina, P., Sposato, A., Sulpizio, R., Zanchetta, G., 2012. The late MIS 5 Mediterranean tephra markers: a reappraisal from peninsular Italy terrestrial records. *Quat. Sci. Revi.* **56**, 31-45. https://doi.org/10.1016/j.quascirev.2012.09.009.

Goldstein, S.L., Denis, P., Oelkers, E.H., Rudnick, R.L., Walter, L.M., 2003. Standards for publication of isotope ratio and chemical data in chemical geology. *Chem. Geol.* **202**, 1-4. https://doi.org/10.1016/j.chemgeo.2003.08.003.

Insinga, D.D., Tamburrino, S., Lirer, F., Vezzoli, L., Barra, M., De Lange, G.J., Tiepolo, M., Vallefuoco, M., Mazzola, S., Sprovieri, M., 2014. Tephrochronology of the astronomically-tuned KC01B deep-sea core, Ionian Sea: insights into the explosive activity of the Central Mediterranean area during the last 200 ka. *Quat. Sci. Revi.* **85**, 63-84. https://doi.org/10.1016/j.quascirev.2013.11.019.

Iorio, M., Liddicoat, J., Budillon, F., Incoronato, A., Coe, R.S., Insinga, D.D., Cassata, W.S., Lubritto, C., Angelino, A., Tamburrino, S., 2014. Combined palaeomagnetic secular variation and petrophysical records to time-constrain geological and hazardous events: An example from the eastern Tyrrhenian Sea over the last 120 ka. *Glob. Planet Change* **113**, 91-109. https://doi.org/10.1016/j.gloplacha.2013.11.005.

Jochum, K.P., Stoll, B., Herwig, K., Willbold, M., Hofmann, A.W., Amini, M., Aarbug, S., Abouchami, W., Hellebrand, E., Mocek, B., Raczek, I., Stracke, A., Alard, O., Bouman, C., Becker, S., Dücking, M., Brätz, H., Klemd, R., de Bruin, D., Canil, D., Cornell, D., de Hoog, C.-S., Dalpé, C., Danyushevsky, L., Eisenhauer, A., Gao, Y., Snow, J.E., Groschopf, N., Günther, D., Latkoczy, C., Guillong, M., Hauri, E.K., Höfer, H.E., Lahaye, Y., Horz, K., Jacob, D.E., Kasemann, S.A., Kent, A.J.R., Ludwig, T., Zack, T., Mason, P.R.D., Meixner, A., Rosner, M., Kisawa, K., Nash, P.B., Pfänder, J., Premo, W.R., Sun, W.D., Tiepolo, M., Vannucci, R., Vennemann, T., Wayne, D., Woodhead, J.D., 2006. MPI-DING reference glasses for in situ microanalysis: New reference values for element concentrations and isotope ratios. *Geochem. Geophys.* **7**:2. https://doi.org/10.1029/2005GC001060.

Keller, J., Ryan, W.B.F., Ninkovich, D., Altherr, R., 1978. Explosive volcanic activity in the Mediterranean over the last 200,000 yr as recorded in deep-sea sediments. *Geol. Soc. Am. Bull.* **89**, 591-604. https://doi.org/10.1130/0016-7606(1978)89%3C591:EVAITM%3E2.0.CO;2.

Koppers, A.A.P., 2002. ArArCALC e software for $^{40}Ar/^{39}Ar$ age calculations. *Comput. Geosci.* **28**, 605-619. https://doi.org/10.1016/S0098-3004(01)00095-4.

Kuehn, S.C., Froese, D.G., Shane, P.A.R., INTAV Intercomparison Participants, 2011. The INTAV intercomparison of electron-beam microanalysis of glass by tephrochronology laboratories: Results and recommendations. *Quat. Int.* **246** (1-2), 19-47. https://doi.org/10.1016/j.quaint.2011.08.022.

Le Maitre, R.W., Streckeisen, A., Zanettin, B., Le Bas, M.J., Bonin, B., Bateman, P., Bellieni, G., Dudek, A., Efremova, S., Keller, J., Lameyre, J., Sabine, P.A., Schmid, R., SØrensen, H., Woolley, A.R., 2002. Igneous Rocks: A Classification and Glossary of Terms. Reccomendation of the International Union of Geological Sciences Subcommission on the Systematics of Igneous Rocks, 2nd Edition. Cambridge University Press, Cambridge. 236 pages.

Lee, J.Y., Marti, K., Severinghaus, J.P., Kawamura, K., Yoo, H.S., Lee, J.B., Kim, J.S., 2006. A redetermination of the isotopic abundances of atmospheric Ar. *Geochim. Cosmochim. Acta* **70** (17),

4507-4512. https://doi.org/10.1016/j.gca.2006.06.1563.
Leicher, Giaccio, B., Zanchetta, G., Sulpizio, R., Albert, P.G., Tomlinson, E.L., Lagos, M., Francke, A., Wagner, B., 2021. Lake Ohrid's tephrochronological dataset reveals 1.36 Ma of Mediterranean explosive volcanic activity. *Sci. Data* **8**, 231. https://doi.org/10.1038/s41597-021-01013-7.
Leicher, N., Zanchetta, G., Sulpizio, R., Giaccio, B., Wagner, B., Nomade, S., Francke, A., Del Carlo, P., 2016. First tephrostratigraphic results of the DEEP site record from Lake Ohrid (Macedonia and Albania). *Biogeosciences* **13**, 2151-2178. https://doi.org/10.5194/bg-13-2151-2016.
Lucchi, F., Keller, J., Tranne, C.A., 2013. Regional stratigraphic correlations across the Aeolian archipelago (southern Italy). In: Geological Society, London, Memoirs, vol. 37, Chapter 6, pp. 55-81. https://doi.org/10.1144/M37.6.
Ludwig, K.R., 2001. Isoplot 3.0a geochronological toolkit for Microsoft Excel. In: Special Publication No. 4. Berkeley Geochronology Center, Berkeley, CA, USA.
Marciano, R., Munno, R., Paola, P., Nicoletta, S., Santo, A., Villa, I., 2008. Late quaternary tephra layers along the Cilento coastline (southern Italy). *J. Volcanol. Geotherm. Res.* **177** (1), 227-243. https://doi.org/10.1016/j.jvolgeores.2007.11.009.
Marianelli, P. & Sbrana, A. Risultati di misure standard di minerali e di vetri naturali in microanalisi a dispersione di energia (In Italian). *Atti Soc. Tosc. Sci. Nat. Resid. Pisa, Mem. Serie A* **105**, 57-63 (1998).
Milner, A.M., Collier, R.E.L., Roucox, K.H., Müller, U.C, Pross, J., Kalaitzidis, S., Christanis, K., Tzedakis, P.C., 2012. Enhanced seasonality of precipitation in the Mediterranean during the early part of the Last Interglacial. *Geology* **40** (10), 919-922. https://doi.org/10.1130/G33204.1.
Milner, A.M., Müller, U.C., Roucoux, K.H., Collier, R.E., Pross, J., Kalaitzidis, S., Christanis, K., Tzedakis, P.C., 2013. Environmental variability during the Last Interglacial: a new high-resolution pollen record from Tenaghi Philippon, Greece. J. *Quat. Sci.* **28**, 113– 117. https://doi.org/10.1002/jqs.2617.
Milner, A.M., Roucoux, K.H., Collier, R.E. L., Müller, U.C., Pross, J., Tzedakis, P.C., 2016. Vegetation responses to abrupt climatic changes during the Last Interglacial Complex (Marine Isotope Stage 5) at Tenaghi Philippon, NE Greece. *Quat. Sci. Rev.* **154**, 169– 181. https://doi.org/10.1016/j.quascirev.2016.10.016.
Monaco, L., Palladino, D.M., Gaeta, M., Marra, F., Sottili, G., Leicher, N., Mannella, G., Nomade, S., Pereira, A., Regattieri, E., Wagner, B., Zanchetta, G., Albert, P.G., Arienzo, I., D'Antonio, M., Petrosino, P., Manning, C., Giaccio, B., 2021. Mediterranean tephrostratigraphy and peri-Tyrrhenian explosive activity revaluated in light of the 430-365 ka record from Fucino Basin (central Italy). *Earth Sci. Rev.* **220**, 103706. https://doi.org/10.1016/j.earscirev.2021.103706.
Morabito, S., Petrosino, P., Milia, A., Sprovieri, M., Tamburrino, S., 2014. A multidisciplinary approach for reconstructing the stratigraphic framework of the last 40 ka in a bathyal area of the eastern Tyrrhenian Sea. *Glob. Planet Change* **123** (A), 121-138. https://doi.org/10.1016/j.gloplacha.2014.10.005.
Munno, R. & Petrosino, P., 2007. The late Quaternary tephrostratigraphical record of the San Gregorio Magno basin (southern Italy). *J. Quat. Sci*. **22**, 247-266. https://doi.org/10.1002/jqs.1025.
North Greenland Ice-Core Project members, Andersen, K.K., Azuma, N., Barnola, J.M., Bigler, M., Biscaye, P., Caillon, N., Chappellaz, J., Clausen, H.B., Dahl-Jensen, D., Fischer, H., Flückiger, J., Fritzsche, D., Fujii, Y., Goto-Azuma, K., Grønvold, K., Gundestrup, N.S., Hansson, M., Huber, C., Hvidberg, C.S., Johnsen, S.J., Jonsell, U., Jouzel, J., Kipfstuhl, S., Landais, A.,Leuenberger, M., Lorrain, R., Masson-Delmotte, V., Miller, H., Motoyama, H., Narita, H., Popp, T., Rasmussen, S.O., Raynaud, D., Röthlisberger, R., Ruth, U., Samyn, D., Schwander, J., Shoji, H., Siggard-Andersen, M.L., Steffensen, J.P., Stocker, T., Sveinbjörnsdottir, A.E., Svensson, A., Takata, M., Tison, J. L., Thorsteinsson, T.,Watanabe, O., Wilhelms, F., White, J., 2004. High-resolution record of the Northern Hemisphere climate extending into the last interglacial period. *Nature* **431**, 147-151.
Niespolo, E.M., Rutte, D., Deino, A.L., Renne, P.R., 2017. Intercalibration and age of the Alder Creek Sanidine $^{40}Ar/^{39}Ar$ standard. *Quat. Geochronol.* **39**, 205-213. https://doi.org/10.1016/j.quageo.2016.09.004.
Pabst, S., Wörner, G., Civetta, L., Tesoro, R., 2007. Magma chamber evolution prior to the Campanian Ignimbrite and Neapolitan Yellow Tuff eruptions (Campi Flegrei, Italy). *Bull. Volcanol.* **70**, 961-976. https://doi.org/10.1007/s00445-007-0180-z.
Pappalardo, L., Civetta, L., D'Antonio, M., Deino, A., Di Vito, M., Orsi, G., Carandente, A., de Vita, S., Isaia, R., Piochi, M., 1999. Chemical and Sr-isotopical evolution of the Phlegrean magmatic system before the Campanain Ignimbrite and the Neapolitan Yellow Tuff eruptions. *J. Volcanol. Geotherm. Res.* **91** (2-4), 141-166. https://doi.org/10.1016/S0377-0273(99)00033-5.
Paterne, M., Guichard, F., Duplessy, J.C., Siani, G., Sulpizio, R., Labeyrie, J., 2008. A 90,000-200,000 yrs marine tephra record of Italian volcanic activity in the Central Mediterranean Sea. J. *Volcanol. Geotherm. Res.* **177**, 187-196. https://doi.org/10.1016/j.jvolgeores.2007.11.028.
Paterne, M., Guichard, F., Labeyrie, J., 1988. Explosive activity of the south Italian volcanoes during the past 80,000 years as determined by marine tephrochronology. *J. Volcanol. Geotherm. Res.* **34**, 153-172. https://doi.org/10.1016/0377-0273(88)90030-3.
Paterne, M., Guichard, F., Labeyrie, J., Gillot, P.Y., Duplessy, J.C., 1986. Tyrrhenian Sea tephrochronology of the oxygen isotope record for the past 60,000 years. *Mar. Geol.* **72**, 259-285. https://doi.org/10.1016/0025-3227(86)90123-4.
Pelullo, C., Cirillo, G., Iovine, R.S., Arienzo, I., Aulinas, M., Pappalardo, L., Petrosino P., Fernandez-Turiel, J.L., D'Antonio, M., 2020. Geochemical and Sr-Nd isotopic features of the Zaro volcanic complex: insights on the magmatic processes triggering a small-scale prehistoric eruption at Ischia island (south Italy). *Int. J. Earth Sci.* **109** (8), 2829-2849. https://doi.org/10.1007/s00531-020-01933-6.
Peccerillo, A., 2017. Cenozoic Volcanism in the Tyrrhenian Sea Region. In: IAVCEI, Advances in Volcanology, 2 ed. Springer, p. 400.
Petrosino, P., Arienzo, I., Mazzeo, F.C., Natale, J., Petrelli, M., Milia, A., Perugini, D., D'Antonio, M., 2019. The San Gregorio Magno lacusrine basin (Campania, southern Italy): improved

characterization of the tephrostratigraphic markers based on trace elements and isotopic data. *J. Quat. Sci.* **34**, 393-404. https://doi.org/10.1002/jqs.3107.

Petrosino, P., Jicha, B.R., Mazzeo, F.C., Ciaranfi, N., Girone, A., Maiorano, P., 2015. The Montalbano Jonico marine succession: An archive for distal tephra layers at the Early-Middle Pleistocene boundary in southern Italy. *Quat. Int*. **383**, 89-103. https://doi.org/10.1016/j.quaint.2014.10.049.

Petrosino, P., Morabito, S., Jicha, B.R., Milia, A., Sprovieri, M., Tamburrino, S., 2016. Multidisciplnary tephrochronological correlation of marker events in the eastern Tyrrhenian Sea between 48 and 105 ka. *J. Volcanol. Geotherm. Res.* **315**, 79-99. https://doi.org/10.1016/j.jvolgeores.2016.02.001.

Poli, S., Chiesa, S., Gillot, P.-Y., Gregnanin, A., Guichard, F., 1987. Chemistry versus time in the volcanic complex of Ischia (Gulf of Naples, Italy): evidence of successive magmatic cycles. *Contrib. Mineral. Petrol.* **95**, 322-335.

Rasmussen, S.O., Bigler, M., Blockley, S.P., Blunier, T., Buchardt, S.L., Clause, H.B., Cvijanovic, I., Dahl-Jensen, D., Johnsen, S.J., Fischer, H., Gkinis, V., Guillevic, M., Hoek, W.Z., Lowe, J.J., Pedro, J.B., Popp, T., Seierstad, I.K., Steffensen, J.P., Svensson, A.M., Vallelonga, P., Vinther, P.M., Walker, M.J.C., Wheatley, J.J., Winstrup, M., 2014. A stratigraphic framework for abrupt climatic changes during the Last Glacial period based on three synchronized Greenland ice-core records: refining and extending the INITIMATE event stratigraphy. *Quat. Sci. Rev.* **106**, 14-28. https://doi.org/10.1016/j.quascirev.2014.09.007.

Regattieri, E., Giaccio, B., Nomade, S., Francke, A., Vogel, H., Drysdale, R.N., Perchiazzi, N., Wagner, B., Gemelli, M., Mazzini, I., Boschi, C., Galli, P., Peronace, E., 2017. A Last Interglacial record of environmental changes from the Sulmona Basin (central Italy). *Palaeogeogr. Palaeoclimatol. Palaeoecol.* **472**, 51-66. https://doi.org/10.1016/j.palaeo.2017.02.013.

Regattieri, E., Giaccio, B., Zanchetta, G., Drysdale, R.N., Galli, P., Nomade, S., Peronace, E., Wulf, S., 2015. Hydrological variability over the Apennines during the Early Last Glacial precession minimum, as revelated by a stable isotope record from Sulmona basin, Central Italy. J*. Quat. Sci.* **30**, 19-31. https://doi.org/10.1002/jqs.2755.

Renne, P.R., Balco, G., Ludwig, K.R., Mundil, R., Min, K., 2011. Response to the comment by WH Schwarz et al. on "Joint determination of 40 K decay constants and $^{40}Ar^*/^{40}K$ for the Fish Canyon sanidine standard, and improved accuracy for $^{40}Ar/^{39}Ar$ geochronology" by PR Renne et al. (2010). *Geochim. Cosmochim. Acta* **75**, 5097-5100.

Rolandi, G., Bellucci, F., Heizler, M.T., Belkin, H.E., De Vivo, B., 2003. Tectonic controls on the genesis of ignimbrite from the Campanian Volcanic Zone, southern Italy. *Mineral. Petrol.* **79**, 3-31. https://doi.org/10.1007/s00710-003-0014-4.

Rosi, M., Sbrana, A., Vezzoli, L., 1988a. Tephrostratigraphy of Ischia, Procida and Campi Flegrei volcanic products (In Italian). *Mem. Soc. Geol. It.* **41**, 1015-1027.

Rosi, M., Sbrana, A., Vezzoli, L., 1988b. Stratigraphy of Procida and Vivara islands (In Italian). *Boll. GNV* **4**, 500-525.

Santacroce, R. & Sbrana, A., 2003. Geological map of Vesuvius, 1:15.000 scale. SELCA, Firenze.

Santacroce, R., Cioni, R., Marianelli, P., Sbrana, A., Sulpizio, R., Zanchetta, G., Donahue, D.J., Joron, J.L., 2008. Age and whole rock-glass compositions of proximal pyroclastics from the major explosive eruptions of Somma-Vesuvius: A review as a tool for distal tephrostratigraphy. *J. Volcanol. Geotherm. Res.* **177**, 1-18. https://doi.org/10.1016/j.jvolgeores.2008.06.009.

Satow, C., Tomlinson, E.L., Grant, K.M., Albert, P.G., Smith, V.C., Manning, C.J., Ottolini, L., Wulf, S., Rohling, E.J., Lowe, J.J., Blockley, S.P.E., Menzies, M.A., 2015. A new contribution to the Late Quaternary tephrostratigraphy of the Mediterranean: Aegean Sea core LC21. *Quat. Sci. Rev.* **117**, 96-112. https://doi.org/10.1016/j.quascirev.2015.04.005.

Scarpati, C., Perrotta, A., Lepore, S., Calvert, A. 2013. Eruptive history of the Neapolitan volcanoes: constraints from ^{40}Ar-^{39}Ar dating. *Geol. Mag.* **150** (3), 412-425. https://doi.org/10.1017/S0016756812000854.

Shackleton, N.J., Fairbanks, R.G., Chiu, T., Parennin, F., 2004. Absolute calibration of the Greenland time scale: implications for the Antarctic time scales and for $\Delta^{14}C$. *Quat. Sci. Rev*. **23** (14-15), 1513-1522. https://doi.org/10.1016/j.quascirev.2004.03.006.

Sinopoli, G., Masi, A., Regattieri, E., Wagner, B., Francke, A., Peyron, O., Sadori, L., 2018. Palynology of the Last Interglacial Complex at Lake Ohrid: palaeoenvironmental and palaeoclimatic inferences. *Quat. Sci. Rev.* **180**, 177-192. https://doi.org/10.1016/j.quascirev.2017.11.013.

Smith, V.C., Isaia, R., Engwell, S.L., Albert, P.G., 2016. Tephra dispersal during the Campanian Ignimbrite (Italy) eruption: implications for ultra-distal ash transport during the large caldera-forming eruption. *Bull. Volcanol.* **78**, 45. https://doi.org/10.1007/s00445-016-1037-0.

Smith, V.C., Isaia, R., Pearce, N.J.G., 2011. Tephrostratigrapy and glass compositions of post-15 kyr Campi Flegrei eruptions: implications for eruption history and chronostratigraphic markers. *Quat. Sci. Rev.* **30**, 3638-3660.

Sulpizio, R., Zanchetta, G., D'Orazio, M., Vogel, H., Wagner, B., 2010. Tephrostratigraphy and tephrochronology of lakes Ohrid and Prespa, Balkans. *Biogeosciences* **7**, 3273-3288. https://doi.org/10.5194/bg-7-3273-2010.

Tomlinson, E.L., Albert, P.G., Wulf, S., Brown, R.J., Smith, V.C., Keller, J., Orsi, G., Bourne, A., Menzies, M.A., 2014. Age and geochemistry of tephra layers from Ischia, Italy: constraints from proximal-distal correlations with Lago Grande di Monticchio. *J. Volcanol. Geotherm. Res.* **287**, 22-39. https://doi.org/10.1016/j.jvolgeores.2014.09.006.

Tomlinson, E.L., Arienzo, I., Civetta, L., Wulf, S., Smith, V.C., Hardiman, M., Lane, C.S., Carandente, A., Orsi, G., Rosi, M., Müller, W., Menzies, M.A., 2012. Geochemistry of the Phlegrean Fields (Italy) proximal sources for major Mediterranean tephras: Implications for the dispersal of Plinian and co-ignimbritic components of explosive eruptions. *Geochim. Cosmochim. Acta* **93**, 102-128. https://doi.org/10.1016/j.gca.2012.05.043.

Tomlinson, E.L., Thordarson, T., Muller, W., Thirlwall, M.T., Menzies, M.A., 2010. Microanalysis of tephra by LA-ICP-MS - strategies, advantages and limitations assessed using the Thorsmork ignimbrite (Southern Iceland). *Chem. Geol.* **279**, 73-89. https://doi.org/10.1016/j.chemgeo.2010.09.013.

Tonarini, S., D'Antonio, M., Di Vito, M.A., Orsi, G., Carandente, A., 2009. Geochemical and Ba-Sr-Nd isotopic evidence for mingling and mixing processes in the magmatic system that fed the Astroni volcano (4.1-3.8 ka) within the Campi Flegrei caldera (southern Italy). *Lithos* **107** (3-4), 135-151. https://doi.org/10.1016/j.lithos.2008.09.012.

Wagner, B., Wilke, T., Francke, A., Albrecht, C., Baumgarten, H., Bertini, A., Combourieu-Nebout, N., Cvetkoska, A., D'Addabbo, M., Donders, T.H., Föller, K., Giaccio, B., Grazhdani, A., Hauffe, T., Holtvoeth, J., Joannin, S., Jovanovska, E., Lust, J., Kouli, K., Koutsodendris, A., Krastel, S., Lacey, J.H., Leicher, N., Leng, M.J., Levkov, Z., Lindhorst, K., Masi, A., Mercuri, A.M., Nomade, S., Nowaczyk, N., Panagiotopoulos, K., Peyron, O., Reed, J.M., Regattieri, E., Sadori, L., Sagnotti, L., Stelbrink, B., Sulpizio, R., Tofilovska, S., Torri, P., Vogel, H., Wagner, T., Wagner-Cremer, F., Wolff, G.A., Wonik, T., Zanchetta, G., Zhang, X.S., 2017. The environmental and evolutionary history of Lake Ohrid (FYROM/Albania): interim results from the SCOPSCO deep drilling project. *Biogeosciences* **14**, 2033-2054. https://doi.org/10.5194/bg-14-2033-2017.

Wagner, B., Vogel, H., Francke, A., Friederich, T., Donders, T., Lacey, J.H., Leng, M.J., Regattieri, E., Sadori, L., Wilke, T., Zanchetta, G., Albrecht, C., Bertini, A., Combourieu-Nebout, N., Cvetkoska, A., Giaccio, B., Grazhdani, A., Hauffe, T., Holtvoeth, J., Joannin, S., Lagoos, M., Leicher, N., Levkov, Z., Lindhorst, K., Masi, A., Melles, M., Mercuri, A.M., Nomade, S., Nowaczyk, N., Panagiotopoulos, K., Peyron, O., reed, J.M., Sagnotti, L., Sinopoli, G., Stellbrink, B., Sulpizio, R., Timmermann, A., Tofilovska, S., Torri, P., Wagner-Cremer, F., Wonik, T., Zhang, X., 2019. Mediterranean winter rainfall in phase with African monsoons during the past 1.36 million years. *Nature* **573**, 256-260. https://doi.org/10.1038/s41586-019-1529-0.

Wulf, S., Hardiman, M.J., Staff, R.A., Koutsodendris, A., Appelt, O., Blockley, S.P.E., Lowe, J.J., Manning, C.J., Ottolini, L., Schmitt, A.K., Smith, V.C., Tomlinson, E.L., Vakhrameeva, P., Knipping, M., Kotthoff, U., Milner, A.M., Müller, U.C., Christanis, K., Kalaitzidis, S., Tzedakis, P.C., Schmiedl, G., Pross, J., 2018. The Marine isotope stage 1-5 cryptotephra record of Tenaghi Philippon, Greece: Towards a detailed tephrostratigraphic framework for the Eastern Mediterranean region. *Quat. Sci. Rev.* **186**, 236-262. https://doi.org/10.1016/j.quascirev.2018.03.011.

Wulf, S., Keller, J., Paterne, M., Mingram, J., Lauterbach, S., Opitz, S., Sottili, G., Giaccio, B., Albert, P.G., Satow, C., Tomlinson, E.L., Viccaro, M., Brauer, A., 2012. The 100-133 ka record of Italian explosive volcanism and revised tephrochronology of Lago Grande di Monticchio. *Quat. Sci. Rev.* **58**, 104-123. https://doi.org/10.1016/j.quascirev.2012.10.020.

Wulf, S., Kraml., M., Brauer, A., Keller, J., Negendank, J.F.W., 2004. Tephrochronology of the 100 ka lacustrine sediment record of Lago Grande di Monticchio (Southern Italy). *Quat. Int*. **122**, 7-30. https://doi.org/10.1016/j.quaint.2004.01.028.

Zanchetta, G., Giaccio, B., Bini, M., Sarti, L., 2018. Tephrostratigraphy of Grotta del Cavallo, Southern Italy: insights of the chronology of Middle to Upper Paleolithic transition in the Mediterranean. *Quat. Sci. Rev.* **182**, 65-77. https://doi.org/10.1016/j.quascirev.2017.12.014.

Ziegler, M., Tuenter, E., Lourens, L.J. 2010. The precession phase of the boreal summer monsoon as viewed from the eastern Mediterranean (ODP Site 968). *Quat. Sci. Rev*. **29** (11-12), 1481-1490. https://doi.org/10.1016/j.quascirev.2010.03.011.

Chapter VI - Application of the tephrostratigraphic method for paleoclimate and volcanological reconstructions

During the Ph.D. Thesis, I contributed to the preparation and publication of several co-authored papers. In these works, I provided the geochemical composition (i.e., major, minor and trace elements by means of EPMA-WDS and LA-ICP-MS) of the investigated tephra layers and contributed to their correlation to the source volcanoes and, when possible, the individual equivalent eruptive event. These works (i.e., Marra et al., 2019; Giaccio et al., 2019, 2021; Bini et al., 2020; Pereira et al., 2020) are here mentioned, with their abstracts, in chronological order of publication.

1. Combined glacio-eustatic forcing and volcano-tectonic uplift: Geomorphological and geochronological constraints on the Tiber River terraces in the eastern Vulsini Volcanic District (central Italy).

Marra, F., Costantini, L., Di Buduo, G.M., Florindo, F., Jicha, B.R., Monaco, L., Palladino, D.M., & Sottili, G., 2019. *Global and Planetary Change*, 182, 103009.

In the present paper, we analyze the regional interplay between glacio-eustasy and volcano-tectonic uplift on the Tyrrhenian Sea margin of central Italy. We reconstruct a succession of fluvial terraces in the Tiber River Valley east of the Vulsini Volcanic District and we provide geochronologic constraints allowing for correlation with the sea-level highstands of the Marine Isotope Stage timescale. Results of this study show that glacio-eustatic forcing affected the hydrographic network of the Tiber River, as far as 70 km inland with respect to the present Tyrrhenian coast, consistent with a regional uplift on the order of several tens of meters that affected this region over the last 250 ky. Using six new $^{40}Ar/^{39}Ar$ dates, we demonstrate the synchronicity between sea-level rise during glacial termination IV and the deposition of a fining-upward sedimentary succession of the Paleo-Tiber River in this area. A detailed reconstruction of the chronostratigraphic setting enabled us to assess local uplift and fault displacement due to volcano-tectonic processes associated with the activities of Bolsena-Orvieto and Latera volcanoes since 350 ka and develop an uplift curve for the different sectors of the investigated area. Moreover, we estimate sedimentation rate during post-glacial sea-level rise. Strong differential uplift, with rates on the order of 0.6–1.2 mm/yr corresponded with the onset of major eruptive phases, whereas a homogeneous regional uplift of 0.24 mm/yr during the last 125 kyr followed this climactic phase. These uplift rates are significantly smaller than sedimentation rate during the glacial termination, consistent with the observed independence of the glacio-eustatic signal.

2. Extending the tephra and palaeoenvironmental record of the Central Mediterranean back to 430 ka: A new core from Fucino Basin, central Italy

Giaccio, B., Leicher, N., Mannella, G., Monaco, L., Regattieri, E., Wagner, B., Zanchetta, G., Gaeta, M., Marra, F., Nomade, S., Palladino, D.M., Pereira, A., Scheidt, S., Sottili, G., Wonik, T., Wulf, S., Zeeden, C., Ariztegui, D., Cavinato, G.P., Dean, J.R., Florindo, F., Leng, M.J., Macrì, P., Niespolo, E., Renne, P.R., Rolf, C., Sadori, L., Thomas, C., & Tzedakis, P.C., 2019. *Quaternary Science Reviews,* 225, 106003

Here we present the first tephrostratigraphic, palaeomagnetic, and multiproxy data from a new ~98 m-deep sediment core retrieved from the Fucino Basin, central Italy, spanning the last ~430 kyr. Palaeoenvironmental proxy data (Ca-XRF, gamma ray and magnetic susceptibility) show a cyclical variability related to interglacial-glacial cycles since the Marine Isotope Stage (MIS) 12-MIS 11 transition. More than 130 tephra layers are visible to the naked eye, 11 of which were analysed (glass-WDS) and successfully correlated to known eruptions and/or other equivalent tephra. In addition to tephra already recognised in the previously investigated cores spanning the last 190 kyr, we identified for the first-time tephra from the eruptions of: Tufo Giallo di Sacrofano, Sabatini (288.0 ± 2.0 ka); Villa Senni, Colli Albani (367.5 ± 1.6 ka); Pozzolane Nere and its precursor, Colli Albani (405.0 ± 2.0 ka, and 407.1 ± 4.2 ka, respectively) and Castel Broco, Vulsini (419-490 ka). The latter occurs at the bottom of the core and has been 40Ar/39Ar dated at 424.3 ± 3.2 ka, thus providing a robust chronological constrain for both the eruption itself and the base of the investigated succession. Direct 40Ar/39Ar dating and tephra geochemical fingerprinting provide a preliminary radioisotopic-based chronological framework for the MIS 11-MIS 7 interval, which represent a foundation for the forthcoming multiproxy studies and for investigating the remaining ~110 tephra layers that are recorded within this interval. Such future developments will contribute towards an improved MIS 11-MIS 7 Mediterranean tephrostratigraphy, which is still poorly explored and exploited.

3. Tephrochronology of the central Mediterranean MIS 11c interglacial (~425-395 ka): New constraints from the Vico volcano and Tiber delta, central Italy.

Pereira, A., Monaco, L., Marra, F., Nomade, S., Gaeta, M., Leicher, N., Palladino, D.M., Sottili, G., Guillou, H., Scao, V., & Giaccio, B., 2020. *Quaternary Science Reviews*, 243, 106470.

Through a systematic integrated approach, which combined lithostratigraphic, geochronological and geochemical analyses of tephra from near-source sections of the peri-Tyrrhenian volcanoes and mid to distal settings, here we provide an improved tephrochronological framework for the Marine Isotope Stage 11c interglacial (MIS 11c, ~425-395 ka) in the Central Mediterranean area. Specifically, we present the complete geochemical dataset and new high-precision $^{40}Ar/^{39}Ar$ ages of the previously poorly characterised earliest pyroclastic products of the Vico volcano (420-400 ka), including the Plinian eruptions of Vico α and Vico β and the immediately post-dating lower magnitude explosive events. Furthermore, we also provide new geochronological and geochemical data for the distal tephra layers preserved in the aggradational succession of the Tiber delta (San Paolo Formation), Roman area, which records sea level rise relating to the MIS 12 (glacial) to MIS 11 (interglacial) transition. Five pyroclastic units were recognized in Vico volcanic area, four out of which, Vico α, Vico β, Vico β_{top} (a minor eruption immediately following Vico β and temporally very close to it) and Vico δ were directly dated at 414.8 ± 2.2 ka, 406.5 ± 2.4 ka, 406.4 ± 2.0 ka and 399.7 ± 3.2 ka respectively (2σ analytical uncertainties). These new data allow a critical reappraisal of the previously claimed identifications of Vico tephra from mid-distal to ultra-distal successions (i.e., Vico-Sabatini volcanic districts, Roman San Paolo Formation and Castel di Guido archaeological site, Sulmona Basin, Valdarno and Lake Ohrid), which were unavoidably biased by the poor and incomplete geochemical and geochronological reference datasets previously available. Such an improvement of the tephrochronological framework brings great benefits to any future investigations (e.g., paleoclimatology, archaeology, active tectonic, volcanology) in the dispersal areas of the studied eruptions at the key point in time that is MIS 11.

4. An end to the Last Interglacial highstand before 120 ka: Relative sea-level evidence from Infreschi Cave (Southern Italy)

Bini, M., Zanchetta, G., Drysdale, R.N., Giaccio, B., Stocchi, P., Vacchi, M., Hellstrom, J.C., Couchoud, I., Monaco, L., Ratti, A., Martini, F., & Sarti, L., 2020. *Quaternary Science Reviews*, 250, 106658.

The timing, duration and evolution of sea level during the Marine Isotope Stage 5e (MIS 5e) highstand is a subject of intense debate. A major problem in resolving this debate is the difficulty of chronologically constraining the sea level fall that followed the peak of the highstand. This was mainly controlled by ice- sheet dynamics, the understanding of which is relevant for assessing future sea-level behavior due to global warming. Here we use stratigraphical and geochronological (U/Th dating and tephra finger- printing) evidence from the Infreschi archaeological cave (Marina di Camerota, Southern Italy) to constrain relative sea level (RSL) evolution during the MIS 5e highstand and younger stages. Uranium- thorium dating of speleothem deposition phases places the maximum highstand RSL at 8.90 ± 0.6 m a.s.l., as indicated by the near-horizontal upper limit of Lithophaga boreholes measured for along a ~3.5 km coastal cliff section. Geochronological data show that RSL fell more than 6 m before ~120 ka, suggesting a duration of the Last Interglacial highstand significantly shorter than proposed in some previous studies. Modelling shows that the RSL trend predicted by the ICE-5G and ICE-6G ice-sheet simulations is consistent with our data, but requires an additional significant reduction of both Greenland and Antarctic ice sheets to match the height of the local maximum highstand if no correction for tectonics is applied. Reconciling field data and models requires an earlier and likely shorter duration of the MIS 5e highstand. This suggests that our new data can constrain global ice-volume variations during the penultimate deglaciation, as well as glacial inception at the end of the Last Interglacial. Ac- cording to our chronology, there is no local evidence of higher-than-present-day sea levels after 120 ka.

5. Tephrochronological constraints on the timing and nature of sea-level change prior to and during glacial termination V

Giaccio, B., Marino, G., Marra, F., Monaco, L., Pereira, A., Zanchetta, G., Gaeta, M., Leicher, N., Nomade, S., Palladino, D.M., Sottili, G., Guillou, H., & Scao, V., 2021. Quaternary Science Reviews, 263, 106976.

Glacial-interglacial variations in ice volume and sea level are essential components of the Pleistocene global climate evolution. Deciphering the timing of change of these key climate parameters with respect to the insolation forcing is central to understanding the processes controlling glacial terminations. Here we exploit the sensitivity of the Paleo Tiber River (central Italy) to sea-level forced changes in the base level and the frequent occurrence of datable tephra layers in its sedimentary successions to reconstruct the timing of the relative sea-level (RSL) change between 450 and 403 ka, i.e., across the glacial termination (T-V) that marks the transition between Marine Isotope Stage (MIS) 12 and MIS 11. The analysis hinges on new stratigraphic data, tephra geochemical fingerprinting, and 40Ar/39Ar dating from a fluvial section that represents the inland counterpart of the near mouth, coastal aggradational successions of the San Paolo Formation (SPF). Tephra correlation indicates that the morpho-stratigraphic record of the inland section is as sensitive to the sea-level change as its coastal counterparts, which makes it ideal to complement previous RSL reconstructions from the Tiber River catchment basin, thereby providing a more detailed picture of the sea-level history across T-V. Combined sedimentological and morphological proxies of the composed inland-coastal SPF record document the occurrence of two phases of relatively rapid sea-level rise, here interpreted as meltwater pulse (MWP) events. The earlier MWP occurred between ~450 and ~445 ka and matches a relatively minor episode of the sea-level rise documented in an existing RSL record, while the younger MWP at ~430 ka corresponds to the high amplitude sea-level rise that marks T-V. We find that both MWPs coincide with episodes of ice-rafted debris deposition in the North Atlantic (Heinrich-like events) and with attendant Southern Hemisphere warming, plausibly associated with the bipolar seesaw.

References

Bini, M., Zanchetta, G., Drysdale, R.N., Giaccio, B., Stocchi, P., Vacchi, M., Hellstrom, J.C., Couchoud, I., Monaco, L., Ratti, A., Martini, F., Sarti L., 2020. An end to the Last Interglacial highstand before 120 ka: Relative sea-level evidence from Infreschi Cave (Southern Italy). *Quaternary Science Reviews* **250**, 106658. https://doi.org/10.1016/j.quascirev.2020.106658.

Giaccio, B., Leicher, N., Mannella, G., Monaco, L., Regattieri, E., Wagner, B., Zanchetta, G., Gaeta, M., Marra, F., Nomade, S., Palladino, D.M., Pereira, A., Scheidt, S., Sottili, G., Wonik, T., Wulf, S., Zeeden, C., Ariztegui, D., Cavinato, G.P., Dean, R.J., Florindo, F., Leng, M.J., Macrì, P., Niespolo, E., Renne, P.R., Rolf, C., Sadori, L., Thomas, C., Tzedakis, P.C., 2019. Extending the tephra and paleoenvironmental record of the Central Mediterranean back to 430 ka: A new core from Fucino Basin, central Italy. *Quaternary Science Reviews* **225**, 106003. https://doi.org/10.1016/j.quascirev.2019.106003.

Giaccio, B., Marino, G., Marra, F., Monaco, L., Pereira, A., Zanchetta, G., Gaeta, M., Leicher, N., Nomade, S., Palladino, D.M., Sottili, G., Guillou, H., Scao, V., 2021. Tephrochronological constraints on the timing and nature of sea-level change prior to and during glacial termination V. *Quaternary Science Reviews* **263**, 106976. https://doi.org/10.1016/j.quascirev.2021.106976.

Marra, F., Costantini, L., Di Buduo, G.M., Florindo, F., Jicha, B.R., Monaco, L., Palladino, D.M., Sottili, G., 2019. Combined glacio-eustatic forcing and volcano-tectonic uplift: geomorphological and geochronological constraints on the Tiber River terraces in the eastern Vulsini Volcanic District (central Italy). *Global and Planetary Change* **182**, 103009. https://doi.org/10.1016/j.gloplacha.2019.103009.

Pereira, A., Monaco, L., Marra, F., Sébastien, N., Gaeta, M., Leicher, N., Palladino, D.M., Sottili, G., Guillou, H., Scao, V., Giaccio, B., 2020. Tephrochronology of the central Mediterranean MIS 11c interglacial (~425-395 ka): New constraints from the Vico volcano and the Tiber delta, central Italy. *Quaternary Science Reviews* **243**, 106-470. https://doi.org/10.1016/j.quascirev.2020.106470.

Chapter VII - General results and main implications of the Thesis

In this Thesis, three original papers, published, in preparation or submitted (i.e., accepted for publication following minor revisions), have been presented in Chapters III, IV and V respectively.

The first two papers, presented in Chapters III and IV, addressed two tephra sequences from Fucino Basin, central Italy, in the time intervals of 430-365 (MIS 11) ka and 250-170 (MIS 6-7) ka. Tephra layers from the two F4-F5 Fucino successions were ascribed to the peri-Tyrrhenian potassic Quaternary volcanoes, including the Vulsini, Vico, Sabatini, Colli Albani, Roccamonfina, Ischia, and Campi Flegrei, based on their geochemical fingerprint. Some of these tephra layers were correlated to known eruptions and/or tephra layers emplaced by the peri-Tyrrhenian volcanoes, but also recorded previously unknown eruptive episodes not yet documented at these volcanoes. Thus, the two Fucino successions provided new integrative information for a more rigorous and complete reconstruction of the explosive history of the peri-Tyrrhenian Italian volcanoes during the Middle Pleistocene.

The third paper (Chapter V) presented a series of medial-proximal pyroclastic units from the Campanian Plain, central Italy, which were correlated to the famous and widespread C-22, X-5, and X-6 tephra MIS 5 marker horizons, as well as to two minor tephra layers (i.e., TM-24a and TM-24b). Thus, results from this study provided new evidence of intense and recurrent activity at Campi Flegrei volcano in the time interval of 109-92 ka.

In these three case studies, as well as in the co-authored publications mentioned in Chapter VI, a dualistic approach has been employed, which combine the study of distal tephra sequences hosted in sedimentary (lacustrine, sub-aerial, marine) successions with analysis of pyroclastic deposits in proximal (i.e., near-vent) volcanic areas. Investigations in proximal areas allowed: (i) a direct comparison between distal tephra layers and proximal pyroclastic units, and (ii) building a glass-geochemistry based reference dataset, not only for these studies, but also for future investigations in the area. This resulted to be essential as most of the previous studies mainly presented whole-rock bulk analysis of the pyroclastic units, which are not directly comparable with glass-based geochemical data aquired on the tephra layers.

Geochemical analysis of the glass-shards and/or pumice fragments were performed with a series of analytical techniques, i.e., EPMA (major and minor elements), LA-ICP-MS (trace elements), TIMS (Sr-Nd isotopes) and $^{40}Ar/^{39}Ar$ dating. The combination of these analyses provided the full geochemical fingerprint of the tephra, which in turn allowed the unambiguous attribution to the source volcano and correlation to known eruptive episodes. In this perspective, data aquired with the same suite of analyses from the proximal deposits resulted to be essential for backtracking the specific source volcano of the tephra layers with unknown origin.

From a broader perspective, results from this Thesis provided new fundamental information for better reconstructing the explosive history of the peri-Tyrrhenian Quaternary Italian volcanoes and sensibly enriched the Mediterranean tephra lattice. The newly presented high-precise $^{40}Ar/^{39}Ar$ ages, which refined the chronology of known eruptions, combined with the discovery of previously undocumented explosive episodes recorded at Fucino, allowed a more precise and updated reconstruction of the explosive history at these volcanoes. In turn, this allowed the refinement of the recurrence time intervals and quiescence periods at the Italian volcanoes, which has relevant implications for hazard assessment in the investigated volcanic areas. For instance, in Chapter V a series of at least five eruptive episodes occurred in a narrow time interval of ~17 kyr, between 109-92 ka, a behaviour previously documented only for the period following the 14 ka eruption of the Neapolitan Yellow Tuff. In Chapter IV, previously undocumented eruptive episodes at Vico, Ischia and Campi Flegrei recorded at Fucino Basin testifies explosive activity during supposedly long quiescence periods. For instance, tephra layers TF-24 and TF-25 (~200 ka) from Vico volcano half the recurrence interval elapsed between the caldera-forming eruptions of Vico Ignimbrite A (~250 ka) and Ignimbrite B (160 ± 3 ka) from ~90 kyr to ~45 kyr (Fig. 1). Similarly, in Chapter III, Fucino tephra layers document explosive eruptions at Vulsini, Vico and Sabatini not documented in proximal settings. In particular, the Fucino record document an eruption cluster at ~399-397 ka occurring at Sabatini volcano, reducing the maximum recorded dormancy period from ~90 kyr to ~70 kyr in this volcanic district (Fig. 1), which is the same interval of time elapsed since the last documented eruption, with implications for hazard assessment in the Roman area.

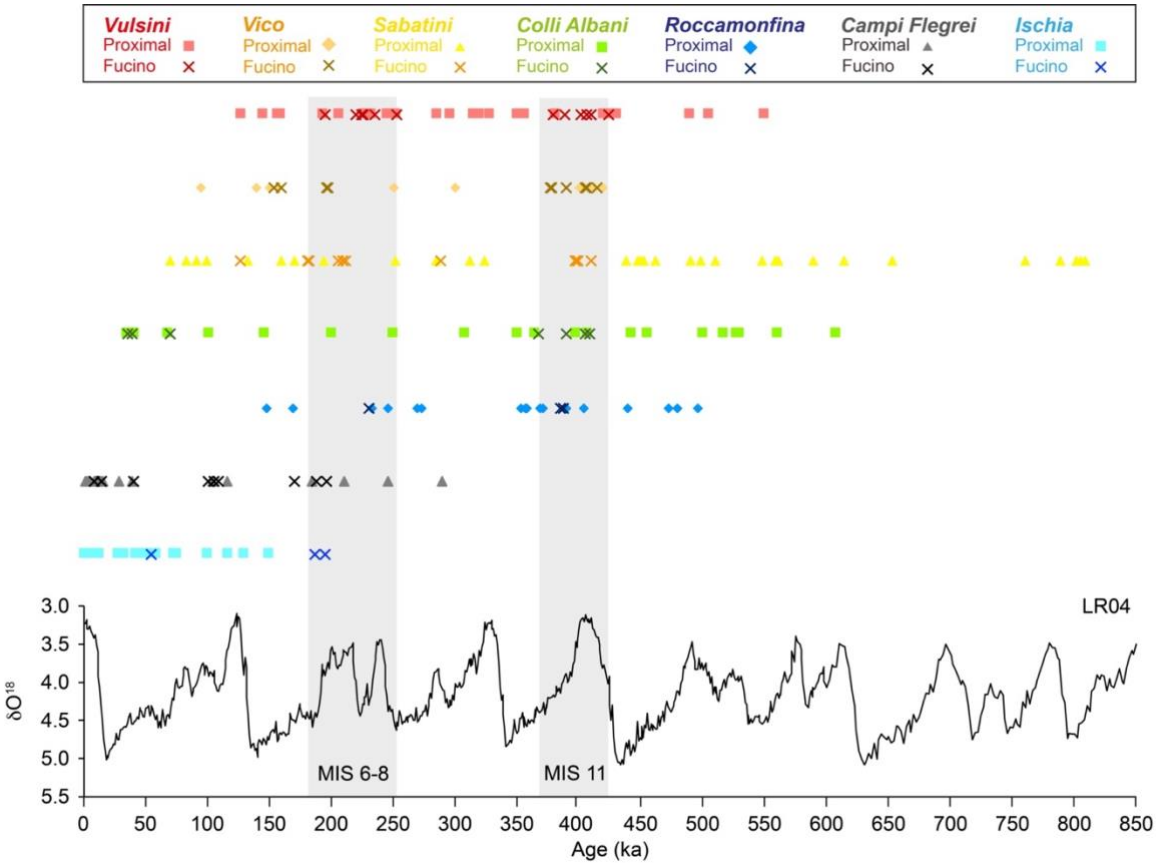

Figure 1. Eruptions from the peri-Tyrrhenian Quaternary volcanoes documented in proximal volcanic areas compared with the Fucino record for the last 850 kyr. LR04 δO^{18} benthic stack record (Lisiecki and Raymo, 2005) is also shown for comparison. Age of the eruptions data source: Fucino basin: Giaccio et al. (2019), Monaco et al. (2021), Monaco et al. (in preparation); Vulsini: Palladino et al. (2010, and references therein); Vico: Perini et al. (1997, and references therein); Sabatini: Marra et al. (2020, and references therein); Colli Albani: Marra et al. (2016, and references therein); Roccamonfina: Rouchon et al. (2008, and refrences therein); Campi Flegrei: Rolandi et al. (2003), Smith et al. (2011, and references therein); Ischia: Poli et al. (1987), Brown et al. (2014).

Despite the big steps forward made with the results from this Thesis, the Middle Pleistocene remains still largely unexplored, and further efforts must be made to collect and analyse pyroclastic deposits of eruptions from Latium (i.e., Vulsini, Vico, Sabatini, and Colli Albani) and Neapolitan (i.e., Roccamonfina, Ischia, Procida, and Campi Flegrei) volcanic areas.

To summarise, the following general conclusions can be drawn:

1) All the tephra layers recovered from the F4-F5 core of Fucino Basin so-far characterised were emplaced by eruptions at the peri-Tyrrhenian and insular potassic Quaternary Italian volcanoes. This shows the relevance of Fucino Basin at regional level for tephra investigations.
2) Tephra layers from the Fucino Basin documented explosive activity so-far unreported in proximal (i.e., near-vent) settings, providing new fundamental insights for eruptive history reconstruction and refinement.
3) Previously known eruptions are now better constrained by the newly acquired $^{40}Ar/^{39}Ar$ ages presented in the studies that constitute this Thesis.
4) Some of the tephra layers recorded at Fucino Basin can be correlated to tephra from other Italian and Mediterranean tephra repositories, allowing to transfer the new high-precise $^{40}Ar/^{39}Ar$ ages determined for Fucino tephra to these successions.
5) On a methodological point of view, major, minor, and trace elements determined on glass shards and/or pumice fragments, respectively by means of EPMA and LA-ICP-MS techniques, showed to successfully allow determination of the tephra layers' source volcano. In most of the cases, these data were also sufficient for identification of the equivalent eruptive episode or tephra layer.
6) On the contrary, Sr and Nd isotopes, although a powerful instrument for determining the volcanic region and/or province, showed a resolution limit that fail to backtrack the specific source volcano and/or eruptive event, due to the similarities shown by products of the peri-Tyrrhenian potassic volcanoes, especially for the Latium ones. Nevertheless, in Chapter V Sr-Nd isotopes contributed to the identification of the Campi Flegrei volcano as the source of the Mediterranean tephra markers highlighting the employement of these isotopes for tephra investigations.
7) Geochemical fingerprinting of the proximal pyroclastic units showed to be essential for volcanic source determination and individual eruptive event identification. Thus, the dualistic approach employed in this Thesis was shown to be successful for tephra investigations in the Italian peninsula and on a broader point of view.

With respect to the objectives and aims of this Thesis, the following conclusions can be drawn:

1) The two tephra sequences from Fucino Basin presented in this Thesis provided fundamental data that enriched the central Mediterranean tephra lattice and partially filled the gap of knowledge relative to the Middle Pleistocene eruptive history. Nevertheless, further investigations are needed, since the F4-F5 Fucino successions covers “only” the last ~430 kyr, meaning there are still ~350 ka to be furtherly investigated. Future investigations at Fucino, as well as other Italian sedimentary successions, such as Sulmona Basin, should focus on these older intervals to completely investigate the Middle Pleistocene.
2) Glass geochemical data provided for the proximal pyroclastic units of Vulsini, Vico, Sabatini, Colli Albani, and Campi Flegrei volcanic districts helped to build a reference dataset for future investigations in the region. However, in order to reach a satisfactory and effective reference dataset, further advancements must be made. Indeed, only specific eruptive intervals of the mentioned volcanoes have been geochemically characterised, and major portions are still unexplored. In particular, glass-geochemistry of the proximal pyroclastic units of Roccamonfina volcano are still missing and, given the occurrence of several Roccamonfina-like tephra in the Fucino succession and other Mediterranean tephra repositories (e.g., Ohrid Lake), their characterisation appears fundamental for further advancements.

References

Brown, R.J., Civetta, L., Arienzo, I., D'Antonio, M., Moretti, R., Orsi, G., Tomlinson, E.L., Albert, P.G., Menzies, M.A., 2014. Geochemical and isotopic insights into the assembly, evolution and disruption of a magmatic plumbing system before and after cataclysmic caldera-collapse eruption at Ischia volcano (Italy). *Contirb. Mineral. Petrol.* **168**: 1035. https://doi.org/10.1007/s00410-014-1035-1.

Giaccio, B., Leicher, N., Mannella, G., Monaco, L., Regattieri, E., Wagner, B., Zanchetta, G., Gaeta, M., Marra, F., Nomade, S., Palladino, D.M., Pereira, A., Scheidt, S., Sottili, G., Wonik, T., Wulf, S., Zeeden, C., Ariztegui, D., Cavinato, G.P., Dean, R.J., Florindo, F., Leng, M.J., Macrì, P., Niespolo, E., Renne, P.R., Rolf, C., Sadori, L., Thomas, C., Tzedakis, P.C., 2019. Extending the tephra and paleoenvironmental record of the Central Mediterranean back to 430 ka: A new core from Fucino Basin, central Italy. *Quat. Sci. Rev.* **225**, 106003. https://doi.org/10.1016/j.quascirev.2019.106003.

Lisiecki, L.E. & Raymo, M.E., 2005. A Pliocene-Pleistocene stack of 57 globally distributed benthic d18O records. *Palaeoceanogr. Palaeoclimatol.* **20** (1), PA1003. https://doi.org/10.1029/2004PA001071.

Marra, F., Castellano, C., Cucci, L., Florindo, F., Gaeta, M., Jicha, B., Palladino, D.M., Sottili, G., Tertulliani, A., Tolomei, C., 2020. Monti Sabatini and Colli Albani: the dormant twin volcanoes at the gates of Rome. *Sci. Rep.* **10**:8666. https://doi.org10.1038/s41598-02-65394-2.

Marra, F., Gaeta, M., Giaccio, B., Jicha, B.R., Palladino, D.M., Polcari, M., Sottili, G., Taddeucci, J., Florindo, F., Stramondo, S., 2016. Assessing the volcanic hazard for Rome: $^{40}Ar/^{39}Ar$ and In-SAR constraints on the most recent eruptive activity and present-day uplift at Colli Albani Volcanic District. *Geophys. Res. Lett.* **43**, 6898-6906. https://doi.org/10.1002/2016GL069518.

Monaco, L., Palladino, D.M., Gaeta, M., Marra, F., Sottili, G., Leicher, N., Mannella, G., Nomade, S., Pereira, A., Regattieri, E., Wagner, B., Zanchetta, G., Albert, P.G., Arienzo, I., D'Antonio, M., Petrosino, P., Manning, C., Giaccio, B., 2021. Mediterranean tephrostratigraphy and peri-Tyrrhenian explosive activity revaluated in light of the 430-365 ka record from Fucino Basin (central Italy). *Earth Sci. Rev.* **220**, 103706. https://doi.org/10.1016/j.earscirev.2021.103706.

Palladino, D.M., Simei, S., Sottili, G., Trigila, R., 2010. Integrated approach for the reconstruction of stratigraphy and geology of Quaternary volcanic terrains: an application to the Vulsini Volcanoes (central Italy). In: Groppelli, G., Viereck, e L. (Eds.), Stratigraphy and Geology in Volcanic Areas. *Geol. Soc. Am. Spec. Pap.* **464**, 66–84.

Perini, G., Conticelli, S., Francalanci, L., 1997. Inferences on the volcanic history of the Vico volcano, Roman Magmatic Province, central Italy: stratigraphic, petrographic and geochemical data. *Mineral. Petrograph. Acta* **40**, 67-93.

Poli, S., Chiesa, S., Gillot, P.-Y., Gregnanin, A., Guichard, F., 1987. Chemistry versus time in the volcanic complex of Ischia (Gulf of Naples, Italy): evidence of successive magmatic cycles. *Contrib. Mineral. Petrol.* **95**, 322-335.

Rouchon, V., Gillot, P.Y., Quidelleur, X., Chiesa, S., Floris, B., 2008. Temporal evolution of the Roccamonfina volcanic complex (Pleistocene), Central Italy. Journal of Volcanology and Geothermal Research, 177, 500-514. https://doi.org/10.1016/j.jvolgeores.2008.07.016.

Smith, V.C., Isaia, R., Pearce, N.J.G., 2011. Tephrostratigrapy and glass compositions of post-15 kyr Campi Flegrei eruptions: implications for eruption history and chronostratigraphic markers. Quaternary Science Reviews, 30, 3638-3660. https://doi.org/10.1016/j.quascirev.2011.07.012.

Acknowledgments

The two external revisors, Prof. R. Cioni (University of Florence) and Dr. S. Wulf (University of Portsmouth), are thanked for providing useful and valuable comments to the manuscript, which greatly benefited from their revision work.

Articles from chapters III and IV of this Theis represent a contribution to the international project "FUcino Tephrochronology Unites Quaternary REcords (FUTURE)", supported by the Italian Ministry of Education, University and Research (MIUR, grant PRIN No. 20177TKBXZ_003; national coordinator: G. Zanchetta). The Fucino project is co-funded by DFG (German Research Foundation) grant WA 2109/16. Prof. G. Zanchetta is thanked for allowing me to contribute to the FUTURE project.

Field investigations and EPMA analysis carried on for the article from Chapter V of this Thesis were financially supported by the project entitled "Tracing the proximal occurrences and modelling the largest Campi Flegrei explosive eruptions preceding the 40 ka Campanian Ignimbrite, souther Italy" (Progetti per Avvio alla Ricerca - Tipo 1, "Sapienza" Università di Roma, N° protocollo: AR120172AD35B81D, PI: L. Monaco).

$^{40}Ar/^{39}Ar$ dating received complementary contribution from the CNRS INSU-LEFE 2018-2020 action to S. Nomade. P.G. Albert is supported by a UKRI Future Leaders Fellowship (MR/S035478/1). INGV-OV laboratories have been also financially supported by the EPOS Research Infrastructure through the contribution of the Italian Ministry of University and Research (MIUR).

M. Sarracino and M. Albano (CNR-IGAG) are thanked for providing valuable technical assistance during SEM and EPMA analysis at the laboratories of the Earth Science Department, "Sapienza" - University of Rome (Rome, Italy). Similarly, Dr. A. Orlando and E. Braschi (CNR-IGG), R. Jedlička and M. Racek (Přírodovědecká fakulta), are thanked for providing valuable technical assistance during EPMA and SEM analysis at the Earth Science Department, University of Florence (Florence, Italy), and at the Institute of Petrology and Structural Geology, Faculty of Science, Charles University (Prague, Czech Republic), respectively.

Dr. Paul G. Albert, Swansea University, is deeply thanked for his assistance during LA-ICP-MS trace element analysis during my visiting period at the Royal Holloway, University of London. He is also thanked for acquiring, elaborating and interpretaing trace element analyses for the original manuscript constituting Chapter V.

Similarly, Dr. Maurizio Petrelli, University of Perugia, is thanked for his assistance during trace element data acquisition via remote connection with the LA-ICP-MS installed at the Physic and Geology Department, as well as his help in data elaboration and interpretation for Chapter IV.

Dr. Alessandro Fabbrizio, Charles University of Prague, is deeply thanked for hosting me at the Přírodovědecká fakulta during my three months-long visiting period at the beautiful city of Prague. I am really looking forward to visit Prague and Alessandro again in the future.

Dr. Sebastien Nomade (LSCE) and Alison Pereira (Paris-Saclay) are thanked for acquiring, elaborating, and providing all the $^{40}Ar/^{39}Ar$ ages presented in this Thesis and I am proud to call them co-authors. On the same wave, Dr. Ilenia Arienzo, of the INGV-OV, is sincerely thanked for acquiring, elaborating, and interpreting the Sr and Nd isotope compostions presented in this Thesis.

All the other co-authors of the published (Chapter III), unpublished (Chapter IV) and submitted/accepted for publication (Chapter V) original manuscripts are thanked for their assistance in the realization of these works, that greetly beneficied from their expertises.

Dr. D. Mannetta is sincerely and deeply thanked for its irreplaceable and fundamental assistance provided during the preparation of the samples studied during the three years-long Ph.D. More importantly, he is thanked for being a sincere friend and a beautiful human being.

I am also greatful to the Ph.D. school and its coordinator, Prof. S. Mollo, for having had me as one of its Ph.D. students, for his advice and suggestions through the the past three years.

Finally, a sincere and deep thank goes to my two supervisors, D. Palladino (“Sapienza” - University of Rome) and B. Giaccio (CNR-IGAG) for their guidance, assistance, and teaching during the Ph.D., which would have not been possible without their experience, knowledge, and friendship.